Modeling and Identification of Electrically Stimulated Muscle

by

Karen I. Palmer

B. S. E. E.
GMI Engineering & Management Institute
(1986)

Submitted to the
Department of Mechanical Engineering

in partial fulfillment of the requirements
for the degree of

Master of Science in
Mechanical Engineering

at the

Massachusetts Institute of Technology

September 1990

Signature of Author _____
Department of Mechanical Engineering
September, 1990

Certified by _____
Professor William K. Durfee
Thesis Supervisor

Accepted by _____
Professor Ain A. Sonin
Chairman, Departmental Committee on Graduate Students

Modeling and Identification of Electrically Stimulated Muscle

by

Karen I. Palmer

Submitted to the Department of Mechanical Engineering
in partial fulfillment of the requirements for the degree of
Master of Science in Mechanical Engineering

Abstract

Functional electrical stimulation, a rehabilitation technique for spinal cord injury, requires an accurate model of electrically stimulated muscles to control the muscle contraction force. This thesis describes a model for electrically stimulated muscle which uses passive and active force generators in parallel. The passive force is the sum of two terms which are dependent on muscle length and velocity. The active force is the product of three terms dependent on stimulation level, length, and velocity. The model parameters are completely identifiable from muscle force measurements when the length, velocity and stimulation levels are known, using a technique based on singular value decomposition.

The model was fit to experimental data from cat medial gastrocnemius and tibialis anterior muscles. Model validity was demonstrated by comparing predicted force to measured force using the same inputs. Characteristic muscle curves – isometric recruitment curve, active length-tension and force-velocity curves, and passive length-tension and force-velocity curves – were derived using classical testing techniques and compared to the estimated model parameters for the same relationships.

Thesis Supervisor: William K. Durfee
Title: Professor of Mechanical Engineering

Acknowledgments

I would like to thank Will Durfee, my thesis advisor, for his help, suggestions, and encouragement during all phases of this project.

I would like to thank the other members of the FES group, both present and past, for their assistance and encouragement. Past group members include Karon MacLean, who tolerated my attempts at modifying her programs while I was learning to program in C, and Andy Robbins who developed the Joint Space Muscle Model on which my work was based. Among the present members, Susan Huang has been an invaluable friend and sounding board for dealing with problems related to the animal experiments.

I would like to thank several friends who have contributed to this work. John Paul Braud lent assistance in the development of the parameter identification algorithm. Greg Troxel has contributed greatly to my understanding of networked computer systems. Mary Phillips taught me the basics of TeX and LaTeX. Cheryl Harris, my roommate, helped me stay productive in the lab by making sure I got enough sleep, food, and yes, even a few leisure activities.

I would also like to thank my family for their love, support, and encouragement during the writing of this thesis. They have contributed to this work in more ways than they will ever know.

This work was funded by the Whitaker Foundation and by the Whitaker Health Sciences Fund, and was conducted in the Eric P. and Evelyn E. Newman Laboratory for Biomechanics and Human Rehabilitation.

Contents

List of Figures

Chapter 1
Introduction

Nearly 177,000 Americans are unable to use their arms and/or legs as a result of spinal cord injury [22]. For these people, tasks which were once simple — climbing stairs, riding a bicycle, holding a pencil, drinking from a cup — have become impossible.

Spinal cord injury is neurological damage to the spinal cord which results in loss of motor control. The communication pathway between the central nervous system (CNS) and the muscles is interrupted, but the muscles and most of the peripheral nervous system remain intact and viable. Rehabilitation is limited to preventing further loss of function from damage to the spinal cord and, for motivated patients, combating muscle atrophy through stretching and strengthening programs. There are no techniques in widespread use today which either repair the damage to the spinal cord or restore function to the limbs.

Functional electrical stimulation, or FES, is being developed as a rehabilitation technique to restore function to those with spinal cord injuries. FES, on a very basic level, delivers electrical pulses to the nerves of the paralyzed limb to cause the muscles to contract so a task can be performed. Figure 1.1 shows the basic strategy for FES.

Electrically stimulating the nerve to cause muscle contraction is relatively easy. The difficult part of FES is in the first word — "functional" — making the muscles contract in a controlled manner so a task can be performed. This is difficult because the physiological command generator (the brain and other parts of the CNS) must be replaced by an artificial command generator or FES controller.

To begin to understand the complexity of controlling muscle contraction, consider the task of picking up a paper cup. Ideally the fingers and thumb are extended as the hand is placed near the cup so that the cup fits into the "V" formed by the fingers and thumb. Then the fingers flex to curl around the cup as the thumb rotates toward the palm. Simple, but several things could go wrong. If the fingers close with too much force, the cup may be crushed. If the thumb rotates before the fingers start to flex, the cup slides across the table and the task must begin again. If the flexing fingers are not at the same height as the thumb, a torque is produced and the cup tips over.

The CNS controller uses force feedback, position sensing, often visual feedback and *a priori* knowledge of how the muscles contract to execute the task. Ideally, an artificial controller would have access to the same information as the CNS. Unfortunately, force feedback, position sensing and visual feedback from the physiological receptors are not easily accessed or decoded. This means that the FES controller design is highly dependent on the understanding of how the muscles are supposed to contract, i.e. the accuracy of the muscle model is important.

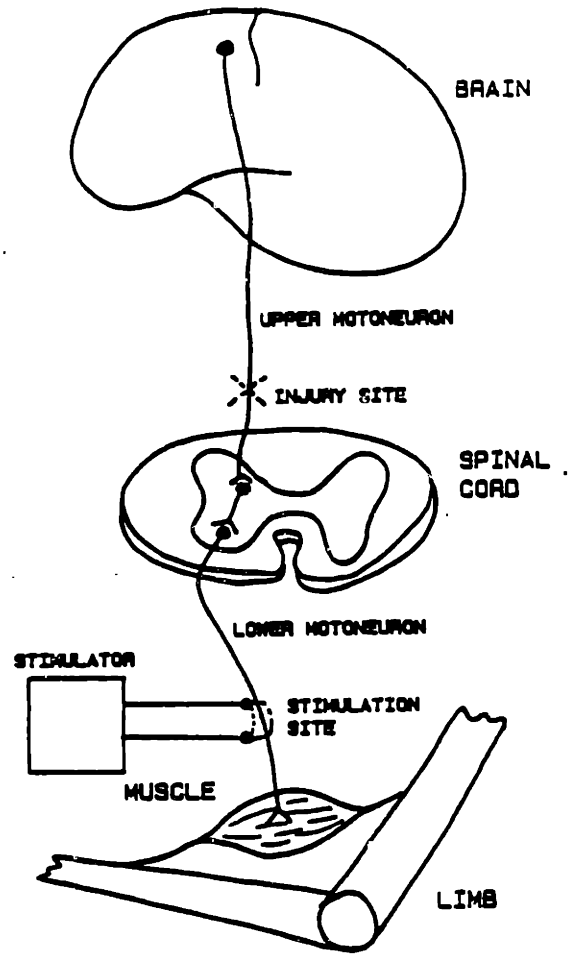

Figure 1.1: **Basic FES strategy.** Voluntary movement commands from the brain are replaced by artificial electrical stimulations [5].

One of the fundamental challenges of FES is to produce a controlled contraction of the muscle. The neuromuscular interface is complex and composed of many motor units which must be independently activated for perfect control. The controller must either have access to adequate feedback channels or a precise knowledge of the muscle's response to stimulation. Without these, the controller cannot deliver the proper stimulation to the muscle to produce the desired contraction.

1.1 Status of Functional Electrical Stimulation

Generating muscle contraction by electrical stimulation is simple. Action potentials can be induced in lower motor neurons through electrical stimulation from an external source. The peripheral nervous system and nerve-muscle interface are not selective in responding to either artificial or naturally generated action potentials. This is not to say that all of the issues related to artificial stimulation have been resolved, merely that exciting muscle tissue to get a contraction is not a major obstacle.

Applications of FES are currently limited to relatively simple, repetitive or cyclic tasks which do not require voluntary monitoring. Examples of common FES applications include: prevention of muscular atrophy, increase in muscular strength and maintenance of range of motion during occupational and physical therapy for a wide range of injuries.

Current FES techniques do not provide active control for tasks which are functional, non-repetitive, or complex such as those relating to hand grasp, postural control, or walking. These applications are the focus of this work.

1.2 Control of Electrically Stimulated Muscle

The success of any control scheme depends on how well the system to be controlled is characterized. Closed-loop control, which uses feedback channels to measure the states of the system, is less dependent upon the quality of the model than is open loop control. With FES there are few reliable sources of feedback, hence an accurate model of stimulated muscle behavior is required.

Characterization of electrically stimulated muscles is complex. In the language of systems modeling, a simple system would be linear, stationary (with respect to time), and have independent variables. Muscles are classified as non-linear, time-varying systems with interdependent variables. Non-linearity refers to the lack of a constant relationship between variables. That is, when force is plotted against velocity, it is not a straight line. Time-varying implies that the curves will tend to change with time. Interdependent variables means that model variables — stimulation, length, velocity, force, etc. — depend on each other. For example, the force-velocity curve changes shape depending on both the stimulation level and the length at which it is measured. Capturing the non-linear, time-varying, interdependent characteristics leads to a complex muscle model.

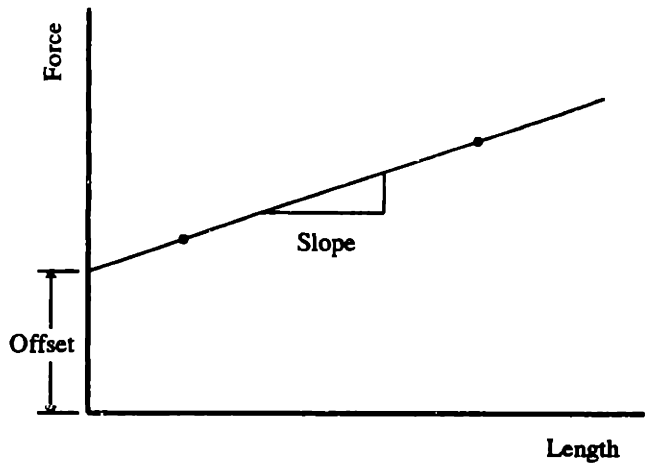

Figure 1.2: Linear model described by two variables

Model complexity is also dictated by the requirements of real time control. The stimulation level must be calculated and the electrical pulse delivered to the nerve within a set length of time in order to maintain control over the muscle contraction. Generally, the shorter this time period, the easier it is to control a fast process such as a muscle contraction. This means that the model should be simple enough to be executed quickly.

These two control issues, model accuracy and real time implementation, require that tradeoffs be made in developing the model. Basically, a model which is to be used for control must be detailed enough to capture the characteristics of a contracting muscle while being simple enough to calculate the control commands quickly.

A third requirement of the muscle model is that it be identifiable. That is, the relationships required by the model must be measurable from muscle contraction data. Since muscles are time varying, the model parameters may change with time. Model calibration is an important factor in designing a muscle model to be used for FES control.

1.3 Identification of Model Parameters

Models are generally developed with many variables which must be determined so that the model describes the actual system. The variables can describe either linear or non-linear relationships between the states of the model. For example, a muscle model needs to know how the force output is related to the length of the muscle. If it were a linear model, force measurements at two different lengths would be required to establish the relationship. It could then be described by two variables — a slope and an offset as in Figure 1.2. For a non-linear model, the force would need to be measured at several lengths and some assumption about the shape of the curve between these points would be required in order to define the force-length relationship at every

length. The model described in this thesis used non-linear relationships which were assumed to be linear between the defined points.

Another issue of parameter estimation is determining what to do when there are more measurements than variables to be fit. In this thesis, chi-squared maximum likelihood estimation was used to resolve the over-determined problem. This criteria states that the best fit line segment is the one which minimizes the sum of the squares of the distances between the line and each data point.

The test of a model's validity, before it is used in an actual controller, is its ability to predict the system's output. This is measured by using the same set of inputs on the fitted model and the actual system. Ideally, the output of the model and the real system would be the same. Realistically, some error is expected and a model is considered acceptable when the error is within a given limit.

1.4 Goal of Thesis

The goal of this thesis was to develop a method for fitting a model to muscle contraction data. A technique was developed and applied to experimental data for the medial gastrocnemius (MG) and the tibialis anterior (TA) of the hind limb of a cat. The fitted model was also used to predict the force output of the same muscles.

1.5 Overview of Contents

The muscle model is described in Chapter 2. Chapter 3 describes the parameter estimation techniques used to fit the model to the muscles. The methods used to generate simulated and experimental data are explained in Chapter 4. Chapters 5 and 6 present and discuss the experimental results, in terms of the muscle characteristics measured by the traditional methods, the estimates of the muscle characteristics for the model, and the predicted output based on the parameter estimates. Chapter 7 presents conclusions and recommendations for future use of the estimation techniques.

Chapter 2
Muscle Model

The purpose of this thesis was to develop a method of organizing information about electrically stimulated muscles. This implies analyzing the information in such a way that it fits a predetermined model.

Modeling electrically stimulated muscles is not a new concept. Many researchers have developed models ranging in levels of sophistication from simple to complex. One of the reasons for the broad spectrum of existing models is the intended use of each. Some researchers wanted to understand the underlying physiological processes of muscle contraction, others wanted to be able to duplicate the details of the contraction, and still others wanted to use the model for controlling the muscle contraction. For reviews of the muscle modeling literature, see [20, 24].

The model used in this research is based on the Joint Space Muscle Model (JSMM) developed by A. H. Robbins [20]. The JSMM was developed for the purpose of controlling electrically stimulated muscles for use with FES. Some objectives for the JSMM were:

1. The model should be simple, while still capturing all of the essential characteristics of muscle dynamics.

2. The model must be completely and phenomenologically identifiable from external measurements (no assumptions about the underlying physiology).

3. All model parameters must be identifiable by correlating known inputs to measurable outputs.

Since this is a real-time control process, the model cannot be too complex. Therefore, several simplifying assumptions were made in the development of this model. These assumptions will be highlighted in the discussion of each part of the model.

The model described in the following sections is based on the JSMM. The reader is encouraged to review Robbins' work to gain an understanding of how this model relates to the physiology of the muscle and to other models which have been developed. Some modifications to Robbins' model have been made and will be discussed in Section 2.4.

2.1 The Musculo-Tendon Unit

The basis of this muscle model is the structure of the musculo-tendon unit (MTU) which is shown in Figure 2.1. The MTU is composed of two parallel sections: one for passive force, the other for active force. The passive force generator consists of

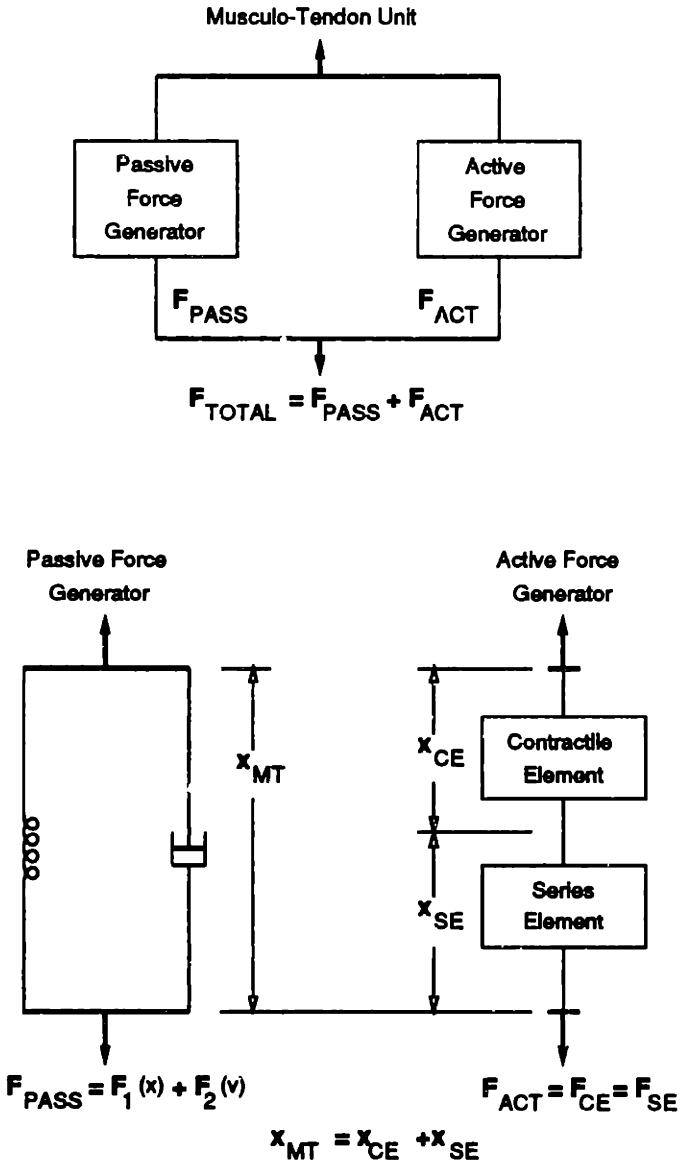

Figure 2.1: The musculo-tendon unit

two elements in parallel: a non-linear spring and a non-linear dashpot. The active force generator has two elements in series: the contractile element (CE) and the series element (SE) (another non-linear spring).

A structure containing two force generators in parallel was used to reduce model complexity by separating the passive and active muscle dynamics. The active force generator only produces force when a stimulus is present. (See Figure 2.1) When the muscle is not stimulated, the developed force is due entirely to the passive characteristics. The force developed by a stimulated muscle is the sum of the passive and the active forces.

$$F_{\text{TOTAL}} = F_{\text{PASS}} + F_{\text{ACT}} \tag{2.1}$$

2.2 Passive Dynamics

When muscle length is changed passively, force is developed. This force is both length and velocity dependent, hence the model contains both a passive spring and a dashpot. The total passive force is the sum of the forces produced by the spring (the passive length-tension relationship (LT_{PASS})) and the dashpot (the passive force-velocity relationship (FV_{PASS}))

$$F_{\text{PASS}} = \text{LT}_{\text{PASS}}(x_{\text{MT}}) + \text{FV}_{\text{PASS}}(\dot{x}_{\text{MT}}). \tag{2.2}$$

When a passive muscle is stretched, it produces a force which is dependent upon the new length. The force increases nonlinearly with length. The relationship between the length and force is commonly called the passive length tension (L-T) curve. A typical L-T curve is shown in Figure 2.2.

The velocity dependency of the stretch of an isolated passive muscle is generally small. It is included here for completeness and for compatibility with the JSMM muscle model. The JSMM model lumps the passive characteristics of all of the muscles acting at a joint into two components — a spring and a dashpot. When the velocity dependencies of all of these muscles and the superficial tissue around the joint are added together, they become significant. So, while some muscle models classify the passive characteristics of a muscle as a "lightly damped" non-linear spring (and use just a spring in the model), this model uses both a spring and a dashpot.

2.3 Active Characteristics

The active force generator of the musculo-tendon unit consists of the contractile element in series with the series elastic element. The contractile element consists of three relationships which are multiplied together to form the total contractile element force. These are the force-recruitment, force-length, and force-velocity dependencies.

$$F_{\text{CE}} = F(\text{stim}) \times F(x) \times F(\dot{x}) \tag{2.3}$$

Each will be discussed in turn.

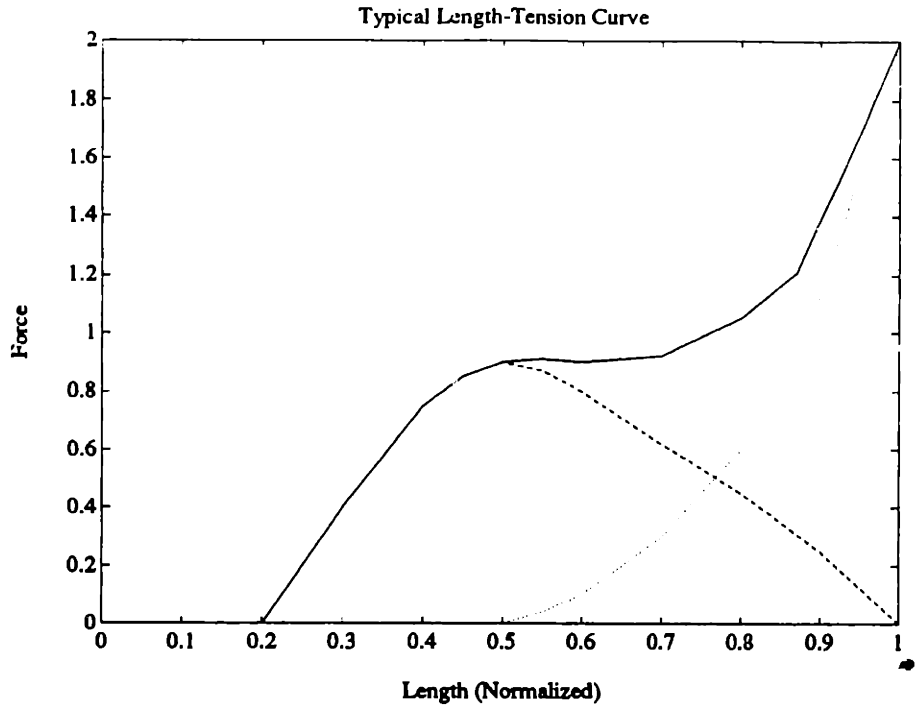

Figure 2.2: Typical length-tension curve: passive (dotted) active (dashed), total (solid).

2.3.1 Series Element

The series element (SE) is modeled as a spring. Figure 2.1 shows the geometric relationship between the CE and the SE. Since the two are in series, the force produced by the CE must be the same as the force in the SE.

$$F_{\mathrm{SE}} = F_{\mathrm{CE}} = F_{\mathrm{ACT}} \tag{2.4}$$

The lengths of the two add to equal the length of the total musculo-tendon unit. Thus the SE relates the force produced by the contractile element to the difference in length between the contractile element and the musculo-tendon unit.

2.3.2 Stimulation Dependence

The model for the relationship between output force and stimulation is based on the work of K. E. MacLean [6, 13]. MacLean used a Hammerstein system consisting of a static non-linear subsystem (SNLS) followed by a dynamic linear subsystem (DLS) as shown in Figure 2.3. The output of the system $Z(t)$ is $Y(t)$ convolved with the impulse response of the DLS, $H(t)$. $Y(t)$ is related to $X(t)$ by the SNLS curve.

The SNLS, the isometric recruitment curve (IRC), is defined as the relationship between stimulus level at a fixed frequency and isometric force output. The IRC of

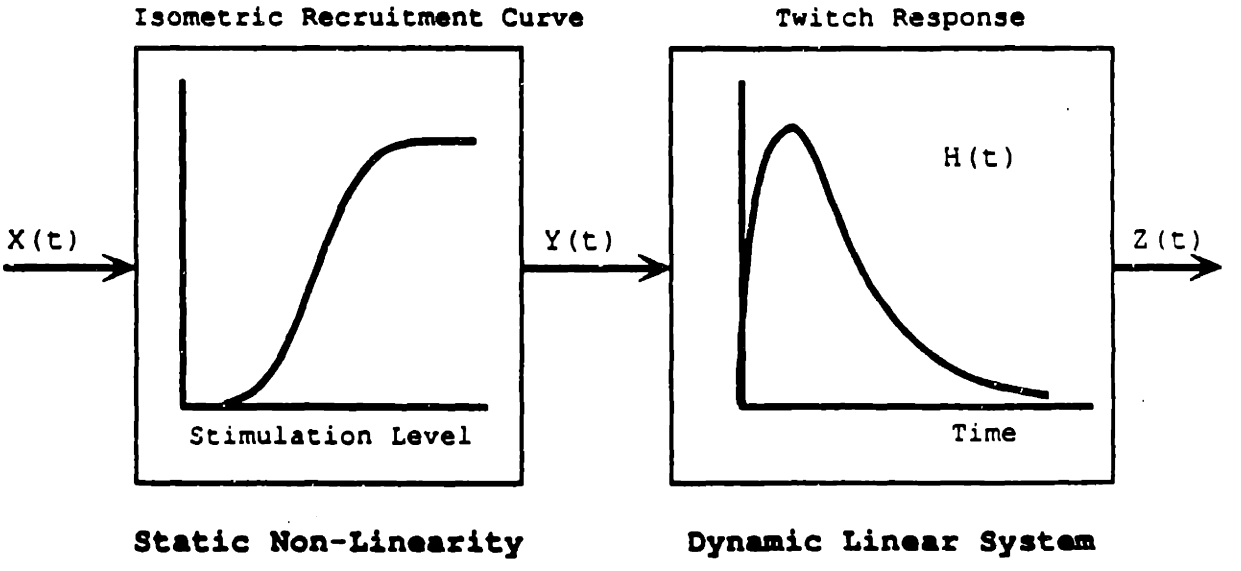

Figure 2.3: Hammerstein activation model [20].

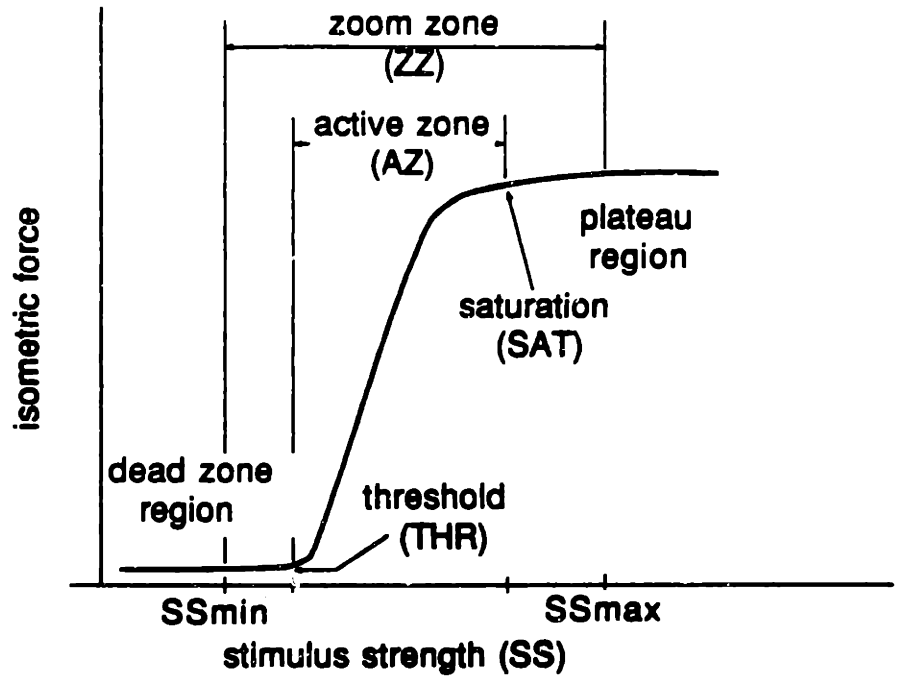

Figure 2.4: The isometric recruitment curve [13].

an artificially stimulated muscle is expected to have a sigmoidal shape as shown in Figure 2.4.

In the Hammerstein system, the DLS is the impulse response of the system which, for the muscle, is the twitch response. It is modeled as a critically damped second order system:

$$h(t) = t\exp(-\lambda t) \tag{2.5}$$

where t is time and λ is the time constant of the impulse response.

2.3.3 Length Dependence

The relationship between length and force development for a stimulated muscle is commonly called the active length-tension (L-T) curve. A typical L-T curve is shown in Figure 2.2. The total force is the measured force output of a stimulated muscle. The active force is the incremental force which is due to the activation of the muscle (the difference between total and passive force).

The length-tension curve changes with stimulation level as shown in Figure 2.5. A simplifying assumption of this model is that this curve does not change shape with

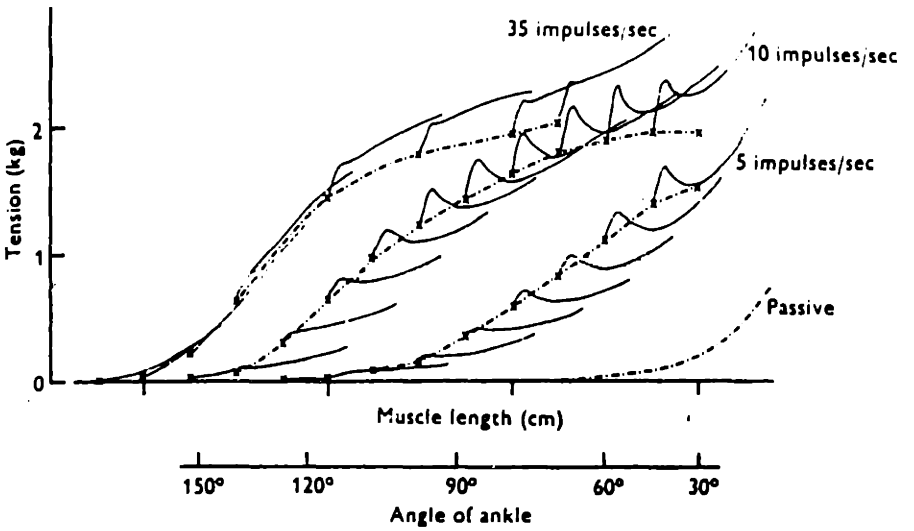

Fig. 3. Tension during extension through different parts of the length range. Tension records from a number of different extensions similar to those shown in Fig. 2 have been traced (continuous line) to show how the tension during lengthening differs from the isometric tension in various parts of the length range. Positions of the ankle joint are shown below corresponding parts of the abscissa.

In each case the muscle was lengthened through 6 mm at 7·2 mm/sec. The interrupted lines are isometric length–tension plots.

Figure 2.5: Length-tension curve as a function of stimulation [10].

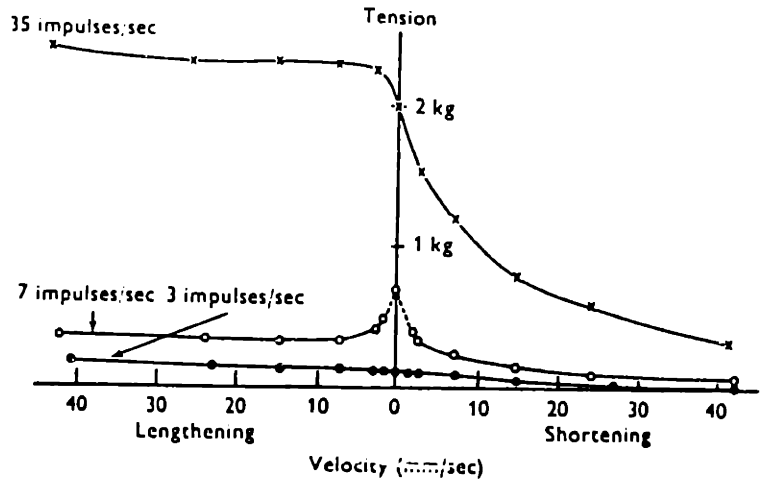

Fig. 5. Tension during movements at various velocities. All tensions were measured at a muscle length corresponding to an angle of 70° at the ankle joint, and all movements began 5 min from that length. Three different stimulus rates were used.

Figure 2.6: Force-velocity curve as a function of stimulation [10].

stimulus level.

2.3.4 Velocity Dependence

A typical force-velocity (F-V) curve is shown in Figure 2.6. The shape of this curve changes with both stimulation and length [10]. This model assumes that the shape is independent of both stimulus and length for simplicity.

2.4 JSMM Model Changes

The model discussed in this section is based on the JSMM model developed by Robbins. The complete model is shown schematically in Figure 2.7. The differences between the model described here and the JSMM are relatively minor and will be discussed below.

The main reason for the differences in models is in the application of the model. Robbins developed the JSMM for use with FES. His goal was a model which could characterize the muscles which act across a human joint. His model placed no limitation on how many muscles acted on the joint nor how many electrodes were used to stimulate those muscles. This research sought to identify the characteristics of

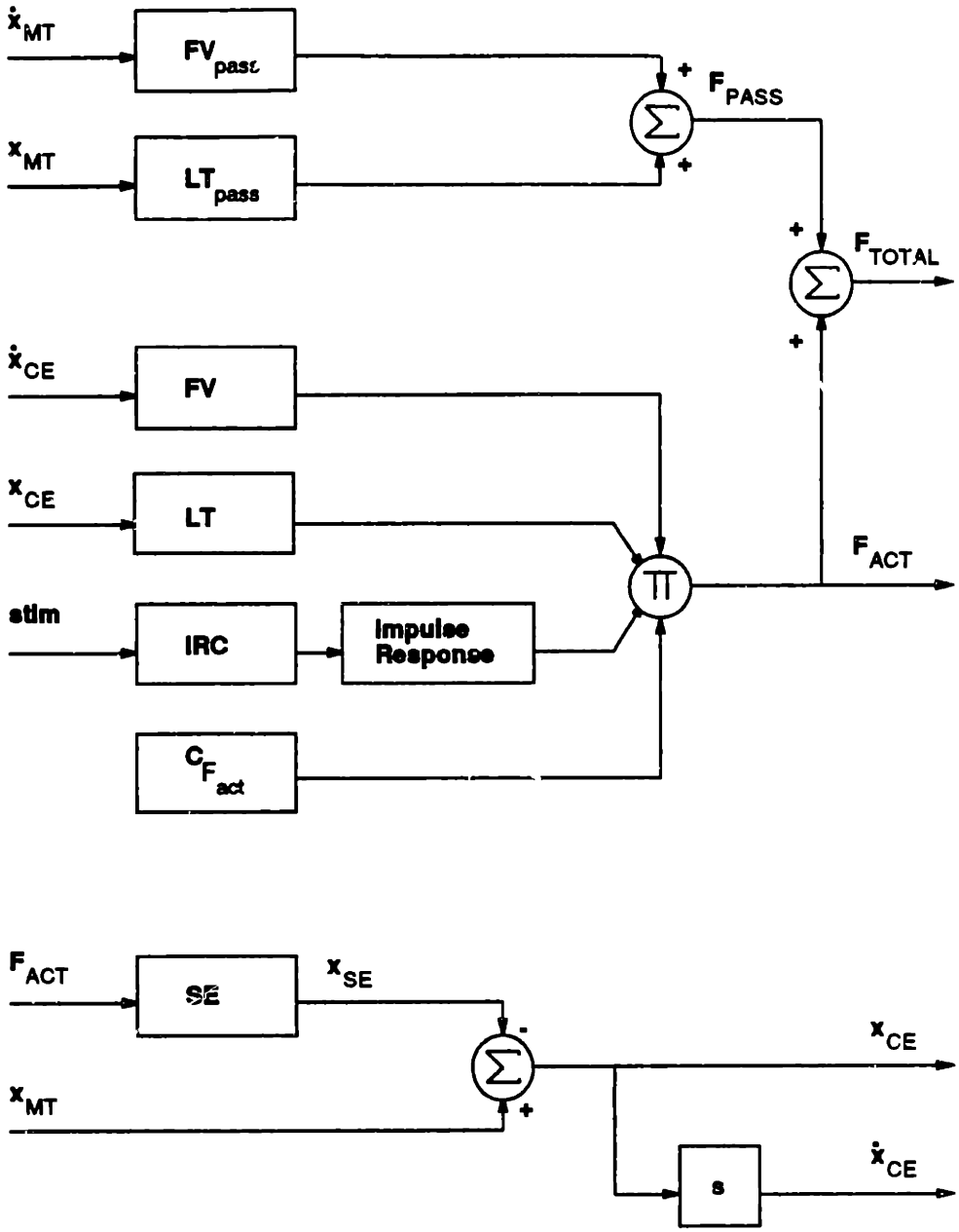

Figure 2.7: Model schematic. Inputs are the stimulation level (STIM), the musculotendon length x_{MT}, and velocity $\dot{x}_{MT}$. The relationships which must be defined are: passive force-velocity (FV_{pass}), passive length-tension (LT_{pass}), active force-velocity curve (FV), active length-tension (LT), isometric recruitment curve (IRC), impulse response (Impulse Response), active force multiplier ($c_{f_{ACT}}$), and the series elastic element (SE). The simulation calculates the active force (F_{ACT}), the contractile element length (x_{CE}), and the contractile element velocity ($\dot{x}_{SE}$) which are used as internal variables. The total force (F_{TOTAL}) is the model output.

isolated muscles which were each stimulated by a single electrode. This fundamental difference resulted in a change from joint space to muscle space.

The space of a model refers to the coordinate system used. The work described here used muscle space — the length of the muscle (in mm) and the velocity (in mm/sec). The JSMM used joint space which measured length and velocity in terms of the angle of the skeletal structure — so length was referred to as joint angle (in degrees) and velocity was measured in units of angular velocity (degrees/sec). The JSMM was intended to be applied to modeling muscle characteristics for muscles which were attached to the skeleton. With such a system, the angle of the joint and the torque about it are easy to measure. The length of the muscle is not so easy to measure *in vivo* and needs to be estimated based on length of the bones, approximate origin and insertion sites of the tendons, and the path of the tendon across the joint. Since the skeleton is not an "ideal" structure, the moment arm of the tendon is not constant with angular rotation of the joint. The conversion of torque to muscle force would need to be and measured torques produced by the muscles would need to be adjusted accordingly. Hence for intact musculo-skeletal systems, using joint space is simpler.

Chapter 3
Parameter Estimation Methods

The model described in Chapter 2 can be used to describe the contraction characteristics of any electrically stimulated (mammalian) muscle. However, the relationships between the model variables are not the same for all muscles. Factors such as muscle size, length of the tendon, and muscle fiber composition (fast versus slow fibers) influence the contraction characteristics of individual muscles. To describe the contraction of a specific muscle, the model must be "fit" to that muscle. This chapter describes the techniques used for estimating the parameters so that the model describes a specific muscle.

3.1 Parameter Description

The parameters of a model are used to define the relationships between the variables. A mathematical relationship can be described in several ways. Two convenient methods for describing SISO, static relations are: 1) a look up table and 2) coefficients of a polynomial or other continuous function. Assuming sufficient detail in the tabular method and a reasonable choice of functions for the continuous method, the two representations are equally valid. The type of description will influence the model implementation and possibly the parameter estimation technique.

For this thesis, a tabular description method was chosen. Two factors influenced this choice: uncertainty of the shape of the curves and the convenience of using the same fitting technique for (almost) all relationships. Although electrically stimulated muscle data existed to describe each relationship, the modeling assumptions led to a degree of uncertainty. For example, the active force velocity curve was known to change with stimulation level as shown in Figure 2.6. But the model assumed that the relationship was the same, independent of the stimulation level. Hence, the fitting technique was expected to produce an average of the curves shown in Figure 2.6 for different stimulation levels. Not knowing the shape of this average curve *a priori* made it difficult to determine the shape of the continuous function which would best describe it.

To describe a continuous function using a table, the values between the table entries must be defined. For this thesis, these values were defined by a linear interpolation between the points. Figure 3.1 illustrates the relationship between a table containing 11 entries to describe the force-velocity relation and the points between. Graphically, the tabulated values represent the endpoints of 10 line segments which define the continuous relationship. The continuous relationship could be made smoother by increasing the number of line segments and hence the number of table

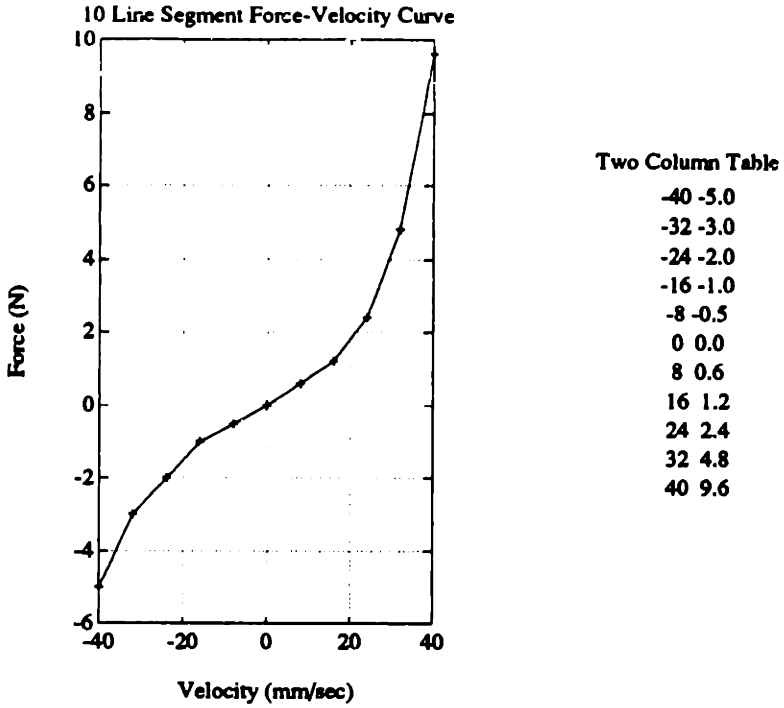

Figure 3.1: Graphical interpretation of linear interpolation between entries in a two column table.

entries.

3.2 Least Squares Fitting

The purpose of parameter estimation is to make the model describe the contraction characteristics of a specific muscle. There are theoretically an infinite number of combinations of curves which can be applied to the model to define the various relationships. The parameter estimation method must choose the best combination for the data being evaluated. This requires a criteria for determining a good fit.

The parameter estimation method known as "least squares fitting" or "chi-squared (χ^2) fitting" is described in Section 3.2.1. The criteria used to determine the best parameters is minimization of the square of the error. The method can be executed in matrix format by using singular value decomposition. Section 3.2.2 discusses the particulars of using least squares fitting with tabular parameter description.

3.2.1 General Least Squares

For general least squares fitting, consider N data points (x_i, y_i), $i = 1, ..., N$. The goal is to find a model which predicts the functional relationship between the

measured independent (x) and dependent (y) variables,

$$y^*(x) = y(x; a_1 ... a_M). \tag{3.1}$$

The least squares fit problem becomes one of minimizing over $a_1 ... a_M$:

$$\sum_{i=1}^{N} [y_i - y(x_i; a_1 ... a_M)]^2. \tag{3.2}$$

This least-squares fitting is a maximum likelihood estimation of the fitted parameters *if* the measurement errors are independent and normally distributed with constant standard deviation [18]. If each data point (x_i, y_i) has its own standard deviation σ_i, then the equation to be minimized becomes the familiar "chi-square"

$$\chi^2 \equiv \sum_{i=1}^{N} \left(\frac{y_i - y(x_i; a_1 ... a_M)}{\sigma_i} \right)^2. \tag{3.3}$$

The general *linear* least squares problem is to determine a linear combination of any specified set of M basis functions of x. For example, linear fitting of a polynomial of degree $M - 1$, would use the functions $1, x, x^2, ..., x^{M-1}$. The linear combination would then be

$$y^*(x) = a_1 + a_2 x + a_3 x^2 + ... + a_M x^{M-1} \tag{3.4}$$

The general form of this type of model is

$$y^*(x) = \sum_{j=1}^{M} a_j X_j(x) \tag{3.5}$$

where $X_1(x), \ldots, X_M(x)$ are arbitrary fixed functions of x, called the basis functions. For multivariable applications, the general equation is

$$y^*(x_1, x_2, \ldots, x_n) = \sum_{j=1}^{M_1} a_j X_j(x_1) + \sum_{j=M_1+1}^{M_1+M_2} a_j X_j(x_2) + \ldots + \sum_{j=M_1+M_2+\ldots+M_{n-1}+1}^{M_1+M_2+\ldots+M_n} a_j X_j(x_n) \tag{3.6}$$

for n dependent variables. Note that the functions $X_j(x)$ can be nonlinear. The term "linear least squares" refers to the model's linear dependence on its parameters a_j.

For linear models, the merit function to be minimized is

$$\chi^2 = \sum_{i=1}^{N} \left(\frac{y_i - \sum_{j=1}^{M} a_j X_j(x_i)}{\sigma_i} \right)^2 \tag{3.7}$$

where σ_i is the measurement error (standard deviation) of the i^{th} data point. The remainder of this discussion assumes σ_i is constant (i.e., no trend in the measurement errors). Therefore, σ_i will be dropped from the equations of the following sections.

Equation 3.7 is easily solved using matrix manipulation techniques. Let **A** be a matrix whose $N \times M$ components are constructed from the M basis functions (X_j) evaluated at the N abscissas x_i, by the formula

$$A_{ij} = X_j(x_i) \tag{3.8}$$

Let **b** define a vector of length N such that

$$b_i = y_i \tag{3.9}$$

and define **a** as the vector of M components to be fitted, $a_1, ..., a_M$. Note that in general $N \geq M$ since there must be more data points than model parameters to be solved for.

In terms of **A**, **b**, and **a**, minimization of χ^2 in (3.7) can be written as

$$\text{find } \mathbf{a} \text{ which minimizes } \chi^2 = |\mathbf{A} \cdot \mathbf{a} - \mathbf{b}|^2 \tag{3.10}$$

This equation can be solved by singular value decomposition (SVD) [18]. SVD puts the **A** matrix into the form $\mathbf{A} = \mathbf{U} \cdot \mathbf{W} \cdot \mathbf{V}^\mathbf{T}$ where **U** is an $M \times N$ column-orthogonal matrix, **W** is an $N \times N$ diagonal matrix, and **V** is an $N \times N$ orthogonal matrix. The **a** which minimizes (3.10) is the solution to $\mathbf{a} = \mathbf{V} \cdot \mathbf{W} \cdot \mathbf{U}^\mathbf{T} \cdot \mathbf{b}$.

3.2.2 Least Squares Fit Applied to Tabular Parameter Description

In fitting the data, the shape function which relates the dependent variable to the independent variable(s) is sought. This shape function could be defined as combinations of polynomials, exponentials, sine functions or linear segments, depending on the true relationship between the variables. SVD will find the best least squares fit to the basis functions as long as they are defined over the entire range of the independent variable and depend linearly upon the SVD coefficients.

The tabular parameter description defines the endpoints of piecewise continuous linear segments. Using linear segments as the basis functions has several advantages. Short linear segments can represent functions which are defined by any other mathematical function. (It is difficult to model a parabola by adding sine waves.) The error between the true shape and the linear function will be small when many short linear segments are used. Linear segments are not subject to "ripple effects" such as when a shape with a flat section is fitted using polynomials. By using linear segments, a wide variety of true shapes can be fitted without changing the definition of the basis functions. (This was referred to as "self modeling" by Lawton, et. al. [11].)

To understand how the linear segments are implemented mathematically, consider the full range of the independent variable (x) divided into $M-1$ smaller ranges where $x_j^*, j = 1, ..., M$ define the end points of the smaller ranges. For each of the $M-1$ ranges, a linear segment is defined which is the best fit of the values of $y_i(x_i)$ for all

x_i in the range of $(x_j^*, x_{j+1}^*]$. Stating this as an equation,

$$y_i^*(x_i) = \sum_{j=1}^{M-1} \left(\frac{a_{j+1} - a_j}{x_{j+1}^* - x_j^*} \left[x_i - x_j^* \right] + a_j \right) \Delta_j(x_i), \text{ for } x_1^* < x_i \leq x_M^* \tag{3.11}$$

where:

$$\Delta_j(x) = \begin{cases} 1 & \text{for } x_j^* < x \leq x_{j+1}^* \\ 0 & \text{otherwise} \end{cases} \tag{3.12}$$

Separating Equation 3.11 into the coefficients of the a_j's, we get:

$$y_i^*(x_i) = \sum_{j=1}^{M-1} a_{j+1} \frac{x_i - x_j^*}{x_{j+1}^* - x_j^*} \Delta_j(x_i) + \sum_{j=1}^{M-1} a_j \left(1 - \frac{x_i - x_j^*}{x_{j+1}^* - x_j^*} \right) \Delta_j(x_i). \tag{3.13}$$

This is in the form of Equation 3.5, the general form of the least squares problem, with the basis functions (X_j) defined as:

$$X_j(x_i) = \begin{cases} 1 - \frac{x_i - x_j^*}{x_{j+1}^* - x_j^*} & x_j^* < x_i \leq x_{j+1}^* \\ \frac{x_i - x_{j-1}^*}{x_j^* - x_{j-1}^*} & x_{j-1}^* < x_i \leq x_j^* \\ 0 & \text{else} \end{cases} \tag{3.14}$$

With the basis functions defined as in 3.14 the **A** matrix can be constructed as in equation 3.8 and the least squares fit solved for by SVD.

3.3 Relating Fit to Model

To this point, this chapter has discussed parameter fitting of models in general. This section will relate the fitting method to the muscle model described in Chapter 2.

The parameters which must be identified describe the curves relating:

- Passive force to musculo-tendon length, $f_1(x)$
- Passive force to musculo-tendon velocity, $f_2(\dot{x})$
- Active force to stimulation, $f_3(\text{stim})$
- Active force to contractile element length, $f_4(x_{\text{CE}})$
- Active force to contractile element velocity, $f_5(\dot{x}_{\text{CE}})$
- Active force to musculo-tendon length and contractile element length, $f_6(x, x_{\text{CE}})$

The parameters were identified in the order in which they are listed above. The passive curves were calculated before the active since $f_{\text{TOTAL}} = f_{\text{PASS}}$ when the muscle is not stimulated. The shape of the isometric recruitment curve (IRC) which relates force to stimulation level was calculated by the ramp deconvolution method described in Section 3.4. The passive parameters and the IRC were used as pre-determined inputs when the active parameters were fit.

3.3.1 Passive Muscle Dynamics

The passive muscle dynamics are of the form:

$$f_{\text{PASS}}(x, \dot{x}) = f_1(x) + f_2(\dot{x}) \tag{3.15}$$

where f_1 represents the passive spring and f_2 is the passive dashpot. To identify the relationship between passive force and length and velocity, muscle data which measured force at N combinations of length and velocity was used.

For the passive dynamics, let M_1 and M_2 be the number of points in the tabular representation of the passive length-tension and force-velocity curves respectively. There were then $M_1 - 1$ and $M_2 - 1$ equal length linear segments in the passive spring and passive dashpot curves, respectively. The **A** matrix which was used for SVD was $N \times (M_1 + M_2)$. The general linear least squares equation (3.5) became:

$$f_{PASS}(x, \dot{x}) = \sum_{j=1}^{M_1} a_j X_{1j}(x) + \sum_{j=M_1+1}^{M_1+M_2} a_j X_{2j}(\dot{x}) \tag{3.16}$$

with X_{1j} and X_{2j} defined as in (3.14) with $\dot{x}_j^*$ replacing x_j^* and $\dot{x}_i$ replacing x_i for X_{2j}. Solving this gave the relative weights of the M_1 a_j's in the passive length-tension curve and the M_2 a_j's in the force-velocity curve. These values were adjusted (by adding a constant to the a_j's associated with the L-T curve and subtracting the same constant from the F-V points) so that the force at zero velocity was zero.

3.3.2 Active Muscle Dynamics

When the muscle is stimulated,

$$f_{\text{TOTAL}} = f_{\text{PASS}} + f_{\text{ACT}} \tag{3.17}$$

The active muscle dynamics were modeled as:

$$f_{\text{ACT}}(\text{STIM}, x, \dot{x}) = f_3^*(\text{STIM}) \times f_4(x_{\text{CE}}) \times f_5(\dot{x_{\text{CE}}}) \tag{3.18}$$

where f_3^* represents the stimulation passed through the isometric recruitment curve and convolved with the impulse response, f_4 is the length-tension relationship, and f_5 is the force-velocity curve.

The shape of the isometric recruitment curve and the impulse response time constant were identified using the deconvolved ramp method of IRC identification developed by MacLean. This method is described in Section 3.4.

The least squares fitting algorithm is well suited to model structures in which the relationships are added together. The active dynamics were to be multiplied, so the logarithm was used. (Recall that $a \times b = \log(a) + \log(b)$.) Since the shape of the

IRC was defined using the ramp deconvolution technique, the unknowns of the active force model reduced to:

$$\log\left(\frac{f_{\text{TOTAL}} - f_{\text{PASS}}(x,\dot{x})}{f_3^*(\text{STIM})}\right) = \log\left(f_4(x)\right) + \log\left(f_5(\dot{x})\right) \tag{3.19}$$

The processing of this fitting routine was similar to the passive fit, after the pre-processing required to calculate the left side of (3.19).

The solution gave the relative weights of the entries for the active length-tension and force-velocity curves. The a_j's were adjusted so that the force at $l = 10$ on the length-tension curve was 1.0 and the force at $v = 0$ on the force-velocity curve was 1.0. The active force multiplier, $c_{f_{\text{ACT}}}$, was calculated as the inverse of the logarithm of the sum of the constants which were added to the length-tension and force-velocity curves to normalize them. The active force multiplier was used in the calculation of the active force, so that Equation 3.18 became:

$$f_{\text{ACT}}(\text{STIM},x,\dot{x}) = f_3^*(\text{STIM}) \times f_4(x_{\text{CE}}) \times f_5(\dot{x_{\text{CE}}}) \times c_{f_{\text{ACT}}}. \tag{3.20}$$

3.4 Ramp Deconvolution

The isometric recruitment curve (IRC) which relates force to stimulation level, was determined by the ramp deconvolution method developed by MacLean [6, 13]. The method is based on the Hammerstein model for activation (shown in Figure 2.3) which assumes the IRC is the static non-linearity and the twitch response is the dynamic linearity. In the model, the stimulation level is passed through the IRC and convolved with the impulse response, as explained in Section 2.3.2.

The deconvolved ramp method inverts the model to find the IRC from impulse and ramped stimulation force measurements. The *rstmclen* and *fastramp* protocols described in Section 4.2.4 were used to generate the required impulse and ramp stimulation data. These protocols stimulated the muscle with four impulses followed by a double ramp of the stimulation level.

Figure 3.2 illustrates the ramp deconvolution process. The four impulses were averaged, normalized and fitted to

$$t\exp(-\lambda t)$$

which is the equation of a second order critically damped impulse response (an assumption of the model). A typical force response from a ramp stimulation is shown in (ii) of Figure 3.2. Note that the time delay between stimulation and force development is also seen in the impulse response. When the force which was generated during the ramp stimulation is deconvolved through the impulse response, the force and the ramp stimulation become aligned in the time domain. The force developed during increasing stimulation is generally lower than the force when the stimulation

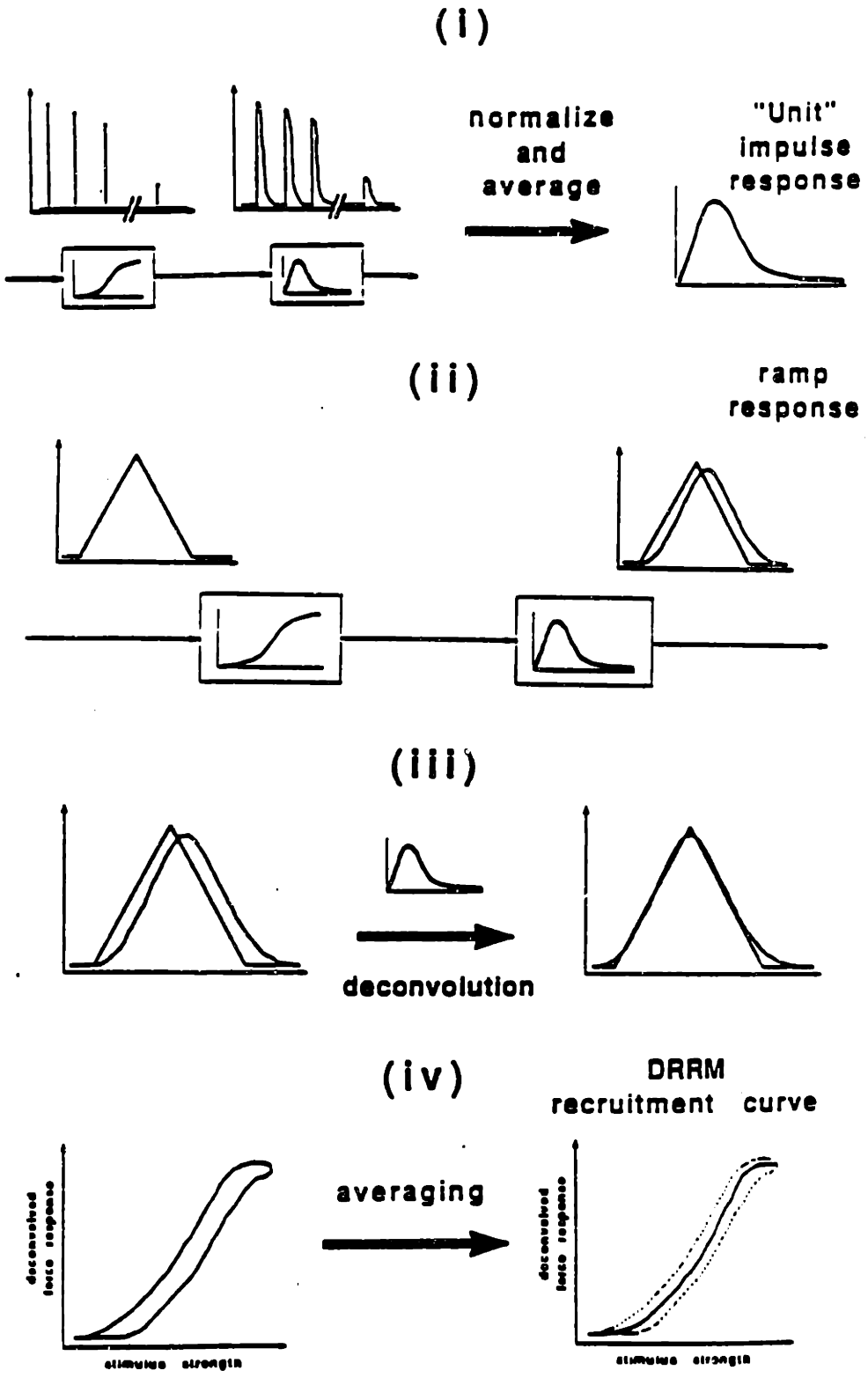

Figure 3.2: Ramp deconvolution process [13].

level is decreasing. The two forces are averaged to produce the isometric recruitment curve as shown in (iv) of Figure 3.2.

The actual deconvolution is performed in the frequency domain. The fast Fourier transform (FFT) of the force from the ramp stimulation is computed. The FFT is low pass filtered to remove artifacts of the stimulation frequency. It is then divided by the Laplace transform of the impulse response

$$H(s) = \frac{1}{(s+\lambda)^2}.$$

(Recall that multiplication in the frequency domain is equivalent to convolution in the time domain.) The inverse FFT is taken of the result to return it to the time domain.

Chapter 4
Methods

Development and validation of the identification techniques described in Chapter 3 required both simulated and experimental data. Noiseless simulated data was used to determine the viability of various fitting techniques. Adding noise to the simulations gave an indication of the robustness and sensitivities of the parameter estimation techniques. Experimental data was obtained from *in vivo* preparations of cat tibialis anterior (TA) and medial gastrocnemius (MG) muscles.

4.1 Simulation

Simulated data was produced using the JSMM Numerical Simulation Method developed by A. H. Robbins [20], with some modifications. This method was derived from the muscle model which was described in Chapter 2. The schematic diagram for the simulation is shown in Figure 4.1 which should be compared to Figure 2.7.

The simulation method, like Robbins' muscle model, defined muscle lengths and velocities as angles and angular velocities. It also lumped together the passive characteristics of all of the muscles attached to a joint. Since the experimental animal model (described in Section 4.2) used only single muscle preparations, the "joint" parameters were changed to single muscle parameters, and lengths and velocities were measured linearly.

4.1.1 Inputs

The inputs to the simulation may be divided into the active and passive muscle parameters. Typical inputs are shown graphically in Figure 4.2. The active muscle parameters which must be defined are: a) the isometric recruitment curve to relate stimulation level to activation, b) the impulse response to define activation as a function of time, c) the force-velocity curve to relate force output to contractile element velocity, d) the length tension curve to define force output as a function of contractile element length, and e) the series elastic element to relate force to the difference between the musculo-tendon length and the contractile element length. The passive muscle parameters include: 1) the length-tension curve to account for the springiness of the passive muscle, and 2) the force-velocity curve to represent the damping effects seen in a passive muscle.

The simulation was designed to allow the user to select any combination of stimulation pattern and length trajectory. The timing of the length and stimulation were user determined. Choices for the stimulation pattern include: fixed stimulation level,

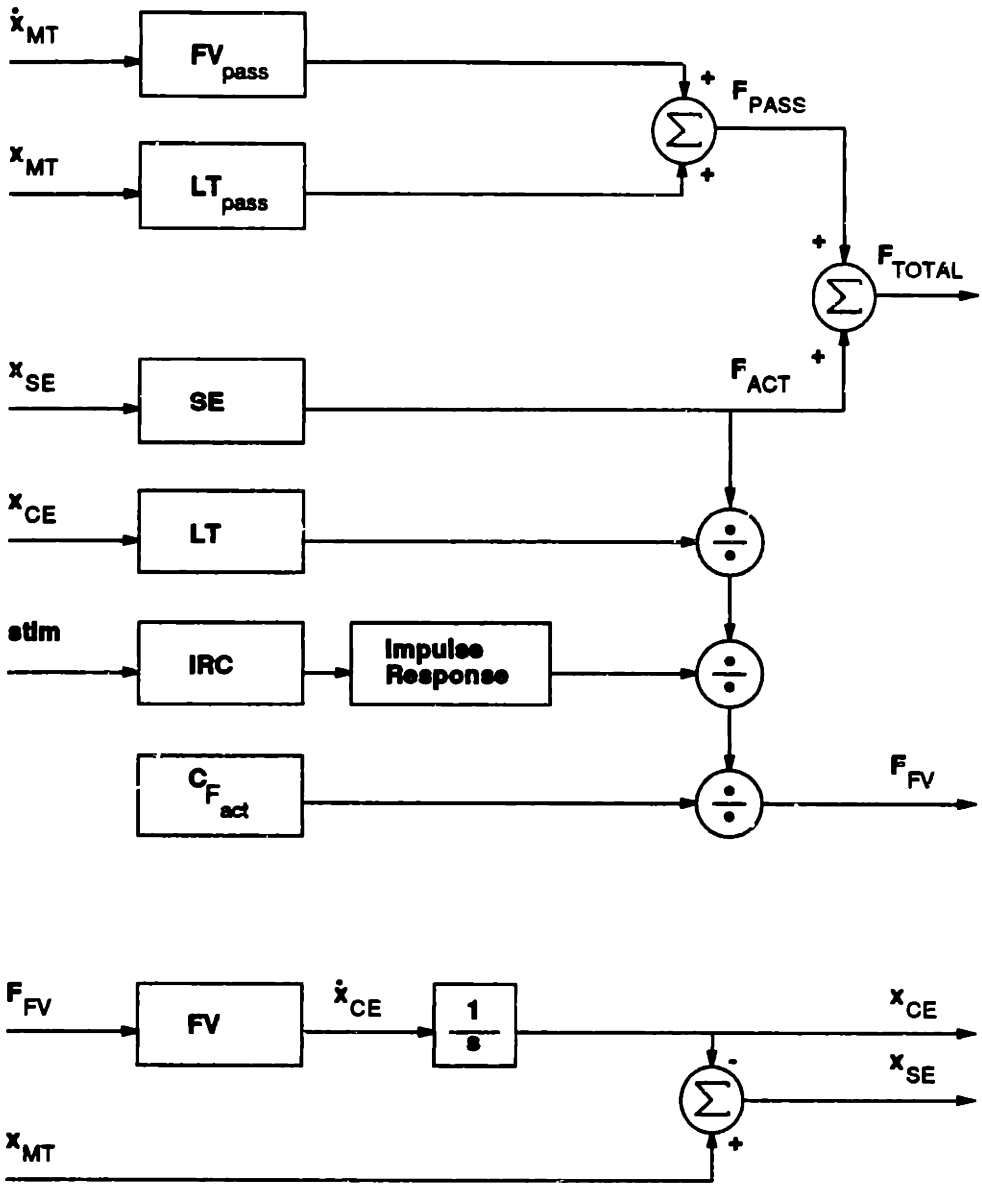

Figure 4.1: Simulation schematic. Inputs are the stimulation level (STIM), the musculo-tendon length x_{MT}, and velocity $\dot{x}_{MT}$. The relationships which must be defined are: passive force-velocity (FV_{pass}), passive length-tension (LT_{pass}), series elastic element (SE), active length-tension (LT), isometric recruitment curve (IRC), impulse response (Impulse Response), active force multiplier ($c_{f_{ACT}}$), and active force-velocity curve (FV). The simulation calculates the active force due to the force-velocity relationship (F_{FV}), the contractile element length (x_{CE}), and the series element length (x_{SE}) which are used internally in the simulation. The total force (F_{TOTAL}) is the simulation output.

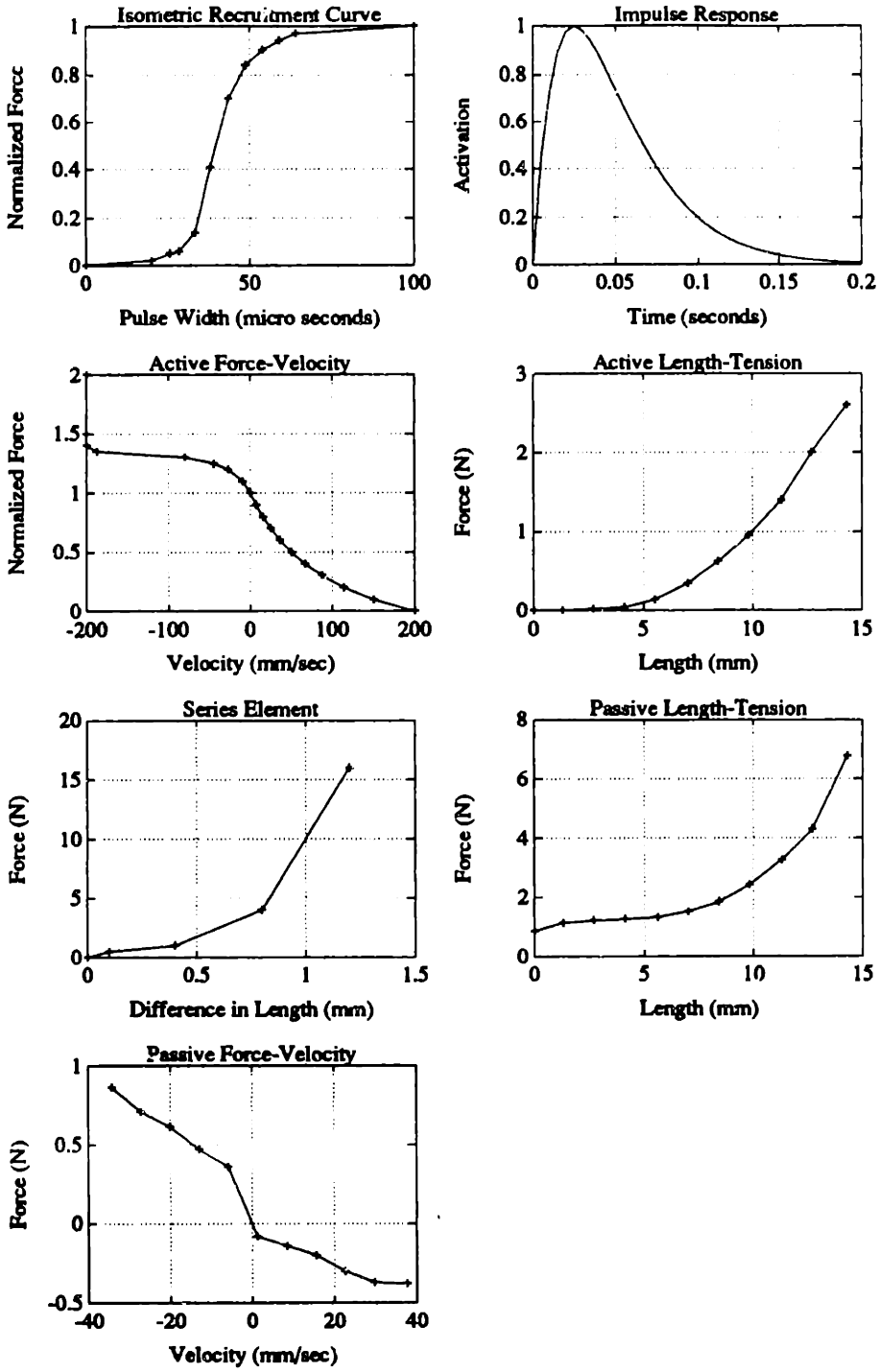

Figure 4.2: Simulation inputs: isometric recruitment curve, impulse response, active force-velocity curve, active length-tension curve, series elastic element, passive length-tension curve, passive force-velocity curve.

step stimulation level, ramp stimulation, double ramp stimulation, impulse stimulation, and passive (no) stimulation. These are shown schematically in Figure 4.3. The defined length trajectories are shown in Figure 4.4. They include: fixed muscle length, step length, ramp length at constant velocity, double ramp length at constant velocity, and random trajectory.

4.1.2 Calculations

The simulation used a set of coupled first order differential equations to calculate the musculo-tendon force. The equations used the following variables to calculate the output force F_{OUT}:

- Activation level, a
- Stimulation level, $u(t)$
- Musculo-tendon velocity, $\dot{x}_{\text{MT}}$
- Musculo-tendon length, x_{MT}
- Contractile element velocity, $\dot{x}_{\text{CE}}$
- Contractile element length, x_{CE}
- Force due to activation, F_{ACT}
- Force due to passive elements, F_{PASS}

The following equations describe the full muscle model simulation:

$$\frac{da}{dt} = \dot{a} \tag{4.1}$$

$$\frac{d\dot{a}}{dt} = -(\alpha + \beta)\dot{a} - \alpha * \beta * a + \text{IRC}(u) \tag{4.2}$$

$$F_{\text{ACT}} = \text{SE}(x_{\text{CE}} - x_{\text{MT}}) \tag{4.3}$$

$$\frac{dx_{\text{CE}}}{dt} = \dot{x}_{\text{CE}} = \text{FV}^{-1}\left(\frac{F_{\text{ACT}}}{a * \text{LT}(x_{\text{CE}})}\right) \tag{4.4}$$

$$F_{\text{PASS}} = \text{LT}_{\text{PASS}}(x_{\text{MT}}) + \text{FV}_{\text{PASS}}(\dot{x}_{\text{MT}}) \tag{4.5}$$

$$F_{\text{OUT}} = F_{\text{PASS}} + F_{\text{ACT}} \tag{4.6}$$

where :

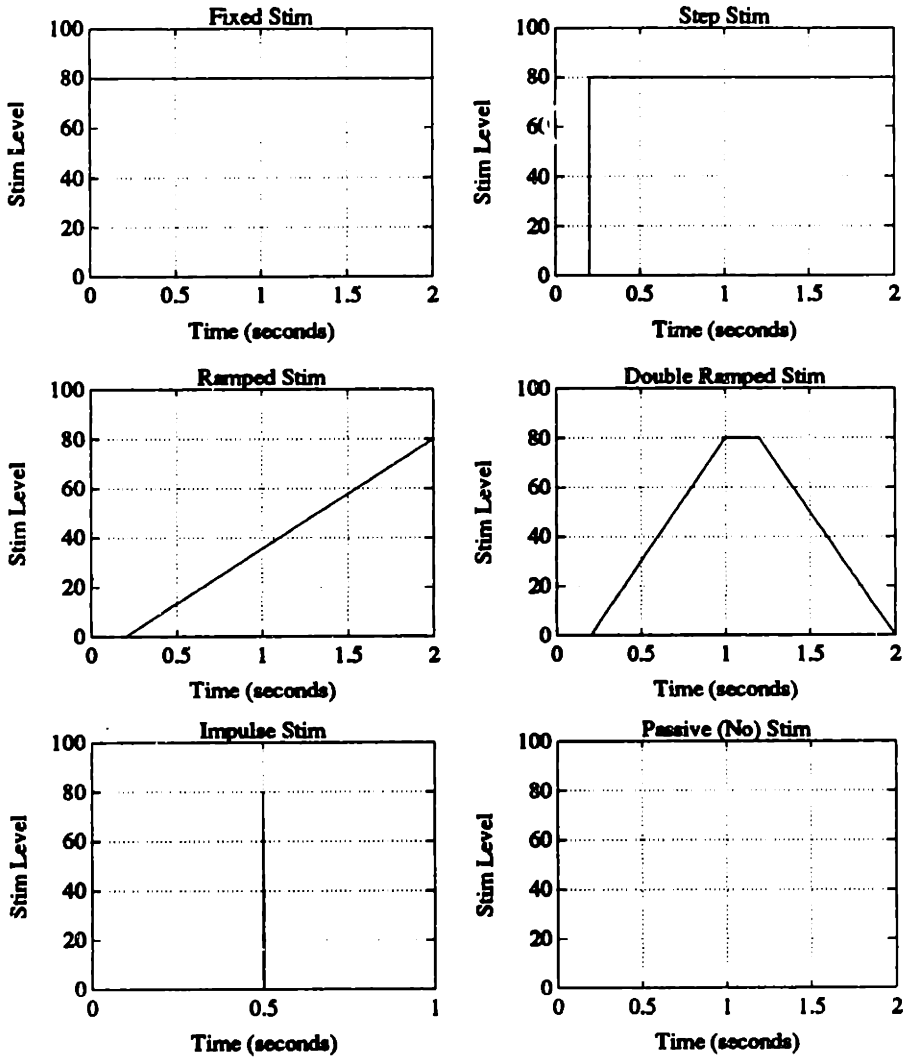

Figure 4.3: Stimulation patterns for simulation: fixed level, step level, ramp, double ramp, impulse, and passive (no) stimulation.

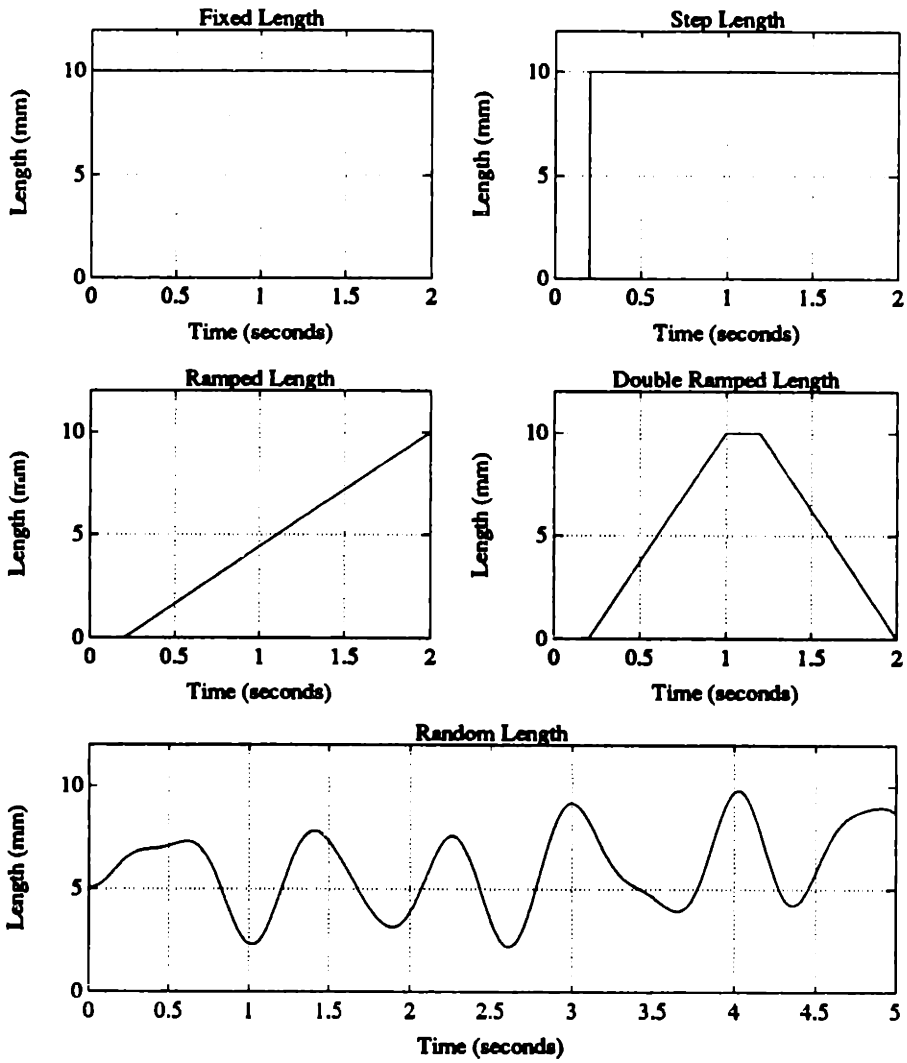

Figure 4.4: Length trajectories for simulation: fixed, step, ramp, double ramp, and random length..

IRC	=	isometric recruitment curve
α, β	=	impulse response time constants
SE	=	series elastic element
FV^{-1}	=	inverse of active force-velocity curve
LT	=	active length-tension curve
LT_{PASS}	=	passive length-tension curve
FV_{PASS}	=	passive force-velocity curve

The selected stimulation pattern $u(t)$ and the impulse response time constants, α and β, determined the activation level by passing the stimulation level through the recruitment curve block and convolving it with the impulse response. (Equations 4.1 and 4.2.) This model used pulse width modulation (PWM) with a basic frequency of 40 Hz. The stimulation was a series of delta functions spaced at 25 ms intervals with width corresponding to the stimulation level. Convolving the delta function with the impulse response led to a continuous activation pattern.

The user selected length trajectory defined the length and velocity of the total musculo-tendon unit (MTU). This length and velocity were used to determine the force due to the passive characteristics of the muscle (Equation 4.5).

The length of the contractile element x_{CE} was shorter than the length of the musculo-tendon unit x_{MT} when the muscle was stimulated. The extra length of the MTU was due to stretching of the series elastic element. The difference in lengths between the total musculo-tendon unit and the contractile element determined the active force F_{ACT} via the series elastic length-tension relationship (Equation 4.3).

Based on the model of Figure 2.7, the active force F_{ACT} is the product of the activation level, a, the force due to the active length-tension relationship, and the force from the active force velocity curve. Using this relationship, the force due to the F-V curve was calculated as in Equation 4.4. The contractile element velocity was solved for by putting this force into the inverse of the active force-velocity relationship (Equation 4.4). The contractile element length was calculated by integrating the contractile element velocity.

Finally, the force output of the musculo tendon unit was calculated as the sum of the active and passive forces (Equation 4.6).

4.1.3 Outputs

Sample outputs of an impulse response at constant length and constant stimulation with ramped length are shown in Figures 4.5 and 4.6.

Two methods were used to create noisy simulated data. The first method was to round off some of the intermediate calculations in the simulation, thereby adding quantization noise. The second method was to add "white noise" generated by the Matlab routine *random()* [16] to the output force. Both methods achieved the goal of generating data which did not exactly fit the model to be parameterized. The

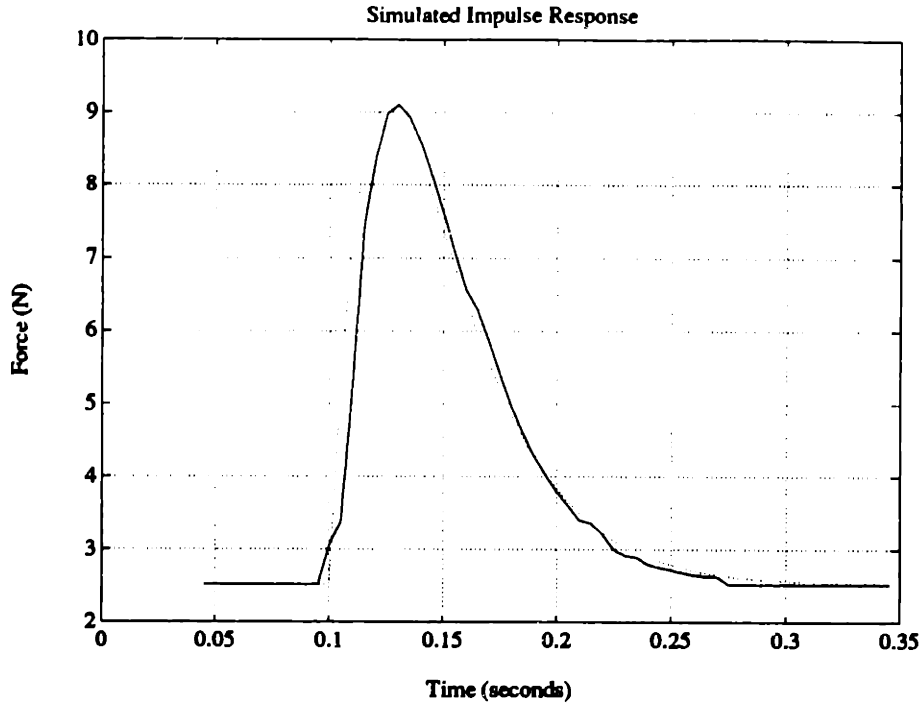

Figure 4.5: Simulated impulse response at constant length. Dotted line is second order critically damped impulse.

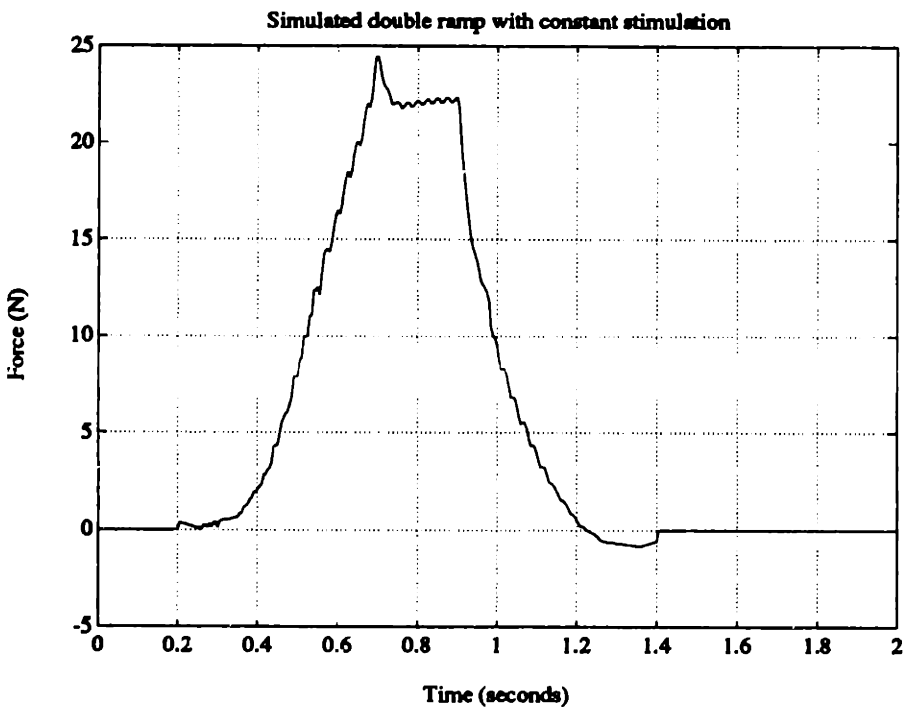

Figure 4.6: Simulated constant stimulation with ramped length.

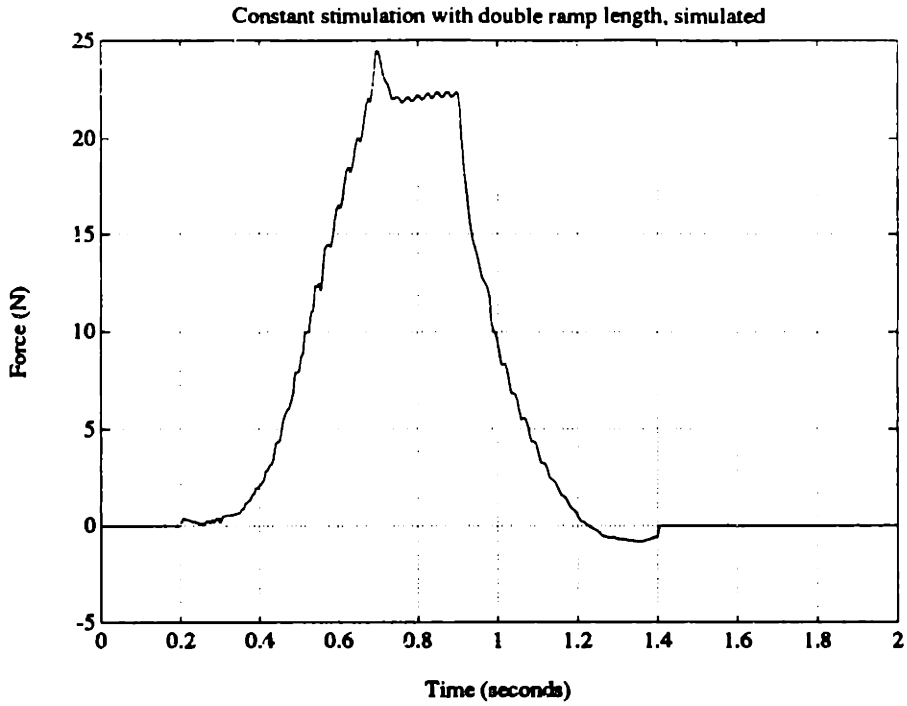

Figure 4.7: Simulated noisy data using white noise.

constant stimulation with ramped length example of Figure 4.6 is shown with added white noise in Figure 4.7.

4.1.4 Modifications to JSMM Simulation

Robbins' JSMM simulation method was used with the following modifications:

1. The program, which was originally written in C, was converted to Matlab [16] macro routines for better graphics portability.
2. The Runga-Kutta numerical integration routine was implemented using *ode45()*, a Matlab function.
3. Joint angle and angular velocity were replaced by muscle length and velocity measurements.
4. Passive joint characteristics were replaced by passive single muscle characteristics.

4.2 Experimental

Wherever possible, simulated data was used for developing the identification techniques. However, if FES is to evolve from an idea to an aid for humans, the muscle

identification techniques must be applied in physiological situations. Several issues dictated the use of the animal model described in this section.

An *in vivo* preparation was required. Since the neuromuscular system is not completely known, no mathematical model, no matter how detailed, will be complete. The simulations described in the preceding section are expected to be inaccurate as a result of the simplifying assumptions Robbins made in the development of his model (see Chapter 2). Thus, simulated data was incomplete and the need for real mammalian muscles in physiological conditions (i.e., in a living animal) was established to validate the parameter identification techniques.

Accurate measurement of force and control of muscle length was required. Since external force measurement and limb position control were considered inadequate, an invasive procedure in an acute animal preparation was dictated.

The animal model used in generating the experimental data was similar to that designed by Durfee and used by MacLean [5, 6, 13]. The experimental apparatus had three basic parts which will be described in detail: the subject animal, the hardware, and the software.

4.2.1 Animal Model

Cats were chosen for the experiments because they are the smallest available animal with muscle size, geometry and fiber composition similar to humans. Rats were considered, but deemed too small to effectively immobilize the skeleton, the muscles were not strong enough, and the nerves were relatively inaccessible. A rabbit's hind limbs were too powerful for the available torque motor to restrain.

The system designed by Durfee allows for length control, electrical stimulation and force monitoring of two antagonist hind limb ankle dorsi- and plantar-flexor muscles. The dorsi-flexor tibialis anterior (TA) and plantar-flexor medial gastrocnemius (MG) were used. (Durfee and MacLean used the same two muscles.) The TA and MG both contain a mixture of fast and slow muscle fibers [2, 4, 14] and have similar dynamic properties, although the MG is capable of generating larger peak forces.

A total of four acute animal experiments were conducted. A surgical plane of anesthesia was maintained throughout the preparatory procedures and the muscle stimulation experiments.

Muscle Isolation and Restraint

Figure 4.8 shows the position of the anesthetized cat on the experiment table. Clamps were used to anchor the animal at the hip, knee and ankle. The clamps also acted to stabilize the superficial tissue around the joints by piercing the tissue with points in the clamping surface. After amputating the foot, the distal tendons of the TA and MG were attached to lightweight airplane cable. The TA tendon was crimped in one side of a 10-12 gauge uninsulated butt splice connector. The cable was crimped to the other side. The insertion of the MG tendon on the calcaneus was left intact.

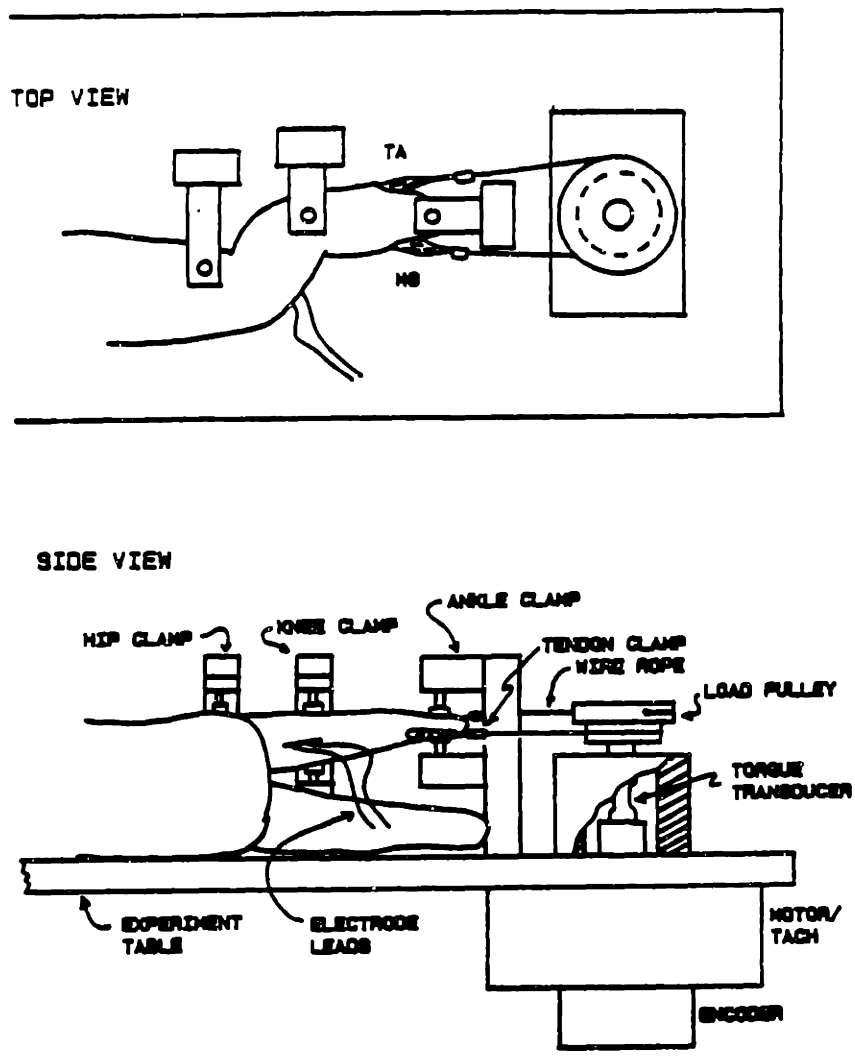

Figure 4.8: Cat restraint configuration [5].

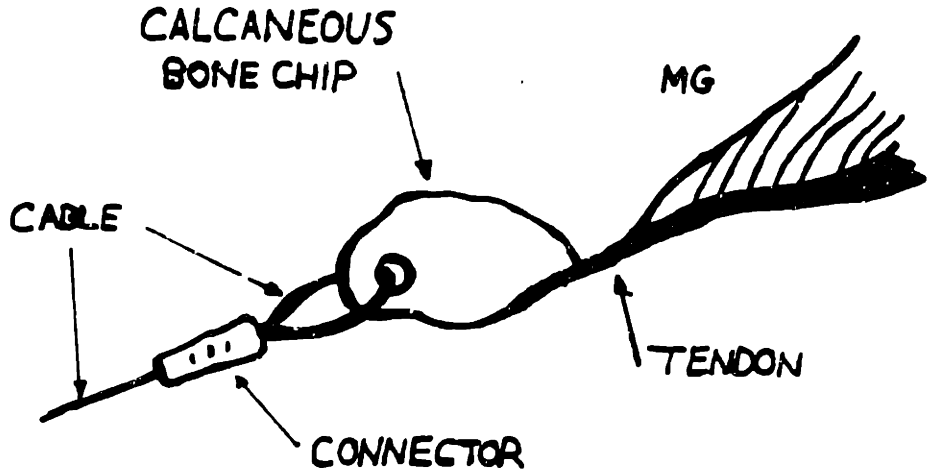

Figure 4.9: MG cable attachment [13].

A hole was drilled in the calcaneus through which airplane cable was threaded and crimped as shown in Figure 4.9.

The two cables were wrapped around a pulley which was coupled through an in-line torque transducer to the shaft of a DC torque motor. The pulley was oriented horizontally to eliminate the effects of gravity. The pulley was used as a pseudo-joint instead of the cat's own ankle for the following reasons: 1) The pulley had a constant moment arm. The moment arm of the muscles across the ankle changed with joint angle, making the geometry non-linear. 2) The pulley had a fixed center of rotation. The complexities of the ankle joint result in a moving center of rotation. 3) The muscles could be surgically isolated. Amputating the foot ensured that other muscles and connective tissue did not influence the measurements on the selected muscles.

The stepped pulley had two rings. The smaller one of diameter 28.4 mm was used for the MG, while the 35.0 mm ring was used for the TA. The unequal moment arms approximated the physiological moment arms found in the ankle and helped to equalize the strength of the two muscles. The tendon cables were attached so that contraction of the TA turned the load shaft clockwise.

Electrodes and Implantation

The two muscles were stimulated via bipolar nerve cuff electrodes, as shown in Figure 4.10. The electrodes were constructed of silastic tubing of external diameter 5 mm for the tibial nerve and 3 mm for the peroneal nerve. The wire leads were seven

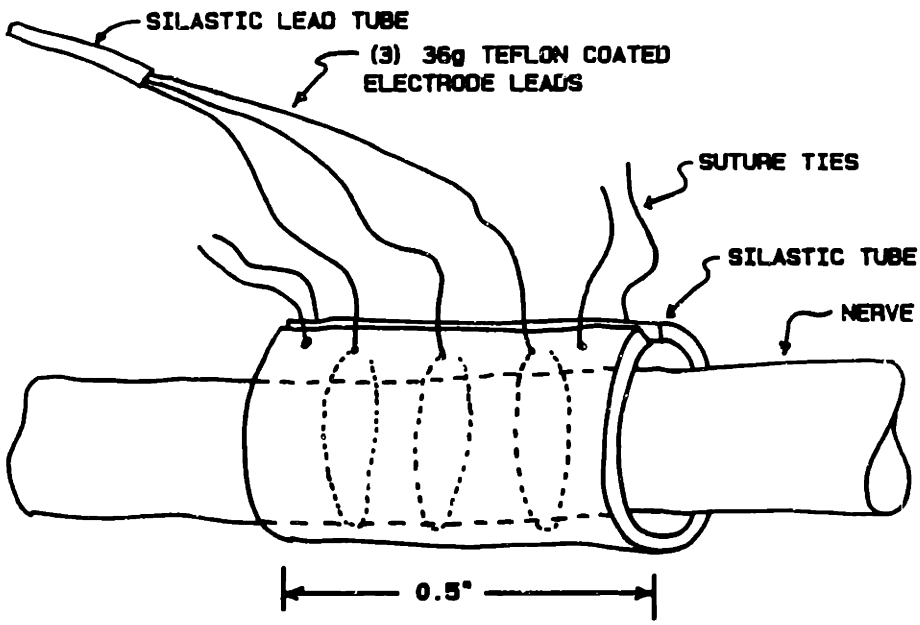

Figure 4.10: Cuff electrode [5].

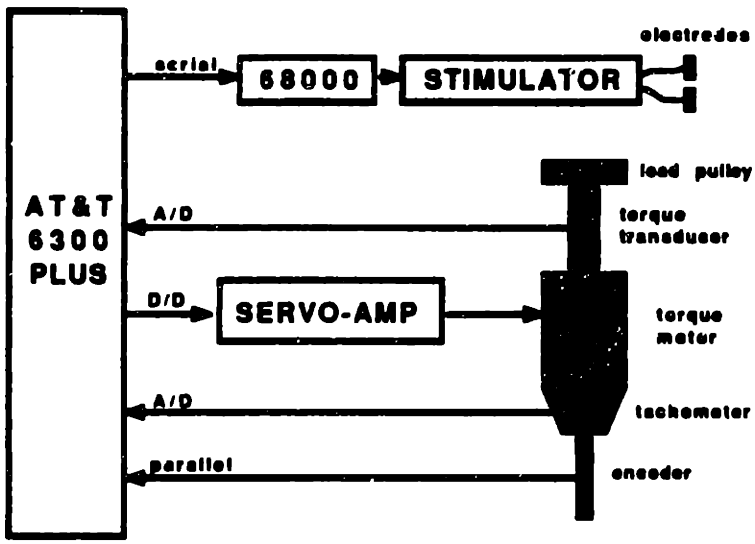

Figure 4.11: Hardware schematic [13].

stranded 36 gauge stainless steel with teflon insulation. The leads were stripped at the contact points and fastened to the silastic tubing with silicon cement.

The electrodes were implanted by wrapping them around the tibial nerve (enervating the MG) and the peroneal nerve (for the TA) and suturing them in place. The tibial trunk of the sciatic nerve was severed proximally from the implanted electrodes to block the transmission of neural signals from the central nervous system to the muscles of the hind limb.

4.2.2 Hardware

The layout of the major hardware components is shown schematically in Figure 4.11. The hardware consists of a personal computer used to control the experiments, the nerve stimulator, the torque motor, and various sensors for control feedback and measurement.

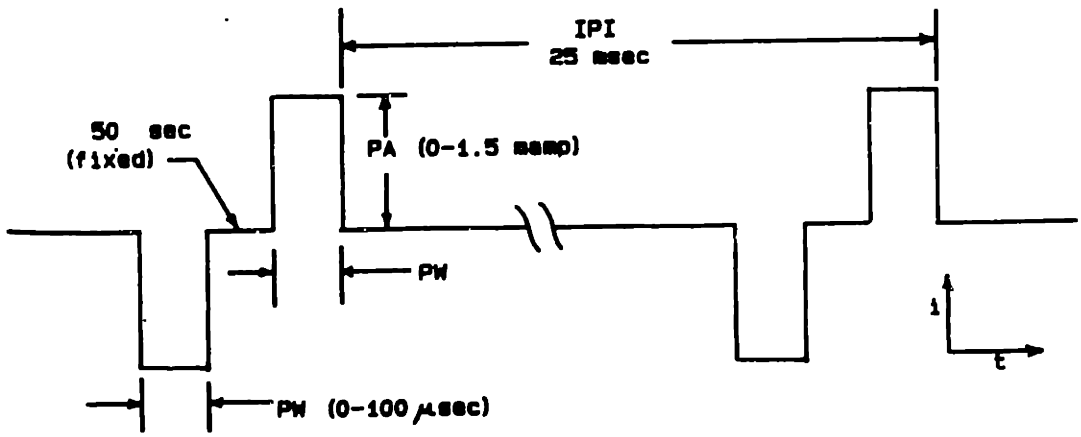

Figure 4.12: Stimulus current waveform [5].

PC Controller

The host CPU was an AT&T 6300 Plus personal computer (an 80286 microprocessor based IBM PC/AT clone), running MS-DOS version 3.1. The unit had 1.2 Mb RAM, an 80287 math coprocessor, and a 40 Mb Seagate hard disk drive with a Western Digital controller. System I/O was handled by a Metrabyte P1012 24-bit parallel digital I/O interface, an Analog Devices RTI-815-A 16-channel A/D and 2-channel digital interface, and an Arnet COMH 100 4-port RS-232 serial interface.

Nerve Stimulator

Electrical stimulation sequences were delivered to the muscles through a two-channel nerve stimulator unit designed and built by Durfee [5]. The stimulator was controlled by a satellite single board microcomputer based on the Motorola 68000 microprocessor. The stimulator was connected to the AT&T 6300 Plus over a 38.4 k baud RS-232 serial line.

The stimulator produced charge-balanced, biphasic square current pulses with 50 μs spacing between pulse phases (Figure 4.12). This waveform was chosen to minimize damage to the nerve tissue [1]. The stimulator provided a continuous range of pulse amplitude (PA) from 0 to 1.5 milliamps. The PA was manually adjusted to approximately 1 milliamp during the muscle calibration procedure. The PA was chosen to minimize the slope of the isometric recruitment curve in order to give the widest possible range of useful pulse width modulation (PWM). The pulse width ranged from 0 to 100.0 μs in steps of 100 ns. The pulse width delivered to the muscle was controlled by the PC and changed for the various experimental protocols as

described in Section 4.2.4. The inter-pulse-interval (IPI) could be adjusted between 0 and 13 seconds in steps of 0.2 milliseconds. For these experiments, IPI was held constant at 25 milliseconds (40 Hz), the shortest interval producing an acceptably tetanized muscle contraction while avoiding rapid fatigue.

The satellite processor computed stimulus PW commands every 5 milliseconds and sent them to two sets of digital and analog circuitry every 25 milliseconds to be converted into the stimulus waveform shown in Figure 4.12.

Torque Motor

A DC torque motor and matching servo amplifier (PMI Motors, Model JR16M-4CH) were coupled directly to the torque load shaft that restrained the muscle tendons. The input to the servo amplifier was connected to a PC analog output port. The voltage level on this port was controlled by the PID algorithm described in Section 4.2.3. Using this control scheme, arbitrary lengths, velocities and torques could be imposed on the torque shaft and the muscles connected to it. The torque motor had a continuous torque rating of 500 oz-in and a peak torque rating of5000 oz-in.

Feedback Channels

The torque motor described above contained an integral tachometer for measuring velocity and an incremental optical encoder for measuring position. Electronic circuits conditioned these signals for computer input [5].

Muscle force was measured by a single in-line torque transducer, based on a full bridge, strain-gauge instrumented aluminum tube, and mounted on the torque load shaft. The sensitivity of the transducer at the strain-gauges was 30.6 micro-strain/lb-in.

Since the difference in force generated by the two muscles was large, (ratios as great as 10/1 have been observed), a dual operational amplifier circuit was used to amplify the single strain-gauge output. The gains for each muscle were independently adjusted with dial potentiometers in order to monitor the torques over the PC's entire A/D input range. The amplified torques were sent to the PC over separate A/D channels and were sampled at 200 Hz to avoid aliasing of the 40 Hz stimulation frequency.

4.2.3 Software

The software used to control the hardware and execute the experimental protocols has evolved to a level of automated testing. Low-level hardware interface routines, written in assembly language by Durfee and MacLean, were implemented in Version 4.0 Microsoft Macro Assembler for speed. Intermediate and high-level routines which execute the tasks required for automated data collection and hardware control were implemented in Version 5.0 Microsoft C.

The animal experiments used various combinations of muscle stimulation patterns and length trajectories as described in Section 4.2.4. Each combination of stimulation and length pattern required a separate program written in C to set up the desired pulse width and position arrays, store the data in files, and provide graphical output of the forces developed.

Control and Data Collection Subroutine

A single subroutine was used to calculate and send the servo commands, send pulse width commands to the stimulator, and measure the state of the muscle. This subroutine contained a 200 Hz loop for the servo calculations and muscle state measurements. The pulse width command was updated at a rate of 40 Hz. The inputs to this subroutine were arrays for the desired position and the desired pulse width. The routine returned the actual position, the tachometer value, and the digitized force measurement.

A proportional-integral-derivative (PID) algorithm was used to calculate the required servo command to maintain the desired position trajectory. The basic equation for the PID controller was:

$$C = K_P \times e + K_I \times \sum e + K_D \times \dot{e} \tag{4.7}$$

where

$$\begin{aligned} C &\Rightarrow \text{motor command} \\ e &\Rightarrow \text{error = desired position} - \text{actual position} \\ \textstyle\sum e &\Rightarrow \text{sum of previous errors} \\ \dot{e} &\Rightarrow \text{velocity} \\ K_P, K_I, K_D &\Rightarrow \text{control constants} \end{aligned}$$

When the desired position remained constant, as for isometric muscle contractions, electrical noise on the tachometer signal adversely affected the servo performance. With the output shaft mechanically locked, tachometer noise was measured. The noise was fed back to the motor since the equation for calculating the servo command used the (noisy) tachometer reading. Hence the servo position oscillated. This problem was alleviated by using an estimated velocity when the tach signal was less than *MAXTACH*. The estimated velocity was calculated by

$$v_{\text{est}} = \frac{actpos_k - actpos_{k-2}}{2 * T} \tag{4.8}$$

where $actpos_k$ was the encoder reading for that time step, $actpos_{k-2}$ was the position two time steps before, and T was the sampling period.

The control values are listed in Table 4.1.

Servo Control Constants	
Control time period, T	0.005 seconds
Proportional gain, K_P	12000
Integral gain, K_I	500
Derivative gain, K_D	55
Estimated tach limit, *MAXTACH*	400

Table 4.1: Control Constants

4.2.4 Experimental Protocols

For each of the experiments, several combinations of muscle stimulation patterns and length trajectories were used. The stimulation patterns were: constant stimulation level, double ramp stimulation, and random stimulation level. The length trajectories were: constant length, double ramp length (constant velocity), and random length (and random velocity).

The patterns of stimulation and length trajectories were arranged in the following protocols (the program names are in parenthesis):

- Constant stimulation, constant length (*stepmapl*)
- Constant stimulation, double ramp length (*rlencstm*)
- Constant stimulation, random length (*cstmrand*)
- Double ramp stimulation, constant length (*rstmclen*)
- Random stimulation, constant length (*randclen*)
- Random stimulation, random length (*randrand*)

These protocols were run in blocks so that data of the same type were generated consecutively. Protocols required 2 to 8 minutes and blocks were scheduled to last 45 to 150 minutes. A block consisted of running the protocol on both muscles 2 to 11 times, with different inputs.

Each of the protocols is described below, along with the type of data expected from each stimulation pattern and length trajectory combination. The complete protocol from the experiment done on July 11, 1990 is included in Appendix A.

References to force measurements imply that the output of the strain gauge torque transducer, as amplified by the operational amplifier circuit, was digitized and recorded. These values were later converted to forces, and are shown in the plots of the following chapters.

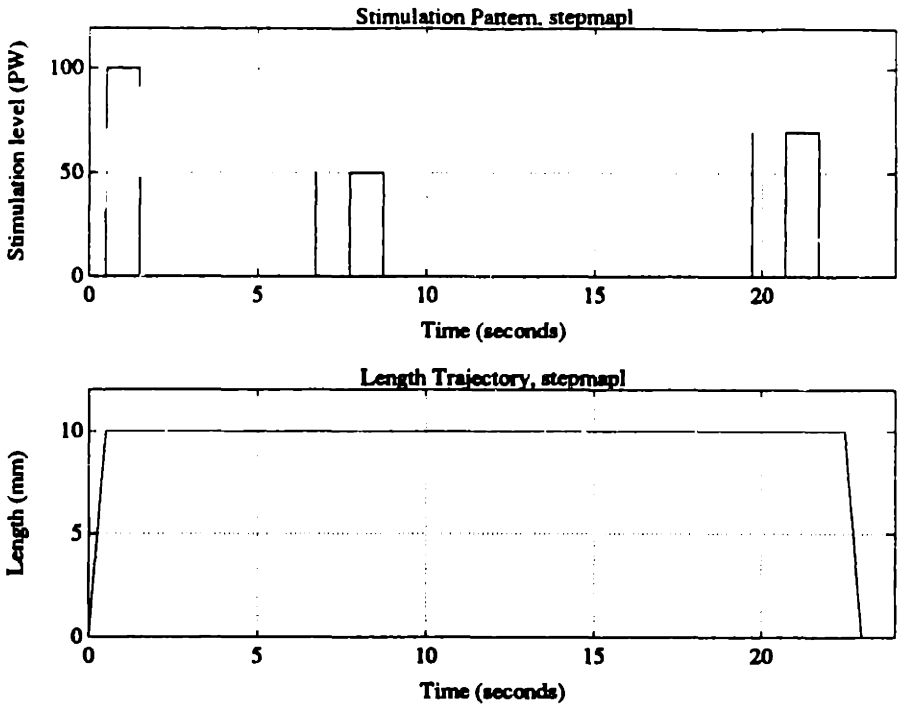

Figure 4.13: Constant stimulation, constant length protocol.

Constant Stimulation, Constant Length (*stepmapl*)

The timing diagram for the constant stimulation, constant length protocol is shown in Figure 4.13. As with all protocols, the initial stimulation was a conditioning pulse. Conditioning pulses were used to take up slack in the muscle and/or tendon which may have developed while the muscle was resting. A conditioning pulse was a 1.0 second stimulation at the maximum stimulus level of the stimulator (100.0 μs). The average force was computed for .25 seconds preceding and 0.25 seconds following the conditioning pulse. These values were used as reference force levels for the muscle at the starting length. Conditioning pulses were always followed by a rest period of 5.0 seconds.

Following the conditioning pulse and associated rest period, a single impulse of stimulation was delivered to the muscle. The stimulation level for this impulse was determined by the user and was the same pulse width as the step stimulation which followed. The force was measured for 0.2 seconds before and 0.8 seconds after the impulse stimulation. The 0.8 seconds was sufficient time for the force associated with the impulse to die away. (A typical impulse response peaked in 35 ms and faded in 300 ms.)

The step stimulation lasted 1.0 second. Force was recorded from 0.2 seconds before until 0.8 seconds after the stimulation. Following a 20.0 second rest, the impulse and step stimulations were repeated, generally at different stimulation levels.

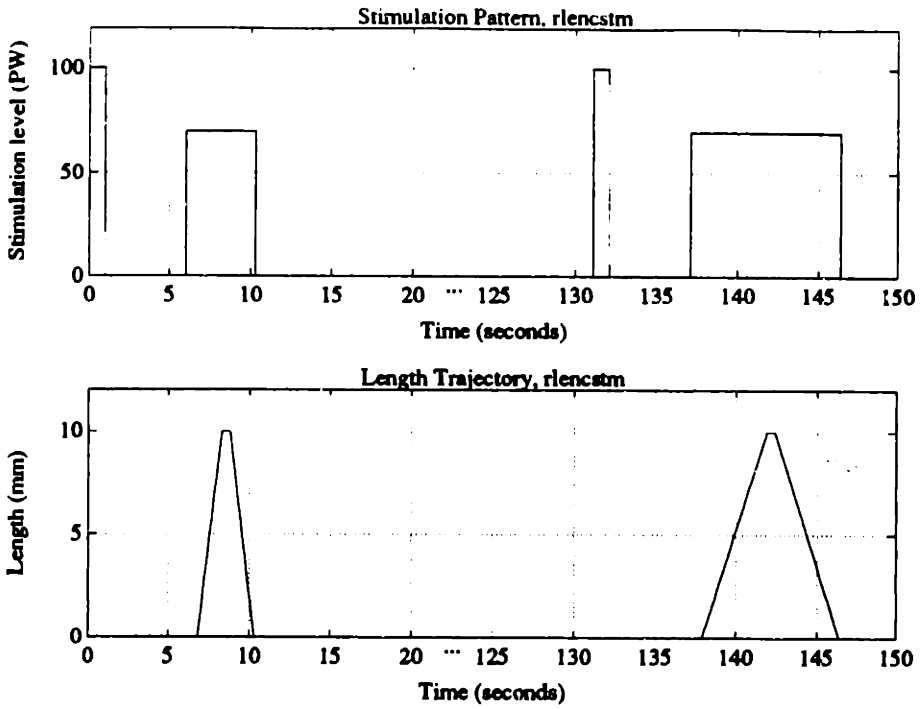

Figure 4.14: Constant stimulation, double ramp length protocol.

The length of the muscle was held constant during the stimulation. As can be seen in Figure 4.13, the servo started at instrumentation zero, ramped to the desired position, maintained that position for the duration of the stimulation, then ramped back to instrumentation zero. The muscle was allowed to rest at instrumentation zero for 120 seconds, then the sequence was repeated, generally at a different test length.

The variables which were input by the user allowed for changing: the number of stimulation levels, the pulse width of the stimulations, the number of lengths to be tested, and the shortest and longest lengths.

This protocol was used to produce length-tension curves for both impulse stimulation and constant stimulation. The data points for an impulse L-T curve were the peak force measurements following the impulse stimulation. The average of the force produced during the last 0.5 second of the 1.0 second constant stimulation was the force used to generate the constant stimulation L-T curve.

Constant Stimulation, Double Ramp Length (*rlencstm*)

The timing diagram for the constant stimulation, double ramp length protocol is shown in Figure 4.14. The conditioning stimulation was followed by a stimulation which began 0.8 seconds before the servo started to ramp the length and continued until the servo finished ramping. The servo ramping went from instrumentation zero to the user determined length, maintained that length for 0.5 seconds, then returned

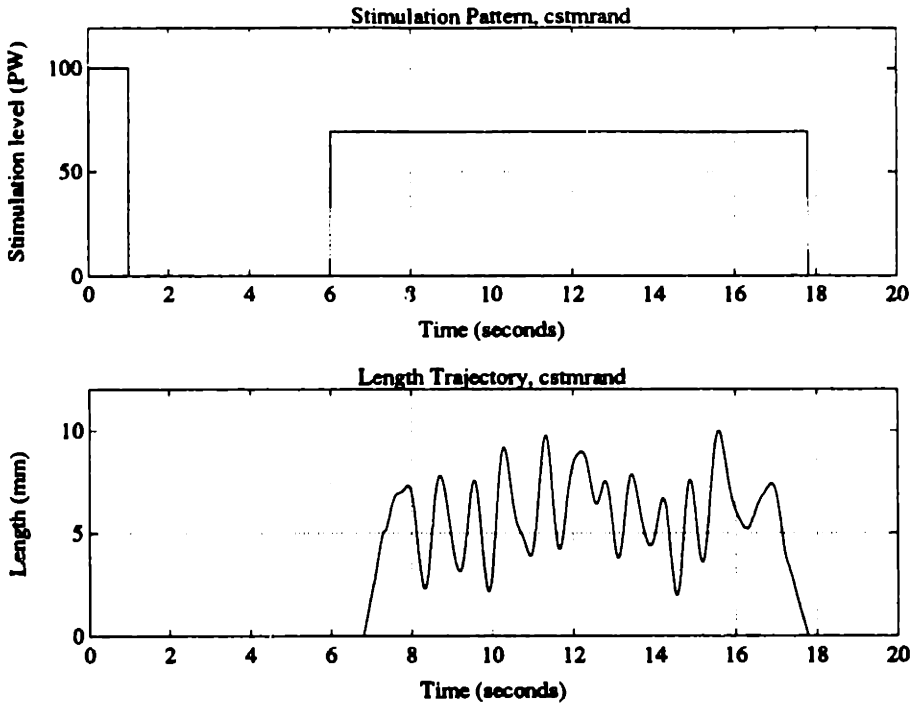

Figure 4.15: Constant stimulation, random length protocol.

to the zero position. The muscle rested at instrumentation zero, with no stimulation, for 120 seconds before the process was repeated. Subsequent ramps were usually at a different velocity. The stimulation level was the same for all ramps in a file.

The user determined: the stimulation level, the distance the muscle was stretched, the number of servo ramps, the duration of each ramp (this determined the velocity), and the time at the longest length (this was constant for all of the ramps).

This protocol was used to produce the force-velocity curve at various stimulation levels, including passive. Using one stimulation level per file, data for several velocities were generated consecutively, thus minimizing the time varying effects of the muscle on the force-velocity curve.

Constant Stimulation, Random Length (*cstmrand*)

The timing diagram for the constant stimulation, random length protocol is shown in Figure 4.15. The stimulation for this protocol consisted of a conditioning pulse followed by the standard 5.0 second rest, then a stimulation which started 0.8 seconds before the servo began to move and lasted the duration of the servoing. The servo maintained the instrumentation zero position for the conditioning stimulation. It then followed a predetermined "random" trajectory for up to 10.0 seconds. The path from the zero position to the beginning of the random sequence, and from the end of the random sequence back to zero, was a constant velocity ramp which required

0.25 seconds. The muscle rested at zero position for 120 seconds before the next conditioning pulse was delivered.

The random trajectories were created in Matlab [12] by filtering random noise signals through a tenth order Butterworth filter with cutoff frequencies ranging from 1.5 to 2.5 Hz. The Matlab commands were:

```
   N  =  2000;
   x  =  random(1:N);
[b,a] =  butter(10,1.5/100);
   y  =  filter(b,a,x);
```

The random position trajectories are shown in Figure 4.16.

The following options were available to the user of the constant stimulation, random position program: number of stimulations, pulse width of the stimulations, range of random lengths (maximum and minimum lengths for the random trajectory to use), choice of predetermined random trajectories, and duration of the random travel.

This data was generated to be used by the fitting algorithms described in Chapter 3. The length trajectories were chosen because they covered the length-velocity phase plane well. That is, when the velocity was plotted against the position, the points did not all lie on top of each other or leave large blank areas. For parameter fitting, many points clustered in one area of the phase plane would unfairly bias the fitting algorithm toward that area and other data points with either the same velocity or length would be poorly fit. Large blank areas in the phase plane would also unfairly bias the fitting algorithm. Figure 4.17 shows the phase plane plots for each of the random trajectories of Figure 4.16.

Double Ramp Stimulation, Constant Length (*rstmclen*)

The timing diagram for the double ramp stimulation at constant length is shown in Figure 4.18. The stimulation sequence consisted of a conditioning pulse followed by four (4) impulses, then a ramp up and ramp down in stimulation level. The four impulses were spaced 1.0 seconds apart and the first began 5.2 seconds after the conditioning pulse ended. The ramp stimulation began 1.0 second after the final impulse and lasted 2.0 seconds – 1.0 second for increasing stimulation level, 1.0 second for decreasing. There was a 120.7 second rest between the end of a ramp and the following conditioning stimulation. The servo took 0.25 seconds to ramp to the desired length, which it achieved 0.25 seconds before the conditioning pulse began. It held the muscle at that length until 0.25 seconds after the ramp stimulation was completed at which time it ramped back to the instrumentation zero position.

The data generated by this protocol was used to construct the isometric recruitment curve. This construction used the ramp deconvolution method described in Section 3.4.

This protocol was implemented in two different programs. One, called *fastramp*,

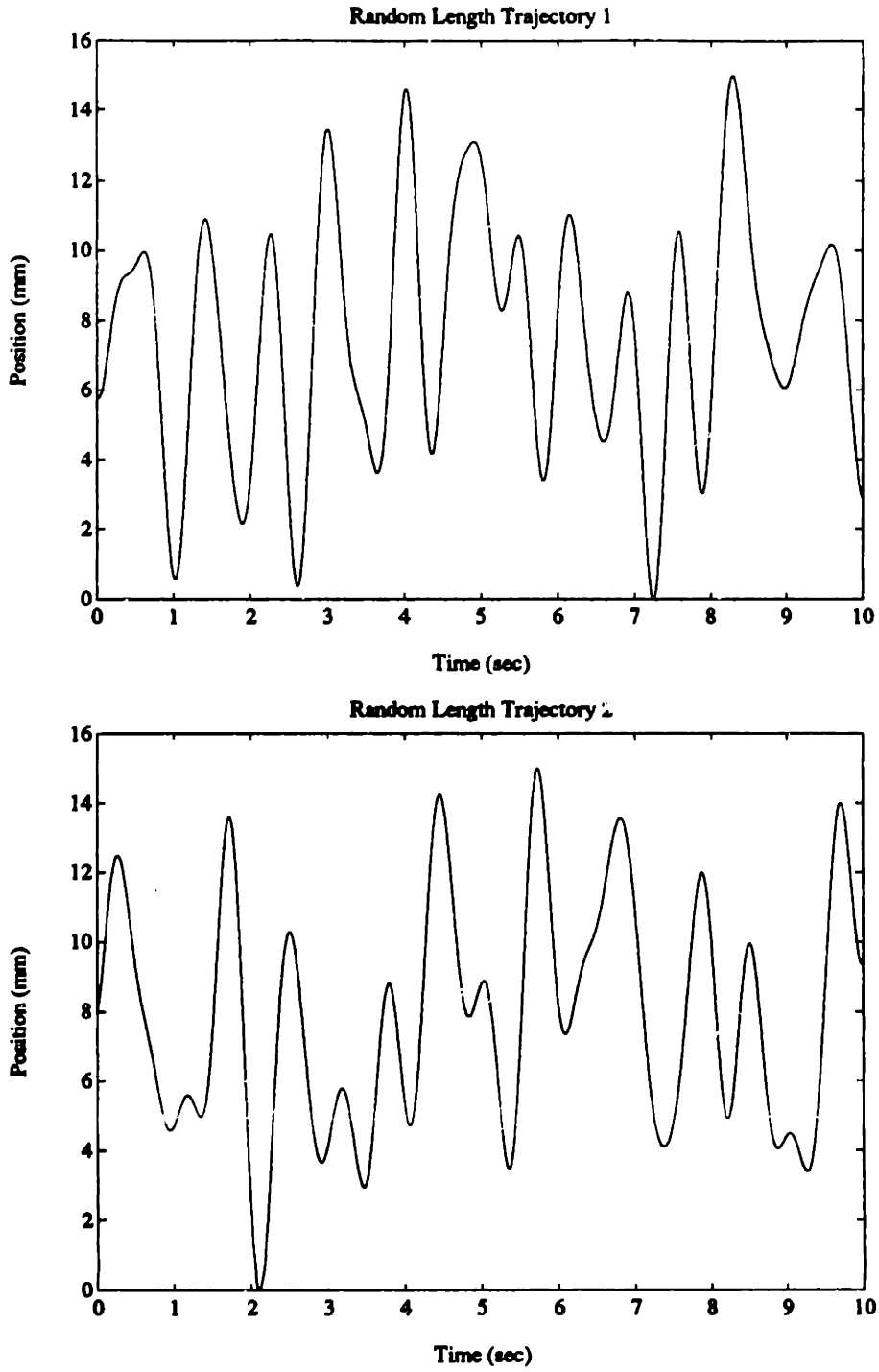

Figure 4.16: Random position trajectories.

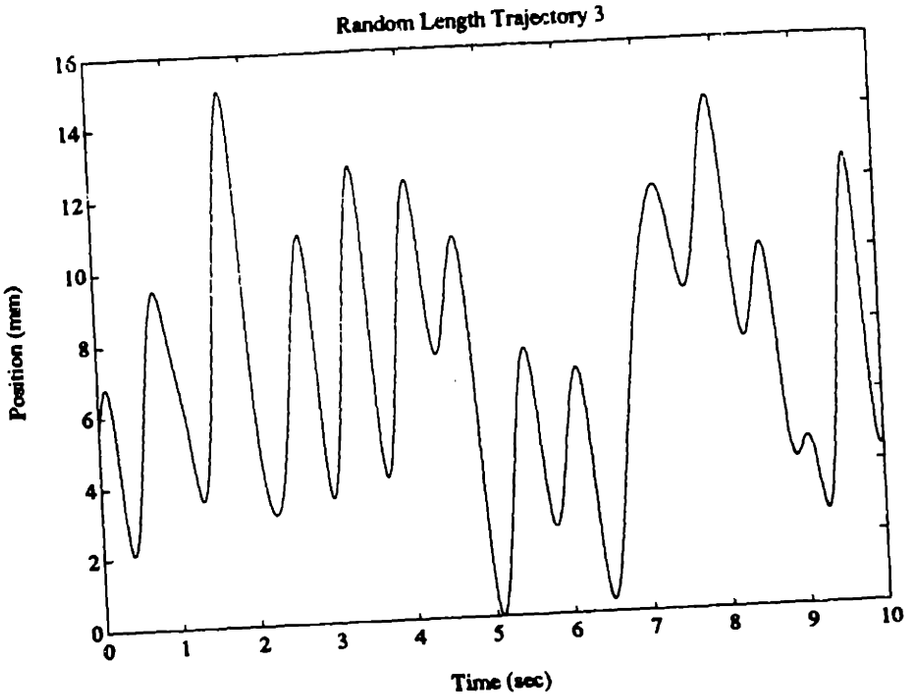

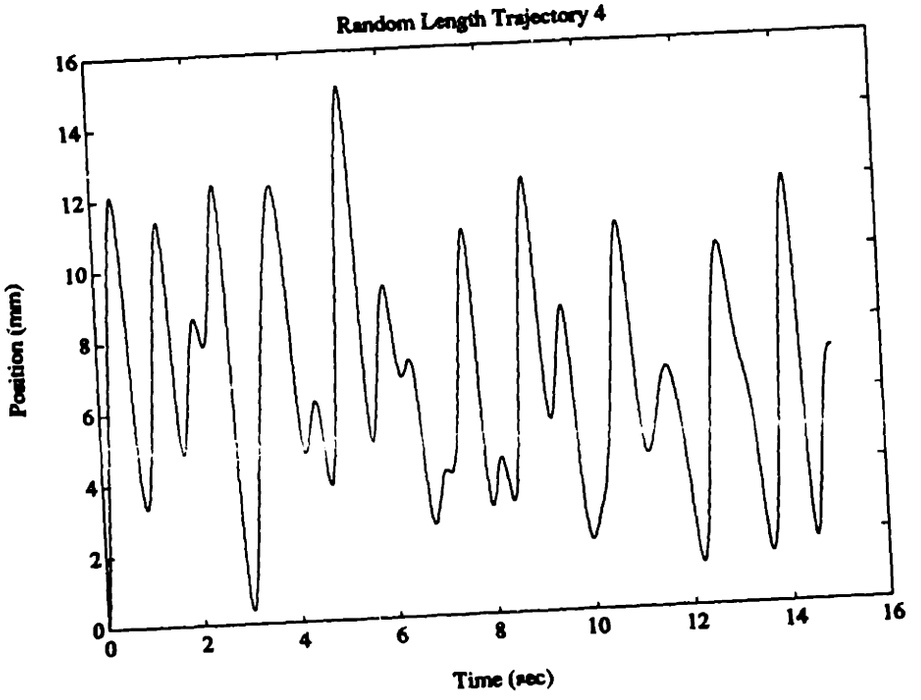

Figure 4.16: Random position trajectories. (cont.)

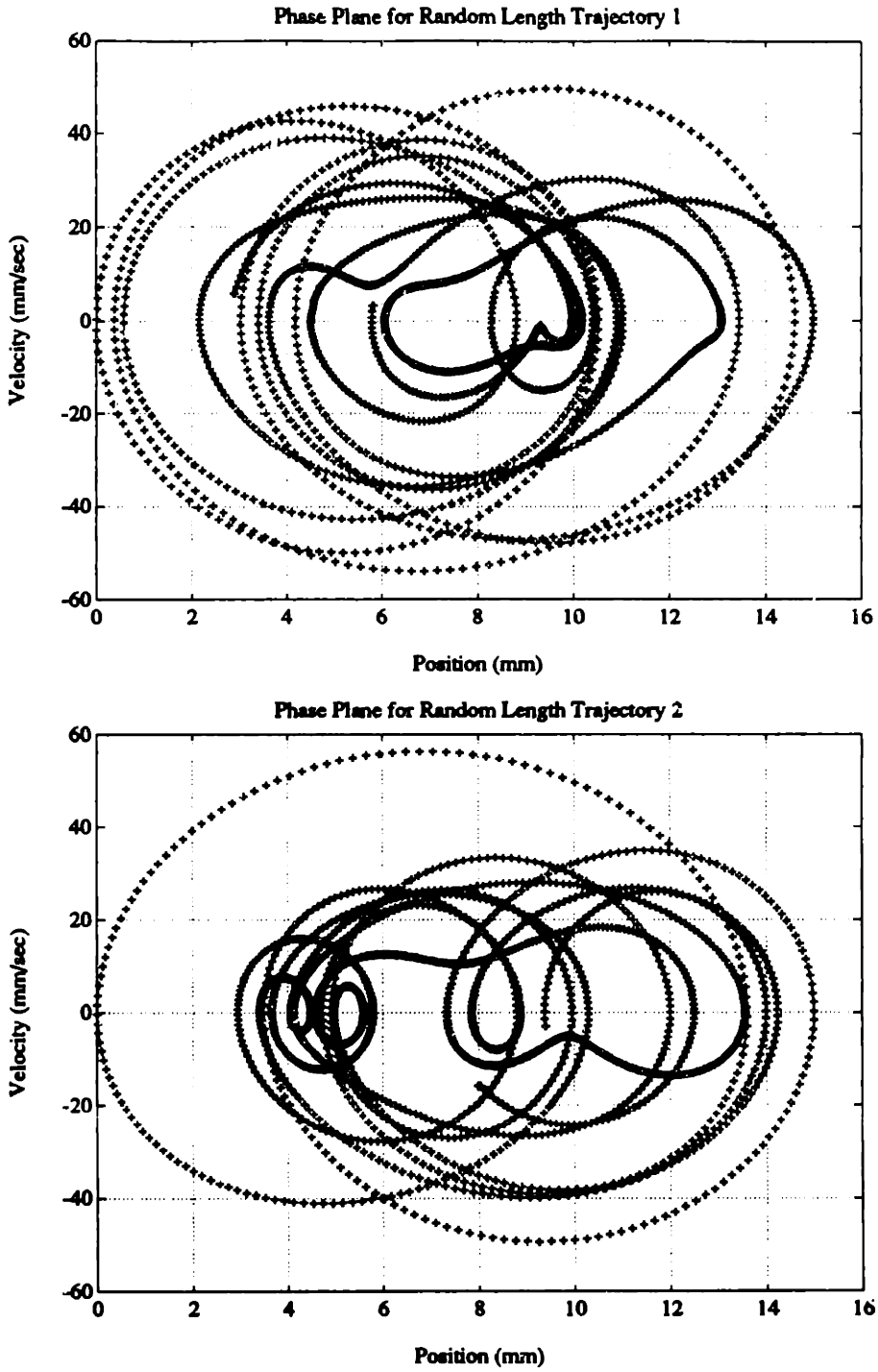

Figure 4.17: Phase planes of random position trajectories.

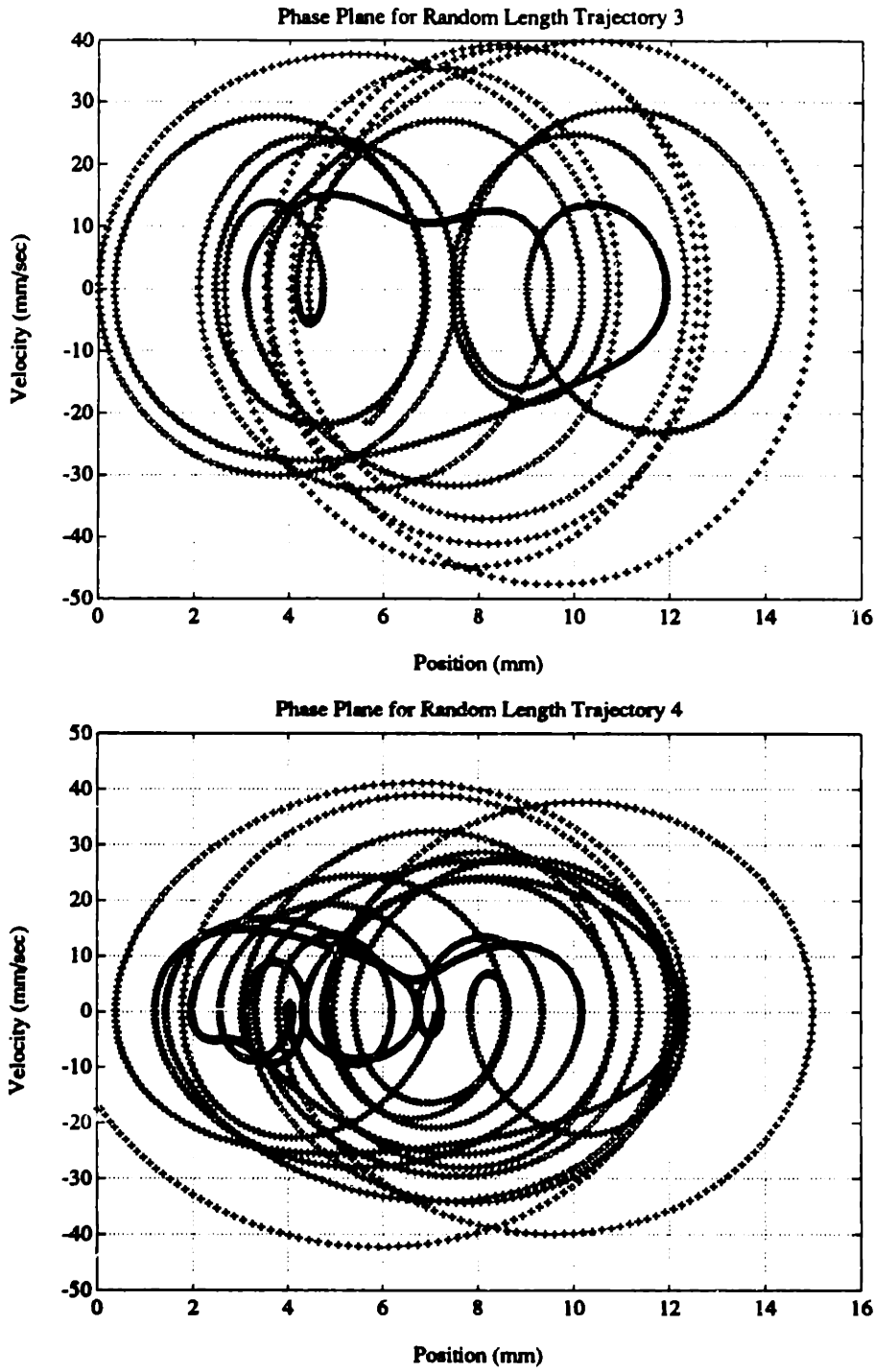

Figure 4.17: Phase planes of random position trajectories. (cont.)

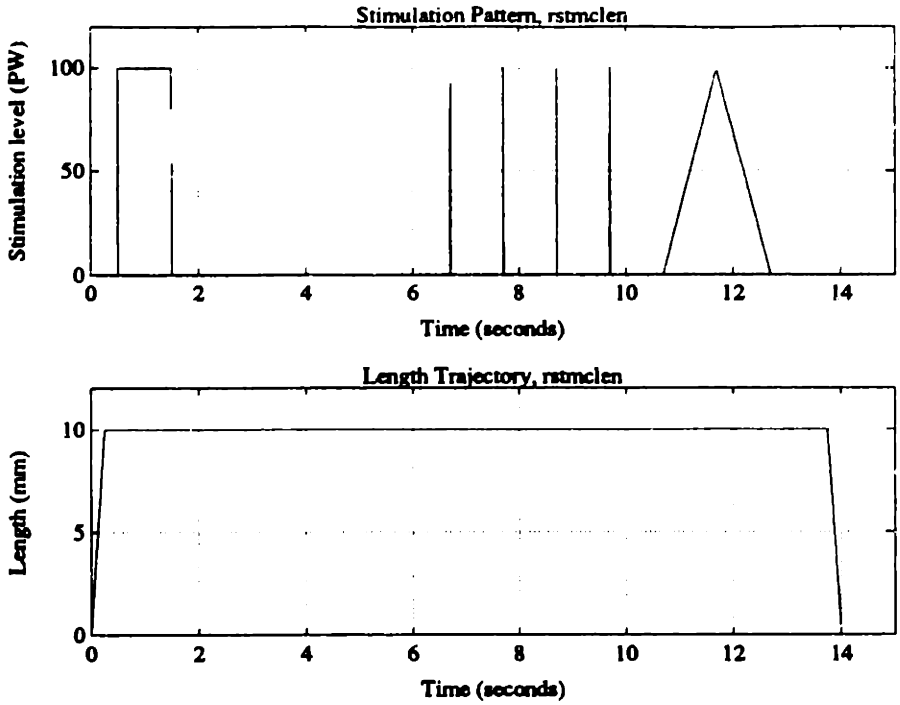

Figure 4.18: Double ramp stimulation, constant length protocol.

was used to determine the "zoom limits," or the activation limits of the isometric recruitment curve. This program was run at the beginning of each block of data. It required the user to input the test length and used 0.0 - 100.0 μs as the default stimulation range. The other program allowed the user to input the number of lengths to be tested, as well as the shortest and longest test lengths. The stimulation range for this program was the zoom limits which were set as a result of running *fastramp*. The zoom limits were used to produce more detail in the isometric recruitment curve in the area of interest.

Random Stimulation, Constant Length (*randclen*)

The timing diagram for the random stimulation at constant length protocol is shown in Figure 4.19. The stimulation sequence for this protocol consisted of the conditioning pulse followed by 5.0 seconds of rest, then random stimulation levels. The range of the random stimulation was determined by the zoom limits. The length trajectory ramped to the test length in 0.25 seconds, held constant at that length, then ramped back to the instrumentation zero. Only one length was tested per file, so there was no timed rest period. One muscle rested while the other muscle was being stimulated.

There were four (4) random stimulation patterns which were predetermined. They are shown in Figure 4.20. The level of randomness varied between the four patterns.

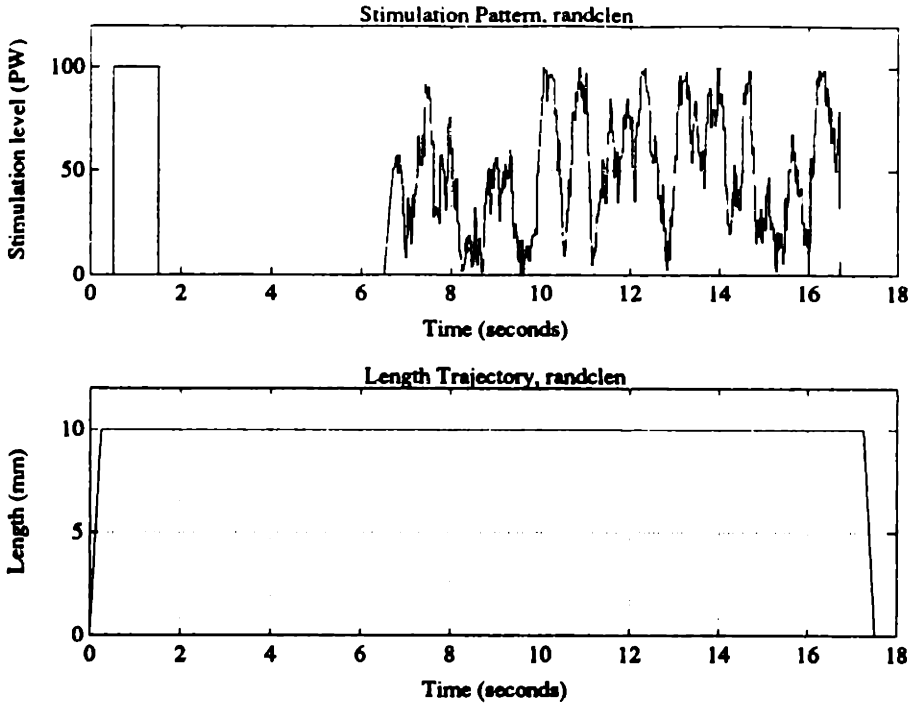

Figure 4.19: Random stimulation, constant length protocol.

The more random ones, 1 and 2, were included to provide a wide range of frequency content (larger bandwidth) in the stimulations. The user input the number corresponding to the random sequence desired, the test position, and the length of time to stimulate.

This data was created to test the parameter identification techniques, particularly the stimulation/activation and the series elastic element blocks. No classical muscle curves were generated directly from this data.

Random Stimulation, Random Length (*randrand*)

The timing diagram for the random stimulation and random length protocol is shown in Figure 4.21. The stimulation patterns were identical to those used for the random stimulation with constant length protocol. The random length trajectories were the same as those used in the constant stimulation, random length protocol.

The user input the number corresponding to the random stimulation and random position sequences desired, limits of the positions for the random length trajectory, and the duration of the two random sequences. The range of the random stimulation was determined by the zoom limits.

This data was generated to test the parameter identification techniques. No classical muscle curves were generated from this data.

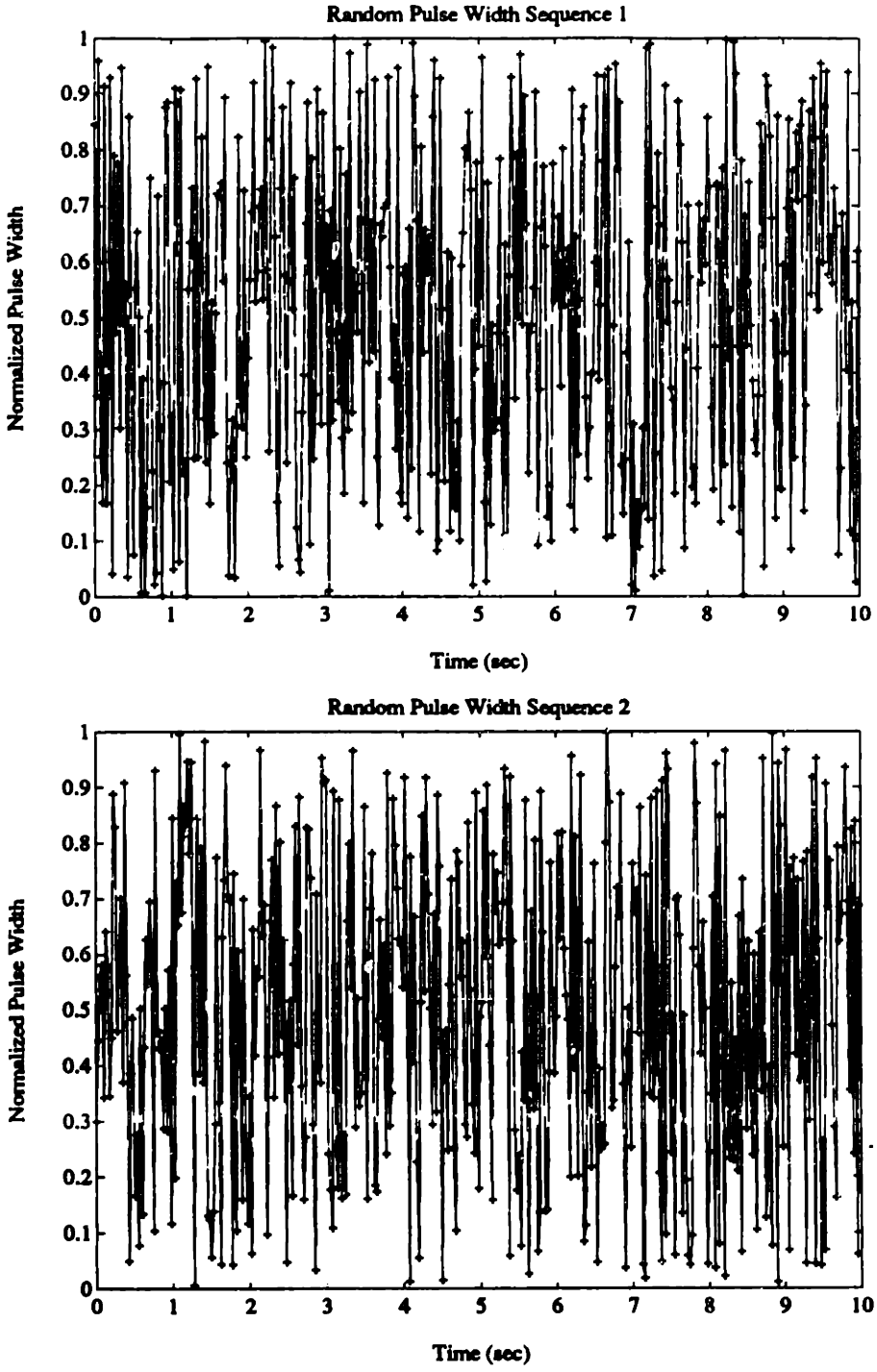

Figure 4.20: Random stimulation patterns

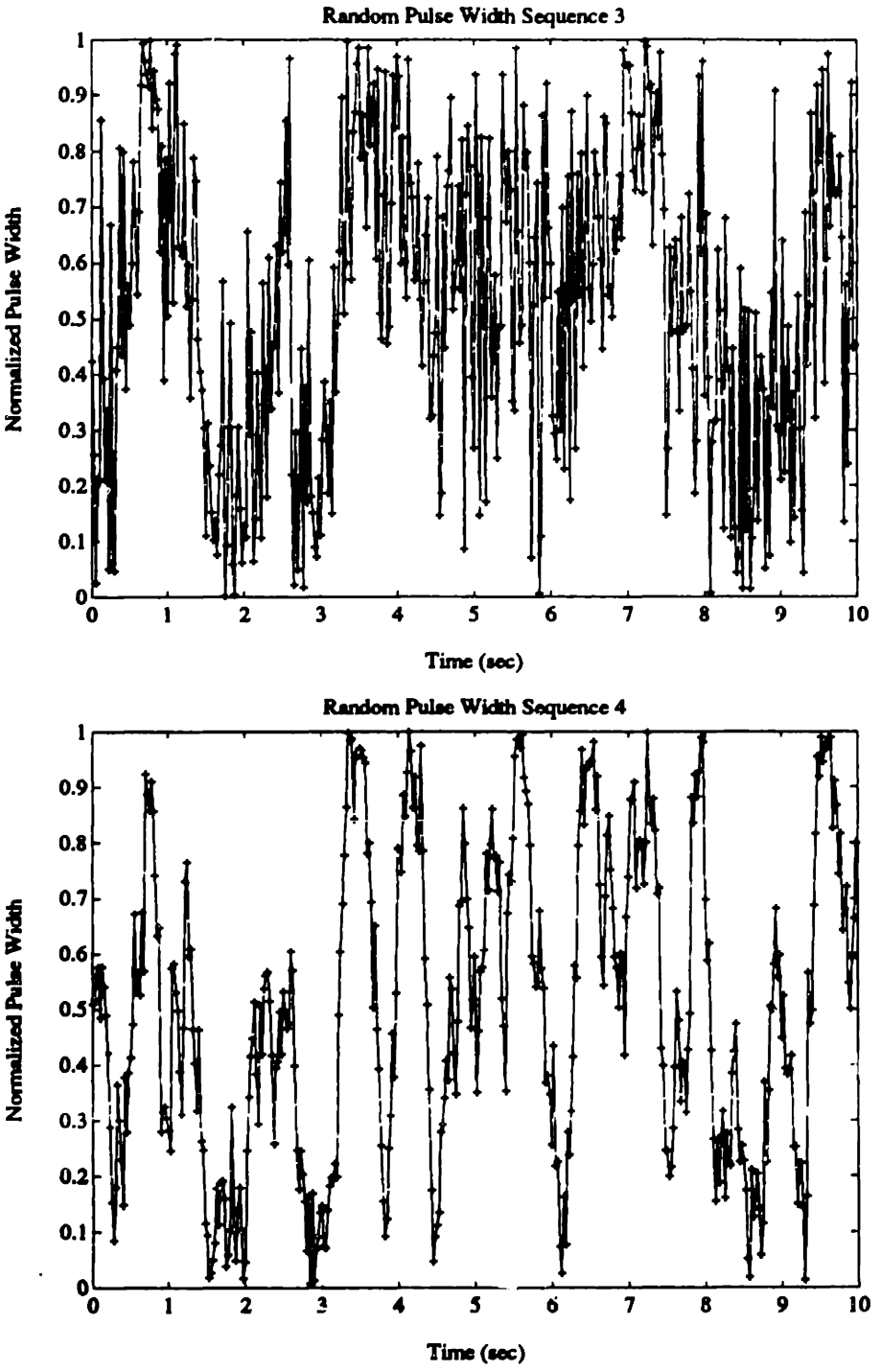

Figure 4.20: Random stimulation patterns (cont.)

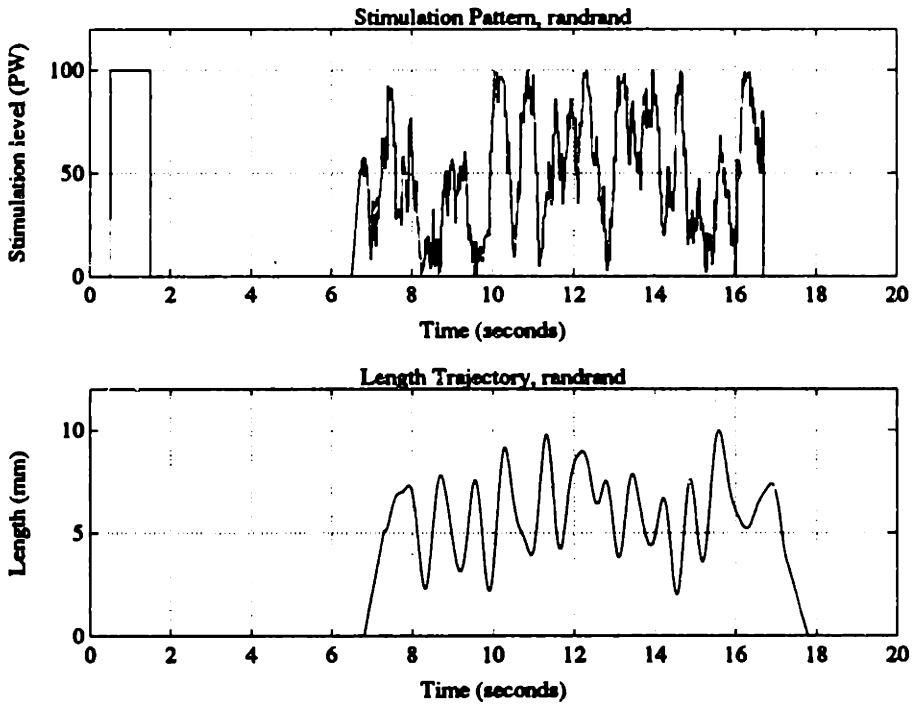

Figure 4.21: Random stimulation, random length protocol.

Chapter 5
Results

The data presented in this chapter was generated during a single animal experiment on July 11, 1990. Two muscles of a cat's hind limb, the tibialis anterior (TA) and the medial gastrocnemious (MG), were stimulated. The protocol for the entire experimental session is included as Appendix A. The individual test protocols are described in Section 4.2.4 and will be referenced in this chapter using the program names listed on page 58.

The reader is reminded that the length measurements for all of the experimental data presented in this thesis are referenced to the instrumentation zero position which is not related to any definable physiologic muscle length. Negative velocities denote muscle shortening.

This chapter is divided into the following sections: muscle characteristics using classical development methods, muscle characteristics from parameter estimation, and prediction of muscle force. The first section presents curves which were produced directly from the force, length, velocity and stimulation data. The second section shows muscle relationships which were generated by applying the parameter estimation techniques discussed in Chapter 3. The final section explores the prediction capability of the model, i.e, given the relationships of the first two sections, use the model to predict the force output.

5.1 Muscle Characteristics using Classical Techniques

5.1.1 Passive Muscle Dynamics

The passive length-tension curves, which were produced using the *stepmapl* experimental protocol, are shown in Figures 5.1 and 5.2. The muscles were passively stretched, stimulated with a conditioning pulse, then held at a constant length. The data points shown in the curve were calculated by averaging the passive force for a half second.

The passive force-velocity curves shown in Figures 5.3 and 5.4 are from the data produced by the *rlencstm* protocol. The muscles were stimulated with a conditioning pulse, then passively ramped in length for 14 mm for the MG and 17.5 mm for the TA at different velocities. The velocities ranged from -40 to 40 mm/sec for the MG, and -50 to 50 mm/sec for the TA. The figures show the passive force-velocity curve at different muscle lengths (as referenced to instrumentation zero). For the MG, 4.0, 6.0, 8.0, 10.0, and 12.0 mm are shown. The TA plot shows the force-velocity relationship at 5.0, 7.5, 10.0, 12.5, and 15.0 mm. The developed force increased with increasing length as shown in Figure 5.5.

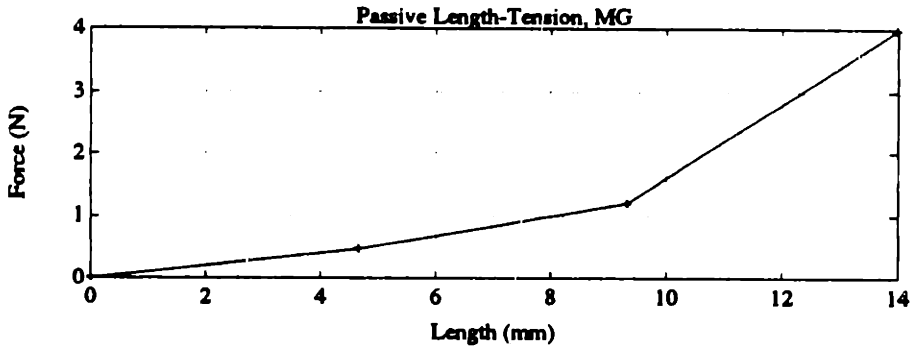

Figure 5.1: Passive length-tension curve for MG, generated by *stepmapl*.

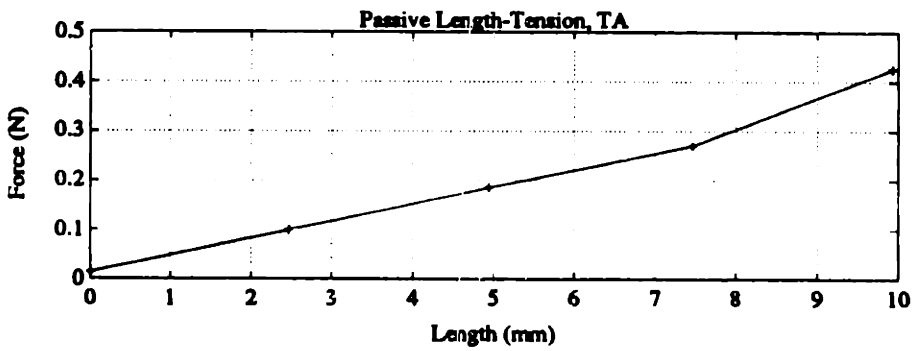

Figure 5.2: Passive length-tension curve for TA, generated by *stepmapl*.

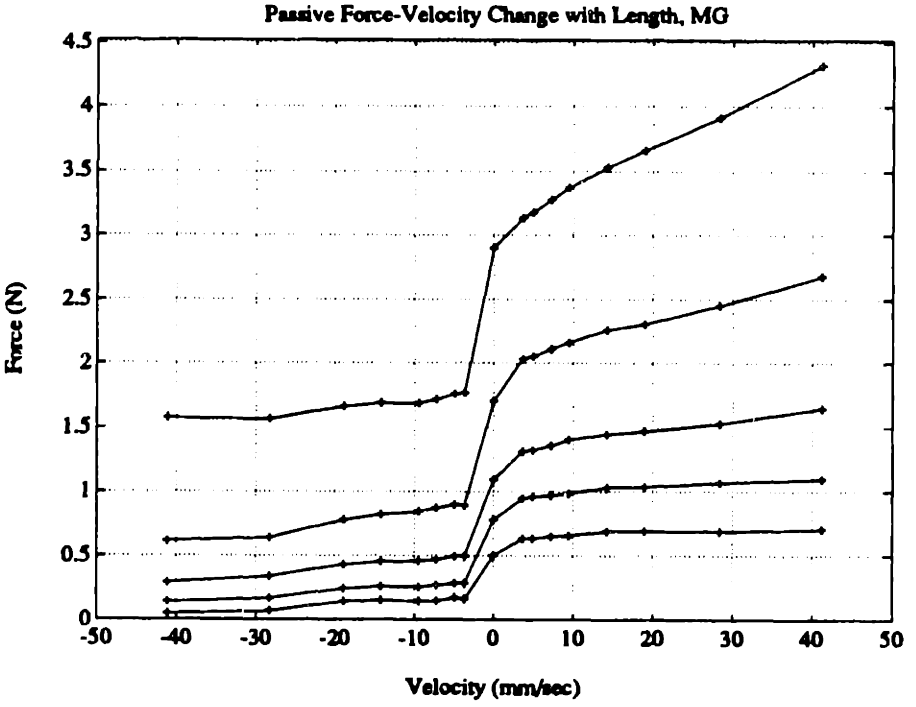

Figure 5.3: Passive force-velocity curve at different lengths, MG, generated by *rlencstm*. Lengths of 4, 6, 8, 10, and 12 mm are shown (bottom to top).

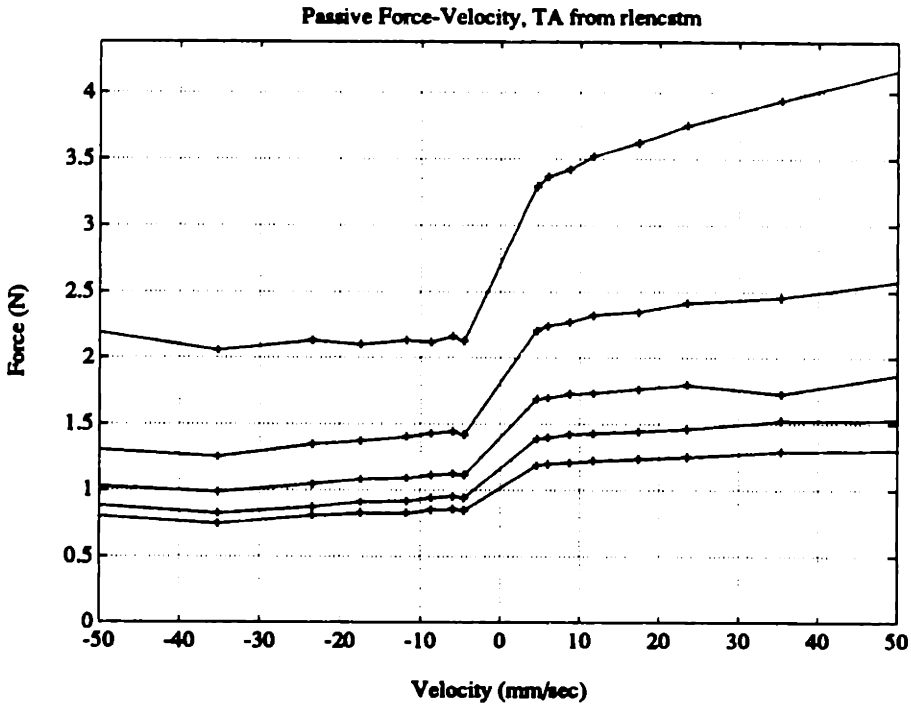

Figure 5.4: Passive force-velocity curve at different lengths, TA, generated by *rlencstm*. Lengths of 5, 7.5, 10, 12.5, and 15 mm are shown (bottom to top).

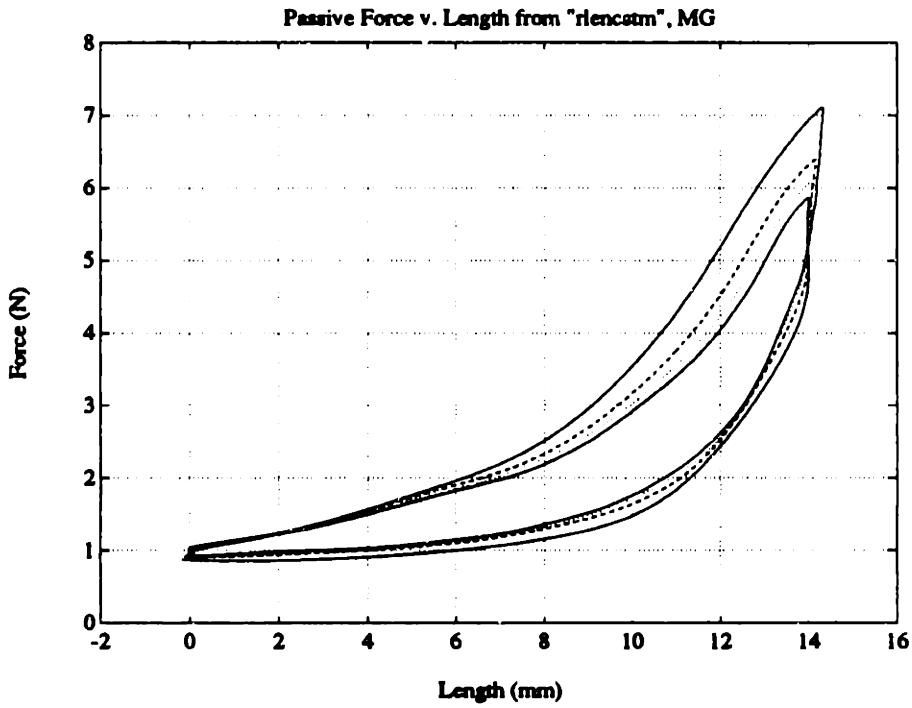

Figure 5.5: Passive force as a function of length, MG, from *rlencstm*. Constant velocity ramps are 4.7 (solid), 9.3 (dotted), 18.7 (dashed), and 40.0 (solid) mm/sec.

5.1.2 Active Dynamics

Length Dependence

The active length-tension curves were generated by two different methods — using the *stepmapl* and *rlencstm* protocols.

The results of the *stepmapl* protocol are shown in Figures 5.6 and 5.7. The force used for these plots was the average force for a half second of stimulation at the given length. The figures show three curves, corresponding to stimulation levels of 20, 40, and 60 μs for the MG and 30, 50 and 70 μs for the TA. These stimulation levels represent low, medium, and high levels of recruitment.

The data points shown on these curves were generated in two distinct runs of *stepmapl*, separated by approximately 30 minutes. This delay between trials resulted in curves which were not smooth for the TA as explained in Section 6.2.1.

The *rlencstm* protocol ramped the length of the muscle at constant velocity. By ramping very slowly, a quasi-static condition existed. Figures 5.8 and 5.9 show the length-tension curves for the servo ramping at 3.5 mm/sec and 4.4 mm/sec, respectively. The stimulation levels were 0, 35, and 50 μs for the MG and 0, 22.5, 27.5 and 35 μs for the TA. Note that the lengthening and shortening ramps produced different force levels at each length as is shown in Figure 5.10. The lengthening and shortening forces were smoothed [25] and averaged to produce Figures 5.8 and 5.9.

Velocity Dependence

The active force-velocity curves were generated using the *rlencstm* protocol. The shape of the curves and the magnitude of the forces produced changed with both length and stimulation level. Figures 5.11 and 5.12 show the force-velocity curves at stimulation levels of 50 and 35 μs for the MG and TA respectively. The curves were measured at lengths ranging from 4.0 to 12.0 mm in increments of 2.0 mm for the MG. The lengths for the TA curves ranged from 5.0 to 15.0 mm in even increments of 2.5 mm. These plots were generated from data which was separated into two files which were measured approximately 20 minutes apart. The TA curves have been plotted by data file in Figure 5.13. Figures 5.14 and 5.15 show the force-velocity curves at several stimulation levels. The length was 8 mm for the MG with stimulation levels of 0, 35, and 50 μs. The TA curves were generated at 10 mm, with stimulation levels of 0, 22.5, and 35 μs.

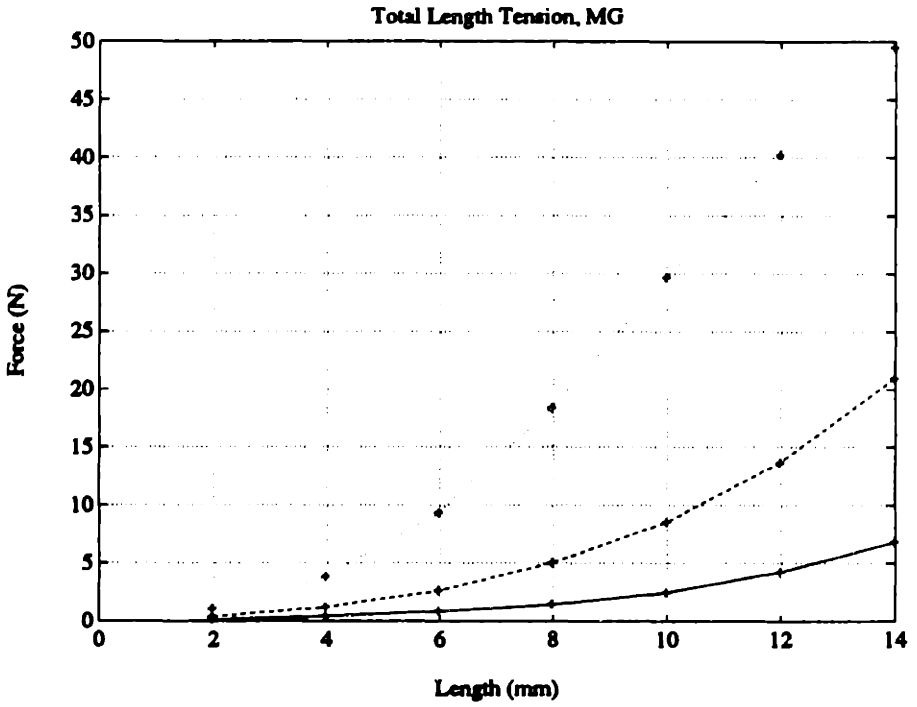

Figure 5.6: Total length-tension curves at different stimulation levels, MG, generated by *stepmapl*. Stimulation levels were 20 (solid), 40 (dashed), and 60 (dotted) μs.

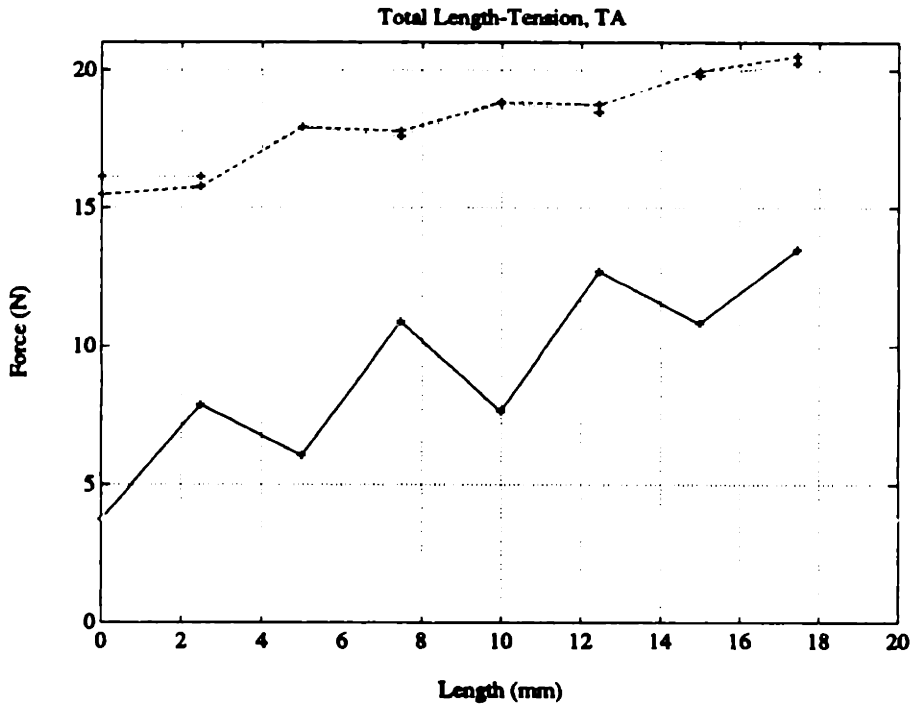

Figure 5.7: Total length-tension curves at different stimulation levels, TA, generated by *stepmapl*. Stimulation levels were 30 (solid), 50 (dashed), and 70 (dotted) μs.

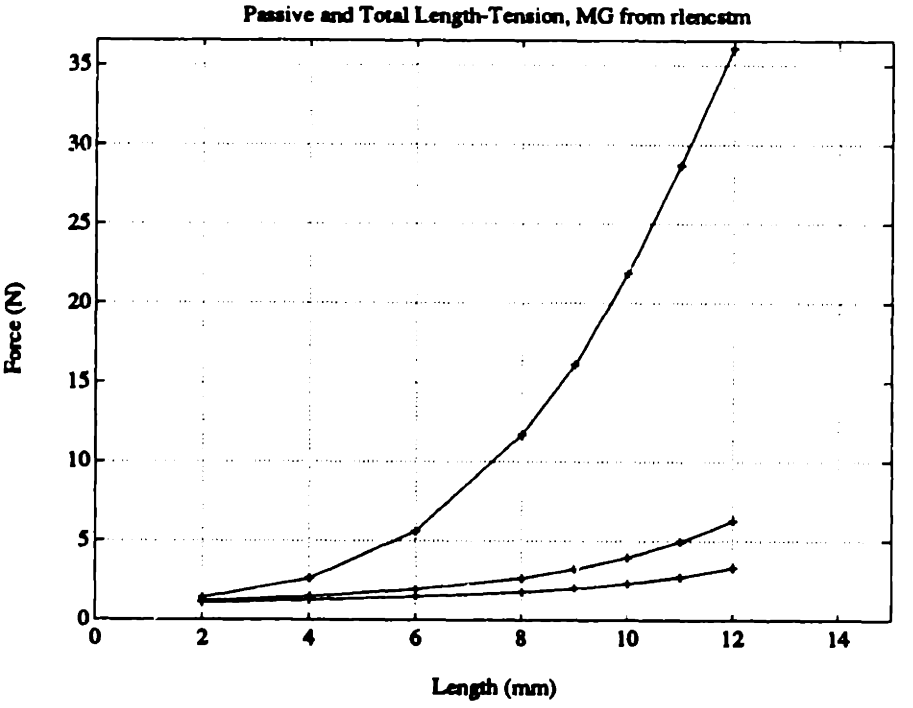

Figure 5.8: Quasi-static length-tension curve at 0, 35, and 50 μs stimulation levels, MG. from *rlencstm*.

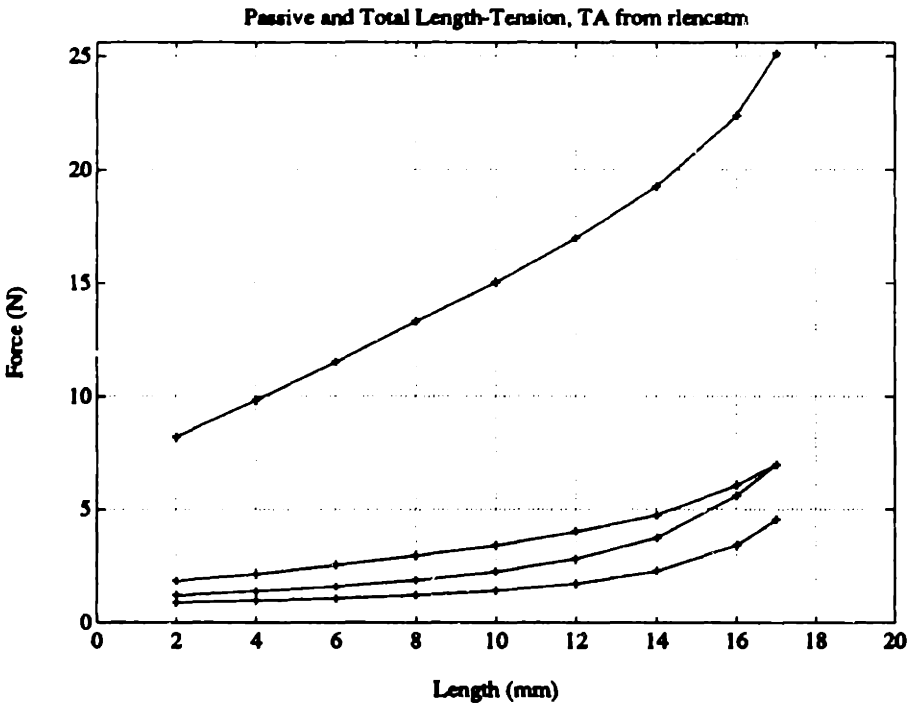

Figure 5.9: Quasi-static length-tension curve at 0, 22.5, 27.5, and 35 μs stimulation levels, TA, from *rlencstm*.

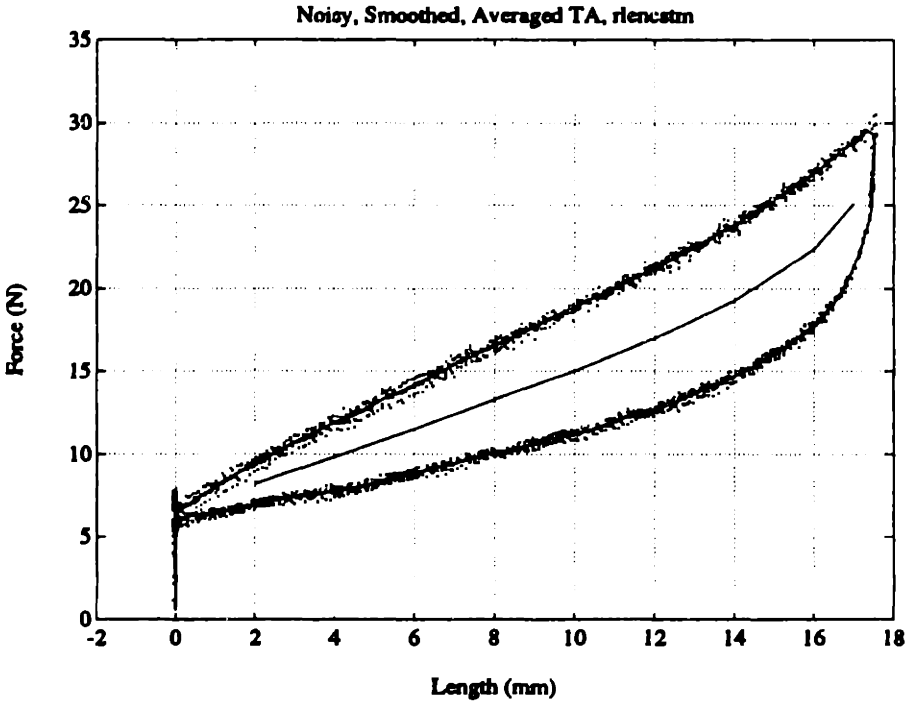

Figure 5.10: Force vs. Length for lengthening (upper) and shortening (lower), from *rlencstm*. Raw data, smoothed, and averaged. TA, PW 35 μs

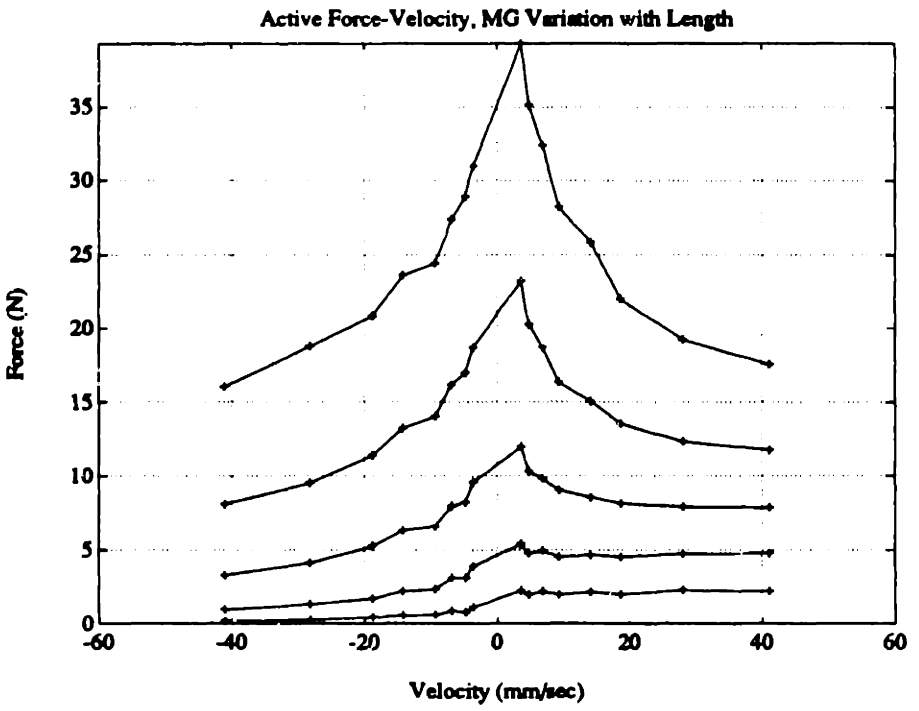

Figure 5.11: Active force-velocity at different lengths, MG, PW 50 μs, from *rlencstm*. Lengths were 4, 6, 8, 10, and 12 mm.

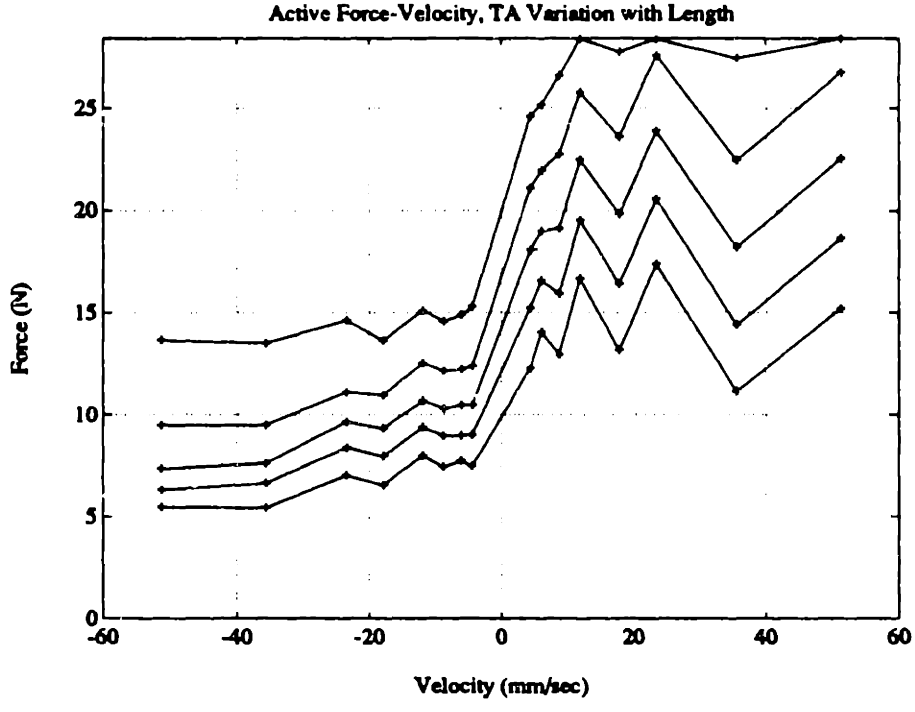

Figure 5.12: Active force-velocity at different lengths, TA, PW 35 μs, from *rlencstm*. Lengths were 5, 7.5, 10, 12.5, and 15 mm. (The analog force input was saturated for $l = 15$mm.)

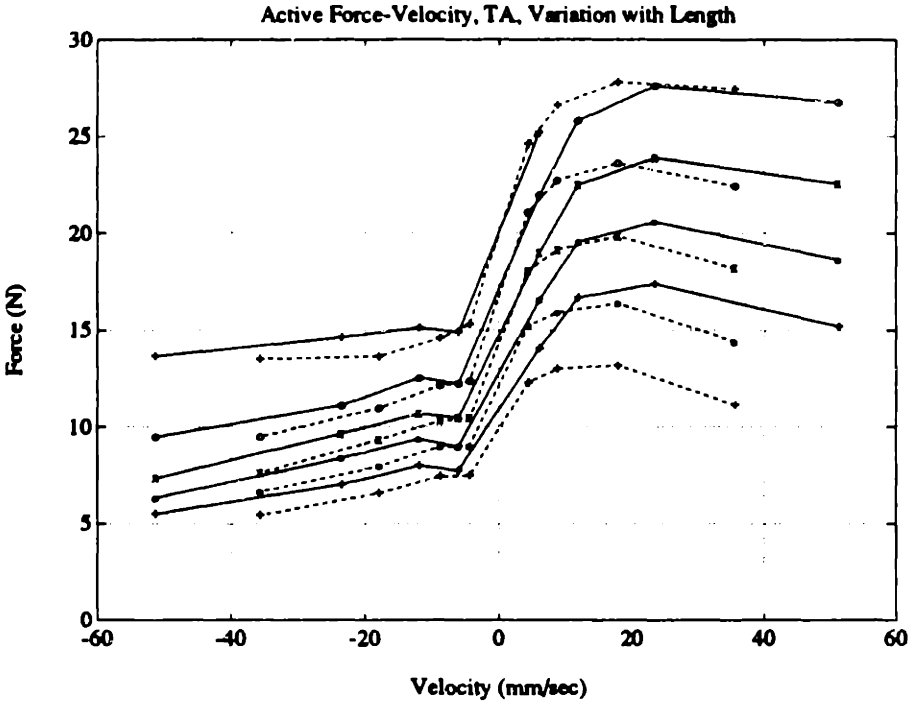

Figure 5.13: Active force-velocity at different lengths, TA, from *rlencstm*. Lengths were 5 (+), 7.5 (*), 10 (o), 12.5 (x), and 15 mm(+). Solid lines were measured 20 minutes before broken.

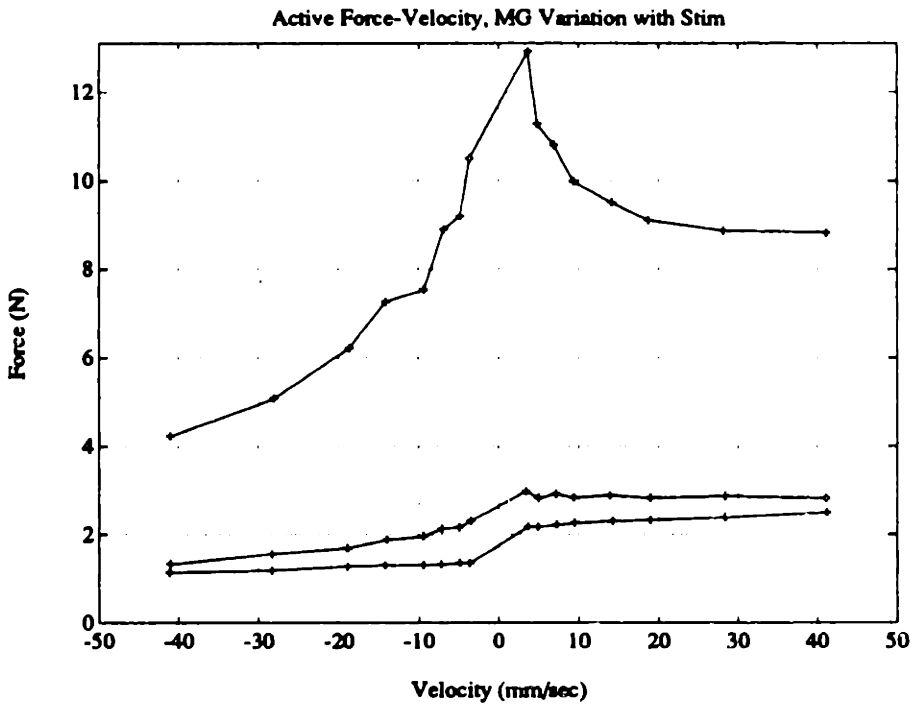

Figure 5.14: Active and passive force-velocity at different stimulation levels, MG, from *rlencstm*. Stimulation levels were passive, 35 and 50 μs.

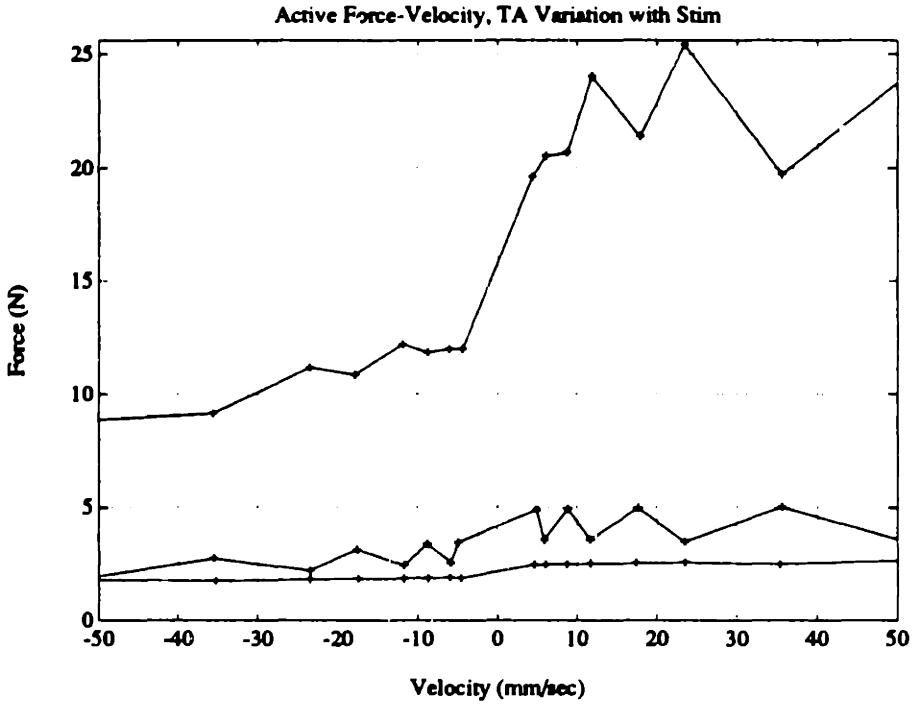

Figure 5.15: Active and passive force-velocity at different stimulation levels, TA, from *rlencstm*. Stimulation levels were passive, 22.5, and 35 μs

5.2 Muscle Characteristics using Parameter Estimation

The structure of the model dictated that the parameters be defined in a specific sequence: 1) passive length-tension and force-velocity curves, 2) stimulation/activation characteristics, and 3) active length-tension and force-velocity curves.

The least squares fitting algorithm described in Section 3.2 was used to determine both the passive and active length-tension and force-velocity relationships. Changing the number of line segments to be fit and the length of the data set yielded different estimated parameters. These variations will be shown.

5.2.1 Passive Muscle Dynamics

The passive muscle force was modeled as the sum of the length dependent and velocity dependent forces, according to Equation 2.2. The *cstmrand* protocol was used to generate data from which the passive force-velocity and length-tension relationships could be estimated. This protocol changed the length of the muscle to follow a random trajectory. The three random trajectories used are shown in Figure 4.16. Figures 5.16 and 5.17 show the force records for random trajectory 3, which are typical. Note that for the first 0.9 second and the last 0.8 second the muscles were held at a constant length (instrumentation zero). For $t = 0.9$ to 1.4 and $t = 11.4$ to 11.9, the velocity was constant as the muscle was ramped to the starting position of the random trajectory.

The fitted passive length-tension curves are shown in Figures 5.18 and 5.19. The passive force-velocity curves are shown in Figures 5.20 and 5.21. The three curves in each figure were generated by parameter estimation using ten (10) line segments to fit the data from three different random trajectories. Random trajectories 1, 2 and 3 produced the solid, dashed, and dotted fitted parameters, respectively.

Figures 5.22 and 5.23 show the difference between the measured force (same as Figures 5.16 and 5.17) and the fitted force for random trajectory 3. The fitted force was calculated from Equation 2.2 using length and velocity inputs defined by the random position trajectory.

The error between the measured and fitted forces was reduced when either more line segments were used, or the data was shortened to eliminate the constant position and constant velocity sections. Figure 5.24 shows the difference between the measured force and the fitted force when twenty (20) line segments were used to estimate the length-tension and force-velocity relationships for the MG. Figure 5.25 was generated using the data between 1.4 and 11.4 seconds (only the random trajectory data). Figures 5.26 and 5.27 show the length-tension and force-velocity relationships estimated from the three estimation variations. The solid line was using ten line segments with the entire data set. The dashed line was twenty line segments and all of the data. The dotted line was for ten segments and only the random part of the data. The average squared errors were 0.0468 and 0.0447 for the full data set with ten and twenty line segments, respectively. The average squared error for $t = 1.4$ to 11.4 was 0.0541 using parameters calculated from the entire data set with ten line segments and 0.0522

Summary of Passive Fitting					
Data Set	Number of Segments	Average Squared Error			
		MG		TA	
		Long	Short	Long	Short
Long	10	0.0468	0.0541	0.0616	0.0720
Long	20	0.0447	0.0519		
Short	10		0.0522		

Table 5.1: Summary of passive parameter estimation.

when the shortened data set was used to estimate the parameters. Table 5.1 summarizes the passive fitting results. The parameters calculated from the entire data set using ten line segments to describe the passive characteristics was used to determine the active characteristics.

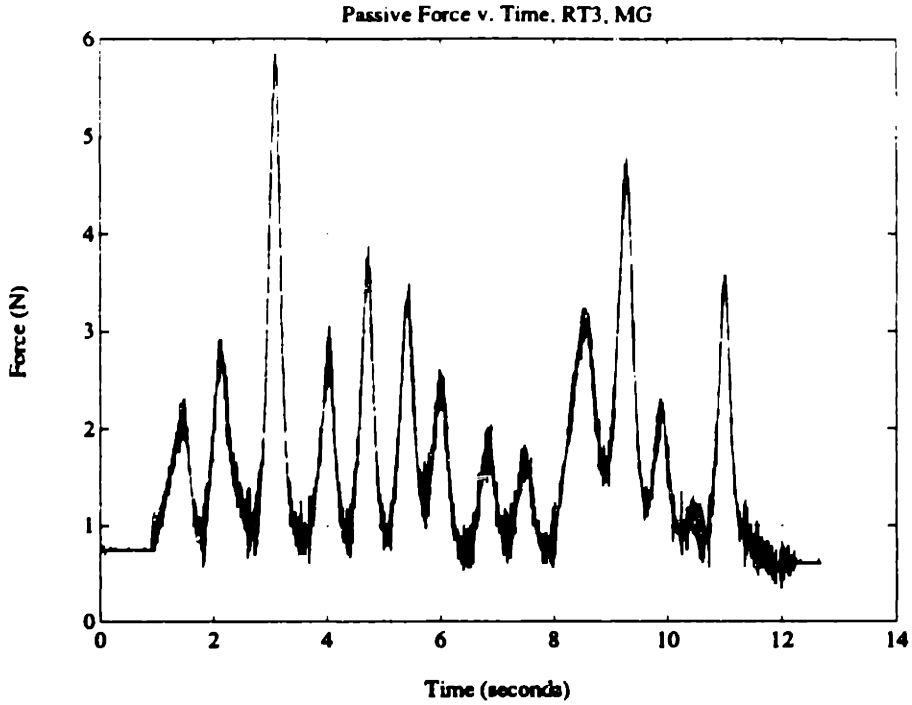

Figure 5.16: Force developed during passive random length trajectory 3, MG.

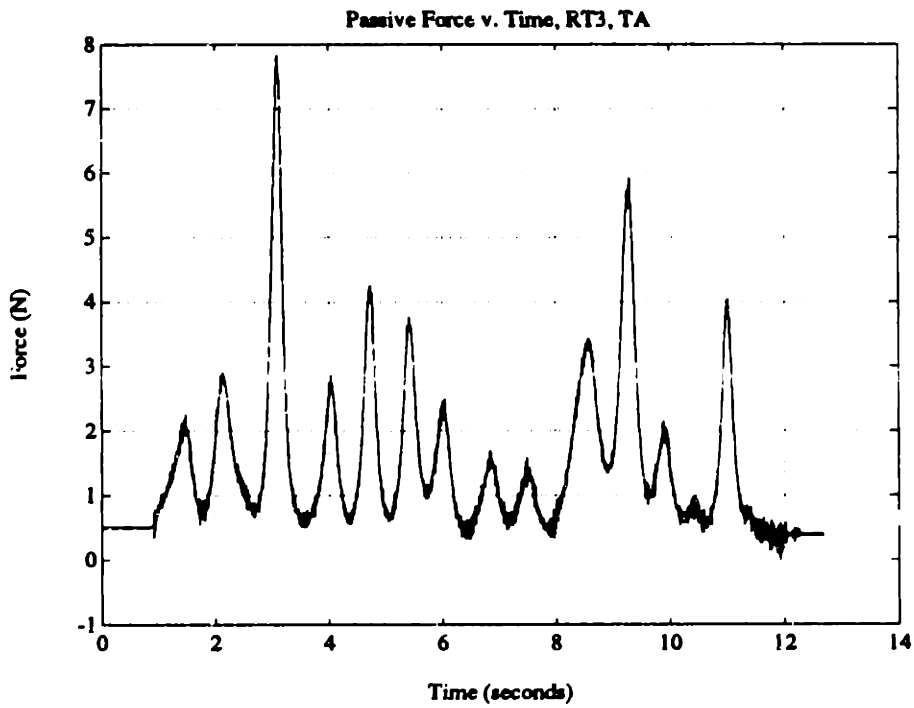

Figure 5.17: Force developed during passive random length trajectory 3, TA.

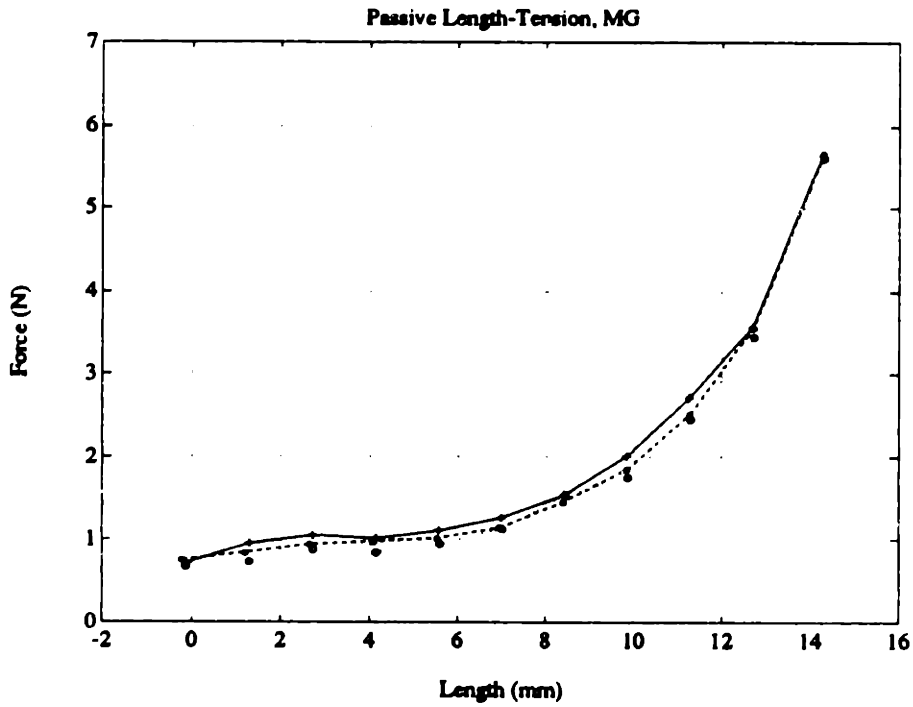

Figure 5.18: Passive length-tension curve for MG, generated by parameter estimation. RT1 (solid,+), RT2 (dashed,*), RT3 (dotted,o).

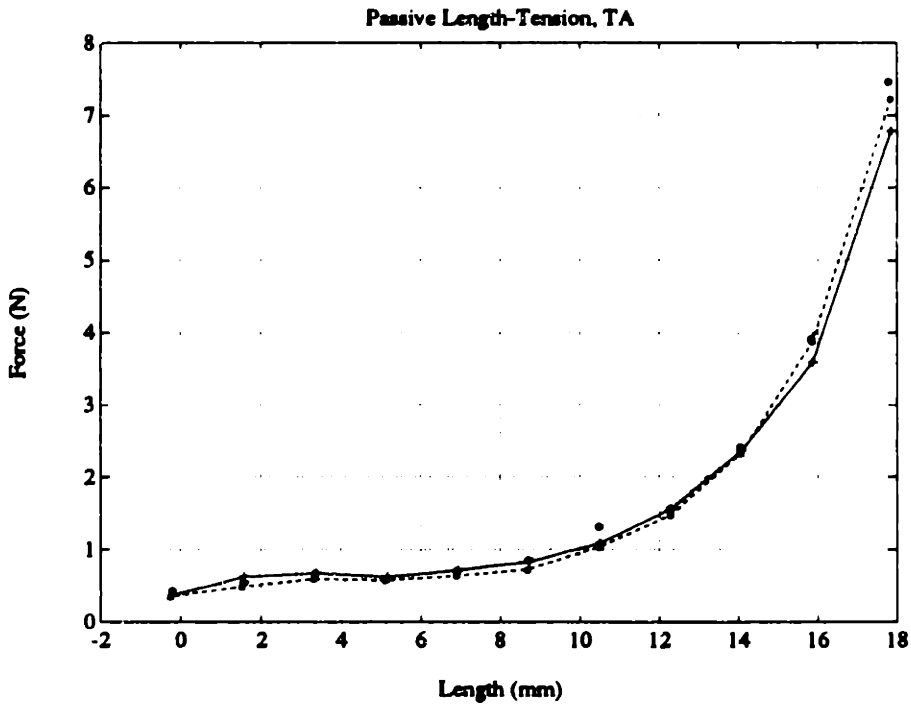

Figure 5.19: Passive length-tension curve for TA, generated by parameter estimation. RT1 (solid,+), RT2 (dashed,*), RT3 (dotted,o).

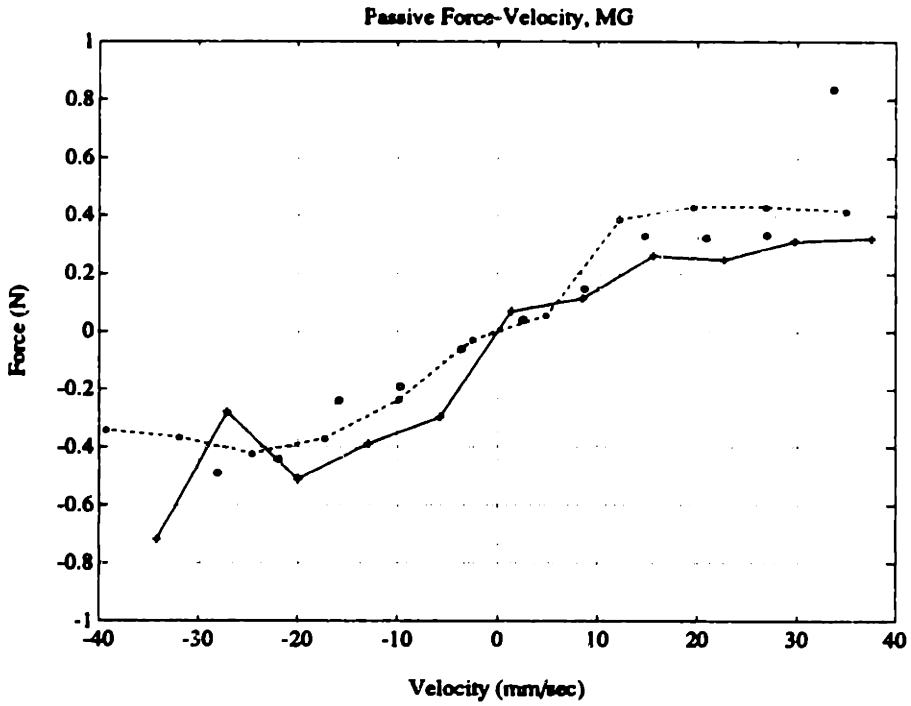

Figure 5.20: Passive force-velocity curve for MG, generated by parameter estimation. RT1 (solid,+), RT2 (dashed,*), RT3 (dotted,o).

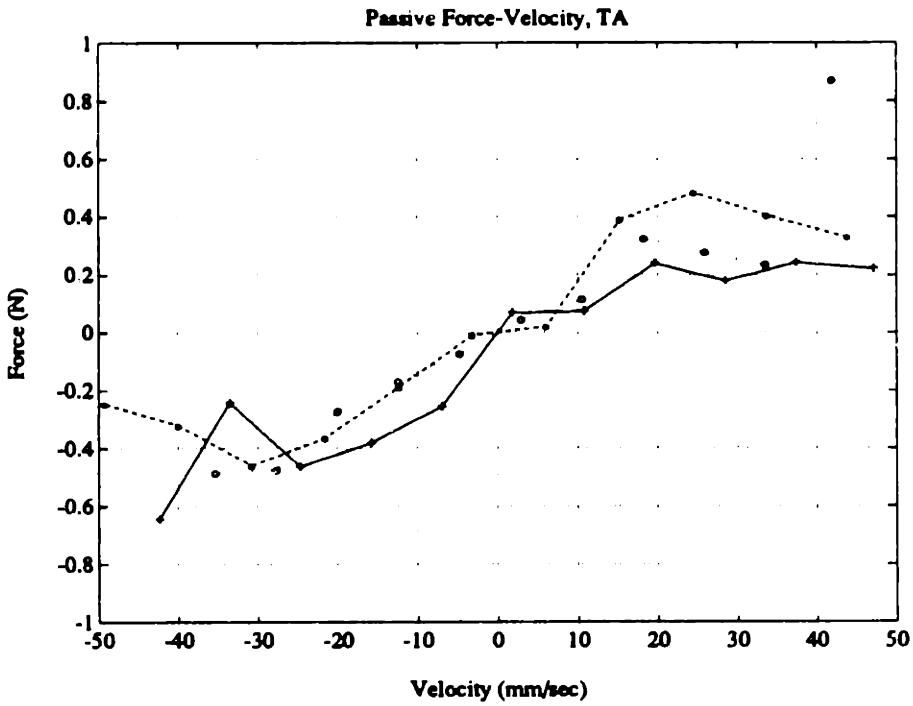

Figure 5.21: Passive force-velocity curve for TA, generated by parameter estimation. RT1 (solid,+), RT2 (dashed,*), RT3 (dotted,o).

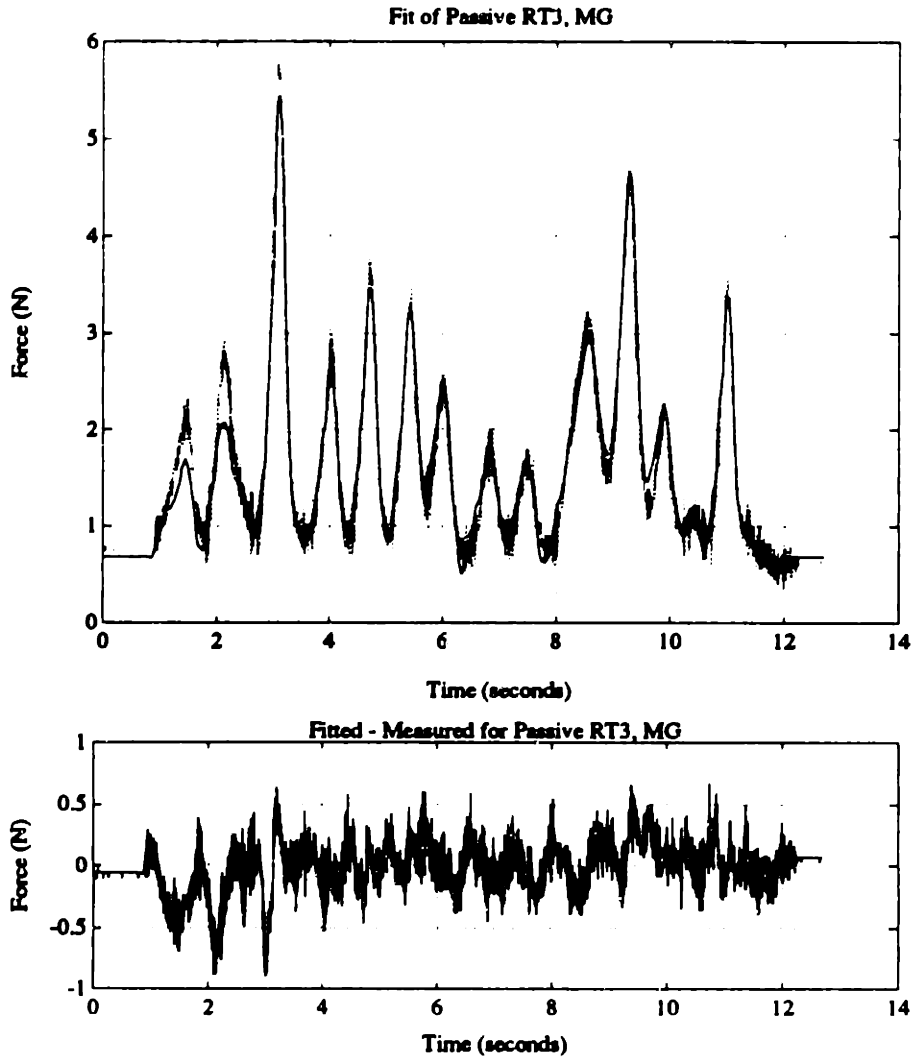

Figure 5.22: Difference between fitted (solid) and measured (dotted) passive force, MG, RT3. Average squared error: 0.0468 for entire data set, 0.0541 for random trajectory.

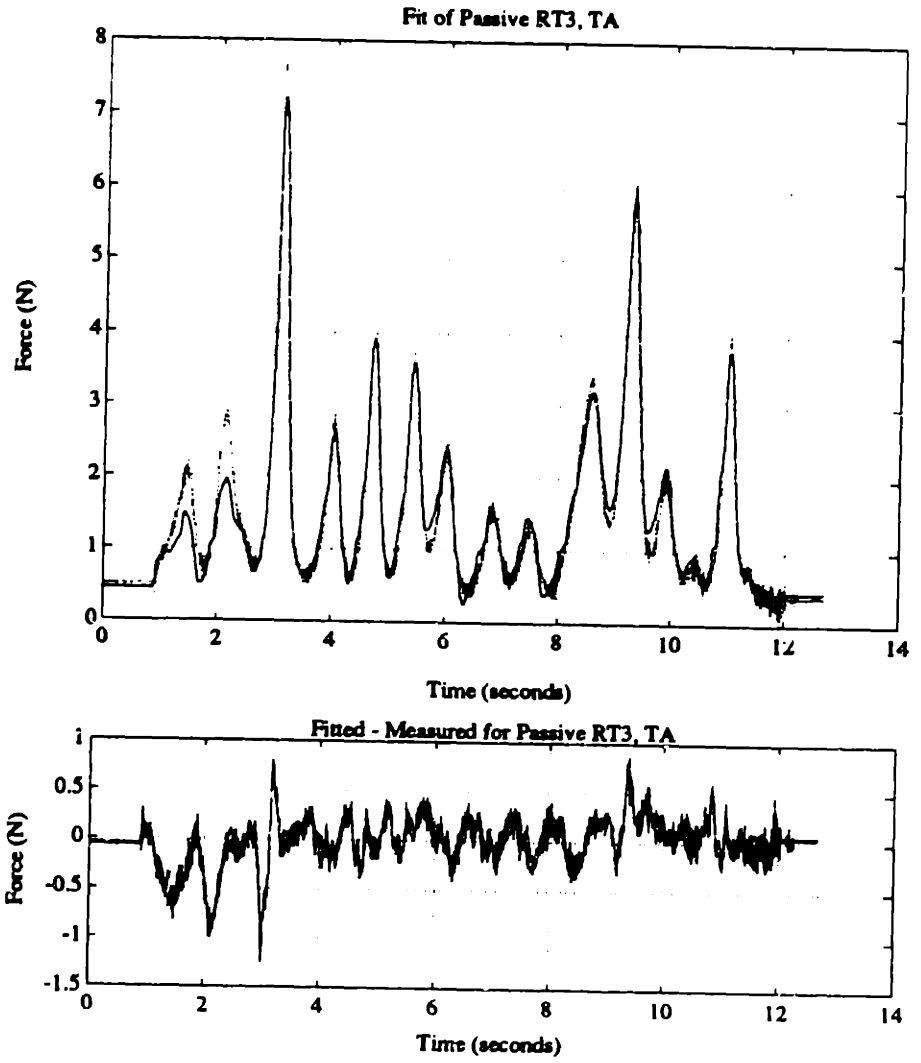

Figure 5.23: Difference between fitted (solid) and measured (dotted) passive force, TA, RT3. Average squared error: 0.0616 for entire data set, 0.0720 for random trajectory.

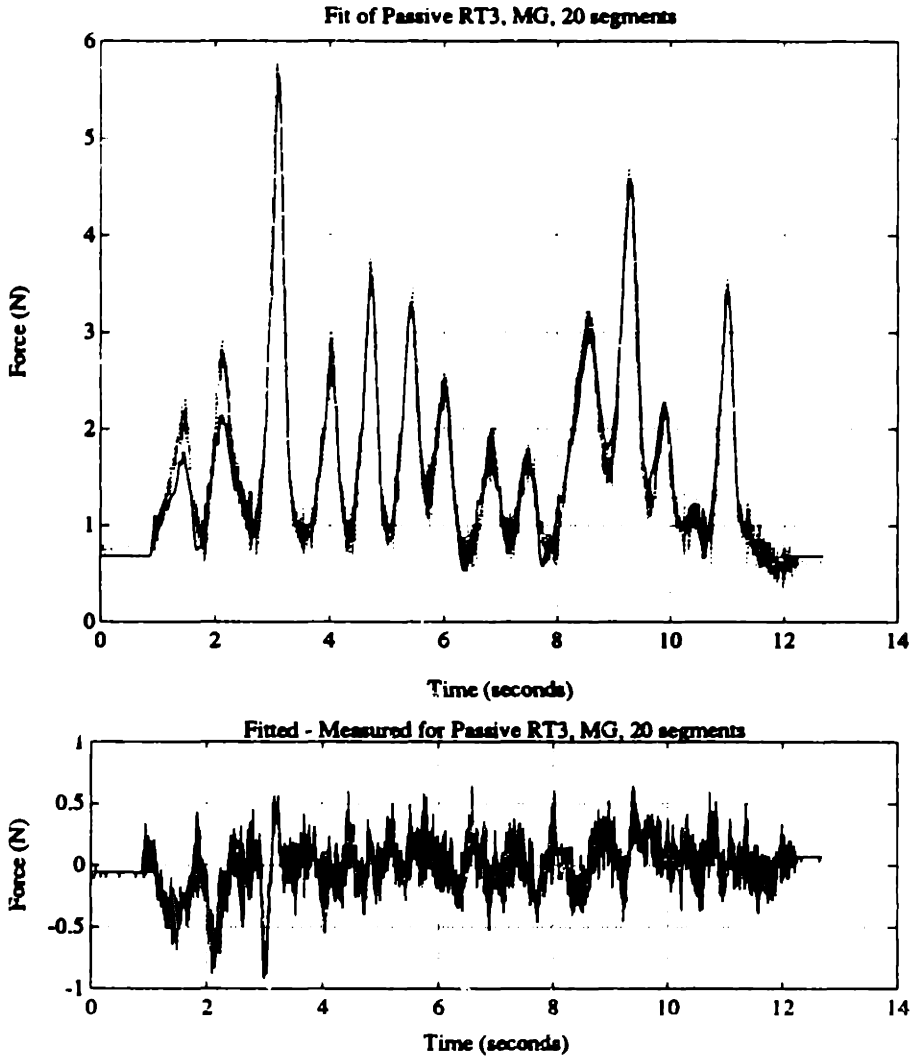

Figure 5.24: Difference between fitted (solid) and measured (dotted) passive force, 20 line segments, MG, RT3. Average squared error: 0.0447 for entire data set, 0.0519 for random trajectory.

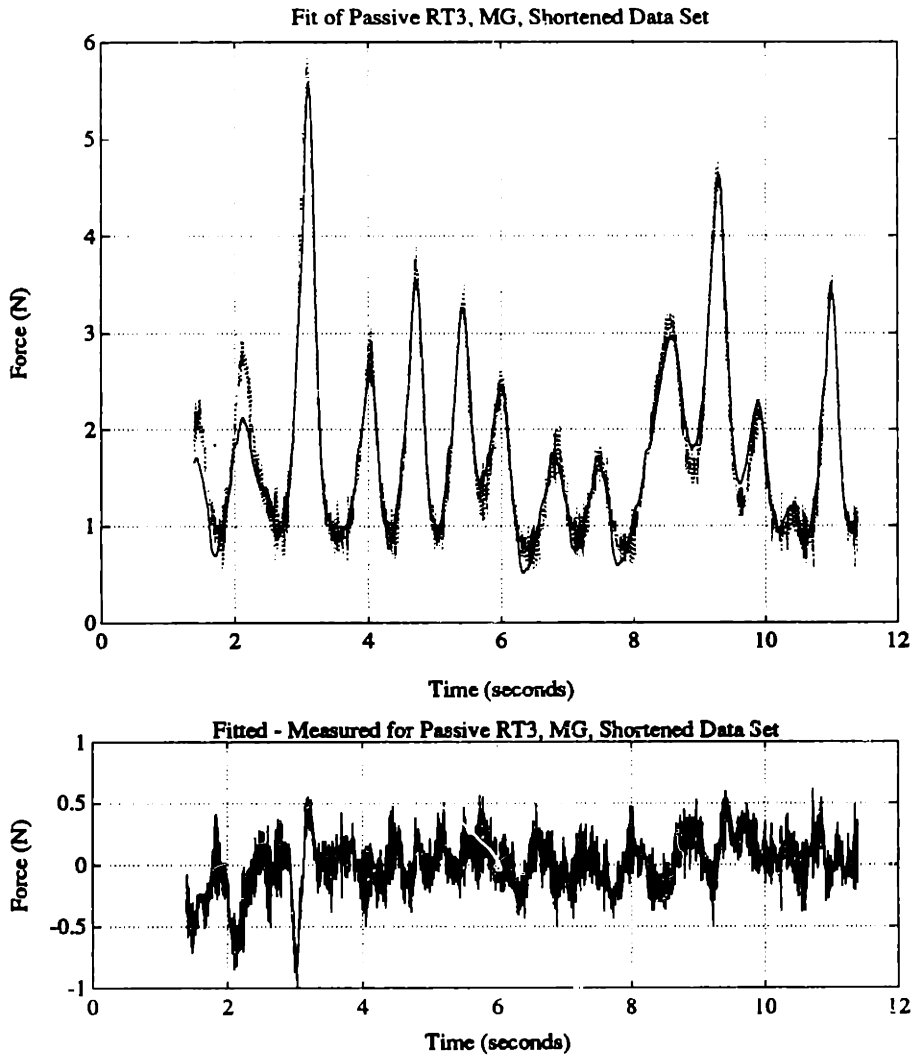

Figure 5.25: Difference between fitted (solid) and measured passive force, shortened data set, MG, RT3. Average squared error: 0.0522 (random trajectory only).

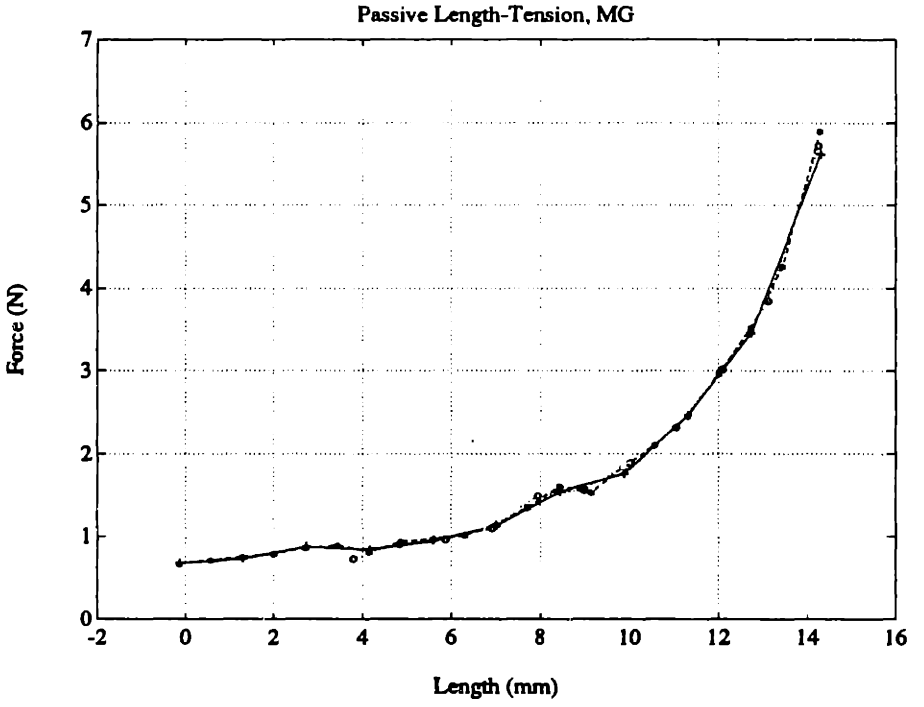

Figure 5.26: Comparison of passive length-tension curves for MG, random trajectory 3. Ten segments (solid,+), twenty segments (dashed,*), short data set (dotted,o).

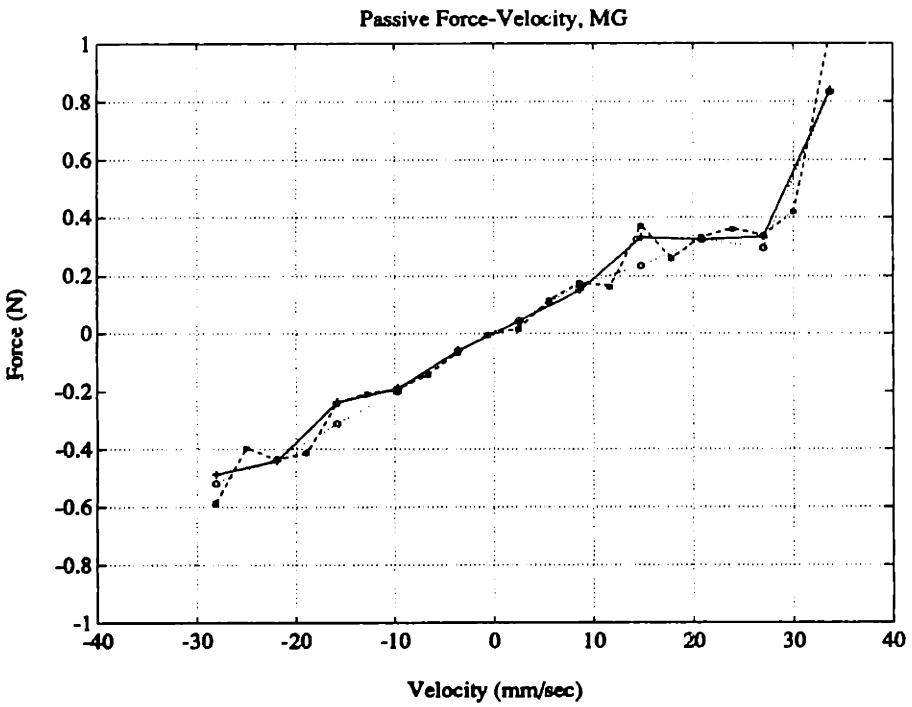

Figure 5.27: Comparison of passive force-velocity curves for MG, random trajectory 3. Ten segments (solid,+), twenty segments (dashed,*), short data set (dotted.o).

5.2.2 Active Dynamics

Parameter estimation of the active dynamics required that the passive dynamics be precomputed since the model defines the total force as the sum of the passive force plus the active force (Equation 2.1). The active force is defined as the product of the activation, a length dependent value, and a velocity dependent value (Equation 2.3). The activation is the stimulation put through the isometric recruitment curve (IRC) and convolved with the impulse response. The IRC was calculated from data generated using the *rstmclen* protocol. The length and force dependent relationships were estimated from data produced by the *cstmrand* protocol.

Stimulation

The data from the *rstmclen* protocol was used to produce the isometric recruitment curve (IRC) which relates the force output to the pulse width (PW) of the stimulation. The muscle was held at a constant length and stimulated with four impulses and a double ramp of the stimulation level. The time constant for the average of the impulse responses was calculated. The force response of the ramp stimulation was deconvolved through the impulse response as explained in Section 3.4.

The upper plots of Figures 5.28 and 5.29 show the shape of the (normalized) recruitment curve measured at different lengths (in relation to instrumentation zero). The lower curves show the peak force generated during the ramp stimulation. These curves were generated between 4:04 and 4:45 pm.

The IRC was measured at several times during the experimental day using the *fastramp* program, a version of the *rstmclen* protocol. The change in shape over time is shown in Figures 5.30 and 5.31. Again, the upper plot is the shape and the lower plot is the maximum force generated during the ramp stimulation.

The *fastramp* recruitment curves were measured at lengths of 8 mm for the MG and 10 mm for the TA. The instrumentation zero changed at 5:01 pm and 10:17 pm, effectively changing the lengths at which the ramp stimulation occurred for both muscles. The tendon clamp for the TA was replaced at 5:01 pm. This resulted in a change in the length of the tendon (less of the tendon was stretching as the muscle contracted since more tendon was in the clamp), as well as a change in the overall length of the muscle.

For estimation of the active length-tension and force-velocity curves, the recruitment curve which was generated closest in time to the data set to be fit was used.

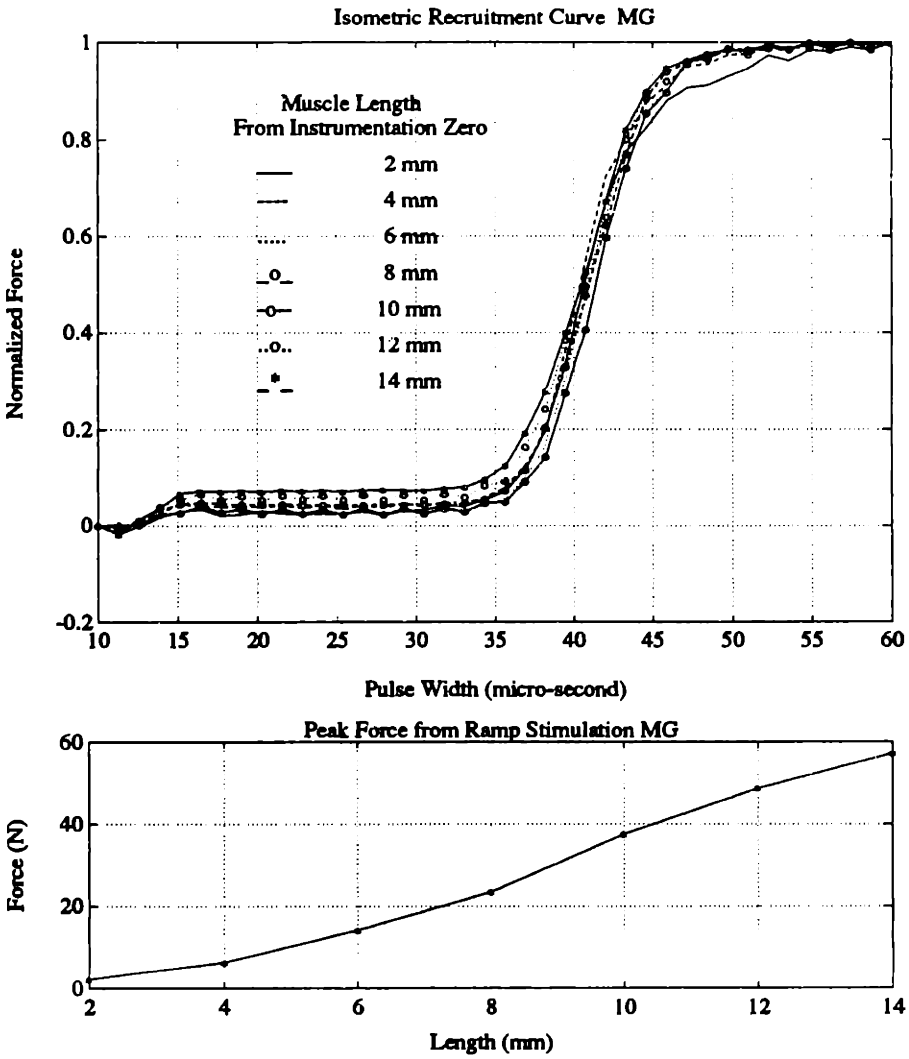

Figure 5.28: Isometric recruitment curve for MG as a function of length

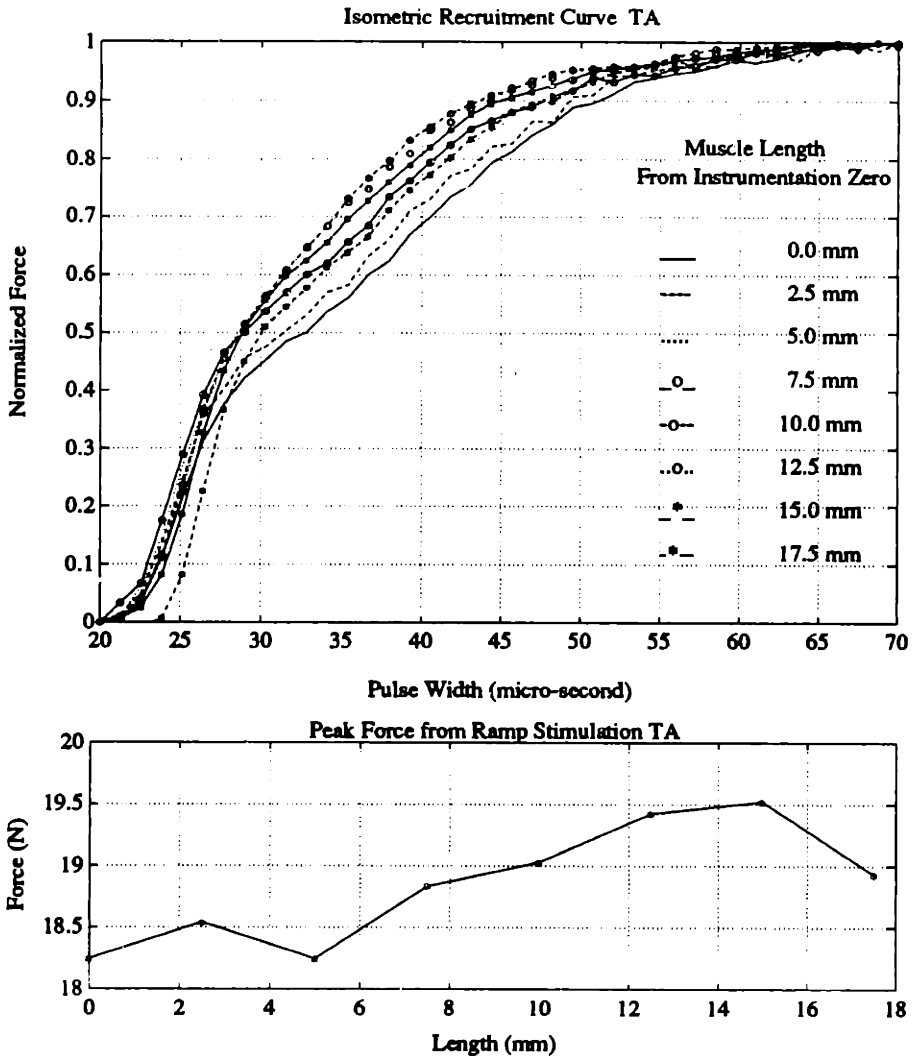

Figure 5.29: Isometric recruitment curve for TA as a function of length

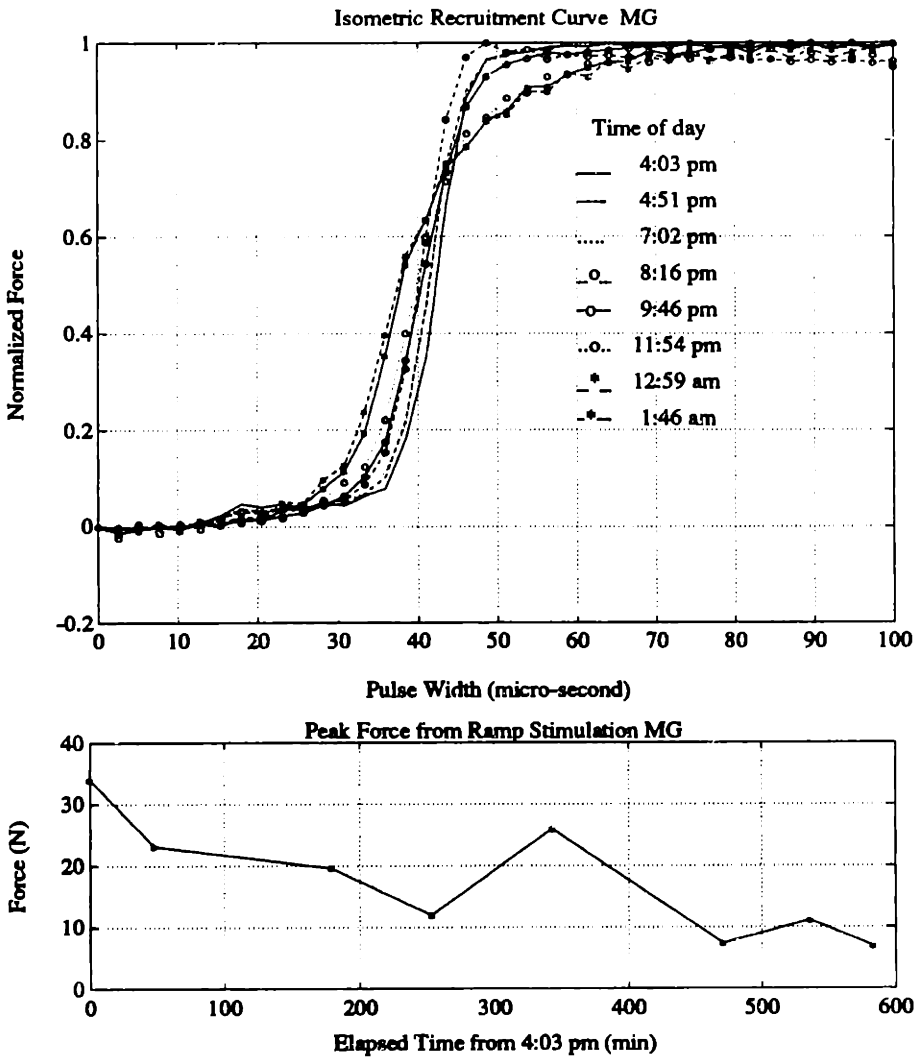

Figure 5.30: Isometric recruitment curve for MG as a function of time.

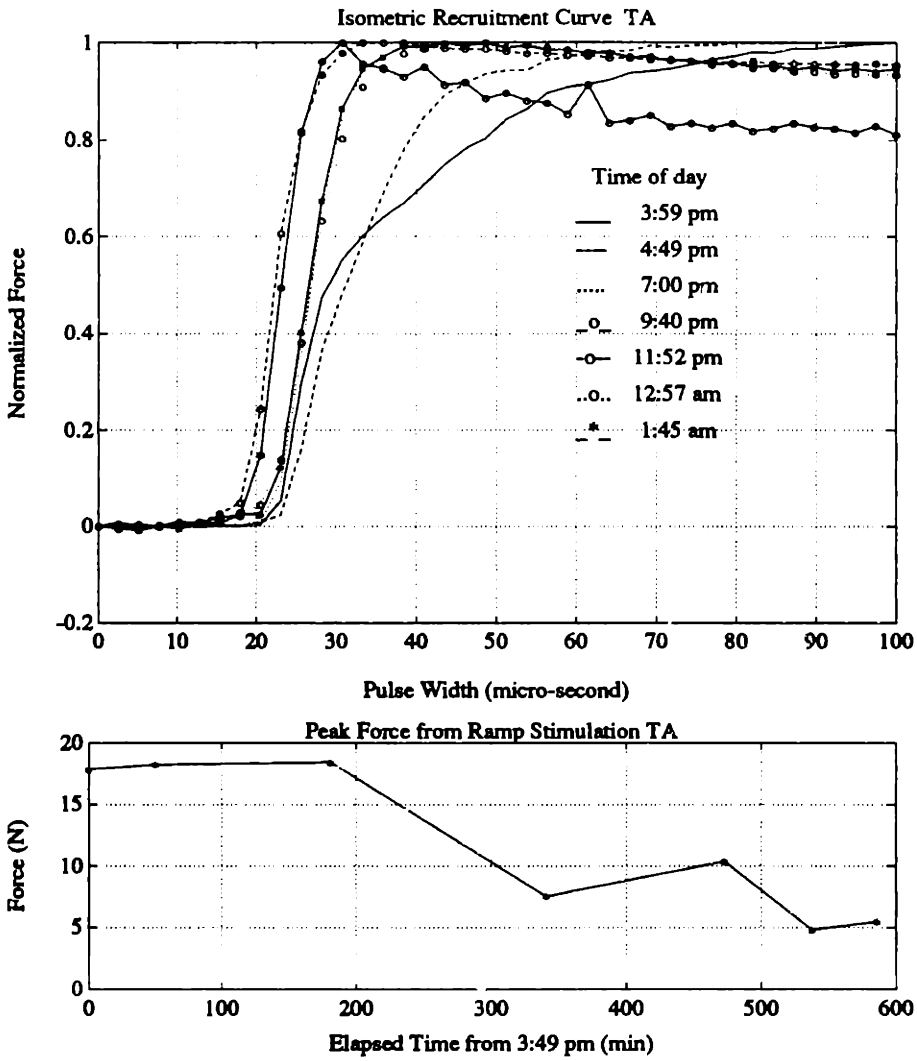

Figure 5.31: Isometric recruitment curve for TA as a function of time.

Length and Velocity Dependence

The *cstmrand* protocol was used to generate data from which the active length-tension and force-velocity relationships could be estimated. Figures 5.32 and 5.33 show the total force produced by the stimulated muscles with the length following random trajectory 3. The stimulation levels were 60 and 35 μs, respectively.

The fitted active length-tension curves are shown in Figures 5.34 and 5.35. Figures 5.36 and 5.37 show the active force-velocity curves. The three curves in each figure were generated by parameter estimation using ten (10) line segments for the active parameters. The contractile element was assumed to be the same length as the total length (compliance of the SE was zero). The parameter estimates for the active length-tension and force-velocity curves are plotted on semi-log scales at the top of each figure. Since the parameter estimation routine adds the logarithm of the force components (Equation 3.19), the linear interpolation between the fitted parameters is done in the logarithmic domain. The lower plot in each figure shows the same curve plotted on linear axes. Note that the straight lines between the data points in these curves are only an approximation to the actual (logarithmically interpolated) values. The force-velocity curve was adjusted so that the force at $v = 0$ was 1.0. The length-tension curve was adjusted so that the force at $l = 10.0$ was 1.0. Random trajectories 1, 2 and 3 produced the solid, dashed, and dot-dash fitted parameters, respectively.

Figures 5.38 and 5.39 show the difference between the measured force and the fitted force for random trajectory 3 (RT3) using the parameters from Figures 5.34–5.37. The averaged sum of the square of the error over the entire data set for RT3 was 15.84 for the MG and 35.29 for the TA. The averaged square of the error for the random portion of the data set ($t = 1.4$ to 11.4) was 13.13 for the MG and 1.67 for the TA.

The error between the measured and the fitted force was reduced by using only the random trajectory portion of the data set for the parameter estimation. Figures 5.40 and 5.41 show the differences between the measured and fitted data for $t = 1.4$ to 11.4 seconds. The average of the square of the errors for RT3 were 9.06 and 1.63, respectively.

Figures 5.42 through 5.45 show the parameter estimates for the three random trajectories using a linear series elastic element with compliance 0.05 mm/N. The entire data set was used to determine these parameters. The difference between the fitted and measured forces for RT3 are shown in Figures 5.46 and 5.47. The averaged sum of the errors for the entire data set were 16.62 and 32.73 for the MG and TA. For the random part of the data set, the errors were 13.70 and 2.11, respectively.

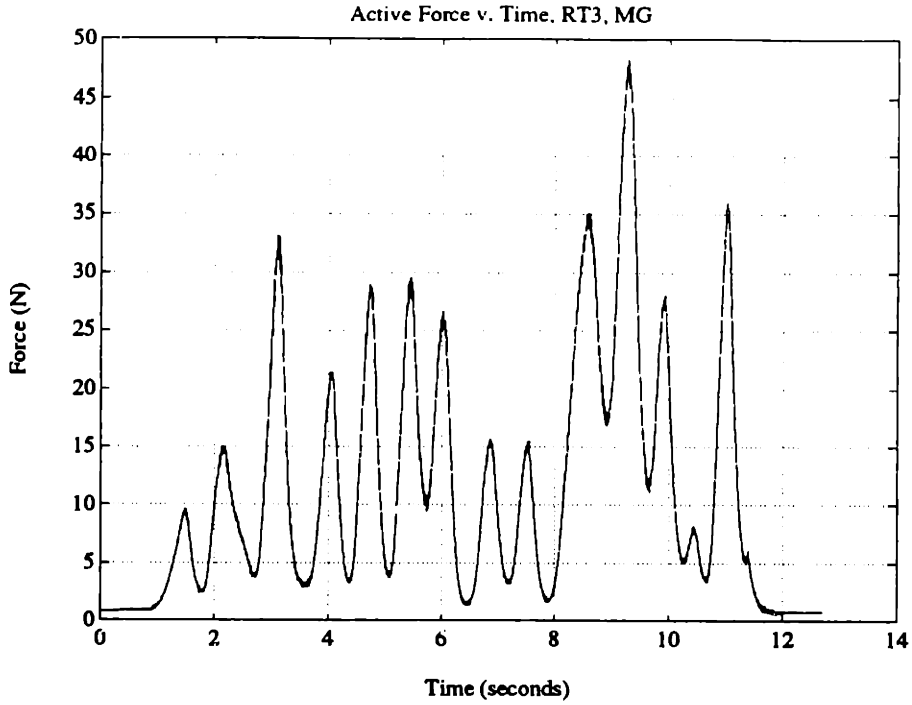

Figure 5.32: Force developed during active RT3, MG, stimulation level 60 μs.

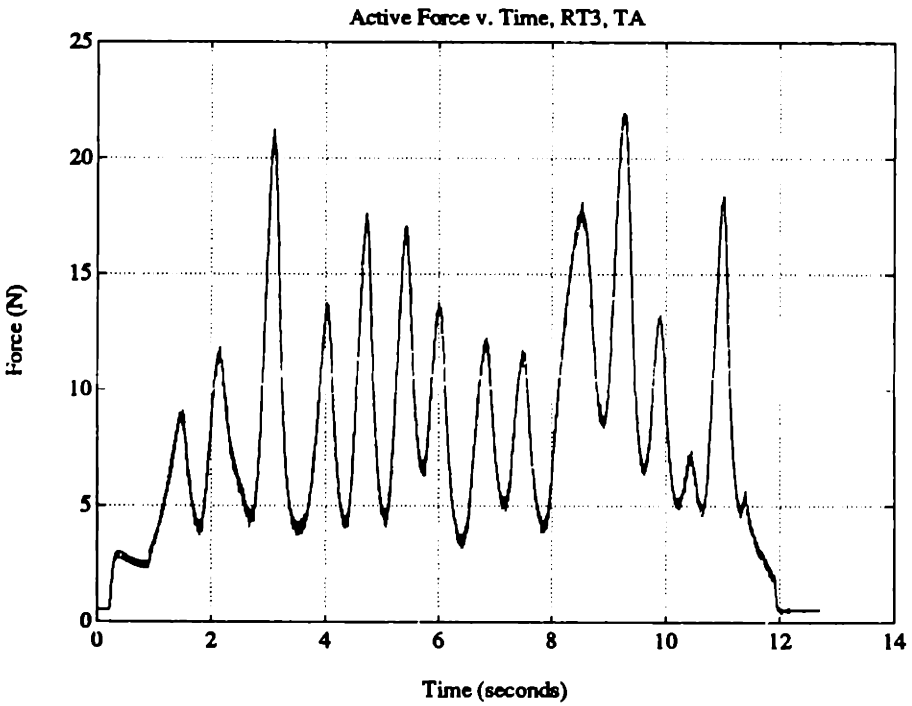

Figure 5.33: Force developed during active RT3, TA, stimulation level 35 μs.

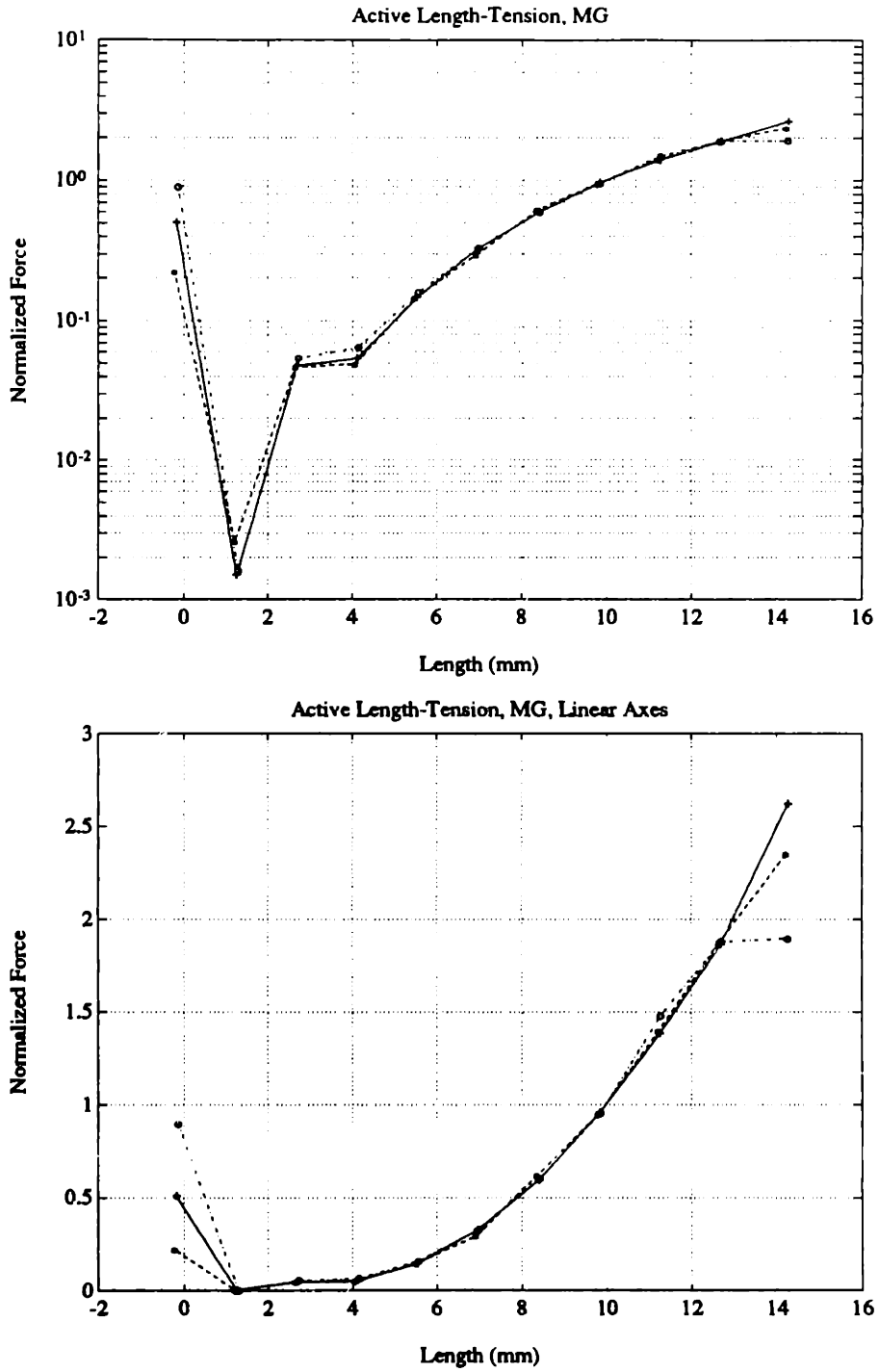

Figure 5.34: Active length-tension curve for MG, generated by parameter estimation. Full data set, 10 line segments, no series compliance. RT1 (solid,+), RT2 (dashed,*), RT3 (dotted,o). Semi-log scale, top, linear scale, bottom.

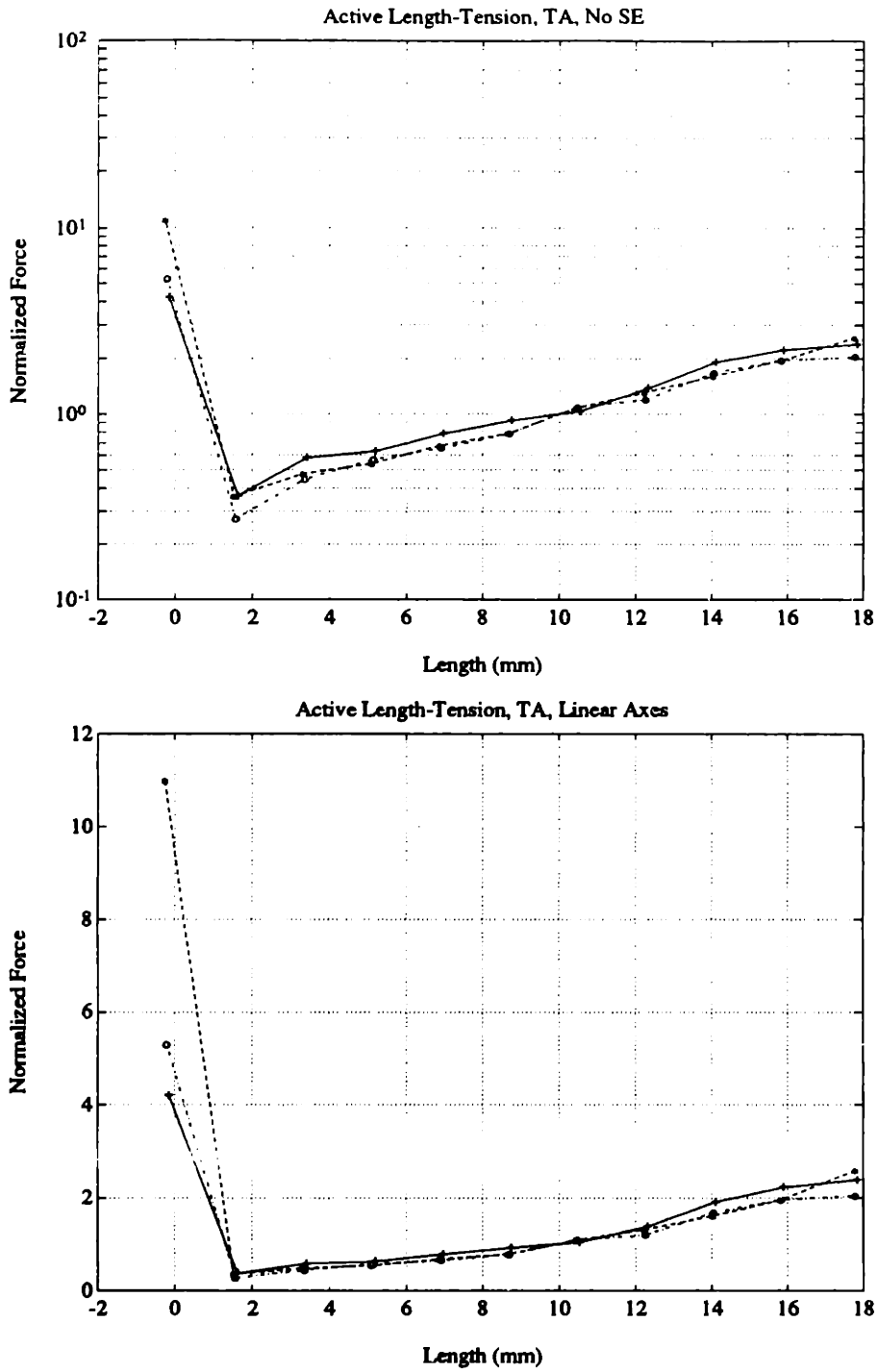

Figure 5.35: Active length-tension curve for TA, generated by parameter estimation. Full data set, 10 line segments, no series compliance. RT1 (solid,+), RT2 (dashed,*), RT3 (dotted,o). Semi-log scale, top, linear scale, bottom.

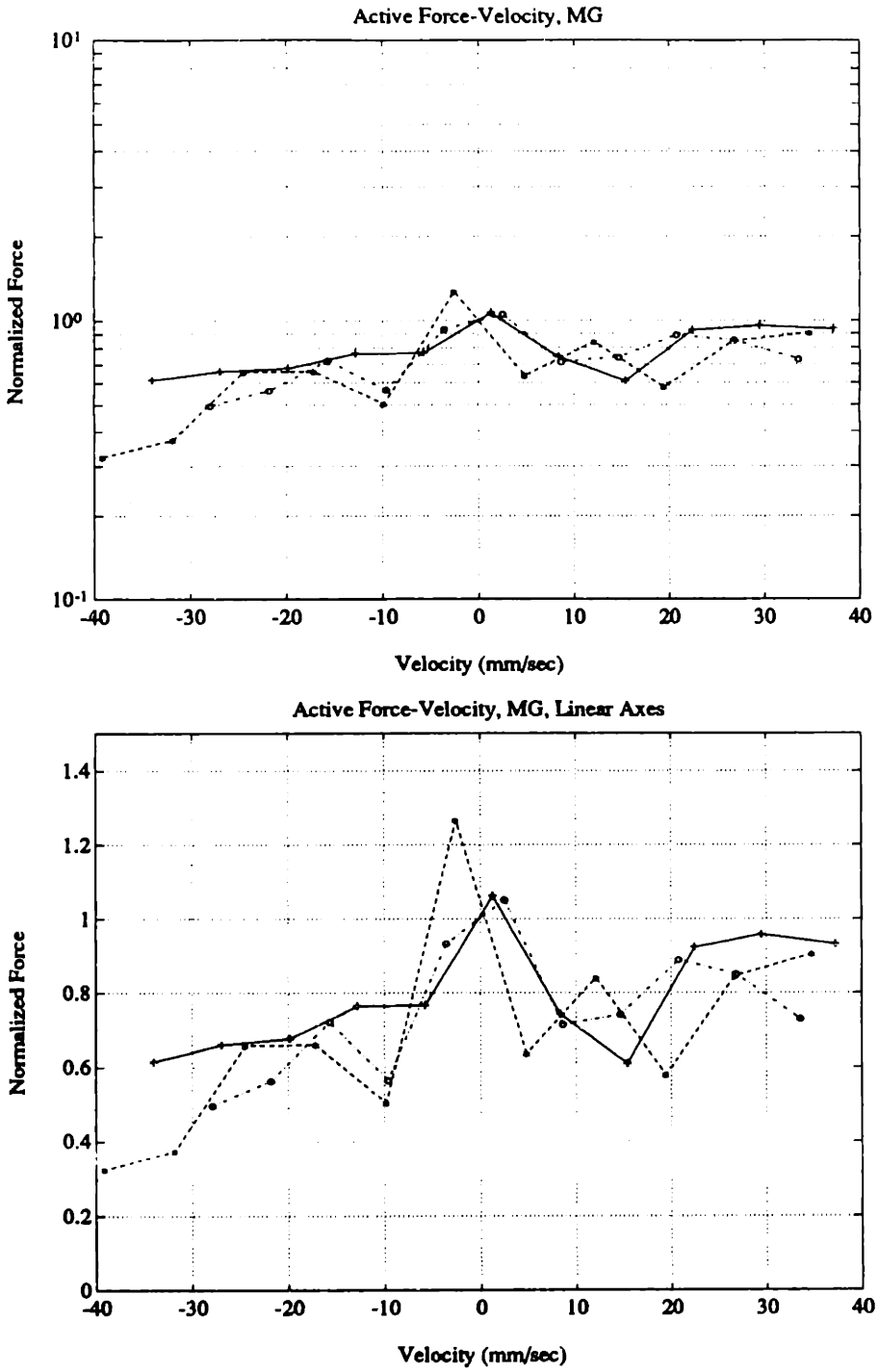

Figure 5.36: Active force-velocity curve for MG, generated by parameter estimation. Full data set, 10 line segments, no series compliance. RT1 (solid,+), RT2 (dashed,*), RT3 (dotted,o). Semi-log scale, top, linear scale, bottom.

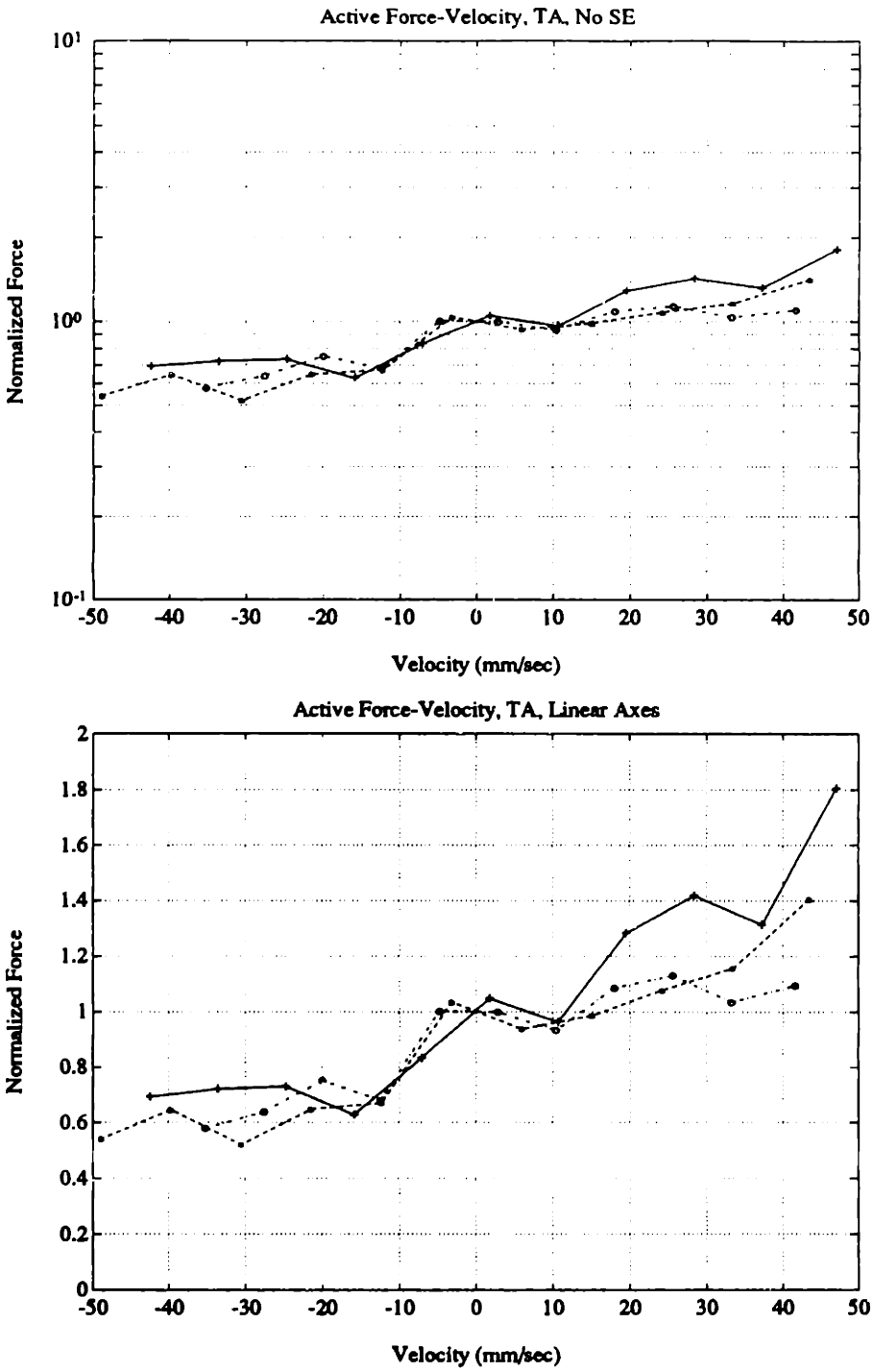

Figure 5.37: Active force-velocity curve for TA, generated by parameter estimation. Full data set, 10 line segments, no series compliance. RT1 (solid,+), RT2 (dashed,*), RT3 (dotted,o). Semi-log scale, top, linear scale, bottom.

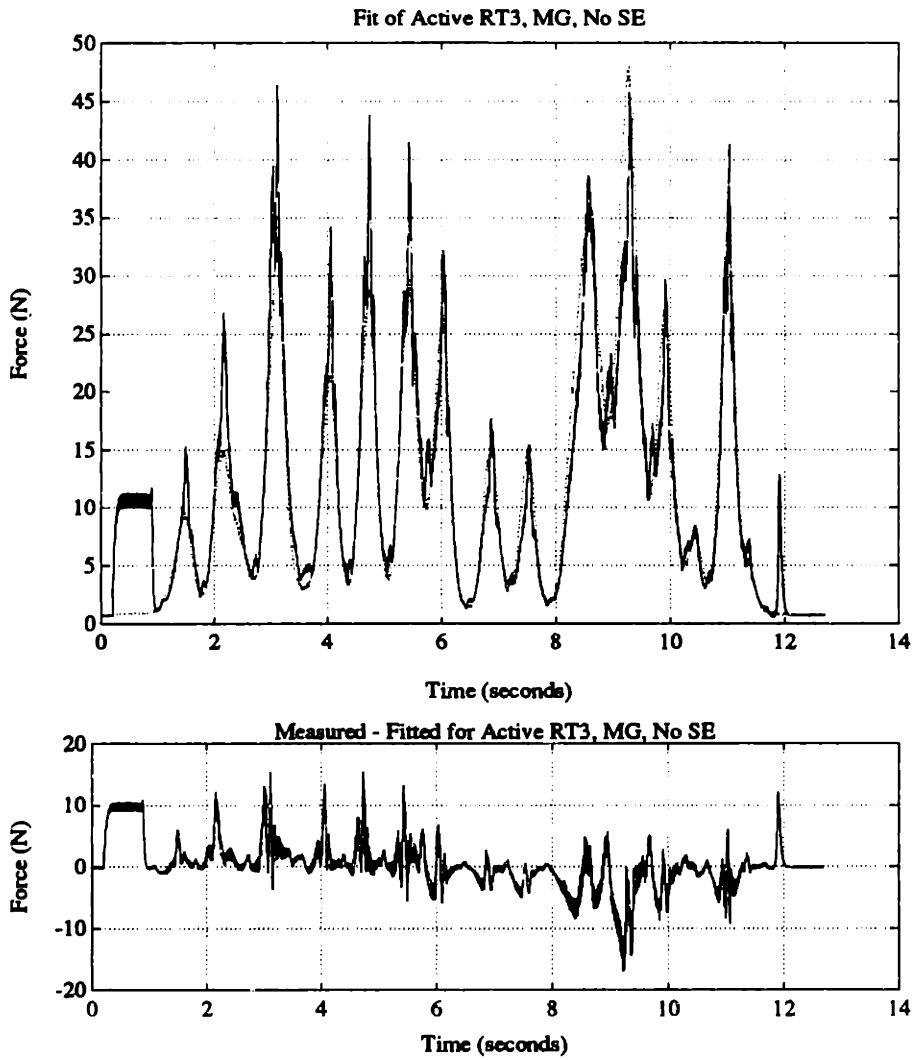

Figure 5.38: Difference between fitted (solid) and measured (dotted) active force, no compliance in series element, MG, RT3. Average squared error: 15.84 for entire data set, 13.13 for random trajectory.

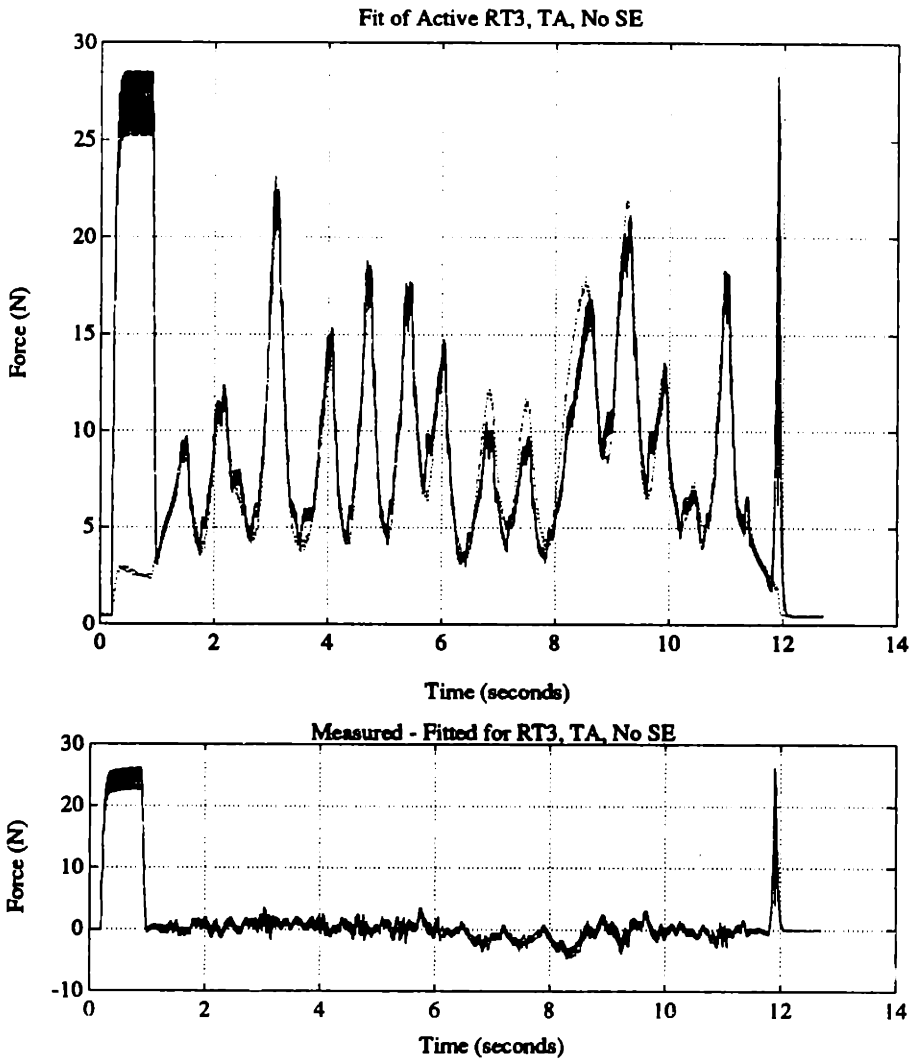

Figure 5.39: Difference between fitted (solid) and measured (dotted) active force, no compliance in series element, TA, RT3. Average squared error: 35.29 for entire data set, 1.67 for random trajectory.

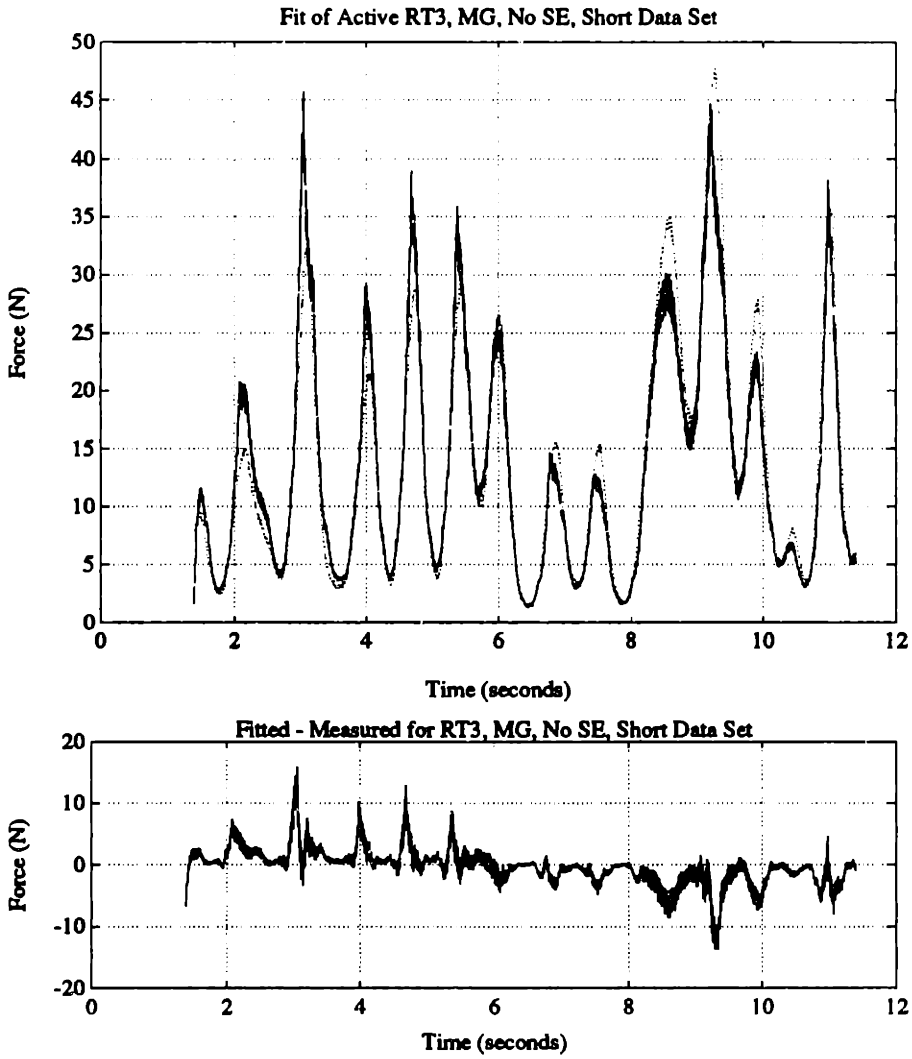

Figure 5.40: Difference between fitted (solid) and measured (dotted) active force, no series element compliance, shortened data set, MG, RT3. Average squared error: 9.06 (random trajectory only).

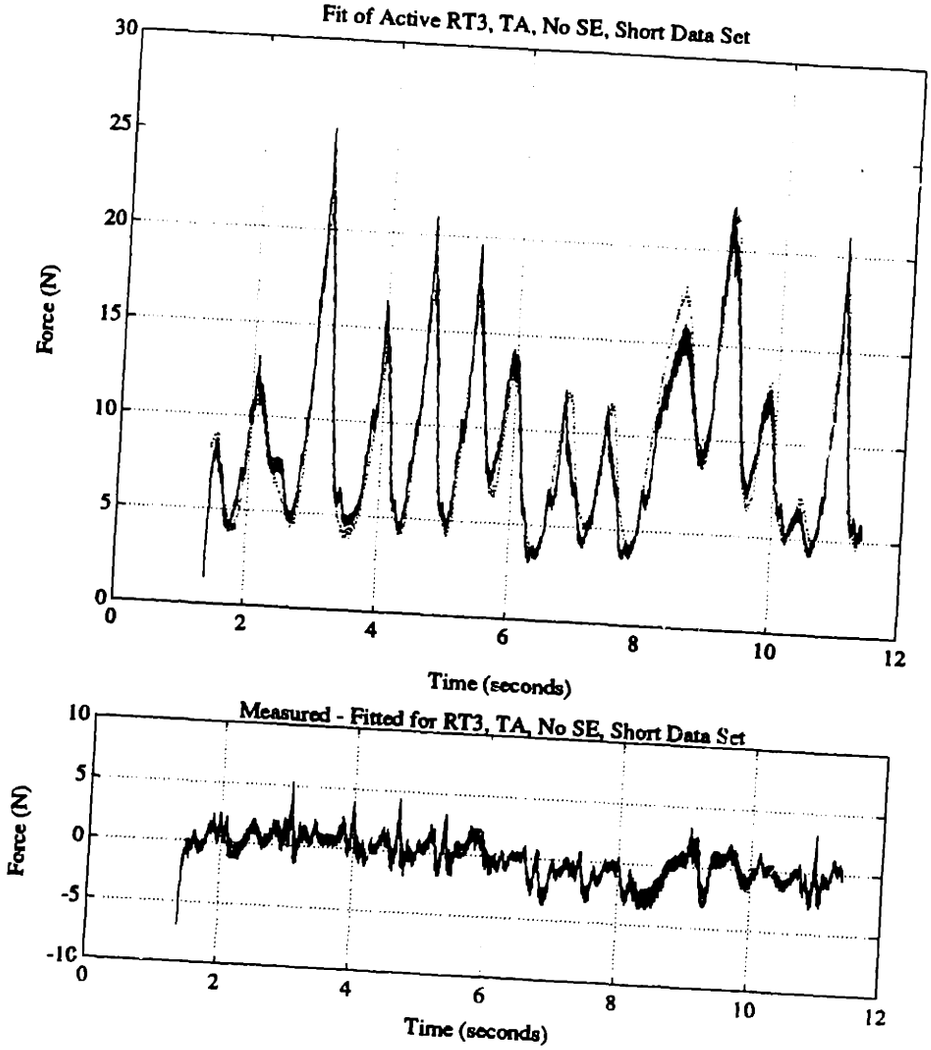

Figure 5.41: Difference between fitted (solid) and measured (dotted) active force, no series element compliance, shortened data set, TA, RT3. Average squared error: 1.63 (random trajectory only).

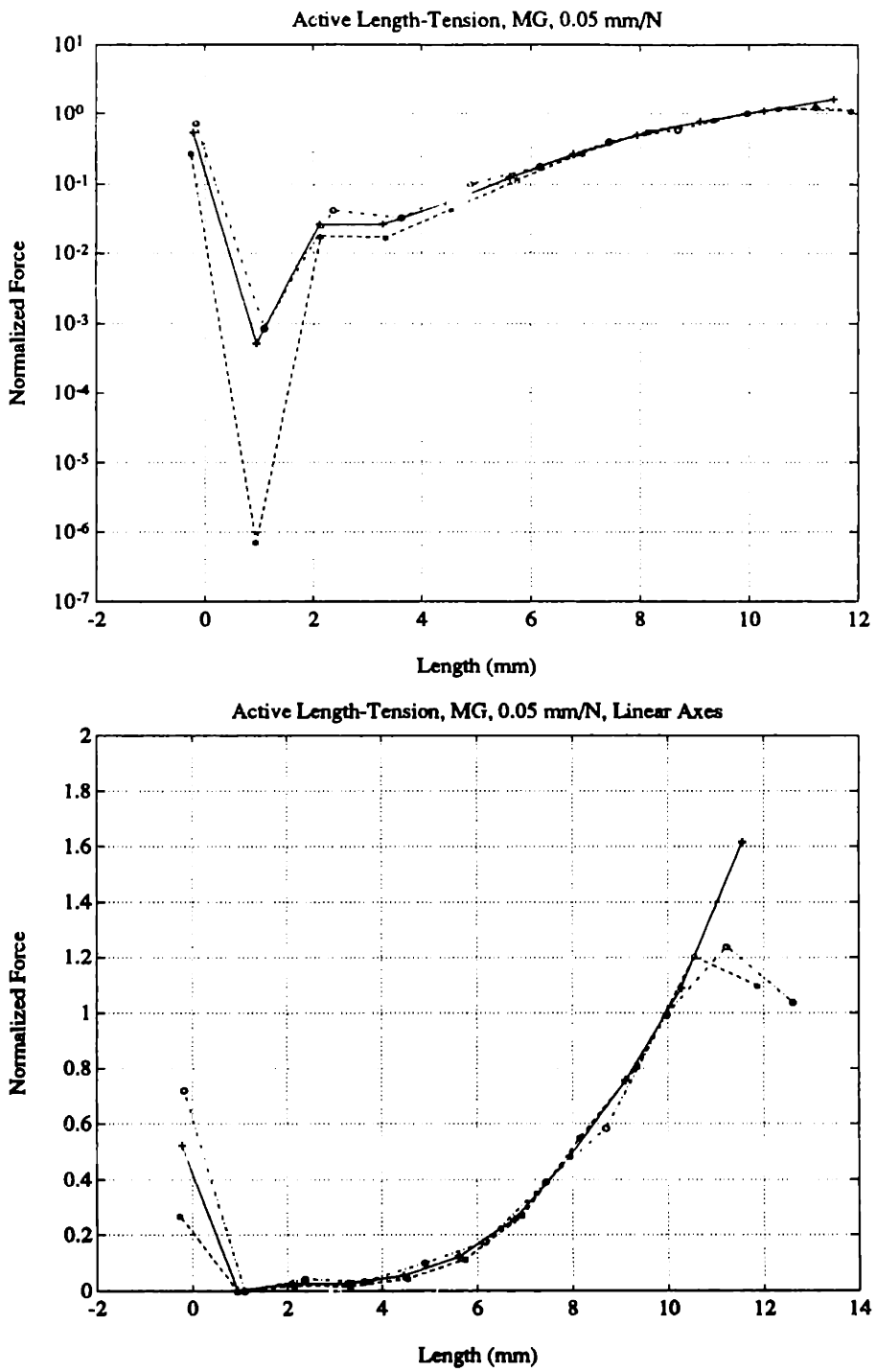

Figure 5.42: Active length-tension curve for MG, generated by parameter estimation, 0.05 mm/N compliance in series element, full data set, 10 line segments. RT1 (solid,+), RT2 (dashed,*), RT3 (dotted,o). Semi-log scale, top, linear scale, bottom.

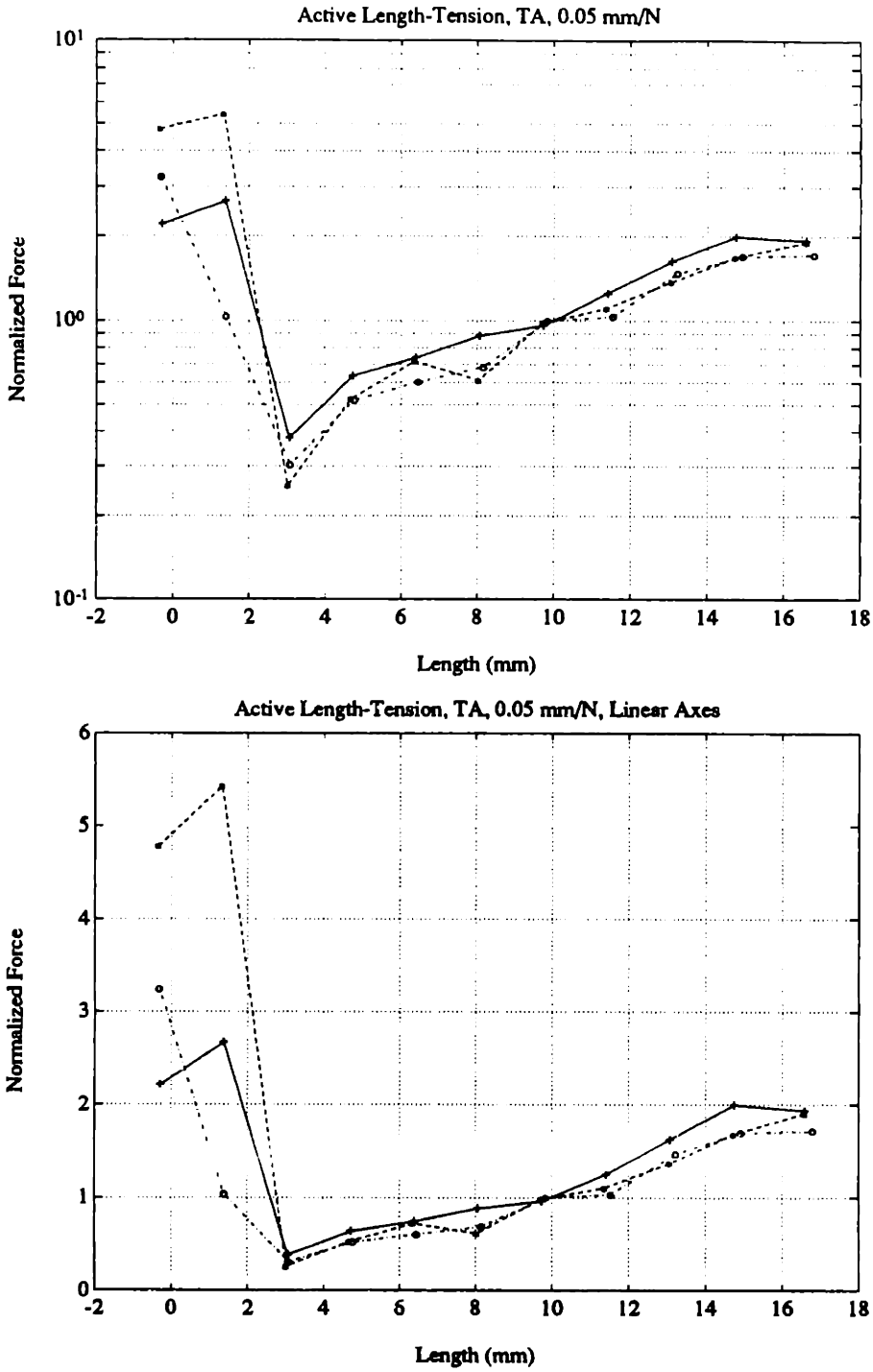

Figure 5.43: Active length-tension curve for TA, generated by parameter estimation, 0.05 mm/N compliance in series element, full data set, 10 line segments. RT1 (solid,+), RT2 (dashed,*), RT3 (dotted,o). Semi-log scale, top, linear scale, bottom.

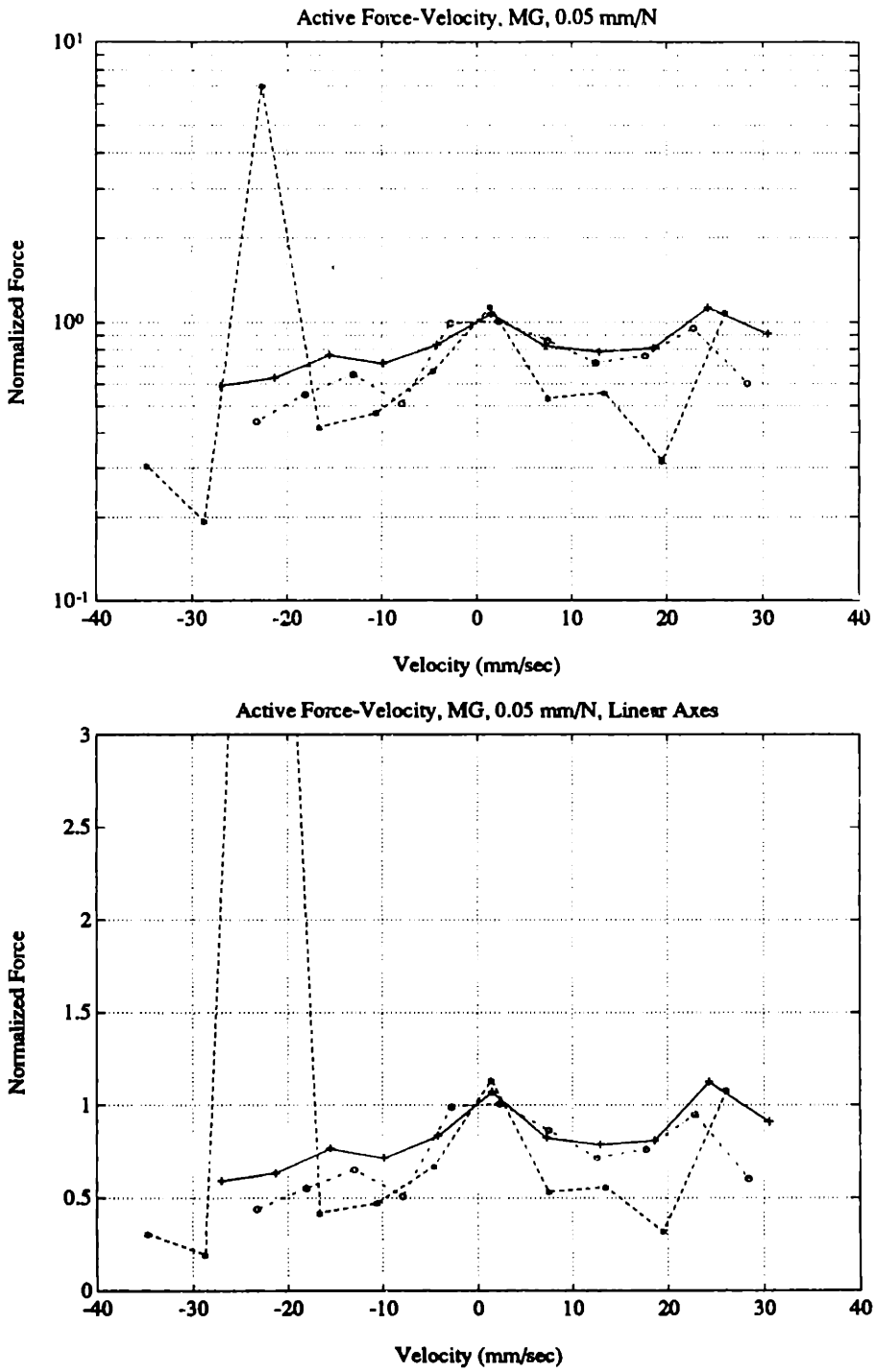

Figure 5.44: Active force-velocity curve for MG, generated by parameter estimation, 0.05 mm/N compliance in series element, full data set, 10 line segments. RT1 (solid,+), RT2 (dashed,*), RT3 (dotted,o). Semi-log scale, top, linear scale, bottom.

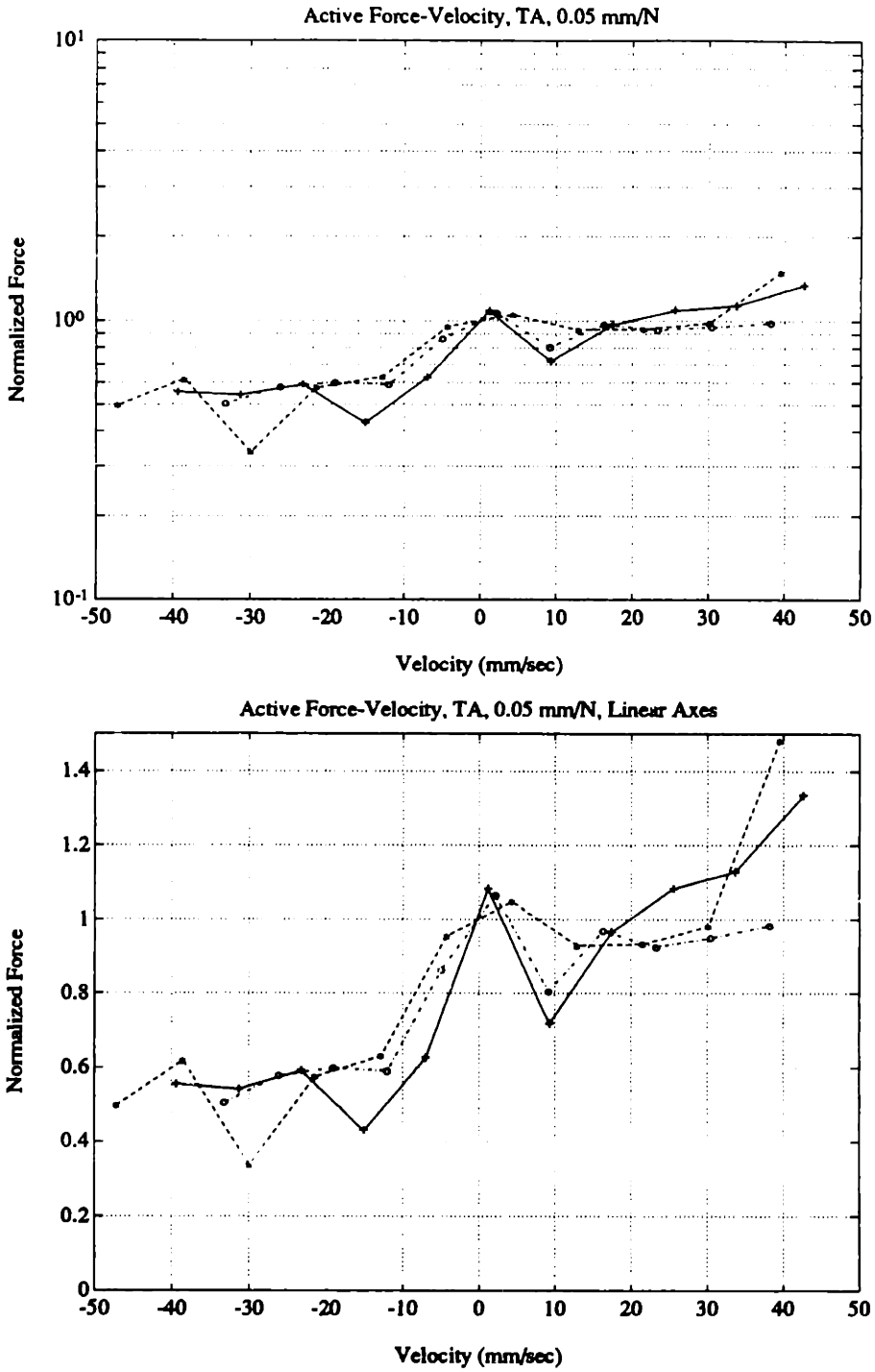

Figure 5.45: Active force-velocity curve for TA, generated by parameter estimation, 0.05 mm/N compliance in series element, full data set, 10 line segments. RT1 (solid,+), RT2 (dashed,*), RT3 (dotted,o). Semi-log scale, top, linear scale, bottom.

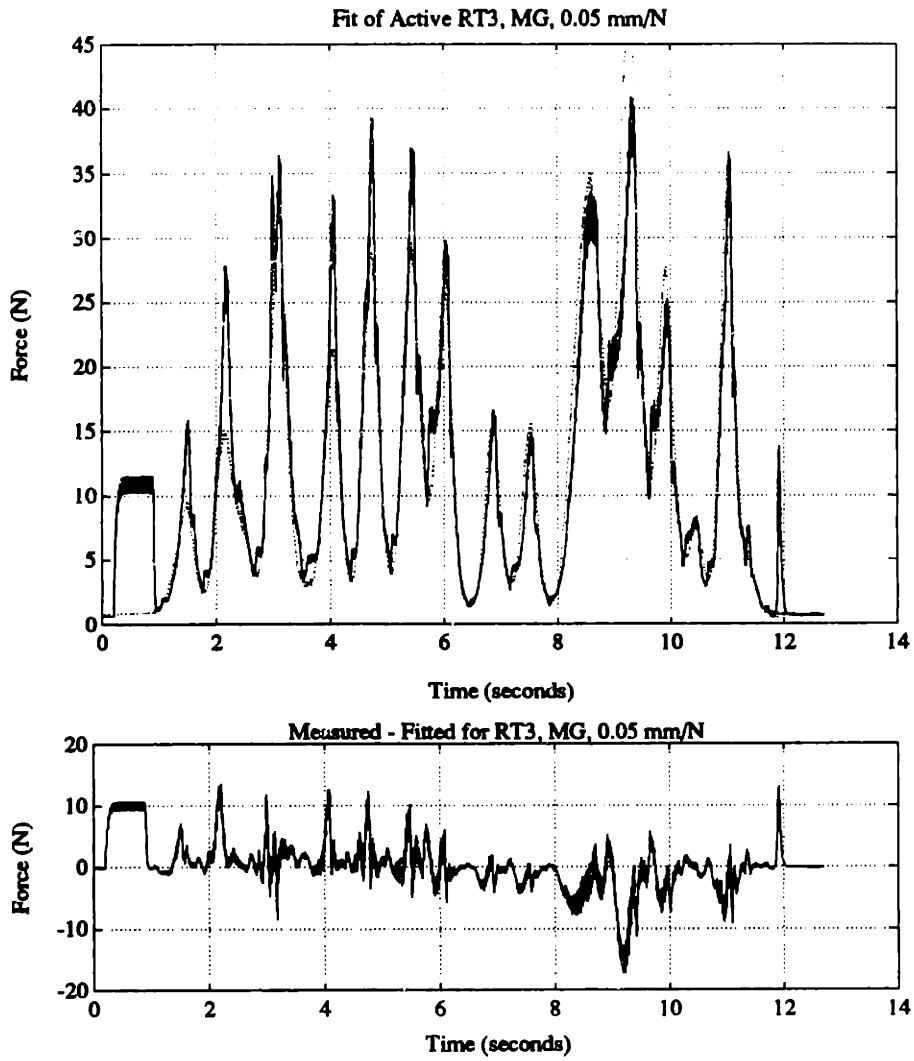

Figure 5.46: Difference between fitted (solid) and measured (dotted) active force, 0.05 mm/N compliance in series element, full data set, MG, RT3. Average squared error 16.62 for entire data set, 13.70 for random trajectory.

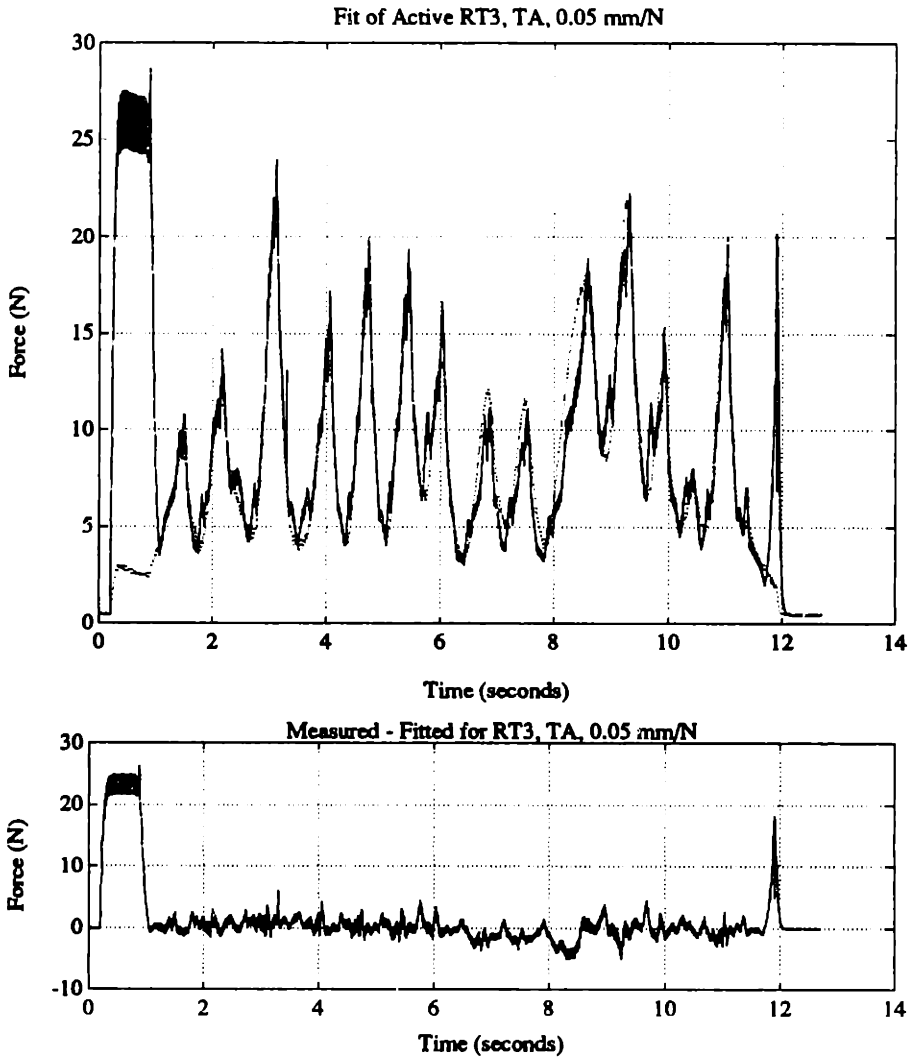

Figure 5.47: Difference between fitted (solid) and measured (dotted) active force, 0.05 mm/N compliance in series element, full data set, TA, RT3. Average squared error 32.73 for entire data set, 2.11 for random trajectory.

Summary of Active Fitting								
Line Type	Line Marker	Data Set	Compliance of SE	Impulse Response	Average Squared Error			
					MG		TA	
					Long	Short	Long	Short
Solid	+	Long	0	Yes	15.84	13.13	35.29	1.67
Solid	*	Short	0	Yes		9.06		1.63
Dashed	*	Long	0.05	Yes	16.62	13.70	32.73	2.11
Broken	o	Short	0.05	Yes		11.86		1.65
Dashed	+	Short	0	No		8.54		1.32

Table 5.2: Summary of active parameter estimation.

Using only the random portion of the trajectories (from t = 1.4 to 11.4 seconds), and the series element with compliance 0.05 mm/N produced the fitted parameters shown in Figures 5.48 through 5.51. Figures 5.52 and 5.53 show the fitted force. The averaged sum of the square of the error was 11.86 for the MG and 1.65 for the TA.

Figures 5.54 and 5.55 show the results of parameter estimation without using the impulse response. The stimulation was passed through the IRC to produce the pseudo-activation. (For all of the preceding active fits, the stimulation was passed through the IRC then convolved with the impulse response to produce the activation.) The errors for this case were 8.54 and 1.32 for the random trajectory.

Figures 5.56 through 5.59 show a summary of the parameters for RT3 presented in this section. The key to the line types for these figures is given in Table 5.2. On the linear scale, the straight lines between the points are approximations — the fitting algorithm used straight lines on the logarithmic axes.

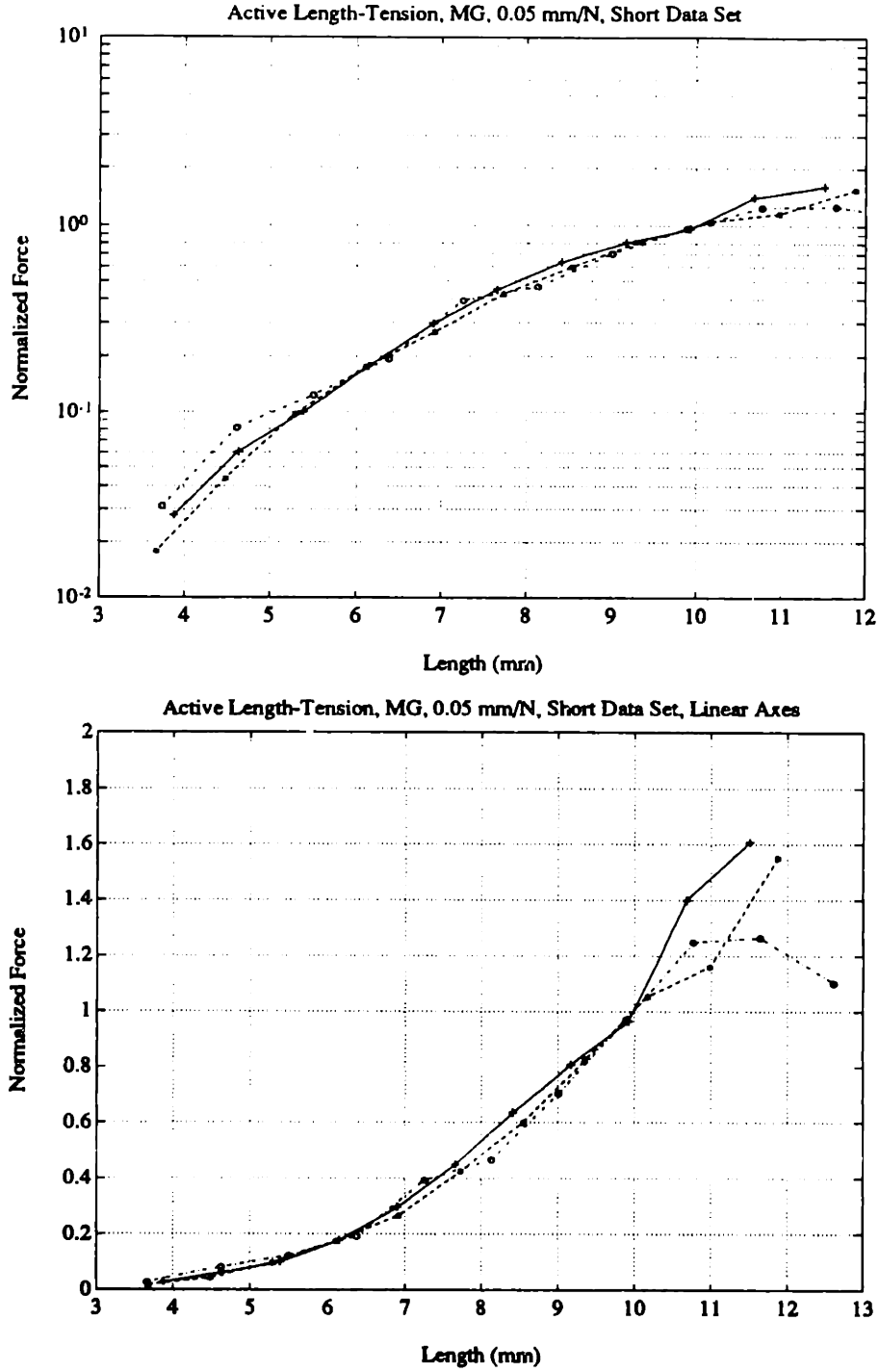

Figure 5.48: Active length-tension curve for MG, generated by parameter estimation, 0.05 mm/N compliance in series element, shortened data set, 10 line segments. RT1 (solid,+), RT2 (dashed,*), RT3 (dotted,o). Semi-log scale, top, linear scale, bottom.

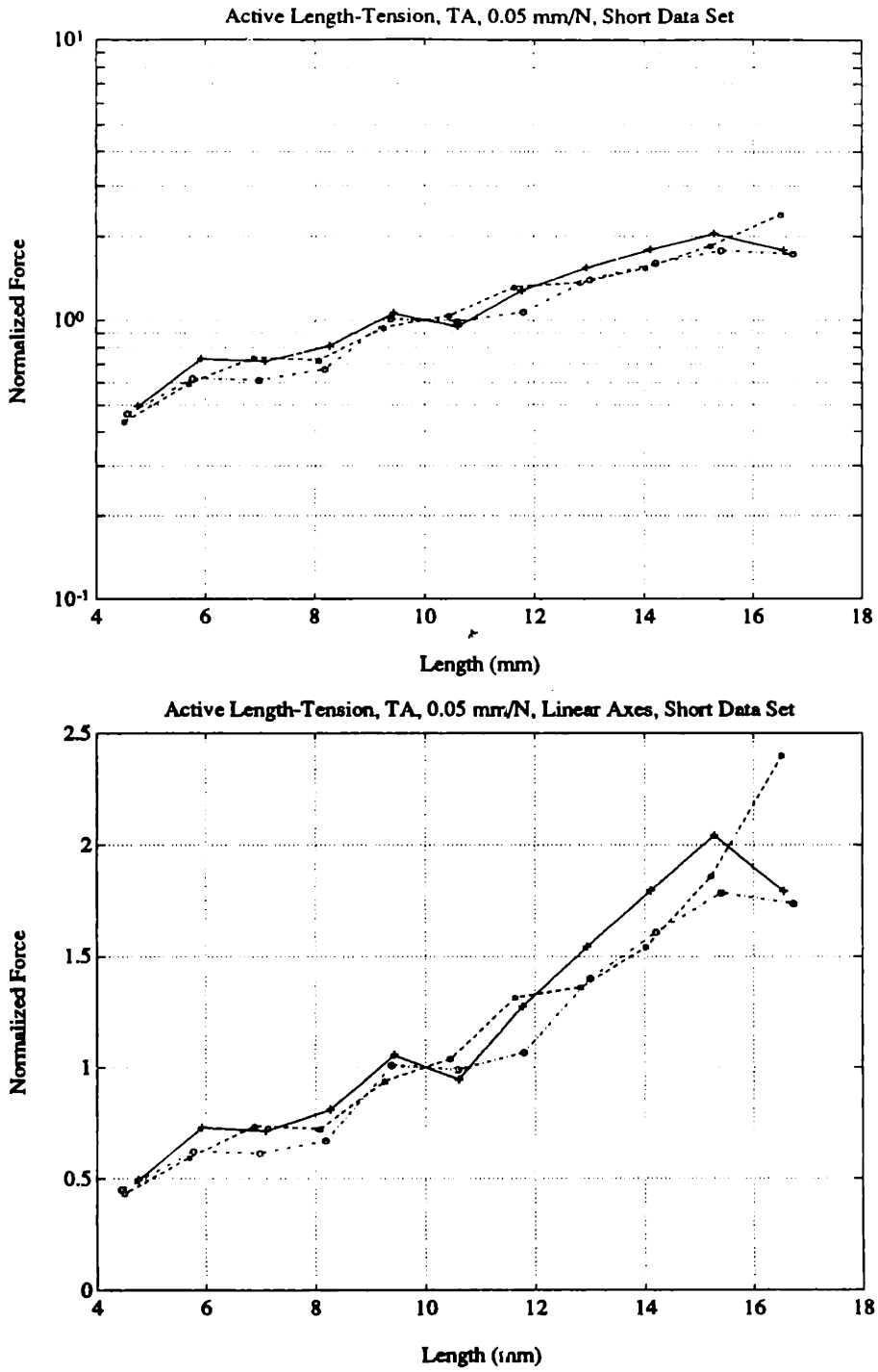

Figure 5.49: Active length-tension curve for TA, generated by parameter estimation, 0.05 mm/N compliance in series element, shortened data set, 10 line segments. RT1 (solid,+), RT2 (dashed,*), RT3 (dotted,o). Semi-log scale, top, linear scale, bottom.

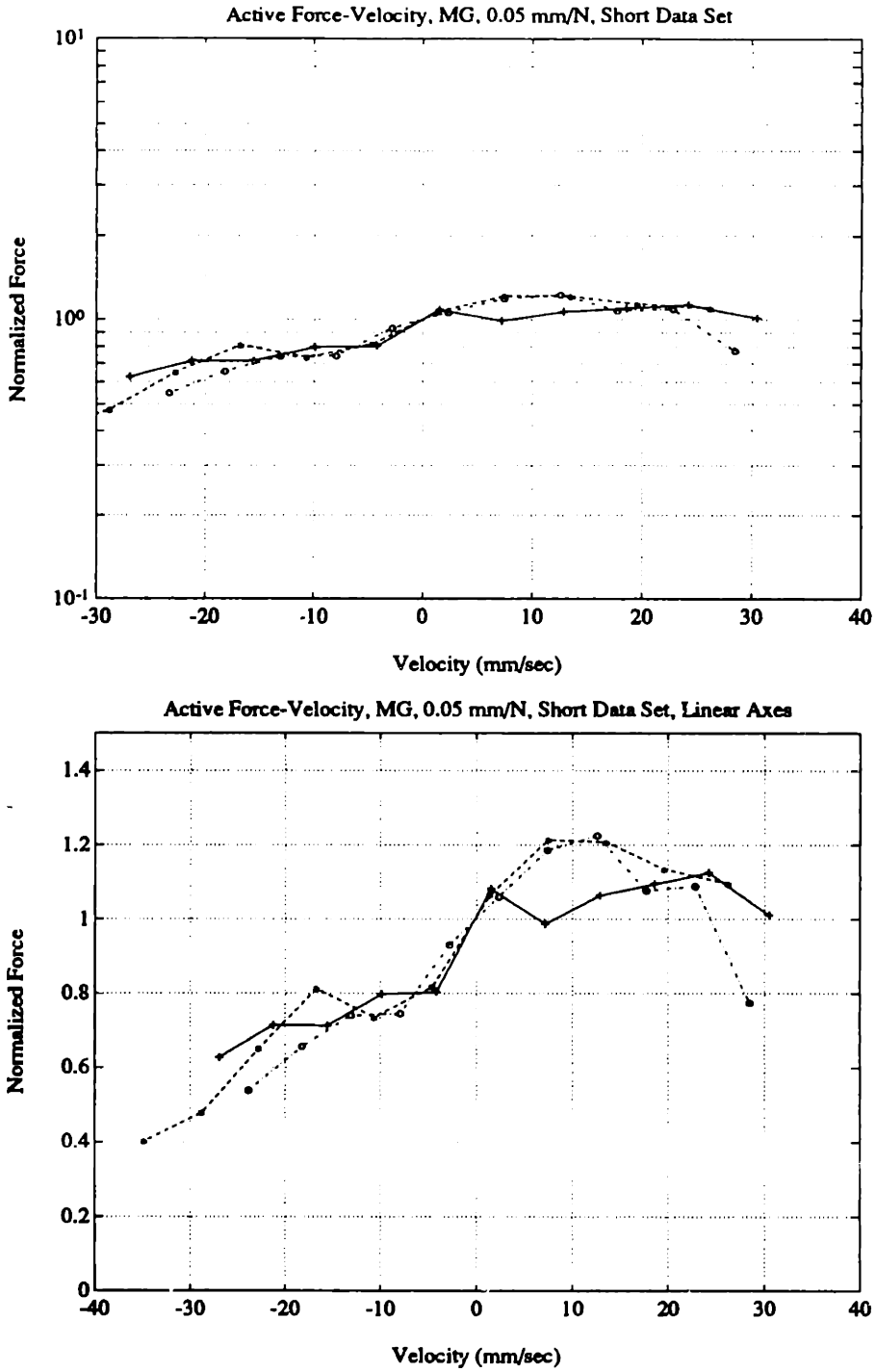

Figure 5.50: Active force-velocity curve for MG, generated by parameter estimation, 0.05 mm/N compliance in series element, shortened data set, 10 line segments. RT1 (solid,+), RT2 (dashed,*), RT3 (dotted,o). Semi-log scale, top, linear scale, bottom.

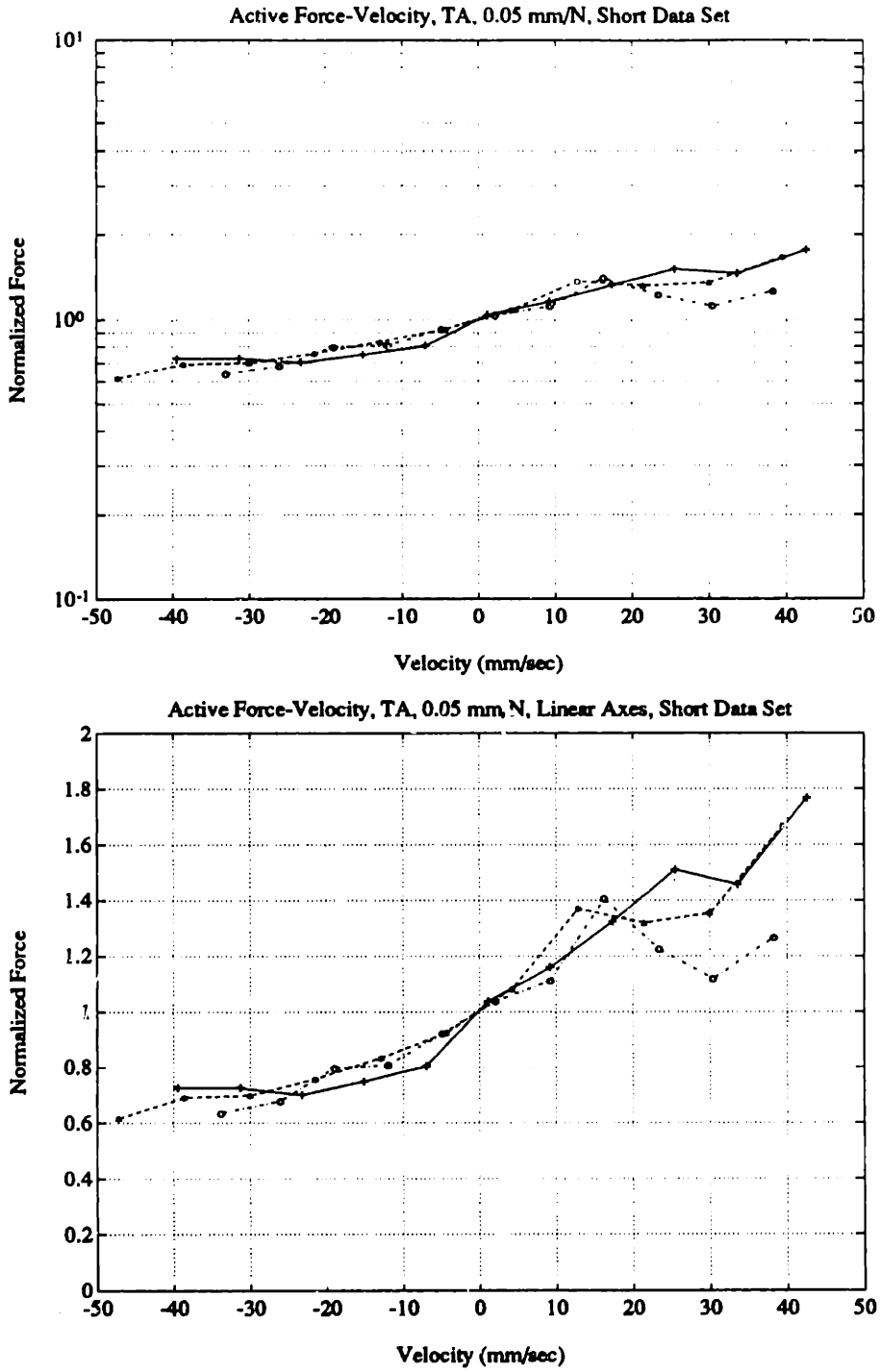

Figure 5.51: Active force-velocity curve for TA, generated by parameter estimation, 0.05 mm/N compliance in series element, shortened data set, 10 line segments. RT1 (solid,+), RT2 (dashed,*), RT3 (dotted,o). Semi-log scale, top, linear scale, bottom.

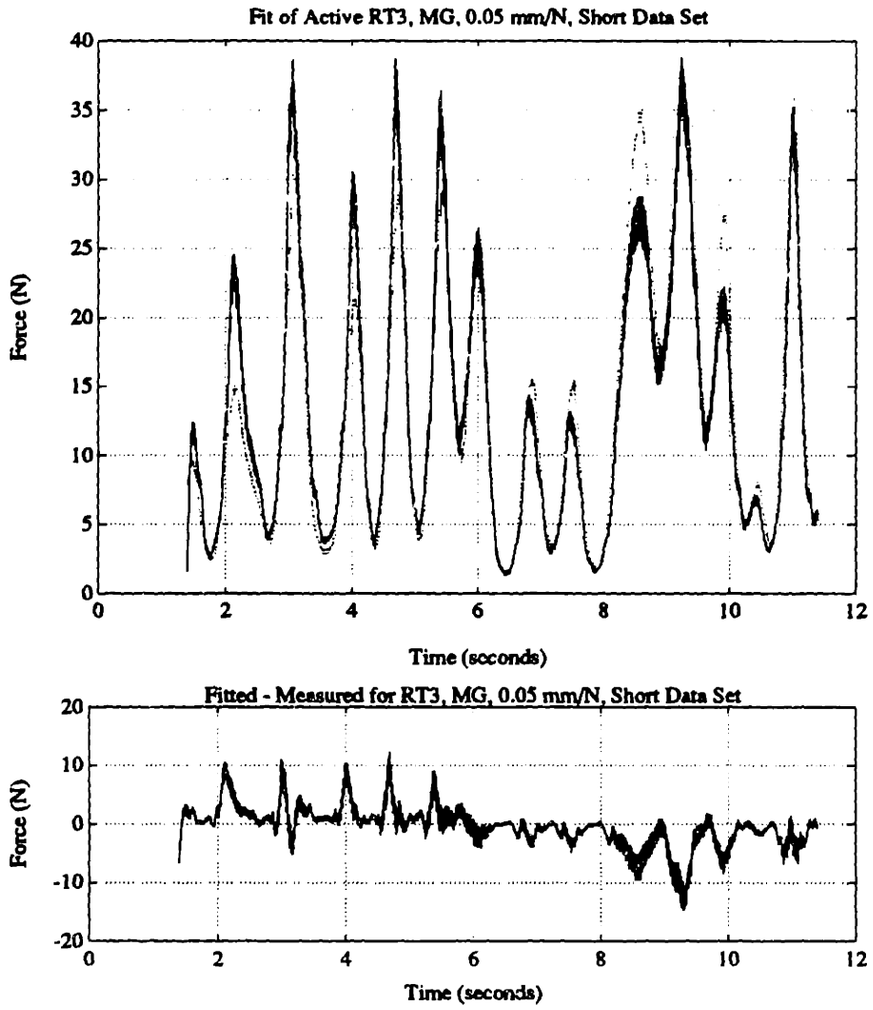

Figure 5.52: Difference between fitted (solid) and measured (dotted) active force, MG, 0.05 mm/N compliance in series element, shortened data set. Average squared error 11.86 (random trajectory only).

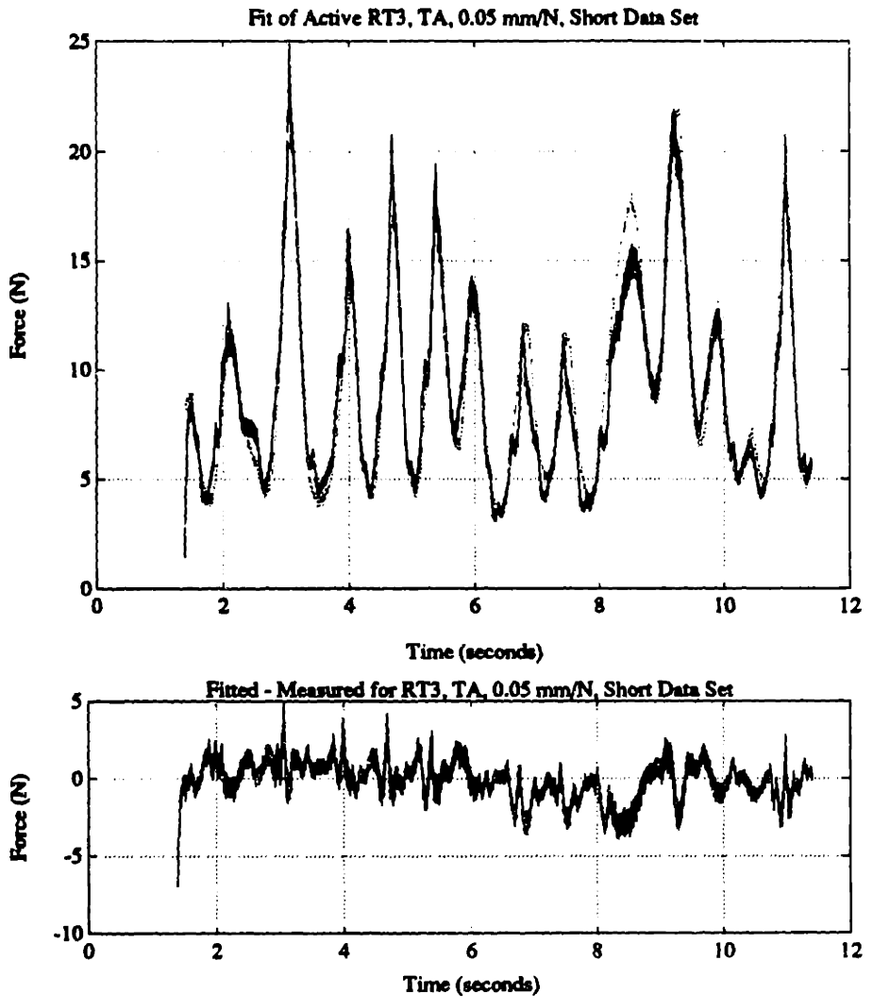

Figure 5.53: Difference between fitted (solid) and measured (dotted) active force, TA, 0.05 mm/N compliance in series element, shortened data set. Average squared error 1.65 (random trajectory only).

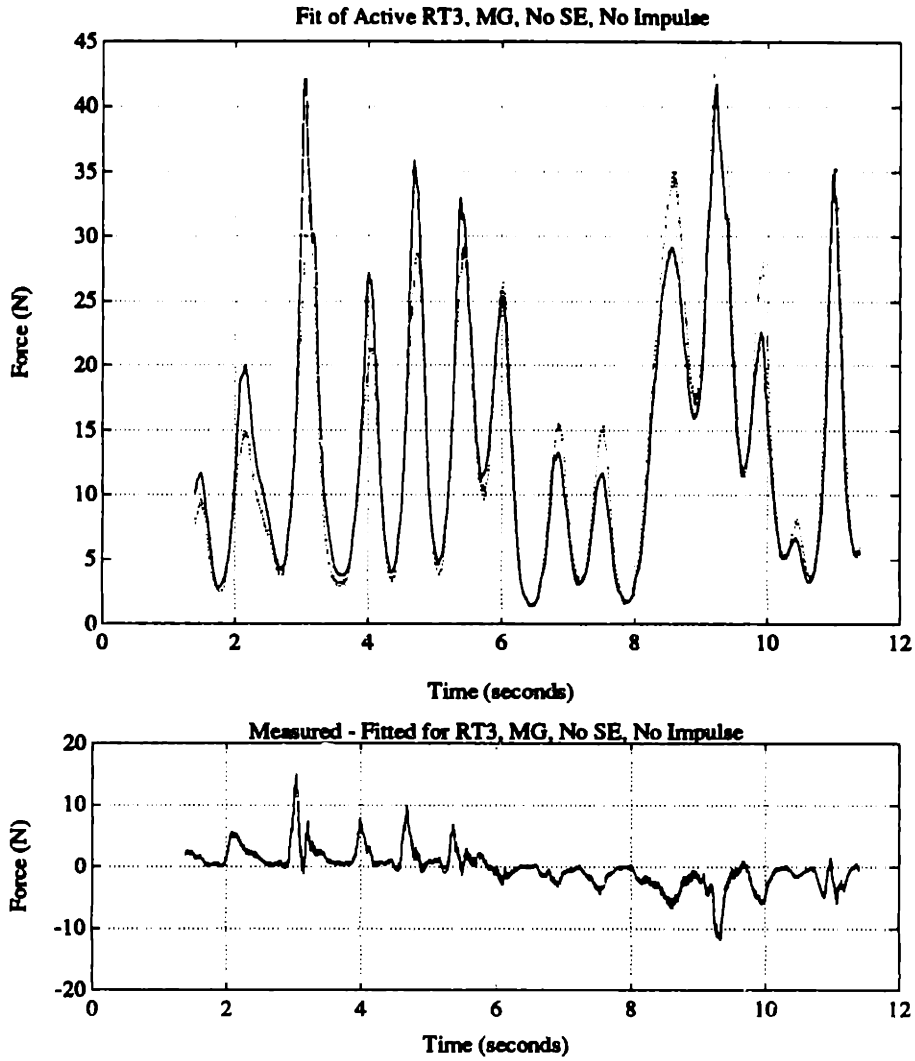

Figure 5.54: Difference between fitted (solid) and measured (dotted) active force, MG, no series element compliance, shortened data set, no impulse response. Average squared error 8.54 (random trajectory only).

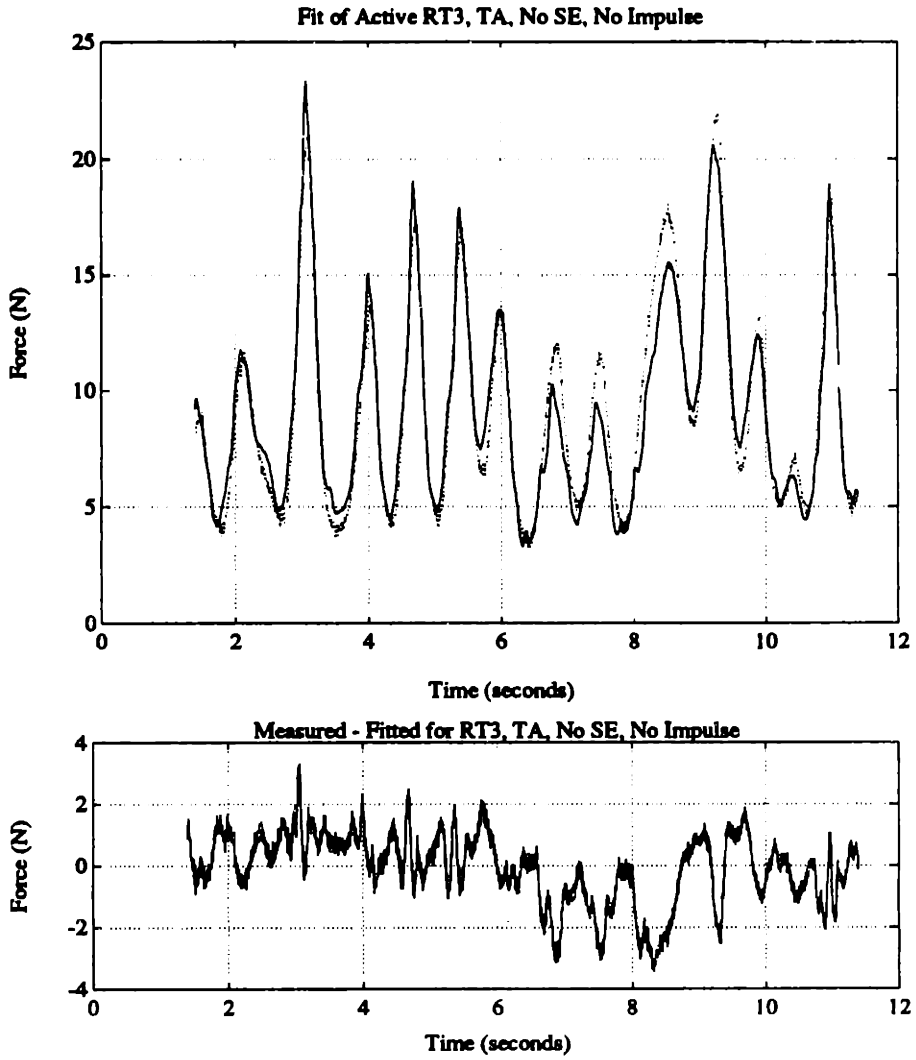

Figure 5.55: Difference between fitted (solid) and measured (dotted) active force, TA, no series element compliance, shortened data set, no impulse response. Average squared error 1.32 (random trajectory only).

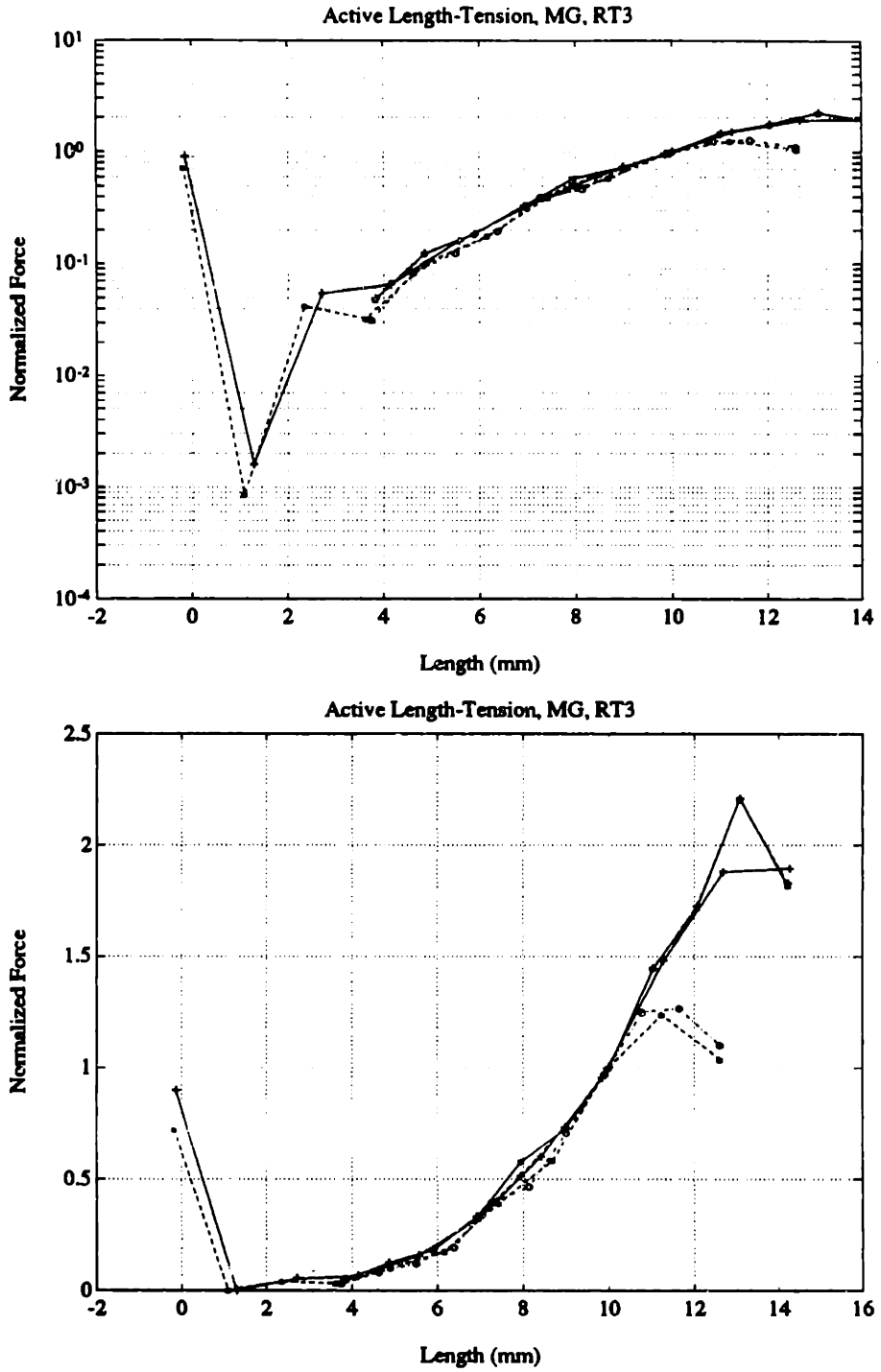

Figure 5.56: Summary of active length-tension parameters, MG, RT3. See Table 5.2 for a description of the line types.

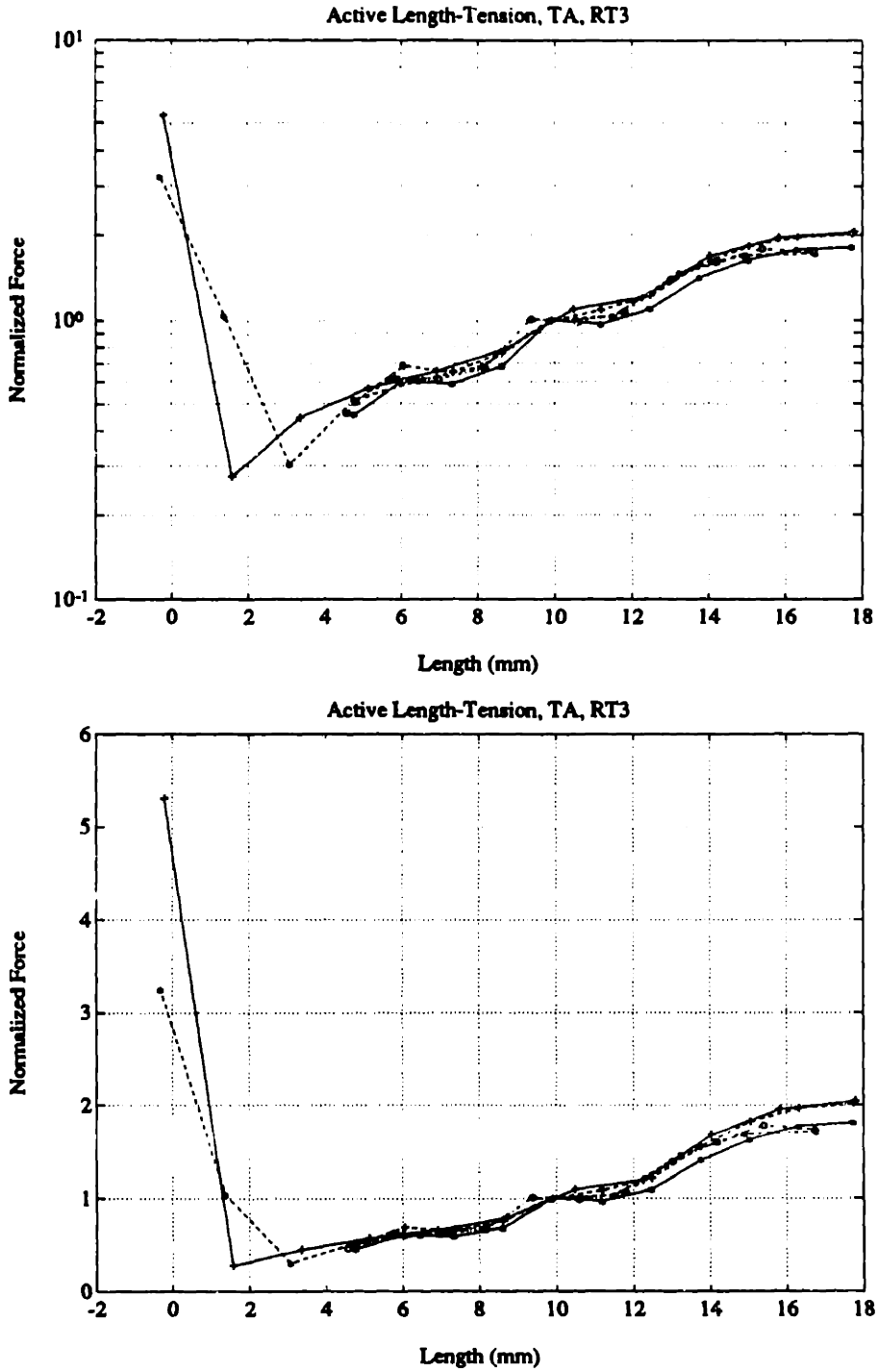

Figure 5.57: Summary of active length-tension parameters, TA, RT3. See Table 5.2 for a description of the line types.

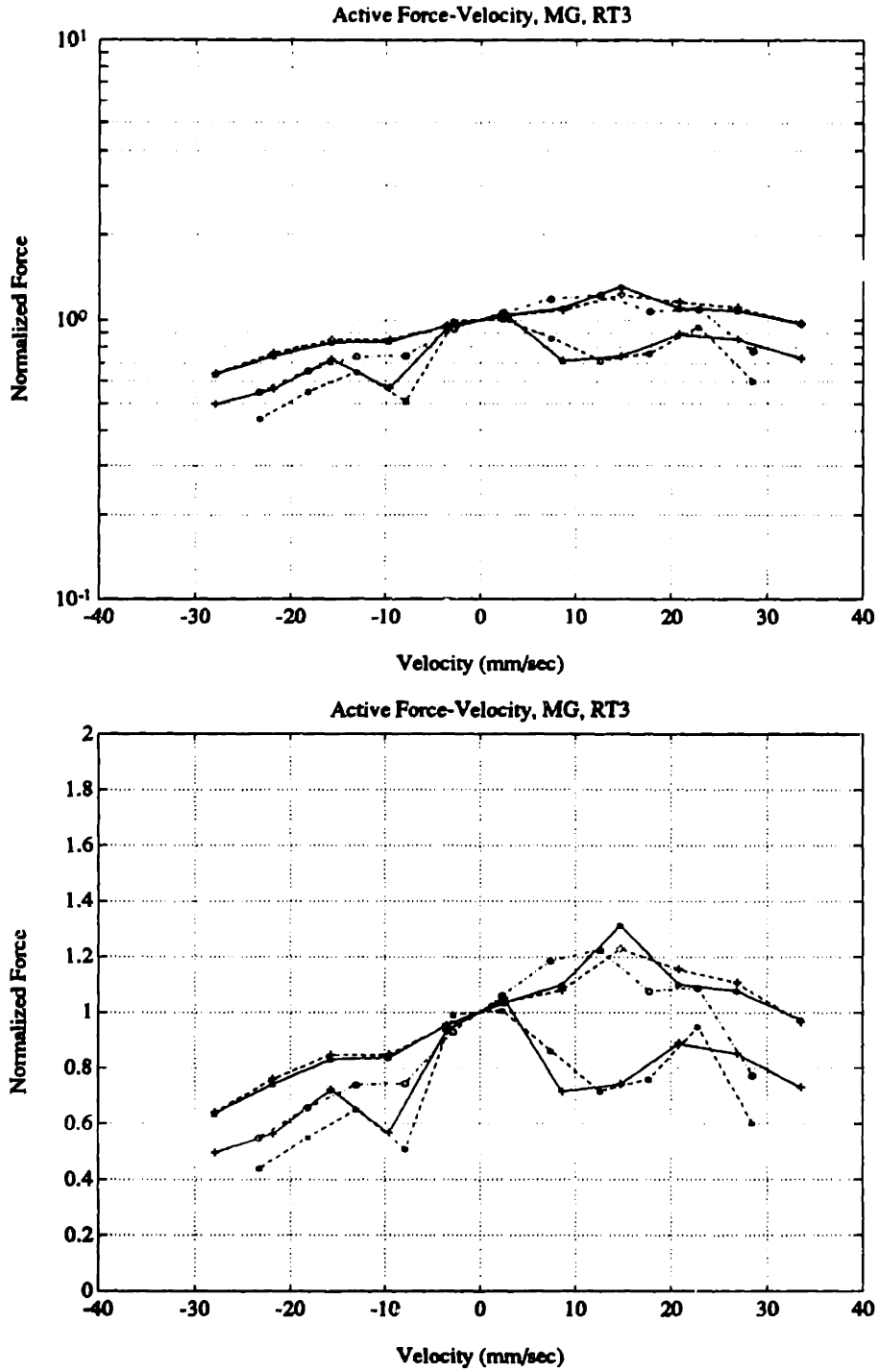

Figure 5.58: Summary of active force-velocity parameters, MG, RT3. See Table 5.2 for a description of the line types.

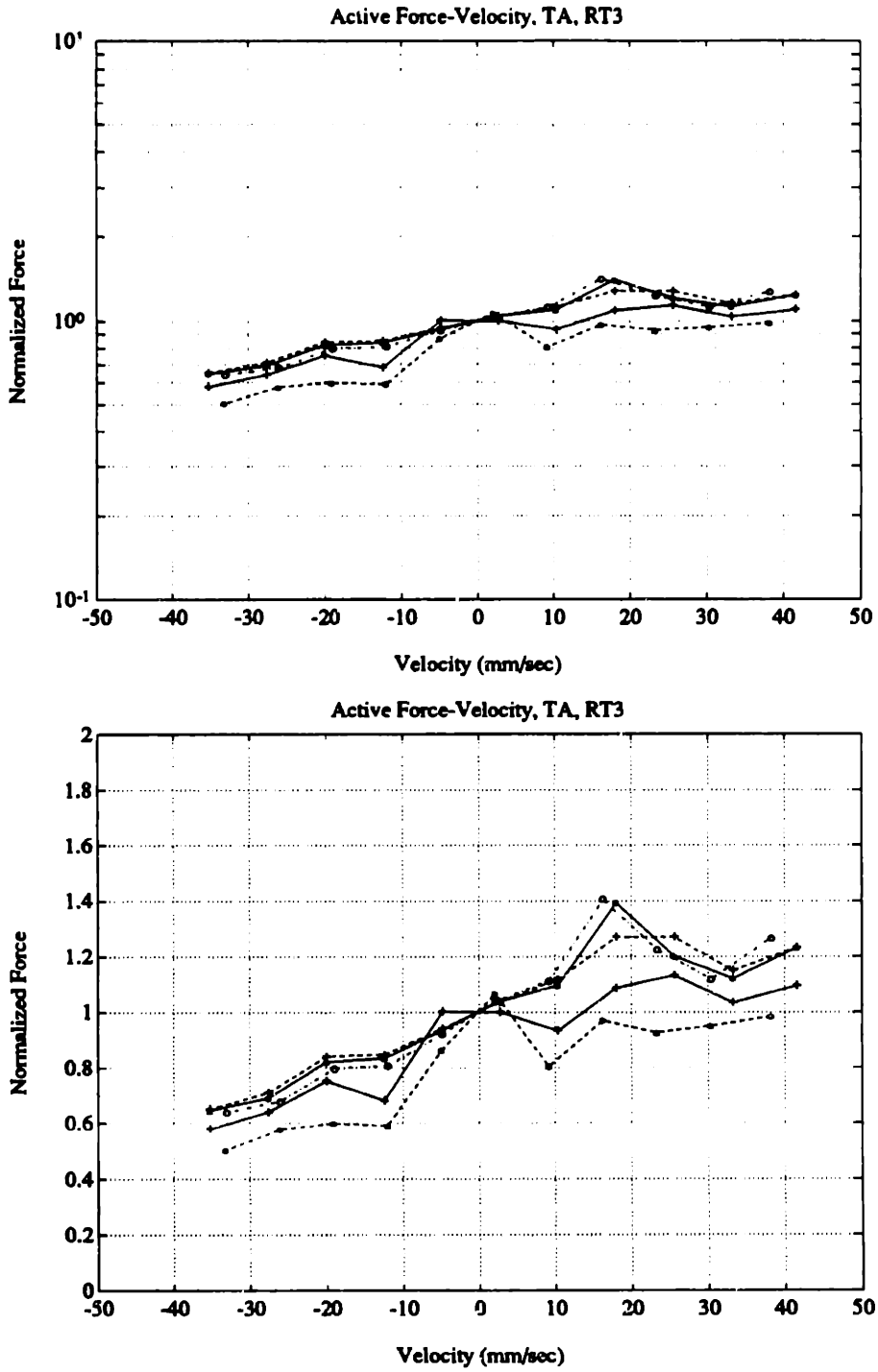

Figure 5.59: Summary of active force-velocity parameters, TA, RT3. See Table 5.2 for a description of the line types.

5.3 Prediction of Muscle Force

Prediction of muscle force is a method of testing the model's validity. The error plots of the previous section show that the model works well in data fitting where the same data set is used for both the parameter estimation and the force prediction. This, however, is not a demanding verification of model validity. The goal of this section is to show that after the model has been fit to a muscle, it can be used to predict the force output using any set of inputs.

The parameter estimates derived from *cstmrand* using random trajectory 3 (RT3) were used as the model parameters. As can be seen from Figures 5.18 - 5.21, 5.34 - 5.37, 5.42 - 5.45, 5.48 - 5.51, the fitted parameters were approximately equivalent for each of the random trajectories. Using the fitted parameters of RT3 to describe the model was an arbitrary decision.

5.3.1 Passive Force Prediction

Figures 5.60 and 5.61 show the passive length-tension and force-velocity parameters which were used to predict the passive force. These were estimated from force measurements from random trajectory 3 in the *cstmrand* protocol. The figures show one and ten segment estimates of the parameters. The single line segment is the best fit of the RT3 data when the L-T and F-V relationships are assumed to be linear.

The dotted line in Figures 5.62 and 5.63 is the measured passive force from *cstmrand* using random trajectory 1. The solid line shows the passive force predicted for random trajectory 1 (RT1) using the parameters estimated from RT3. The parameter estimates used ten line segments to describe the passive force-velocity and length-tension curves. Random trajectory 1 was used as the input to *cstmrand* approximately 42 minutes before RT3. The average squared error was 0.085 for the MG and 0.128 for the TA, compared to 0.060 and 0.065 for the predicted passive force for RT1 using the parameters estimated from RT1.

Figures 5.64 and 5.65 show the difference between the predicted and measured force for RT1 using only one line segment to describe the force-velocity relationship and ten line segments for the length-tension curve. The parameters were estimated from RT3 and are shown in Figures 5.60 and 5.61. The average of the squared errors was 0.083 for the MG and 0.126 for the TA.

Figures 5.66 and 5.67 show the difference between the predicted and measured forces for RT1 using only one line segment to describe both the F-V and L-T relationships. The average squared errors were 0.341 and 0.584.

Figures 5.68 and 5.69 show the actual and predicted force for *rlencstm*. The constant velocity ramps were at $\pm$ 14 mm/sec and $\pm$ 17.5 mm/sec for the MG and TA, respectively. The parameter estimates from RT3 with ten line segments were used to generate the predicted forces. The ramped length data was measured 232 minutes before RT3 was used. The average squared errors were 0.217 and 0.551.

Summary of Passive Force Prediction for RT1				
Parameter Source	Number of Segments		Average Squared Error	
	F-V	L-T	MG	TA
RT1	10	10	0.060	0.065
RT3	10	10	0.085	0.128
RT3	1	10	0.083	0.126
RT3	1	1	0.341	0.584

Table 5.3: Summary of passive force prediction for RT1.

Table 5.3 shows a summary of the passive prediction errors for random trajectory 1 in the *cstmrand* protocol.

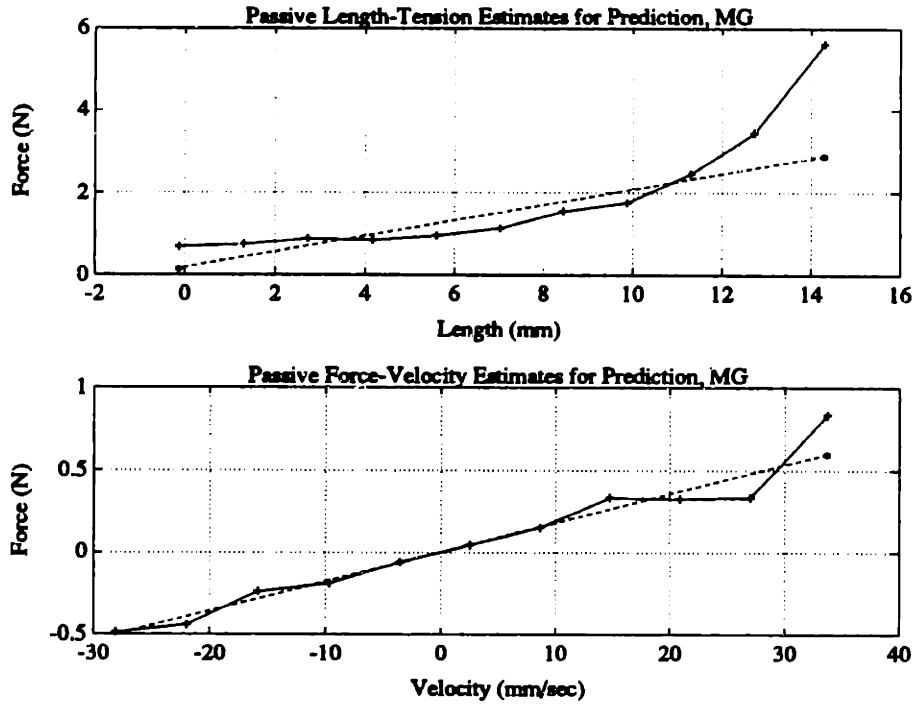

Figure 5.60: Passive length-tension and force-velocity estimates for MG from RT3. 10 segments and 1 segment.

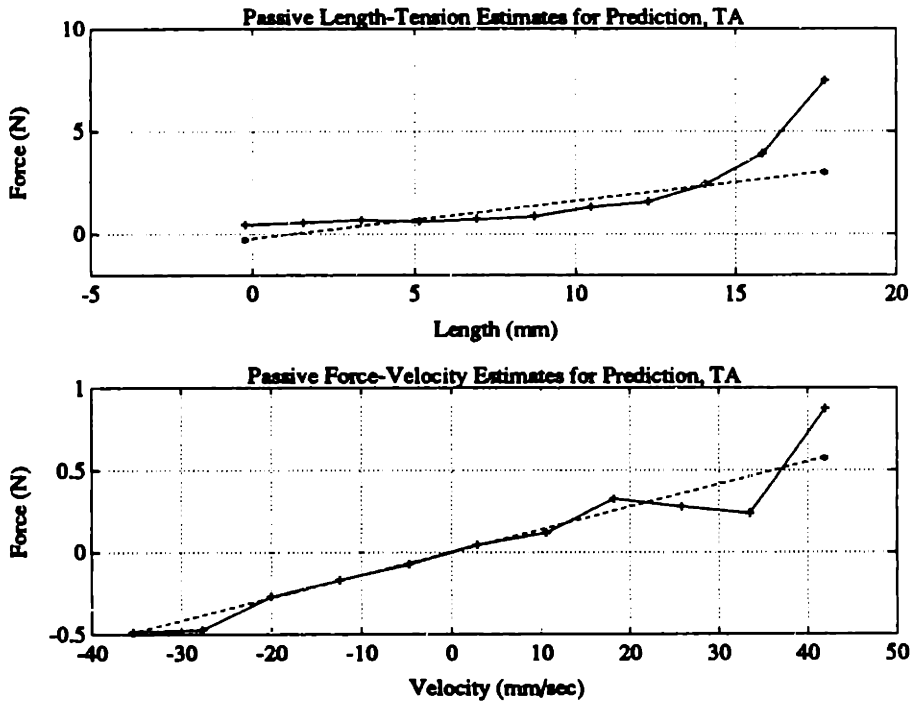

Figure 5.61: Passive length-tension and force-velocity estimates for TA from RT3. 10 segments and 1 segment.

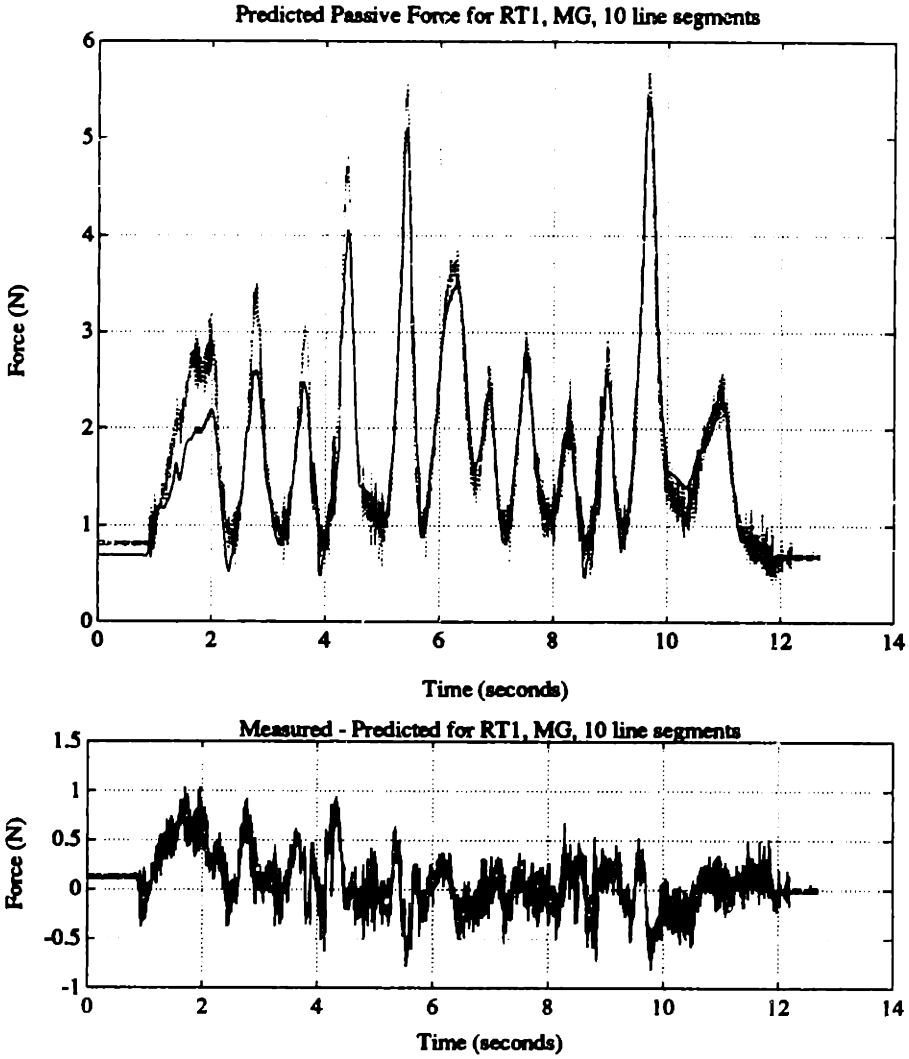

Figure 5.62: Difference between predicted (solid) and measured (dotted) passive force, MG, RT1, 10 line segments. Average squared error: 0.085 for entire data set, 0.101 for random trajectory.

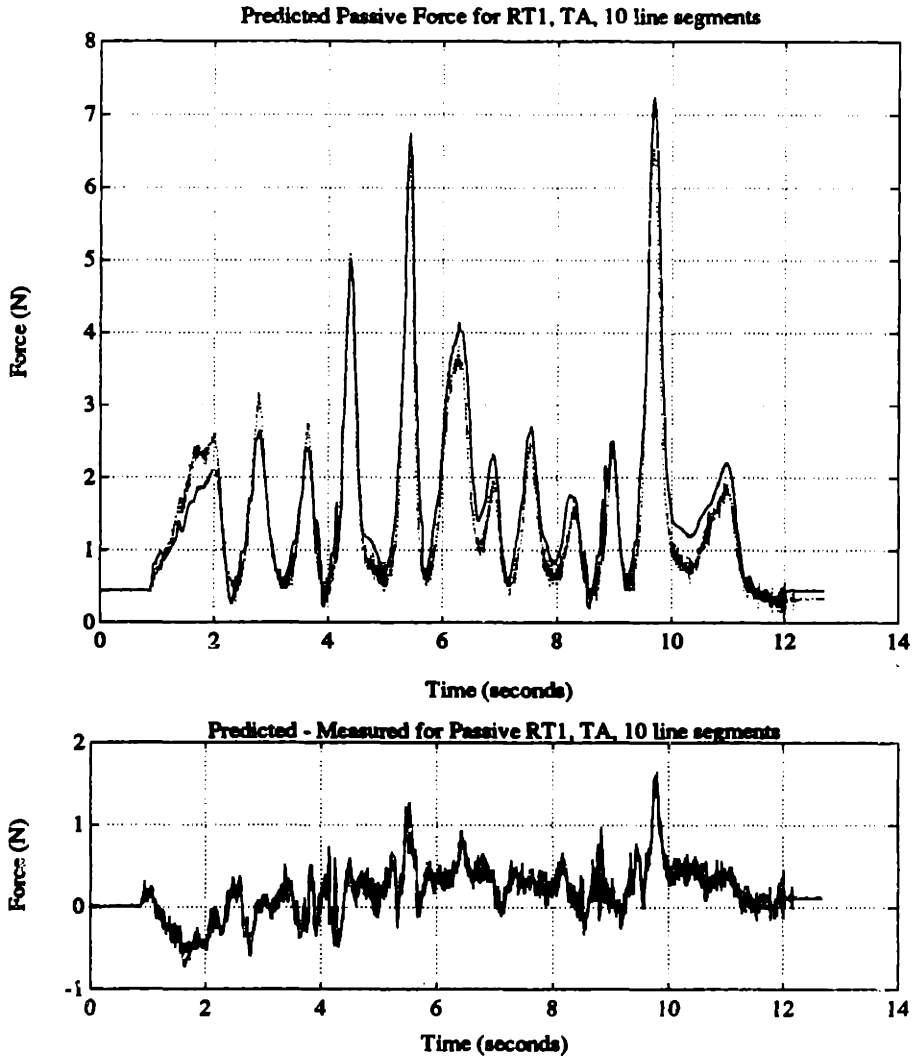

Figure 5.63: Difference between predicted (solid) and measured (dotted) passive force for RT1, TA, 10 line segments. Average squared error: 0.128 for entire data set, 0.160 for random trajectory.

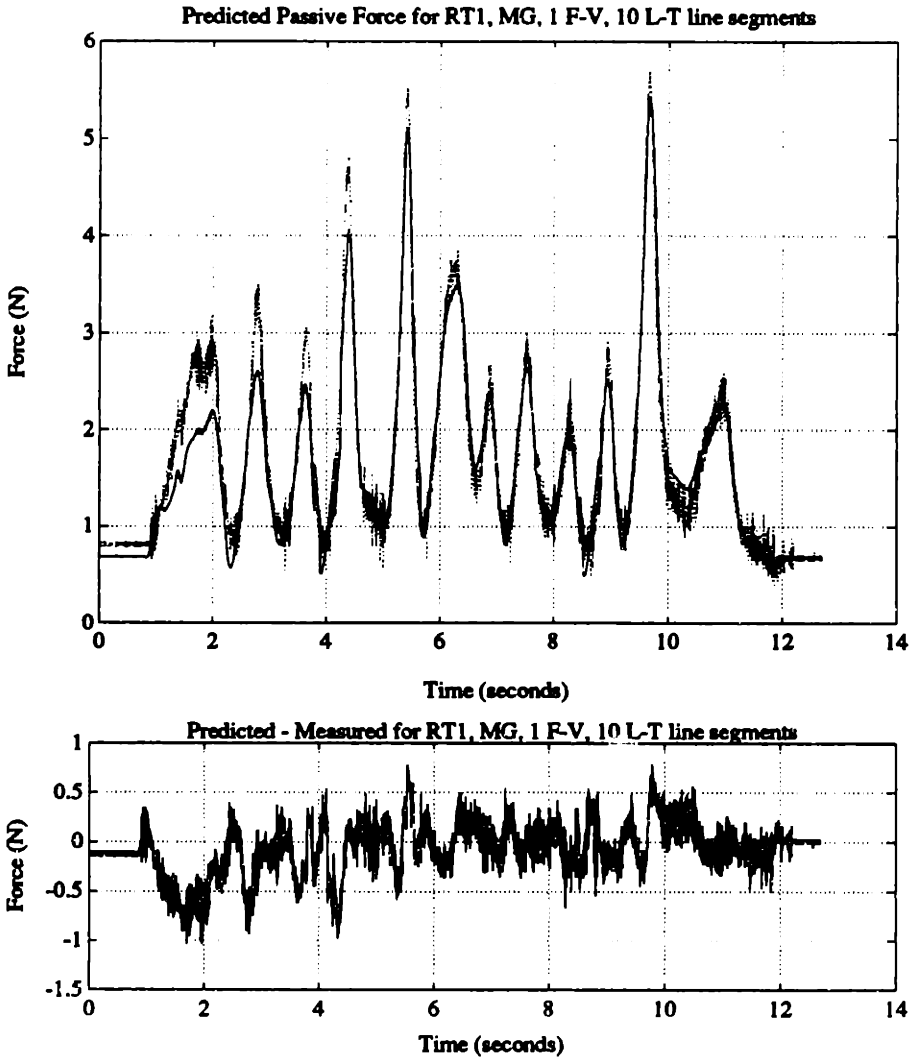

Figure 5.64: Difference between predicted (solid) and measured (dotted) passive force for RT1, MG, 1 line segment for F-V, 10 line segments for L-T. Average squared error: 0.083 for entire data set, 0.097 for random trajectory.

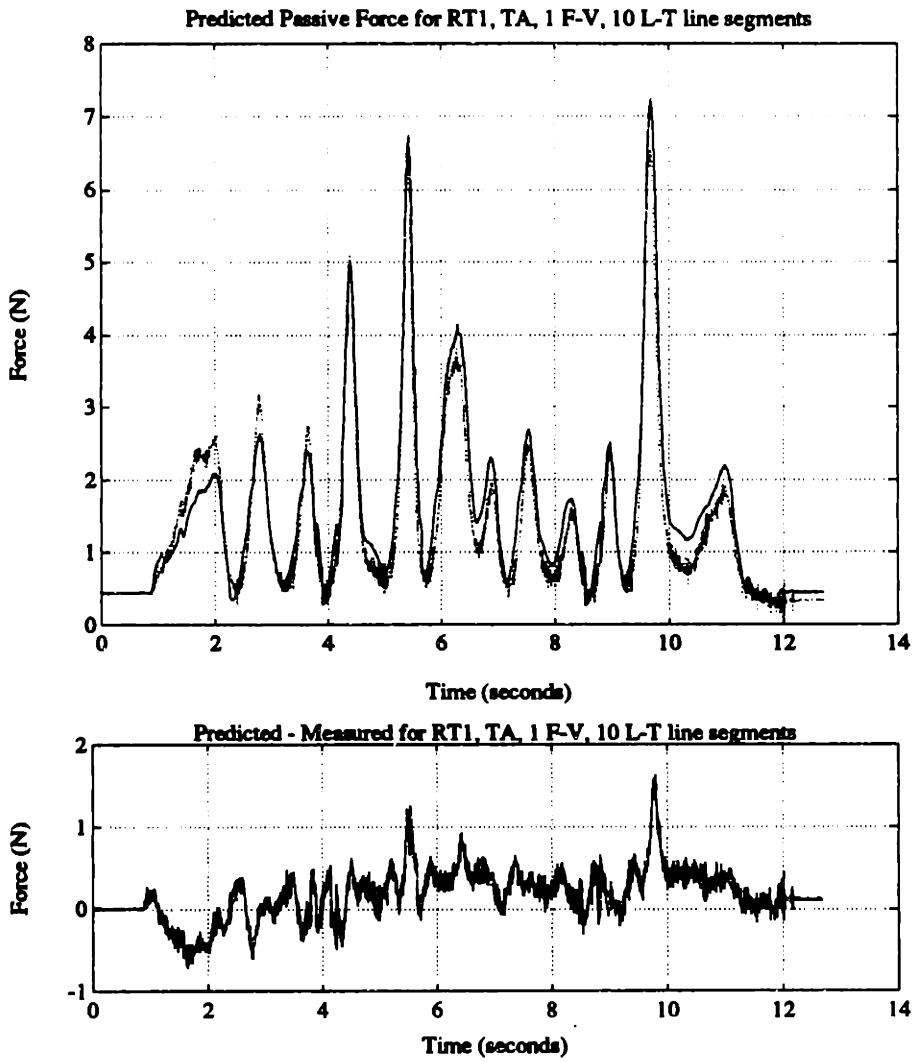

Figure 5.65: Difference between predicted (solid) and measured (dotted) passive force for RT1, TA, 1 line segment for F-V, 10 line segments for L-T. Average squared error: 0.126 for entire data set, 0.157 for random trajectory.

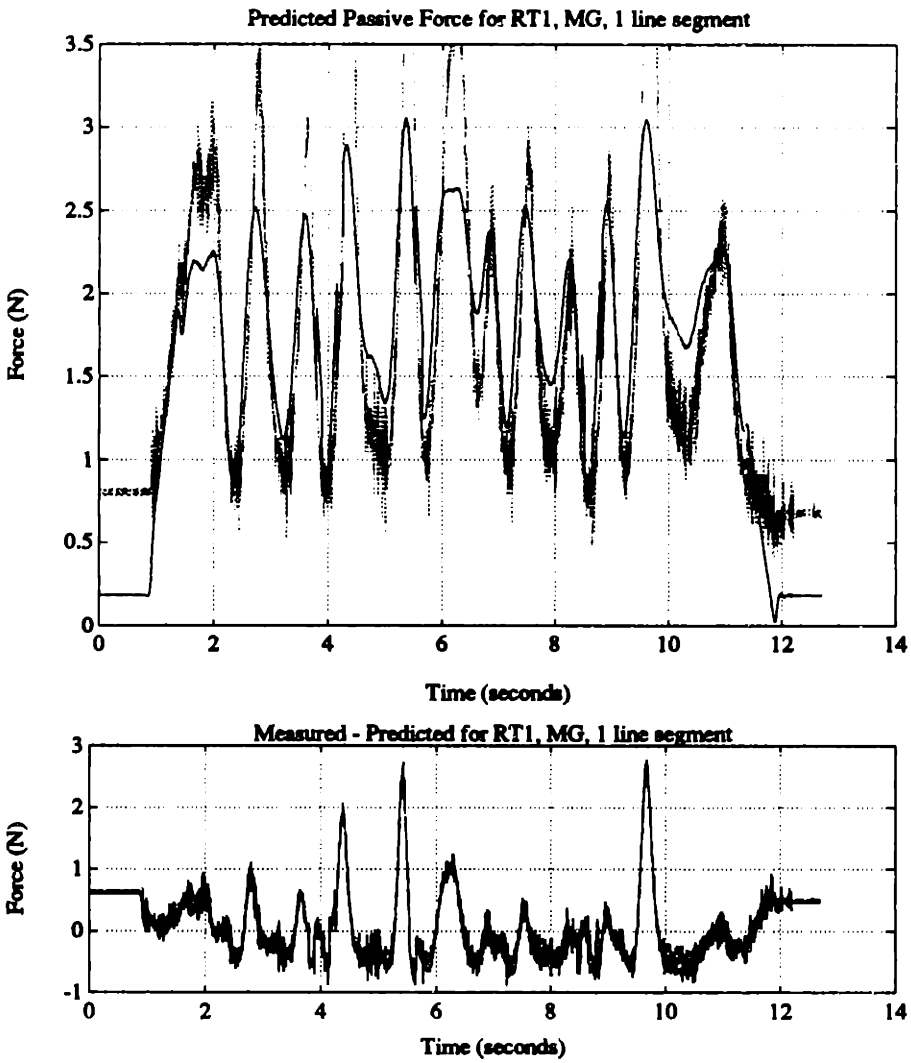

Figure 5.66: Difference between predicted (solid) and measured (dotted) passive force for RT1, MG, 1 line segment. Average squared error: 0.341 for entire data set, 0.371 for random trajectory.

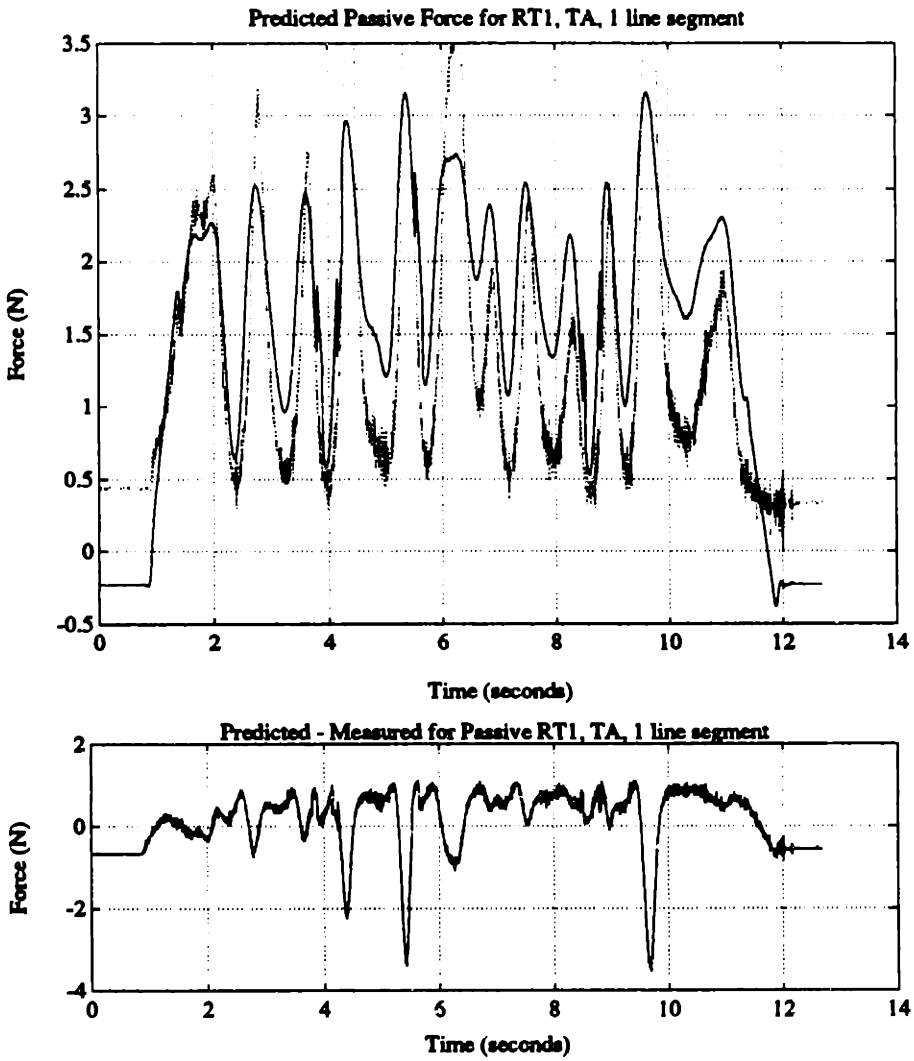

Figure 5.67: Difference between predicted (solid) and measured (dotted) passive force for RT1, TA, 1 line segment. Average squared error: 0.584 for entire data set, 0.664 for random trajectory.

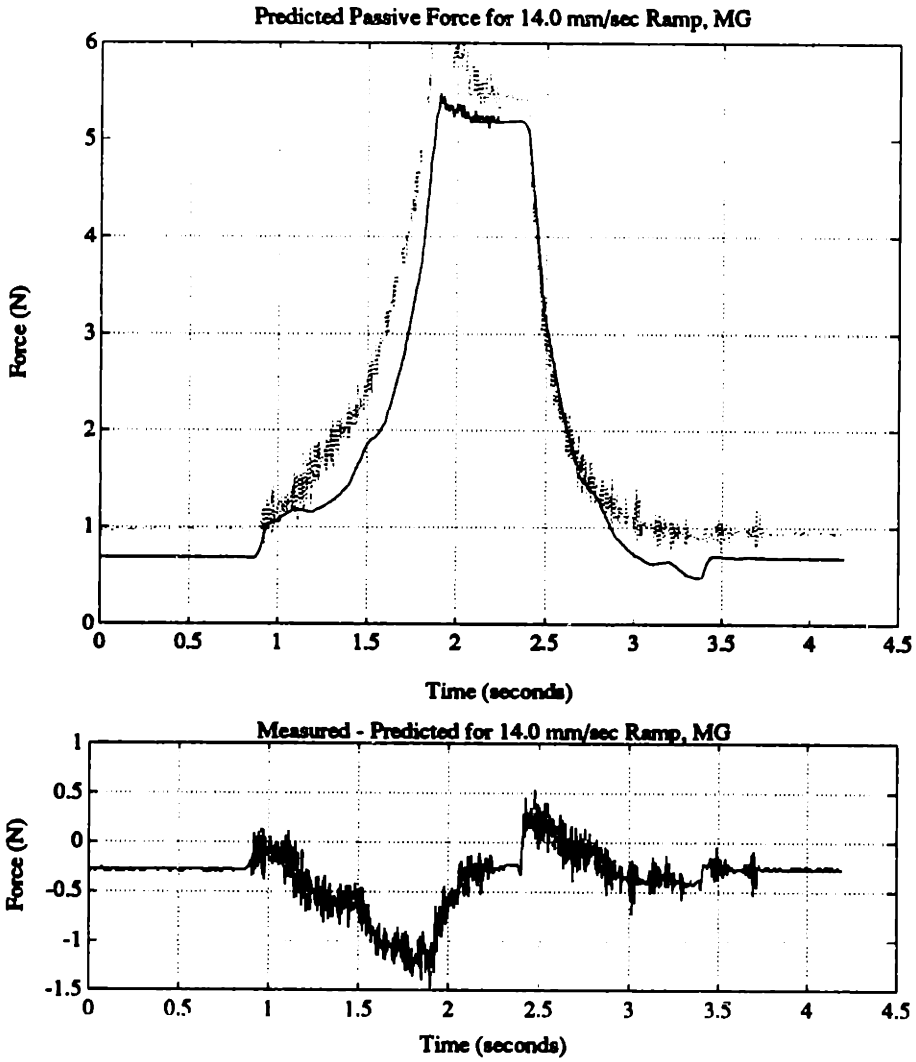

Figure 5.68: Difference between predicted(solid) and measured (dotted) passive force, constant velocity of 14.0 mm/sec, MG, 10 line segments. Average squared error: 0.217.

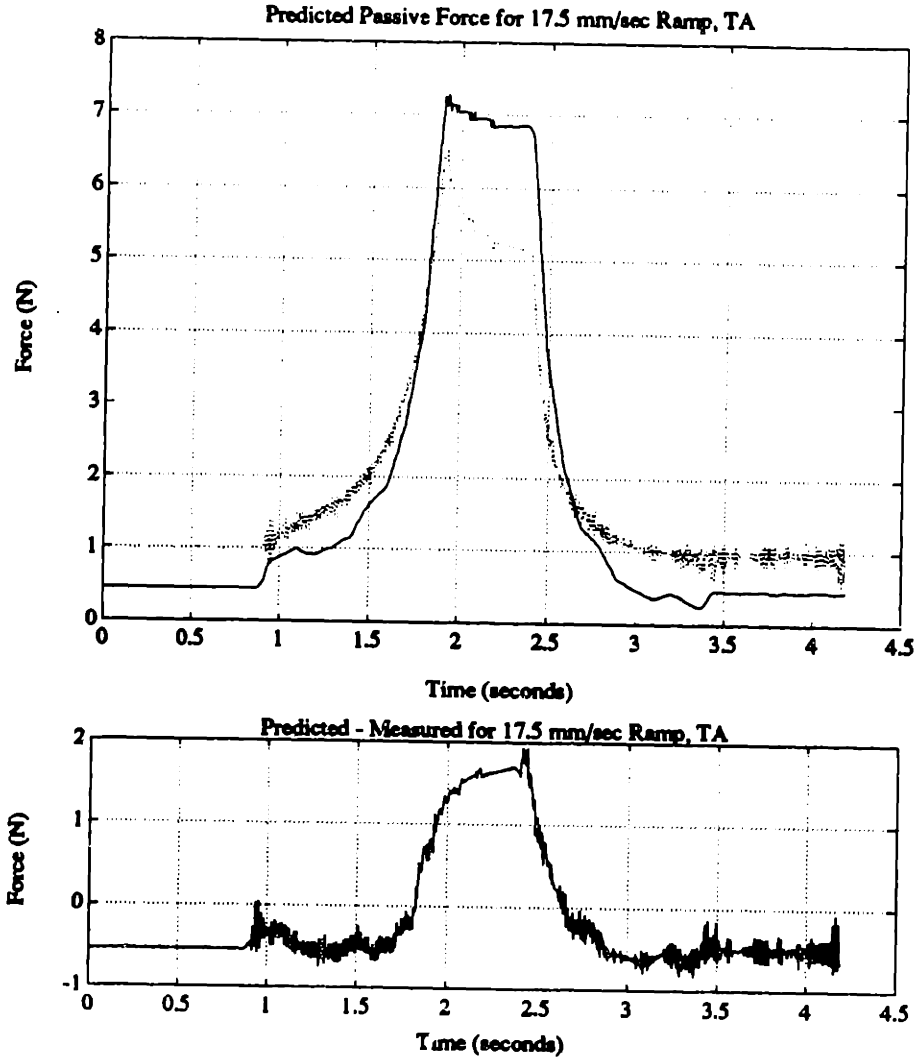

Figure 5.69: Difference between predicted (solid) and measured (dotted) passive force, constant velocity of 17.5 mm/sec, TA, 10 line segments. Average squared error: 0.551.

5.3.2 Active Force Prediction

The model used parameter estimates generated from active and passive tests using RT3 in the *cstmrand* protocol. The active length-tension and force-velocity parameters are shown in Figures 5.70 and 5.71. The ten line segment estimates for both muscles and the dashed one line segment estimate of the MG parameters were generated from the entire data set assuming no series compliance. The solid one line segment estimates for both muscles used only the random trajectory portion of the RT3 data set. (Using the full data set for a one line segment estimate of the TA parameters resulted in a negative slope for the active length-tension curve since the estimated force at $l = 0$ was greater than the force at $l = 17.5$ mm.) The passive model parameters were from RT3 with ten line segments (Figures 5.60 and 5.61). The isometric recruitment curves used were measured at approximately 11:50 pm, close to the time of RT3 in *cstmrand*.

The prediction algorithm for active force includes a "free variable" since the IRC, force-velocity and length-tension parameters are shape characteristics only. They have been normalized so that

$$F(\text{stim} = 0) = 0,$$

$$F(\text{stim} = 100) = 1.0,$$

$$F(v = 0) = 1, \text{ and}$$

$$F(l = 10) = 1$$

according to Equation 3.20. The active force multipliers, $c_{f_{ACT}}$, used for normalizing the curves in Figures 5.70 and 5.71 were 1568 and 537 for ten line segments, 876 and 573 for the single segment parameter estimates for the MG and TA respectively.

Figures 5.72 and 5.73 show the results of predicting the force produced by RT1 using the parameters from RT3. The *cstmrand* protocol was used with stimulation levels of 60 μs for the MG and 35 μs for the TA. The average of the squared errors for the entire data sets were 24.61 and 43.02, for the MG and TA respectively. The average squared error for t = 1.4 – 11.4 (the random trajectory portion) was 20.55 and 5.62. The force multipliers were 1954 and 673. The average error for prediction of RT1 using the parameters from RT1 were 13.28 and 42.54 for the entire data set, 14.41 and 5.60 for the random portion. The data for RT1 was generated approximately 40 minutes before RT3.

Figures 5.74 through 5.76 show the prediction errors for the same set of inputs, using only one line segment to describe the parameters from RT3. The parameters for Figure 5.74 were estimated using the entire data set. The average squared error was 40.33 for the entire data set, 47.90 for the random trajectory only. The force multiplier was 1275. Figures 5.75 and 5.76 were generated using single line segment parameters estimated from the shortened data set. The average squared errors were 58.57 and 7.90 for the entire data set, 37.33 and 6.96 for the shortened data set(random

Summary of Active Force Prediction for RT1									
Parameter Source	Data Set	Number of Segments		Force Multiplier		Average Squared Error			
						MG		TA	
		F-V	L-T	MG	TA	Long	Short	Long	Short
RT1	Long	10	10	1876	670	13.28	14.41	42.54	5.60
RT3	Long	10	10	1954	673	24.61	20.55	43.02	5.62
RT3	Long	1	1	1275		40.33	47.90		
RT3	Short	1	1	1372	667	58.57	37.33	7.90	6.96

Table 5.4: Summary of active force prediction for RT1 in *cstmrand*.

only). The force multipliers were 1372 and 667. The prediction errors for RT1 are summarized in Table 5.4.

In Figures 5.77 and 5.78, random pulse width pattern 4 (from Figure 4.20) was used with the *randclen* protocol at constant lengths of 14.0 and 17.5 mm for the MG and TA. This data was generated approximately 288 minutes before RT3 was used in the *cstmrand* protocol. The predicted force had average squared errors of 25.01 and 9.47. The force multipliers were 2031 and 300.

Figures 5.79 and 5.80 show the predicted and measured active force for the *randrand* protocol using random pulse width pattern 4 and random trajectory 4. The averaged sum of the squared errors were 6.02 and 7.05 for the entire data set, 5.28 and 2.97 for the random trajectory portion only. The force multipliers were 1243 and 329. The *randrand* data was measured 62 minutes after RT3 was used in *cstmrand*.

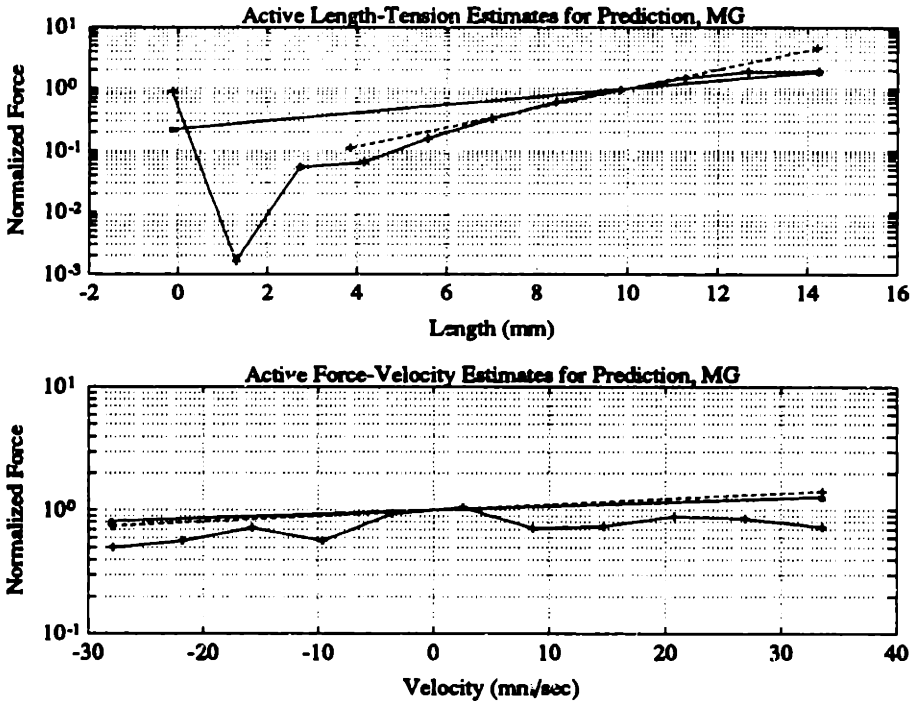

Figure 5.70: Active length-tension and force-velocity estimates for MG from RT3. 10 segment and 1 segment. Long data set (solid), short data set (dashed).

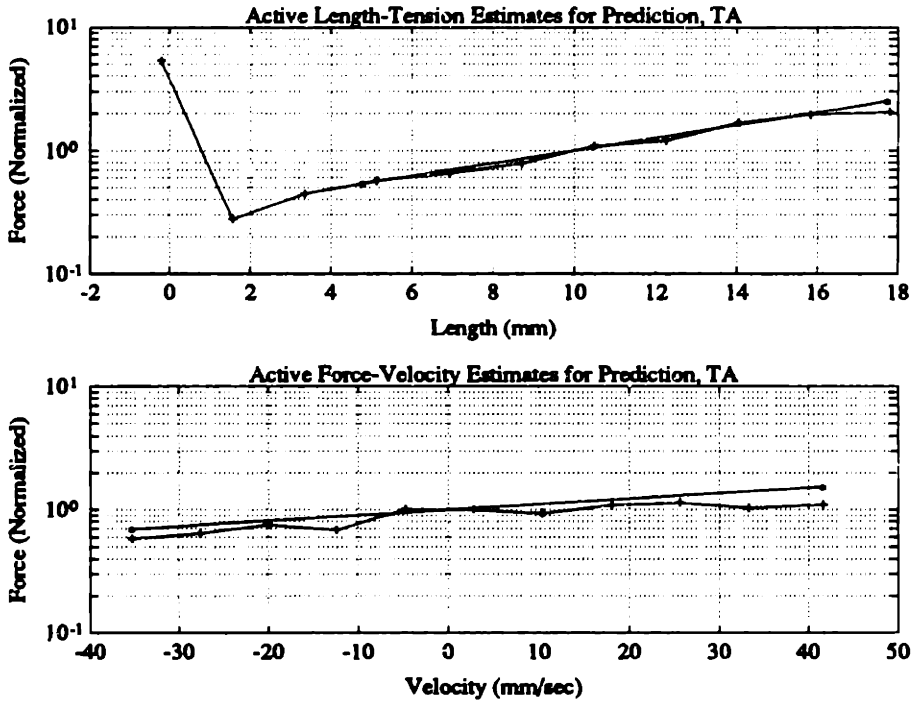

Figure 5.71: Active length-tension and force-velocity estimates for TA from RT3. 10 segment and 1 segment. Long data set (solid), short data set (dashed).

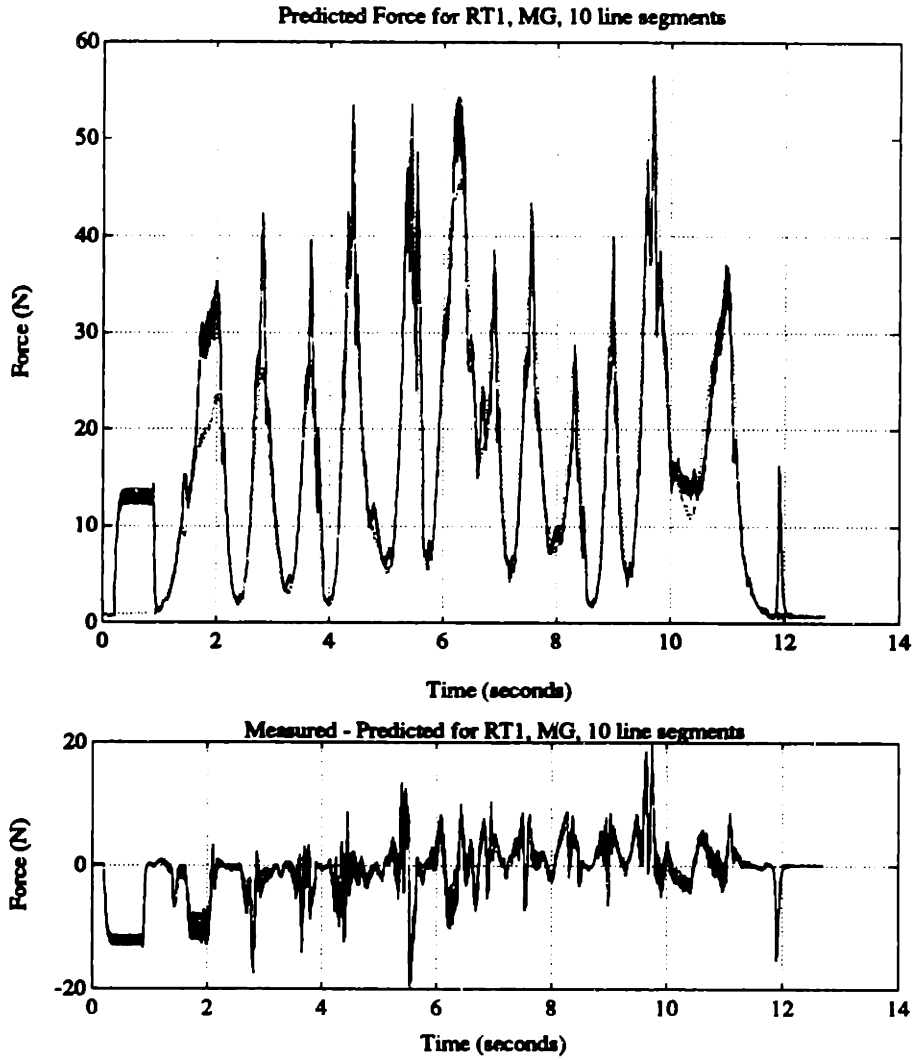

Figure 5.72: Difference between predicted (solid) and measured (dotted) active force, MG, 10 line segments. Average squared error: 24.61 for entire data set, 20.55 for random trajectory. Stimulation level: 60 μs.

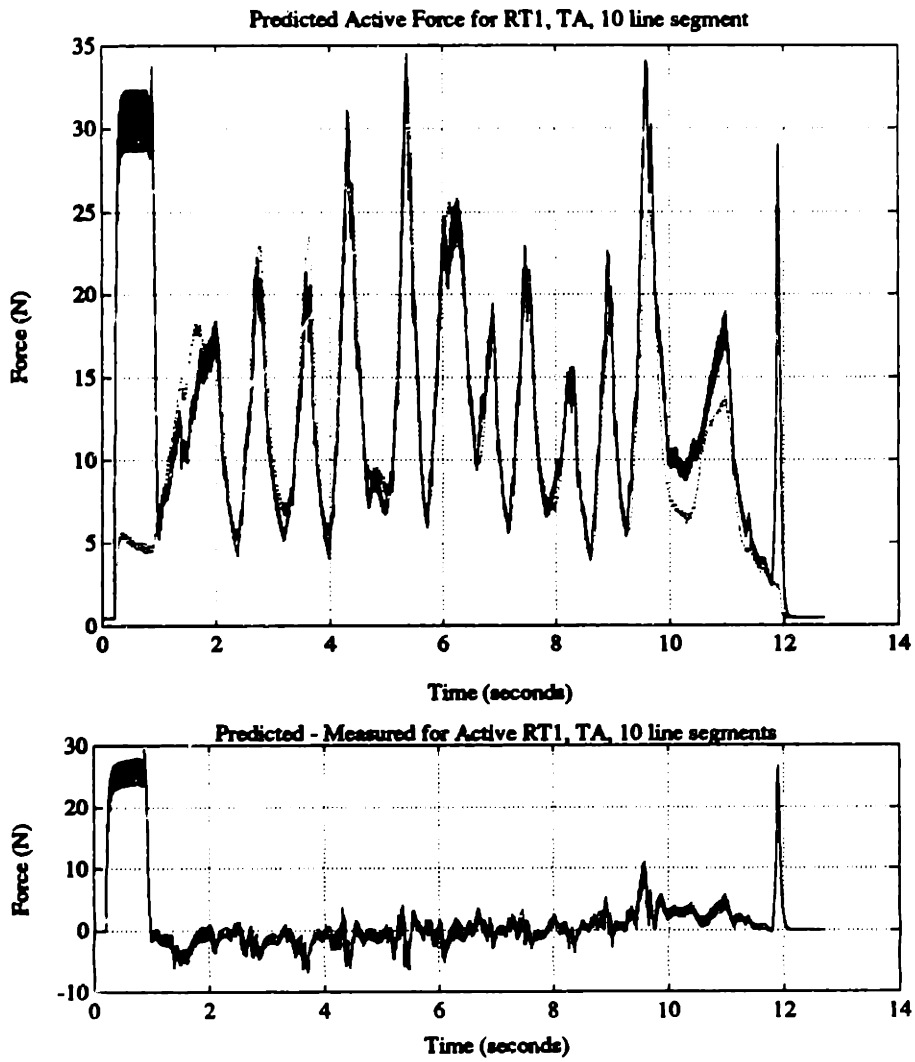

Figure 5.73: Difference between predicted (solid) and measured (dotted) active force, TA, 10 line segments. Average squared error: 43.02 for entire data set, 5.62 for random trajectory. Stimulation level: 35 μs.

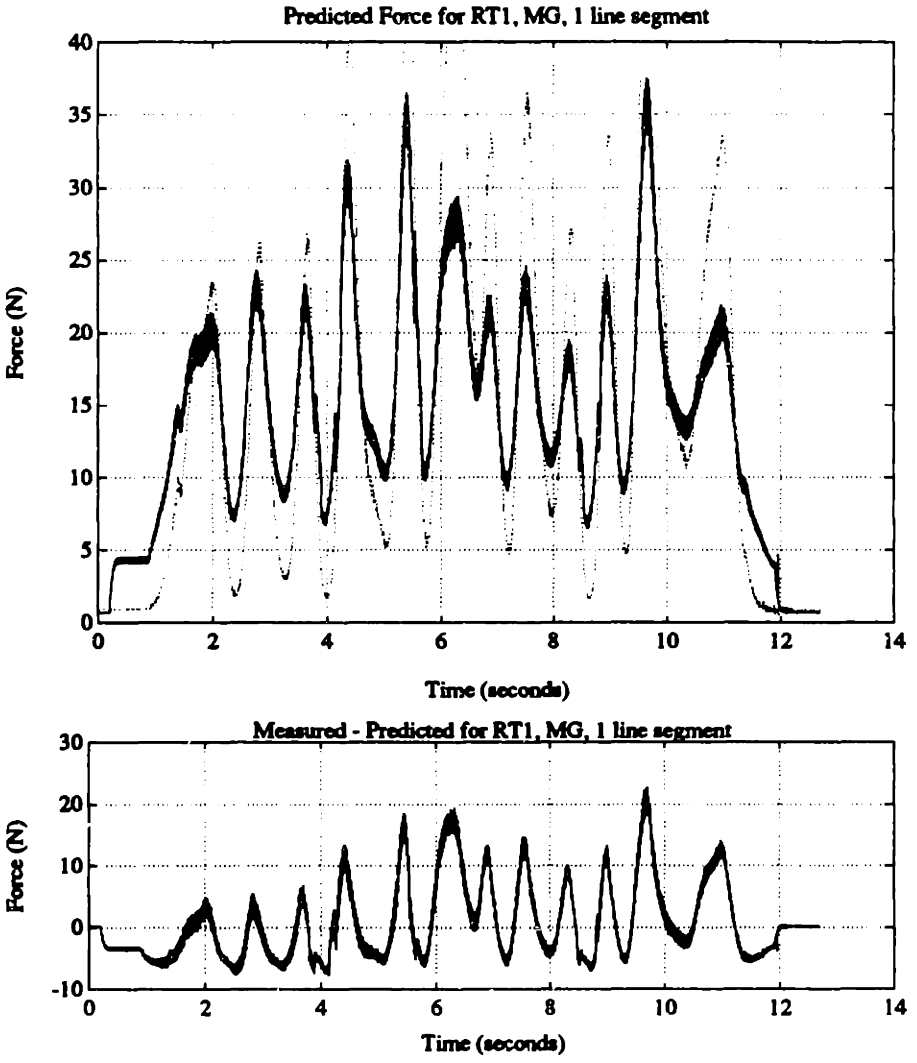

Figure 5.74: Difference between predicted (solid) and measured (dotted) active force, MG, 1 line segment estimated from entire data set. Average squared error: 40.33 for entire data set, 47.90 for random trajectory. Stimulation level: 60 μs.

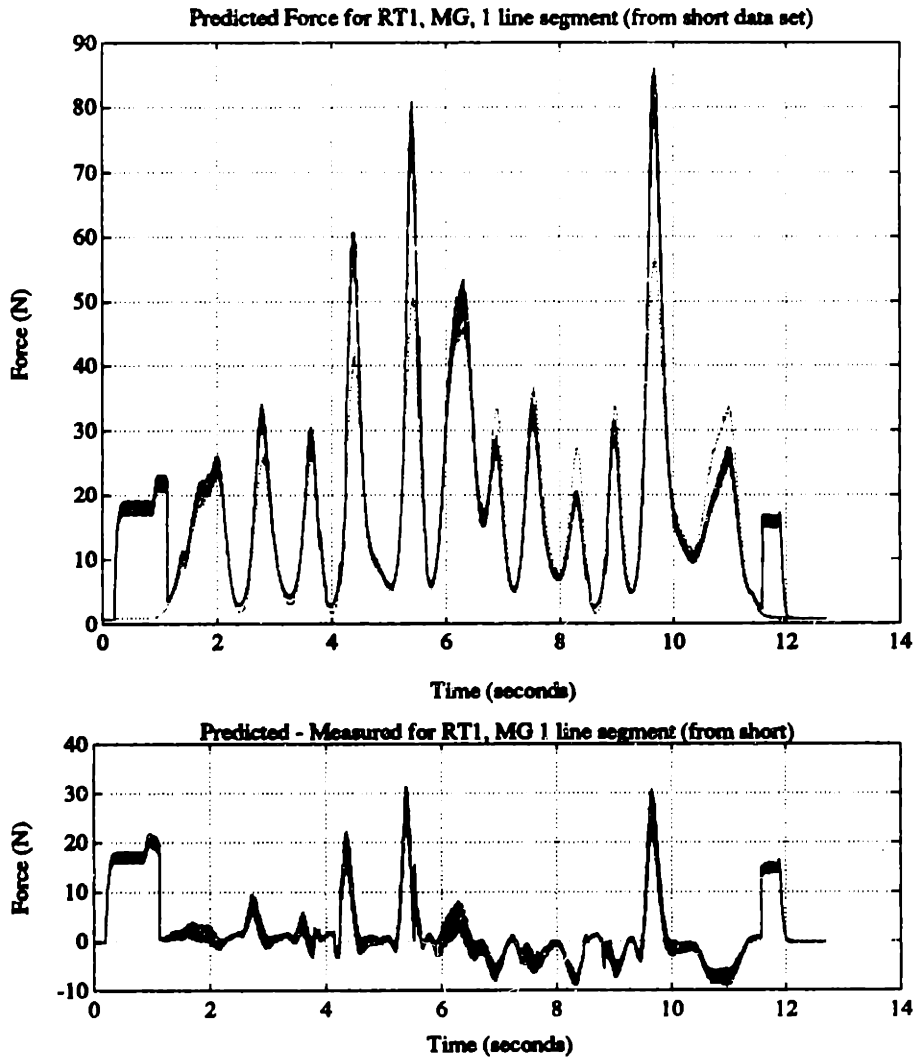

Figure 5.75: Difference between predicted (solid) and measured (dotted) active force, MG, 1 line segment estimated from short data set. Average squared error: 58.57 for entire data set, 37.34 for random trajectory. Stimulation level: 60 μs.

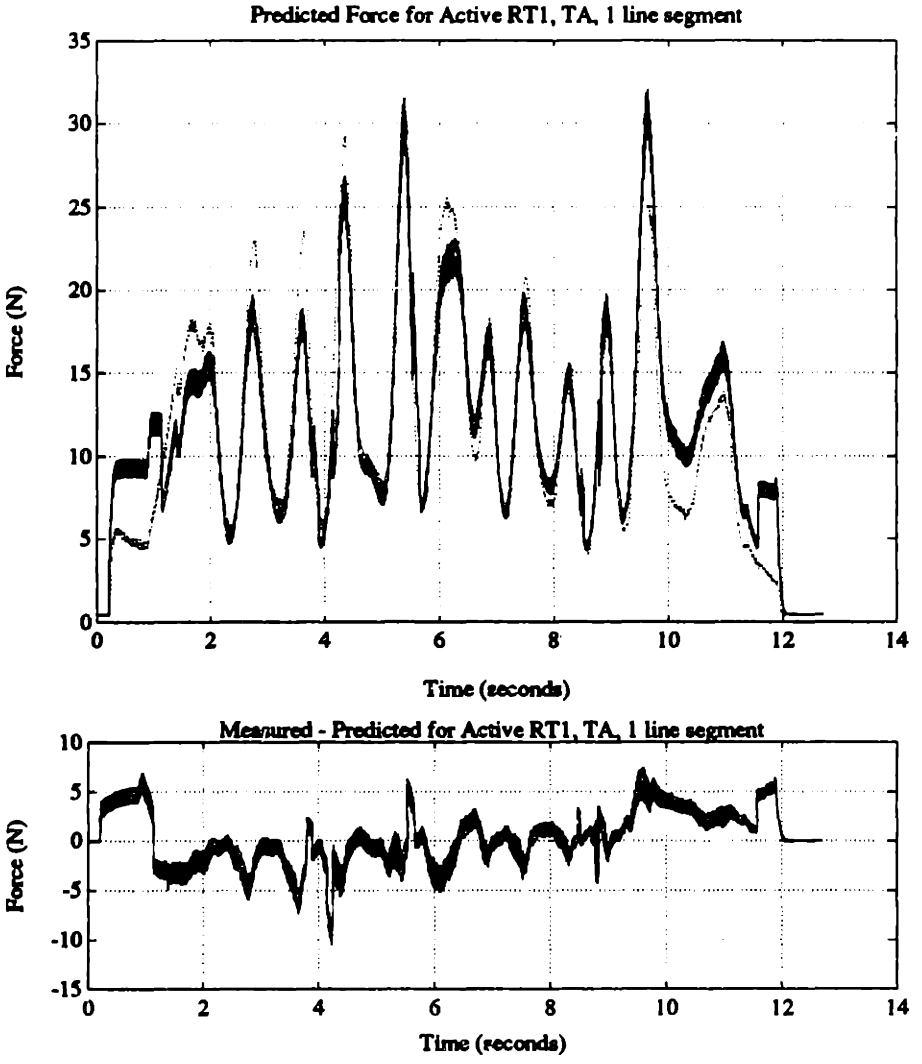

Figure 5.76: Difference between predicted (solid) and measured (dotted) active force, TA, 1 line segment estimated from short data set. Average squared error: 7.90 for entire data set, 6.96 for random trajectory. Stimulation level: 35 μs.

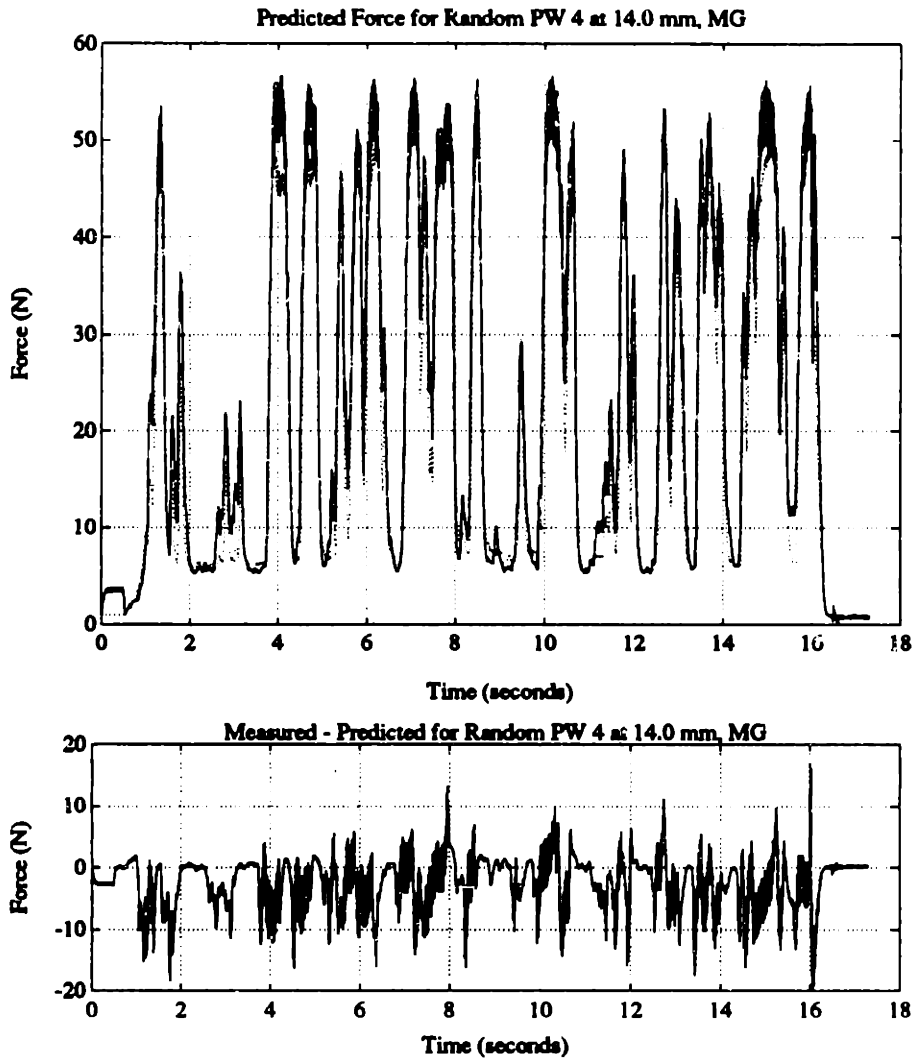

Figure 5.77: Difference between predicted (solid) and measured (dotted) active force, MG, *randclen*, random stimulation 4, 14.0 mm. Average squared error: 25.01 for entire data set, 26.82 for random pulse width. Stimulation range: 10 - 60 μs.

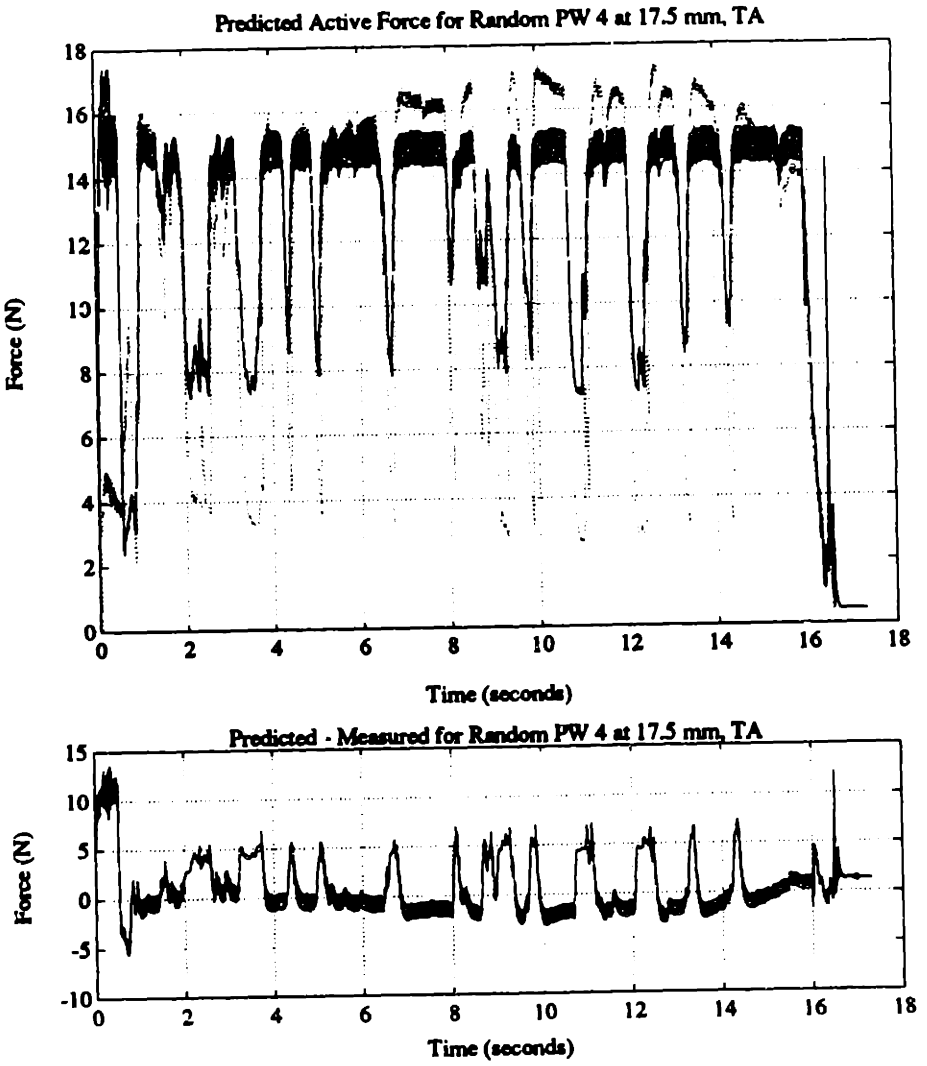

Figure 5.78: Difference between predicted (solid) and measured (dotted) active force, TA, *randclen*, random stimulation 4, 17.5 mm. Average squared error: 9.47 for entire data set, 6.40 for random pulse width. Stimulation range: 15 – 50 μs.

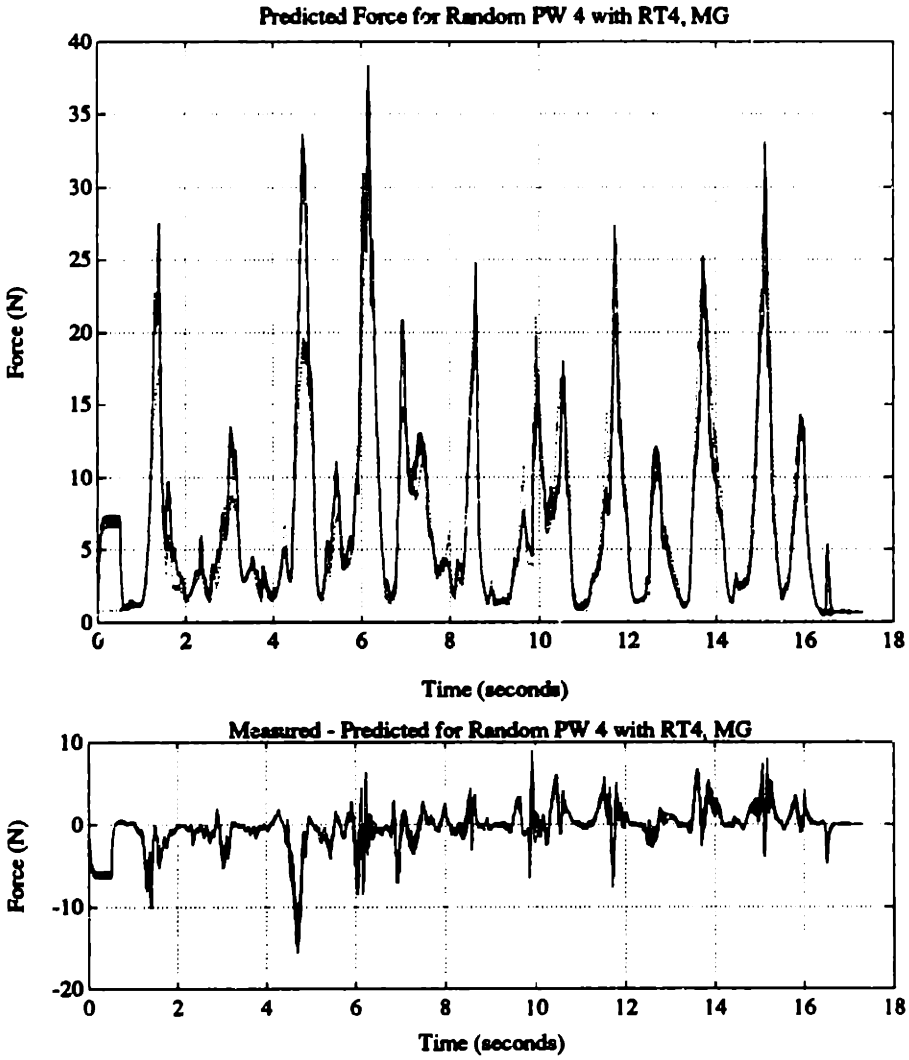

Figure 5.79: Difference between predicted (solid) and measured (dotted) active force, MG, *randrand*, PW4, RT4. Average squared error: 6.02 for entire data set, 5.28 for random trajectory and pulse width. Stimulation range: 20 –70 μs.

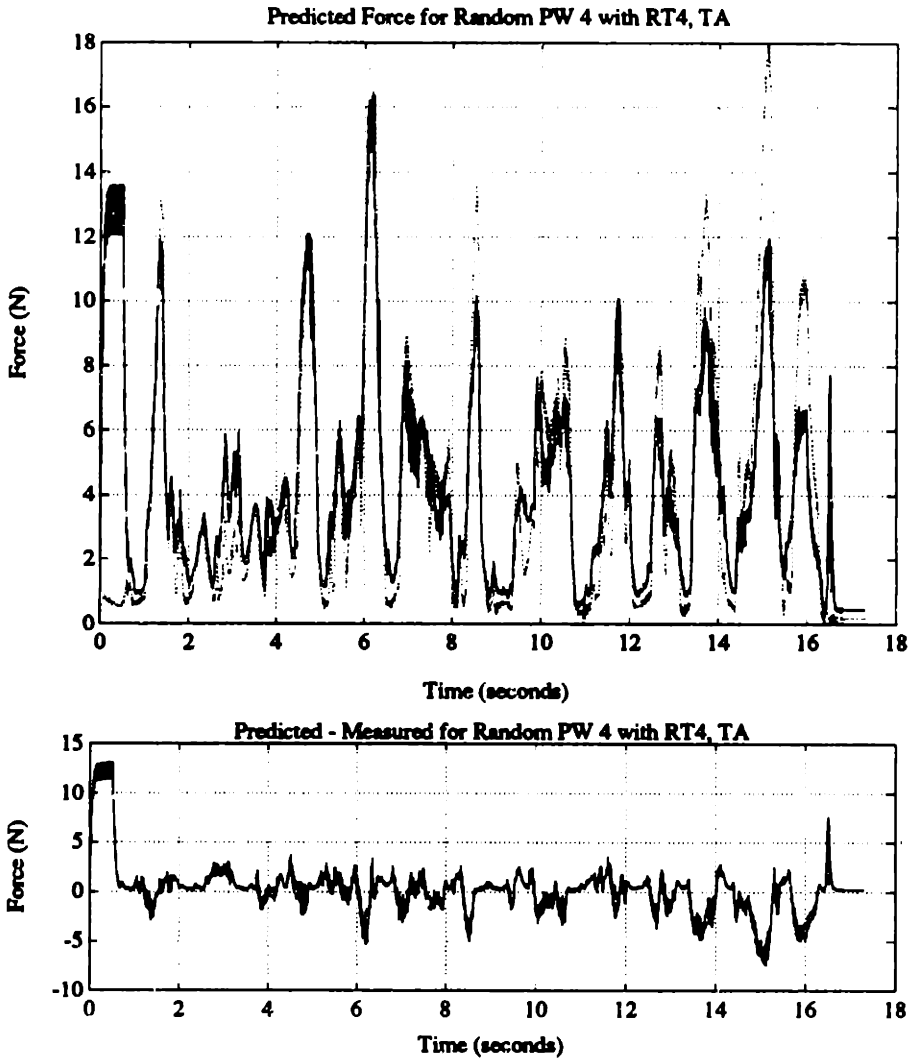

Figure 5.80: Difference between predicted (solid) and measured (dotted) active force, TA, *randrand*, PW4, RT4. Average squared error: 7.05 fro entire data set, 2.97 for random trajectory and pulse width. Stimulation range: 10 – 40 μs.

Chapter 6
Discussion

6.1 Passive Muscle Dynamics

6.1.1 Length Dependence

The passive length-tension relationships from the *stepmapl* data, shown in Figures 5.1 and 5.2 were consistent with the findings of Durfee [5] which are reprinted in Figures 6.1 and 6.2. The force developed by the passive MG was expected to increase exponentially with length. The force of the TA was expected to remain approximately flat over the range of lengths tested.

The passive length-tension curves generated by parameter estimation revealed similar shape characteristics (Figures 5.18 and 5.19). The force shown in the fitted curves is higher than the forces from the *stepmapl* protocol. Several factors influenced this. Experimentally, the instrumentation zero changed and the tendon clamp for the TA was replaced in the 7 hours between the generation of the two sets of data. In terms of the parameter estimation, the passive length-tension and force-velocity parameters were estimated simultaneously. The fitting algorithm produced the shape of the two curves, while post-processing determined the force offset. The force-velocity curve was adjusted so that zero force corresponded to zero velocity. This moved the passive length-tension curve to a higher force.

6.1.2 Velocity Dependence

The passive force-velocity curves were expected to resemble those of Figure 2.6 at very low stimulation levels. The curves shown in Figures 5.3 and 5.4 contained an obvious discontinuity between the lengthening and shortening forces which are not apparent in the figure published by Joyce, et. al. [10]. The difference in the curves could be accounted for either by the testing method or the test equipment and animal model.

Considering the test method, Joyce, Rack and Westbury started the lengthening movement from 5.0 mm shorter than the position they measured. For shortening, the constant velocity movement was started 5.0 mm longer than the measured length. The muscle was either stretched or shortened, never both, on a single run. Figures 5.3 and 5.4 were produced from the data generated by the *rlencstm* protocol, which gave a conditioning stimulation, waited 5.0 seconds, then ramped the length at a constant velocity (lengthening followed by shortening) for 14.0 mm for the MG and 17.5 mm for the TA. Figure 5.5 shows the passive force plotted against the length at several velocities. Note that there is hysteresis between the lengthening (upper)

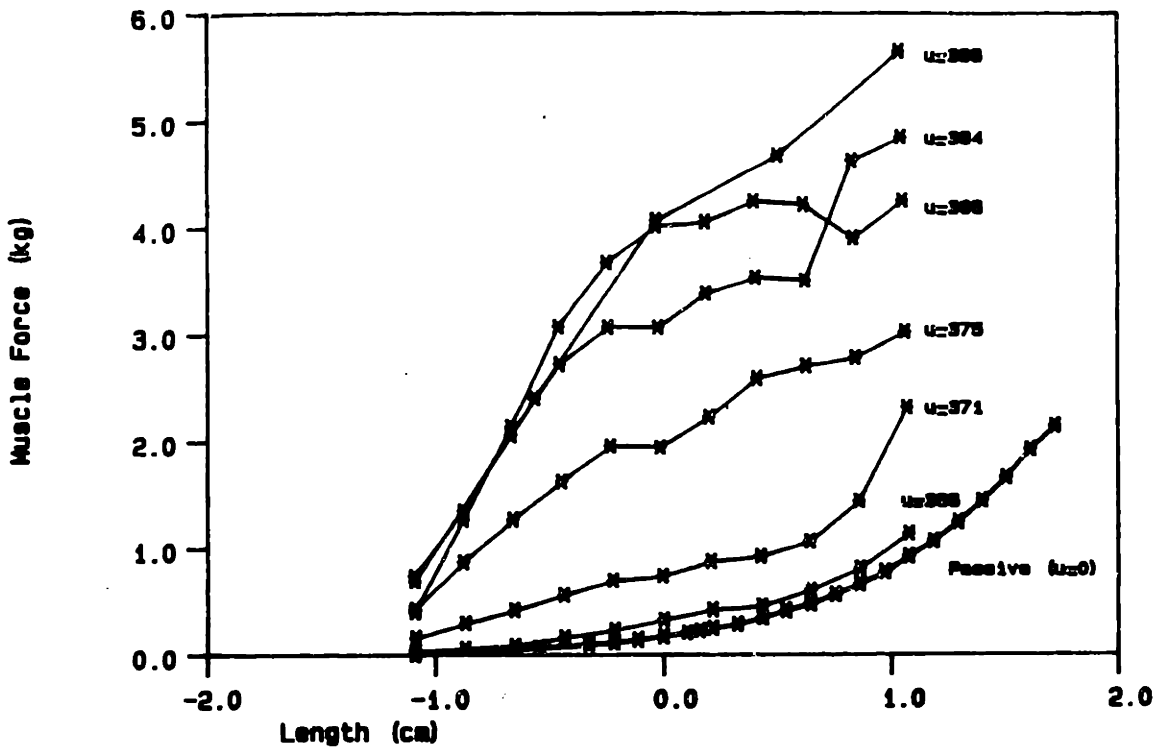

Figure 6.1: Active and passive length-tension curves for MG at several stimulation levels [5].

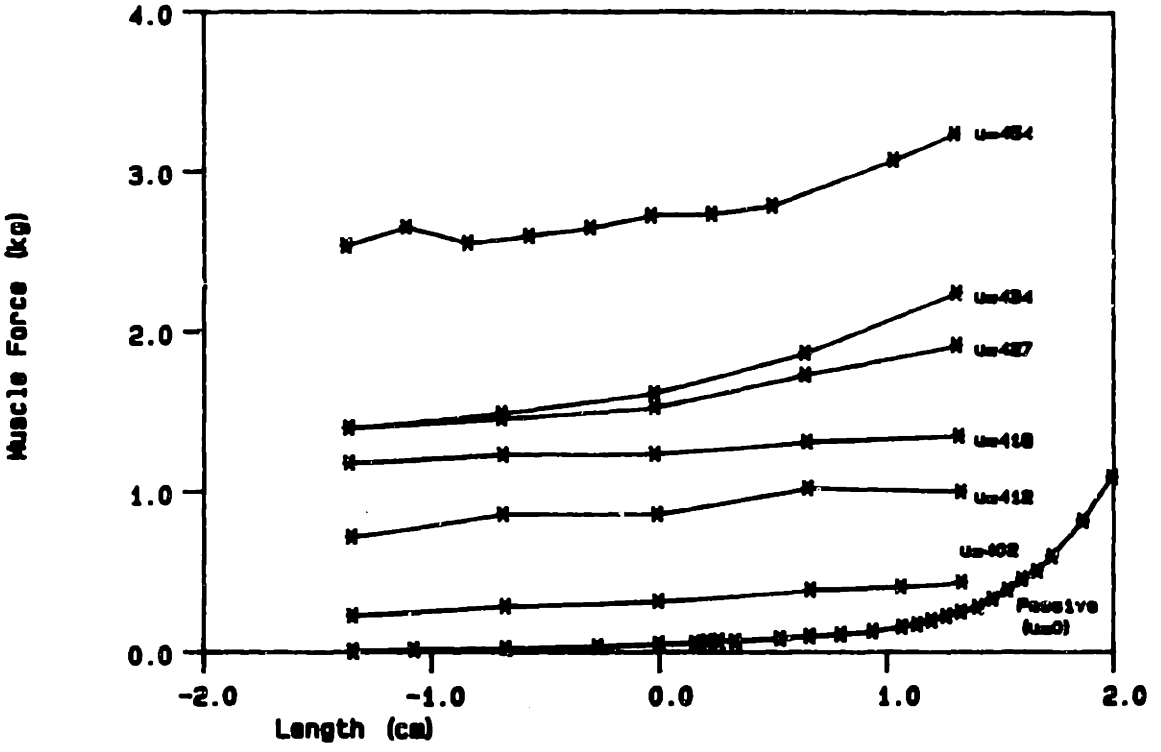

Figure 6.2: Active and passive length tension curves for TA at several stimulation levels [5].

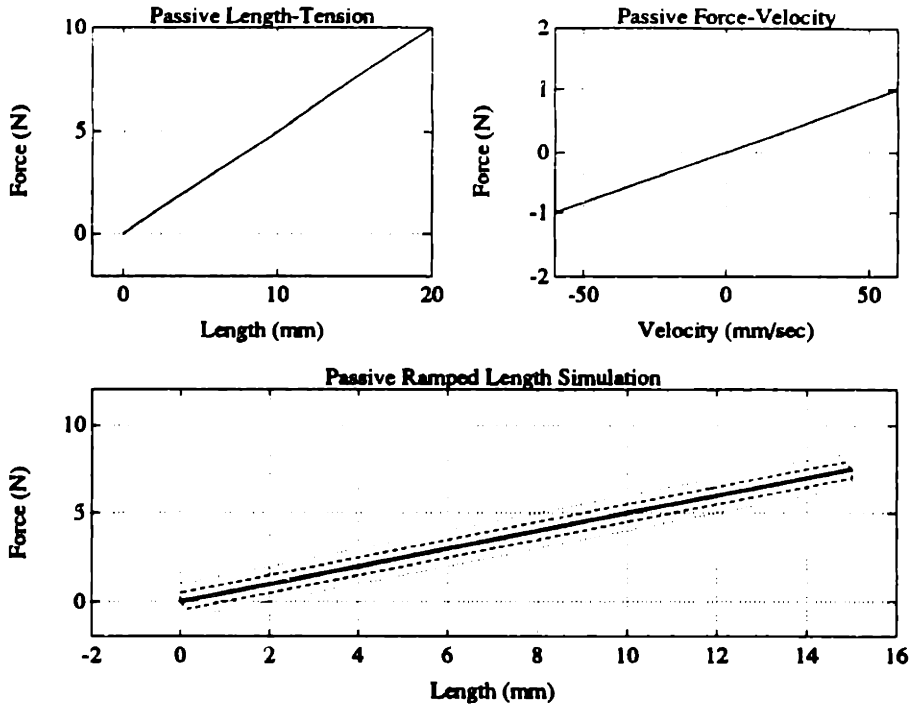

Figure 6.3: Passive stretching, with continuous linear length-tension and force-velocity curves, simulated. Velocity: 3.0 (solid), 30 (dashed), 60 (dotted) mm/sec.

and shortening (lower) curves, even for slow velocities. According to Winters [24], hysteresis results when passive tissue is stretched and then allowed to shorten, due to the viscoelastic nature of the material. Also, the amount of hysteresis is expected to vary with both the speed of ongoing extension and the history of recent extensions.

Figures 6.3 and 6.4 show simulated passive lengthening and shortening data. The first set was generated from linear, continuous passive force-velocity and length tension relationships. Note that the amount of hysteresis decreases with decreasing velocity. The simulations shown in Figure 6.4 were generated from the same length-tension curve as the first set. The force-velocity relationship had the same slope as the first one, but there was a discontinuity at $v = 0$. The hysteresis decreases with decreasing velocity, but it is never less than the value at the discontinuity. These simulations illustrate that if the hysteresis does not go to zero at slow velocities, there must be a discontinuity or other non-linearity in the passive force-velocity curve.

Another possible explanation for the discontinuity is residual effects of the conditioning stimulation. When the stimulation was turned off, the cross bridges in the contractile element did not spontaneously break. They were still attached and generated force in the contractile element when the muscle was passively stretched. As the muscle was stretched, the bonds broke and did not reform since there was no stimulation. If this was indeed what happened, the lengthening phase of the "passive" force-velocity curves in Figures 5.3 and 5.4 are a combination of active and passive

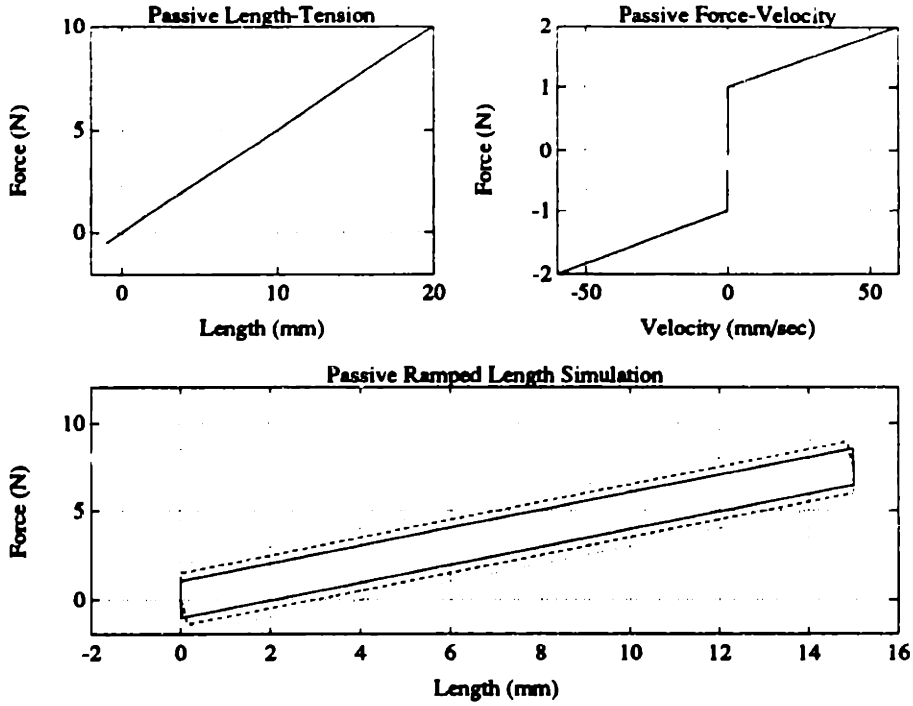

Figure 6.4: Passive stretching, with continuous linear length-tension curve and discontinuous linear force-velocity curve, simulated.

length-tension and force-velocity characteristics. This hypothesis is supported by the small errors in Figures 5.22 through 5.25 which show passive random position trajectories fit using force-velocity curves which did not have a discontinuity at zero velocity.

Another possible explanation for the discontinuity is Coulomb friction in the animal preparation or test setup. When the servo and torque transducer were checked without the animal preparation, there was no evidence of Coulomb friction. Hence, if the discontinuity is due to friction, it must be in the animal preparation. Possible sources could be: the tendon clamps sliding over the skin distal to the wound, the tendon and muscle sliding between the flaps of skin around the wound, or friction as the muscles moved within the body.

The passive force-velocity curves shown in Figures 5.3 and 5.4 change shape with length. For both muscles, the curves are nearly flat (excluding the discontinuity at zero velocity) for short lengths. At longer lengths, the shortening side remains relatively flat, but the lengthening half has a definite positive slope.

The fitted force-velocity curves of Figures 5.20 and 5.21 are approximately the same magnitude as those generated by the *rlencstm* protocol at lengths of 6–8 mm for the MG and 10–12.5 mm for the TA. The passive velocity dependent forces are small in comparison to the passive length dependent forces. (See fitted length-tension curves in Figures 5.18 and 5.19.) Since the passive force is not highly dependent

upon the velocity. it may be possible to simplify the model by either using fewer line segments to define the passive force-velocity relationship or eliminating it completely when the model is used to describe isolated muscle characteristics. However, the passive force may be more dependent on the velocity when intact muscles and joints are modeled. Further testing should be done to explore these possibilities.

6.1.3 Varying the Parameter Estimation Conditions

Changing the conditions for the passive parameter estimation did not significantly affect the fitted parameters as can be seen in Figures 5.26 and 5.27.

When twenty line segments were used to identify the passive length-tension and force-velocity curves, the length-tension curve was nearly identical to the ten segment curve. The most significant differences in the force-velocity curves were around ± 15 mm/sec. These were the approximate speeds of the constant velocity ramps between the instrumentation zero and the initial and final positions of the random trajectories. Using twenty line segments, the average squared error was reduced by 4.5 %. This means that each fitted point was 2.3 % closer to the measured point, not a significant improvement considering the additional computing time required to execute the more detailed model in an FES controller.

Omitting the constant velocity ramps by only using the data between t =1.4 to 11.4 seconds, improved the passive fitting. The ramps were at 15.44 and -13.96 mm/sec for random trajectory 3. The forces at these velocities were smaller when the constant velocity ramps were not used in the estimation. The average squared error was 3.5 % less for the shortened data set, so each point was 1.8 % more accurate. The conclusion to be drawn is that the passive force-velocity and length-tension curves can be estimated from either the entire data set or the shortened data set. Periods of constant velocity do not significantly affect the passive parameter estimates.

6.2 Active Dynamics

6.2.1 Stimulation

The isometric recruitment curves shown in Figures 5.28 through 5.31 exhibited the expected sigmoidal shapes. The shape is dictated by the location and size distribution of the individual motor unit axons. Large diameter axons have a lower stimulus activation threshold than small diameter axons [8 15].

The consistency in the shape of the curves measured at different lengths was unexpected. Hausdorff [9] found a significant length dependence in the shape of the IRC for human quadricep and hamstring muscles using surface stimulation. Crago, et. al. [3] also found that the IRC is dependent on the muscle length-tension curve.

The lack of time dependence in the shape of the recruitment curve for the MG was also unexpected. The replacement of the tendon clamp for the TA at 5:01 pm resulted in a shorter effective tendon length. The recruitment curves measured before

and after this event show substantial variation, but the curves for the two groups have approximately the same shapes. Hausdorff [9] and Durfee and MacLean [6, 13] found significant changes in the shape of the recruitment curve over both short and long time intervals.

Length Dependence

The total length-tension curve generated by *stepmapl* for the MG (Figure 5.6) was similar to the relationship shown in Figure 6.1. With a low stimulation level, the slope of the curve increased with length. As the stimulation level was increased, the curves became increasingly steeper.

The total length-tension curve for the TA, shown in Figure 5.7, is not smooth primarily due to the delay between measurement of adjacent points. In an effort to keep the data files to a reasonable size, the test lengths were split into two files. The first, third, fifth, and seventh points were measured approximately 30 minutes before the second, fourth, sixth and last points. By connecting the points in a single set, it is apparent that the slope of the curve does not change much, and that the force does not increase rapidly with length. This corresponds to Durfee's findings which have been reprinted in Figure 6.2.

The quasi-static length-tension curves of Figures 5.8 and 5.9 which were generated by averaging the forces developed during slow ramping of the length, are similar to the curves measured at constant length. The absolute value of the forces differ, but the change in shape as a function of stimulation is similar between the two sets of data.

The estimated active length-tension curves shown in Figures 5.56 and 5.57 were calculated from maximally stimulated muscle data and were expected to resemble the upper lines of Figures 5.6 through 5.9. The estimated curves show shape only, not absolute force. Once again, the MG shows a much steeper relationship between force and length than the TA.

The normalized forces for lengths shorter than 2.0 mm are high for both muscles due to an artifact of the experimental and fitting techniques. The data from which these curves were created was generated following the *cstmrand* protocol. The muscles were stimulated from 0.2 seconds to 0.9 seconds while held at the instrumentation zero length (no contractile element velocity when the series element compliance was zero). Both muscles developed some force during this initial stimulation. There were other force measurements which corresponded to zero velocity, but there were no other active points measured at zero length. When the fitting algorithm was used to minimize the errors of the entire data set, the shape of the force-velocity curve was influenced by other data points, and only showed a small bump at zero velocity. The length-tension curve was dominated by the zero length, zero velocity points and shows a large deviation from the general slope of the relationship. In Figures 5.56 and 5.57 the force computed with 0.05 mm/N compliance in the series element (dashed-starred line) is smaller for both muscles at the short lengths compared to the force computed

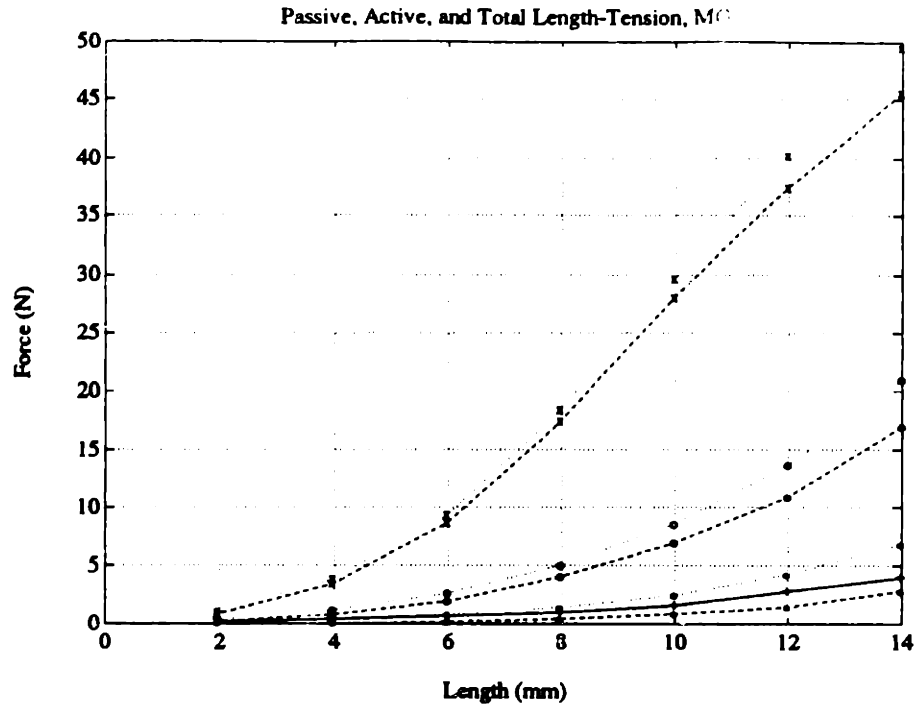

Figure 6.5: Total (dotted), active (dashed) and passive (solid) length-tension from *stepmapl*, MG. Stimulation levels: 0 (+), 20 (*), 40 (x) and 60 (o) μs.

by ignoring the compliance of the series element (solid-crossed line). The conclusion to be drawn from this analysis is that constant length and/or constant velocity position trajectories adversely affect the parameter estimation technique, and data associated with these trajectories should not be used as input to the parameter estimation routines.

The active length-tension parameter estimates show a flattening trend at long lengths which were not evident in either set of measured total length-tension curves. The estimated active curves were calculated after subtracting the passive force from the data. The shape of the estimated curves should be compared with the measured active length-tension curves, which is the total force less the passive force. These are shown in Figures 6.5 and 6.6. (Recall from Figure 2.2 that the total force is the sum of the active and passive forces.)

Velocity Dependence

The shape of the measured force-velocity curves (Figures 5.11 – 5.15) were expected to be similar to Figure 2.6, repreinted from Joyce, Rack and Westbury [10] which used the soleus muscle of the cat. The isometric force is not shown in Figures 5.11 – 5.15 because it was only measured once, approximately 6 hours before the other data points and at different stimulation levels.

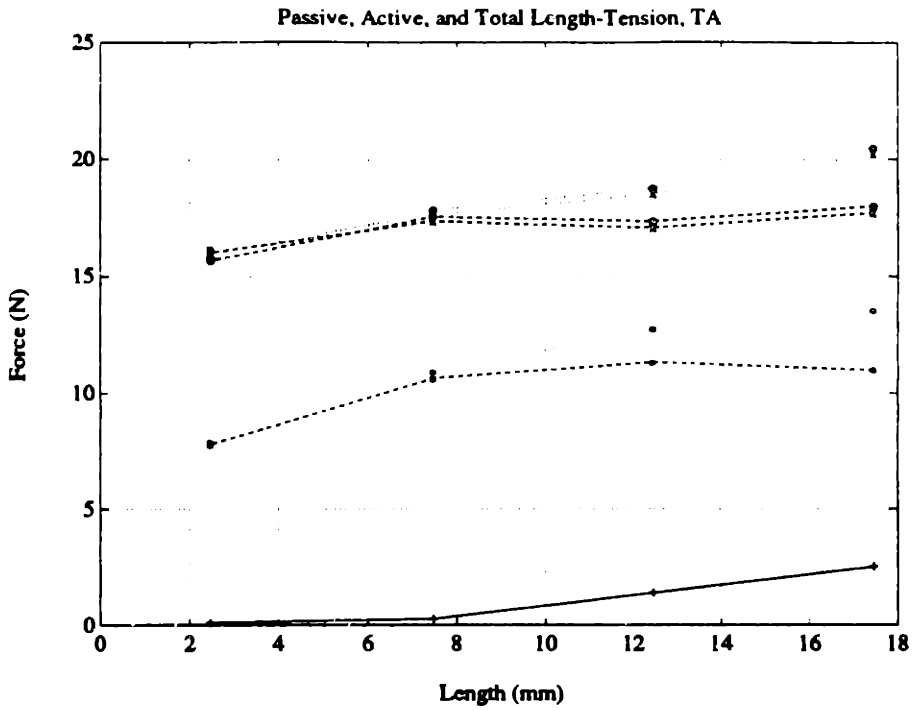

Figure 6.6: Total (dotted), active (dashed) and passive (solid) length-tension from *stepmapl*, TA. Stimulation levels: 0 (+), 30 (*), 50 (x) and 70 (o) μs.

The force-velocity curves for the lengthening MG, shown in Figures 5.11 and 5.14 did not have the expected shape. The force was expected to remain constant or increase slightly with increasing velocity. The actual relationship shows a decrease in the force with increasing velocity of lengthening.

The time varying characteristics of the MG, combined with the experimental protocol, may explain the unexpected shape of the force-velocity curve. The force output of the stimulated MG increased over time. The parameter estimation technique produced the best fit to the measured force by splitting the error - half positive and half negative. In the error plots of Figures 5.38, 5.40, 5.46, 5.52, and 5.54, the measured force is consistently less than the fitted for the first six seconds of the stimulation. After six seconds, the measured force is consistently larger than the fitted. There was a gradual increase in the measured force as a function of time. This is also evident in the force measurements for random trajectory 1, the dotted line in Figure 5.72. The length trajectory for the periods between $t = 1.5$ to 2.25 and $t = 10.5$ to 11.25 were nearly identical in terms of position and velocity, but the measured force was approximately 11 N higher for the second time period. These observations are applicable to the active force-velocity curves when the protocol is examined closely. Figure 6.7 shows selected ramp length trajectories from the *rlencstm* protocol as a function of time. Note that for the fastest constant velocity ramp, the lengthening force measurement at $l = 12$ mm was read after 1.1 seconds of stimulation. As the ramps became

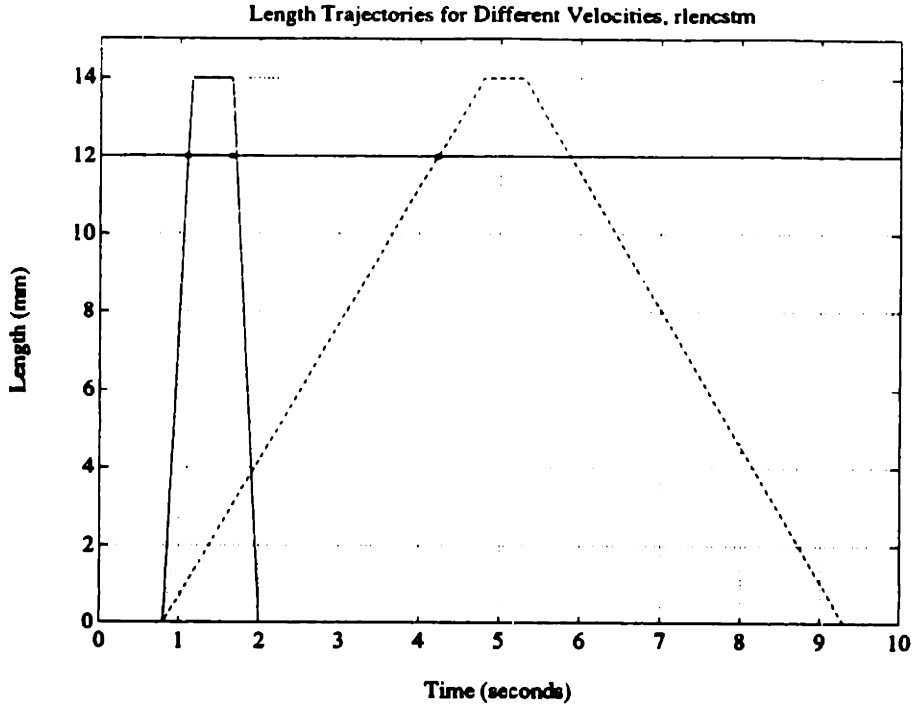

Figure 6.7: Length as a function of time for current *rlencstm* protocol. Stimulation starts at $t = 0$. Constant velocities of 40 (solid), 14 (dotted), and 3.5 (dashed) mm/sec shown. Muscle was stimulated for 1.1, 1.7, and 4.2 seconds when lengthening force at 12 mm was measured.

slower, the corresponding force measurements were taken after increasing periods of stimulation. For the slowest constant velocity ramp, the MG was stimulated for 4.23 seconds before the force was measured at a length of 12 mm. Since the MG exhibited an increase in force with the time period of stimulation, the force measurements for fast velocities were lower than they would have been if all force measurements were taken at the same time. For future experiments, the series of length/stimulation patterns shown in Figure 6.8 or 6.9 should be considered.

The decreasing force with increasing lengthening velocity trend was not evident in the data from a prior animal experiment shown in Figure 6.10. For that experiment, the *rlencstm* protocol was slightly different. Instead of using the same stimulation level at different velocities to define a "run," the velocity was held constant and the stimulation level was varied. The run always started with a passive ramp followed by a ramp with the stimulation level at 100 μs, then five stimulus levels within the zoom range. The protocol was changed for the experiment of July 11, 1990 because the earlier data showed fatigue during the slower ramps at the end of the run.

The force-velocity curves for the TA, shown in Figures 5.12, 5.13, and 5.15 were approximately the expected shape. The oscillations in the curves are a result of measuring the different velocities in runs separated by approximately 20 minutes.

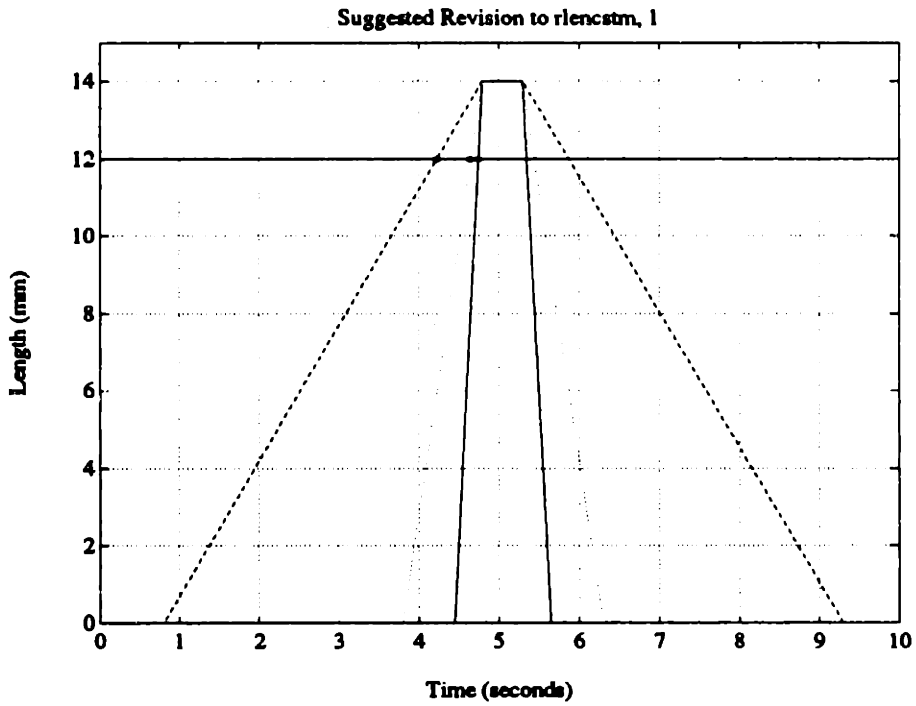

Figure 6.8: Suggested revision to *rlencstm* protocol. Stimulation starts at $t = 0$. Constant velocities of 40 (solid), 14 (dotted), and 3.5 (dashed) mm/sec shown. Muscle would be stimulated for 4.75, 4.66, and 4.23 seconds when lengthening force at 12 mm was measured.

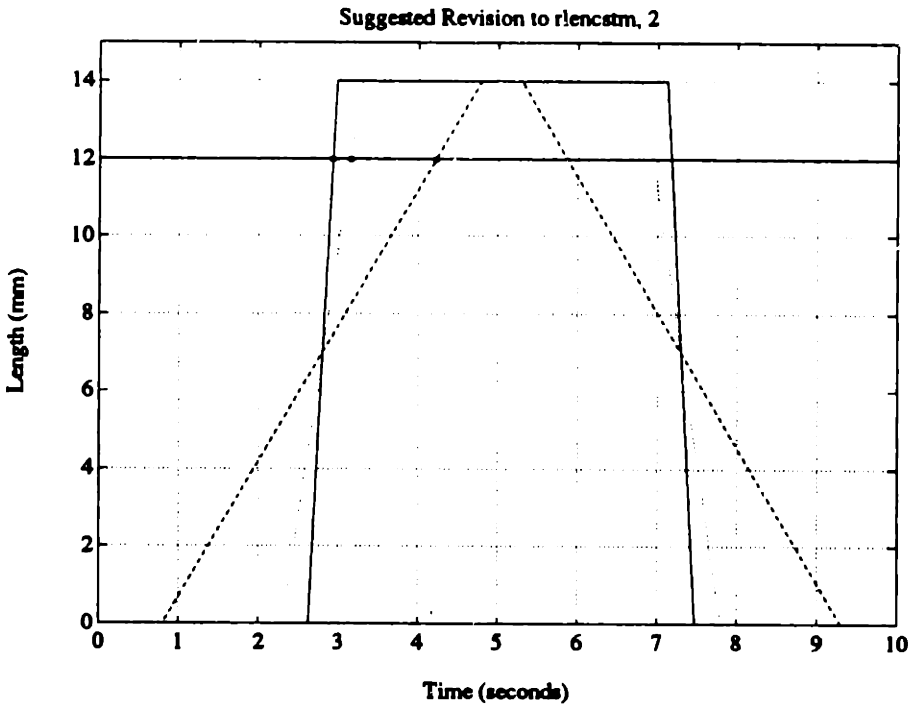

Figure 6.9: Suggested revision to *rlencstm* protocol. Stimulation starts at $t = 0$. Constant velocities of 40 (solid), 14 (dotted), and 3.5 (dashed) mm/sec shown. Muscle would be stimulated for 2.25, 3.16, and 4.23 seconds when lengthening force at 12 mm was measured.

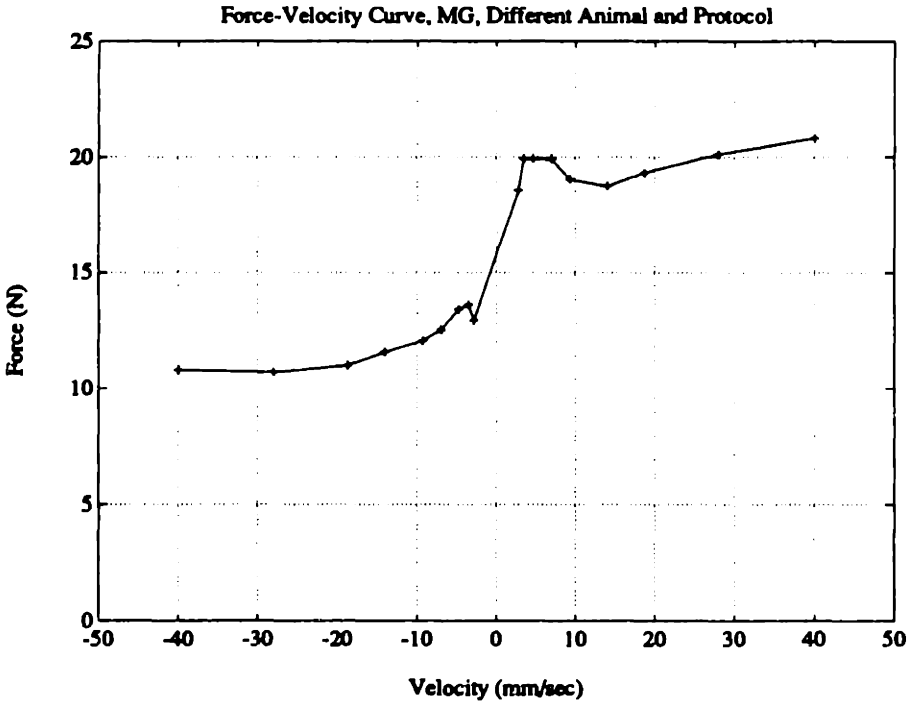

Figure 6.10: Active force velocity curve for MG, different animal, different protocol. Length: 12 mm, stimulation level: 100 μs. Active ramped lengths were separated by 82 minutes (fastest to slowest). Each active ramp was preceded by a passive ramp at same velocity.

The first, third, fifth, and seventh fastest data points at each stimulation level were measured before the others.

The estimated active force-velocity curves shown in Figures 5.36 and 5.37, which were generated from three different random position trajectories, are different from each other. The cause of these differences are the ramps between the instrumentation zero and the beginning and ending points of the random trajectories. The servo moved at a constant velocity for 0.5 seconds. This generated many force measurements at one velocity. The parameter estimation technique, while minimizing the errors for the whole data set, was heavily influenced by the constant velocity ramps. The line segments which included those velocities were skewed. Since each random trajectory had a different starting point, the ramp velocities were not the same. This let to differences in the force-velocity curves.

The shape of the estimated force-velocity curves for the shortened data sets, shown in Figures 5.58 and 5.59, are similar to those shown in Figures 5.11 through 5.15. For the MG, the estimated curves are most like those shown at shorter lengths and lower stimulation levels.

6.2.2 Varying the Parameter Estimation Conditions

Data Set Length

The length-tension curve parameter estimates which used the entire data set had an obvious discontinuity at lengths less than three (3) mm. (Figures 5.34, 5.35, 5.56, and 5.57.) This was an artifact of the fitting technique as described in Section 6.2.1. When force predictions were made from these length-tension curves, large errors were generated at short lengths when the stimulation was on. This explains the large errors between $t = 0.2 - 1.2$ and $11.8 - 12.0$ in Figures 5.38, 5.39, 5.46, and 5.47.

Using only the random trajectory portion of the *cstmrand* data to estimate the parameters yielded a better fit to the data and smoother length-tension and force-velocity curves as seen in Figures 5.56 through 5.59. For the full data set, the constant velocity ramps between the instrumentation zero and the initial and final positions of the random trajectories significantly influenced the force-velocity curves at those velocities. The activation at instrumentation zero and zero velocity resulted in high values in the length tension curve at lengths below 3 mm. These factors did not affect the shortened data set which went from $t = 1.4$ to $t = 11.4$ seconds.

One disadvantage of using the shortened data set was that the length-tension curve was not defined at short lengths. The *cstmrand* protocol started at the instrumentation zero position. The random trajectory range was set to 4 to 14 mm for the MG, 5 to 17.5 mm for the TA. The only force measurements for lengths less than 4 mm for the MG and 5 mm for the TA were made at $0 < t < 1.4$ and $t > 11.4$. The short data set eliminated all of these measurements resulting in estimated length-tension curves which were only defined at lengths greater than 4 mm for the MG and 5 mm for the TA. As a result, the parameter estimates from the short data sets could not

be used for force prediction of protocols which tested the muscle at lengths less than 4 and 5 mm.

Linear Series Element

The series elastic element was expected to significantly reduce the data fitting errors. Parameter estimates using the entire data set with 0.05 mm/N linear series compliance are shown in Figure 5.42 through 5.45. This value for compliance gave the lowest average error for both muscles, although there was no improvement in fit compared to parameter estimates which used zero compliance. Also, the correlation between parameter estimates from each of the three random trajectories was lower. (Compare Figures 5.42 - 5.45 with 5.34 - 5.37.)

Parameter estimates for the shortened data set with 0.05 mm/N compliance in the series element are shown in Figures 5.48 through 5.51. The correlation between estimates for each of the random trajectories is much better than when the full data set was used (Figures 5.42 - 5.45). The errors for the short data set with the series element were 30.9% and 1.2% worse than with no compliance for the MG and TA respectively.

The series elastic element was assumed to be linear with zero offset. This was only one of the possible representations listed by Winters [24]. Other structures which could be used to model the series element include: a spring with an initial concavity followed over a large part of the operating range by a linear region [26]; a traditional concave upward exponential curve, with a linear relationship between stiffness and force; a viscoelastic model including one of the aforementioned springs; a series connection of two (or more) nonlinear springs [21], with one spring modulated by force and the other by activation; a single stiffness value which is a weighted function of force and activation, with element extension determined via integration.

The other implementations partially take into account the multiple sources of series compliance. These include the effects of pennation angle, compliance within the cross bridges, change in compliance with activation level, non-linearity of the tendon force-length curve, and the visco-elastic properties of the tendon [7]. By using a linear spring, the sources of compliance are limited to the tendon. The 0.05 mm/N compliance, which was found to be the optimal value for the linear spring in these data fitting routines, is supported by the findings of others for the compliance of tendons. Rack and Westbury [19] reported the compliance of cat soleus tendon to be 0.05 mm/N. Morgan [17] found cat soleus tendon to have compliance between 0.03 and 0.08 mm/N. Walmsley and Proske [23] found 0.05 mm/N for cat soleus and 0.06 mm/N for cat medial gastrocnemius (MG) tendons.

It was beyond the scope of this thesis to investigate other implementations of the series elastic element. Future work with this model and identification technique should include efforts to characterize the series element more accurately.

No Impulse Response

Figures 5.54 and 5.55 show the results of fitting the data without using the impulse response. The stimulation level was put through the IRC then held constant over the 0.025 ms between stimulations. The other data fitting results used the stimulation through the IRC then convolved with the impulse response to define the activation levels between the stimulation delta functions. Convolution with the impulse response results in an activation record which has 40 Hz ripple. The ripple accounts for approximately 12 % of the total value of the activation.

The improvement in the data fitting was marked when no impulse response was used. The average squared error was reduced by 5.7 and 19.0 % for the shortened data sets. The fitted data was much smoother, more like the measured data. The active parameter estimates in Chapter 5 were done on data generated at high stimulus levels (60 μs for the MG, 35 μs for the TA). At these stimulation levels, the contraction was expected to be fused and relatively free of ripple. Significant ripple is characteristic of low stimulation levels and/or slower stimulation rates (compared to 40 Hz). Parameter estimation and data fitting at lower stimulation levels should be performed to determine if the impulse response block is required in a model to be used for FES control.

6.3 Prediction of Muscle Force

Muscle force prediction is a method of testing the model's validity. A good model should use the estimated parameters calculated from a set (or sets) of input-output data to predict the output of any other set of inputs. Some error in the force prediction should be expected due to measurement errors and muscle characteristics changing with time.

Another factor which influences the model's ability to accurately predict the output force is the detail of the estimated parameters. The active and passive length-tension relationships shown in Sections 5.1 and 5.2 are non-linear. A model which uses only one line segment to represent these relationships will not predict the force as accurately as if the same model used several line segments. However, at some point, additional line segments will not significantly improve the model's prediction ability and will merely increase the computation time required to predict the output force.

6.3.1 Passive Force Prediction

The passive force for random trajectory 1, predicted using the parameters estimated from random trajectory 3 are shown in Figures 5.62 through 5.67. The prediction errors were lowest when one line segment was used to describe the force-velocity relationship and 10 line segments were used for the length-tension curve. It is counter-intuitive that using only one line segment to describe the passive force-velocity relationship results in more accurate force prediction than when using ten line

segment descriptions. The passive force-velocity curve is nearly linear as evidenced by the solid line in Figures 5.60 and 5.61. The maximum lengthening and shortening velocities for the MG on random trajectory 3 were 33.11 and -28.08 mm/sec. For RT1, the maxima were 36.8 and -34.2 mm/sec. The maximum velocities for the TA were also greater for RT1 compared to RT3. Since the parameters for the prediction were from RT3 (which had the smaller range of velocities), the prediction routine estimated the force corresponding to velocities which were outside the range of the defined velocities by using the same slope as the fastest and slowest line segments. Since the slopes of these line segments deviated from the general trend of the force-velocity curves, error was introduced when the ten segment force-velocity curves were used.

Using the passive parameter estimates from RT3 to predict the output of the *rlencstm* protocol is shown in Figures 5.68 and 5.69. The constant difference between the predicted and measured forces at zero length and zero velocity is a result of the length change when the instrumentation zero changed. For the TA, the passive force during the ramp would have been predicted more accurately by a less steep passive length tension curve. In the 242 minutes between the ramped length and the random trajectory test runs, it appears that the TA's passive characteristics shifted from a relatively flat length-tension curve toward a steeper one. This may have been the result of a change in the effective length of the muscle when the instrumentation zero changed, a change in the passive characteristics due to tendon creep or other time varying properties, or an artifact of the testing procedure since there were many passive tests before the ramped length test, but the passive random length trajectory was preceded by an active random length trajectory test (residual cross bridges may have resulted in a steeper "passive" length-tension curve).

6.3.2 Active Force Prediction

The active length-tension and force-velocity parameters which were used to predict the active muscle force are shown in Figures 5.70 and 5.71. They were generated from the output of *cstmrand* using RT3 as the random trajectory. The ten line segment TA and both the ten and one segment MG parameters were estimated using the entire data set (including the constant velocity ramps at the beginning and end of the random length section) assuming no compliance in the series elastic element. The one segment (dashed line) parameters used the short data set (t = 1.4 to 11.4) with no series compliance. Obviously other conditions for the parameter estimation would have given slightly different parameters. The results presented in Table 5.2 suggest that other model assumptions may have produced better active force predictions since they produced smaller fitting errors. Future use of this model should explore force prediction using other model assumptions.

The force predictions using RT1 with the *cstmrand* protocol are shown in Figures 5.72 through 5.76. Using ten line segments to describe the active length-tension and force-velocity relationships for the MG produced much better predictions than

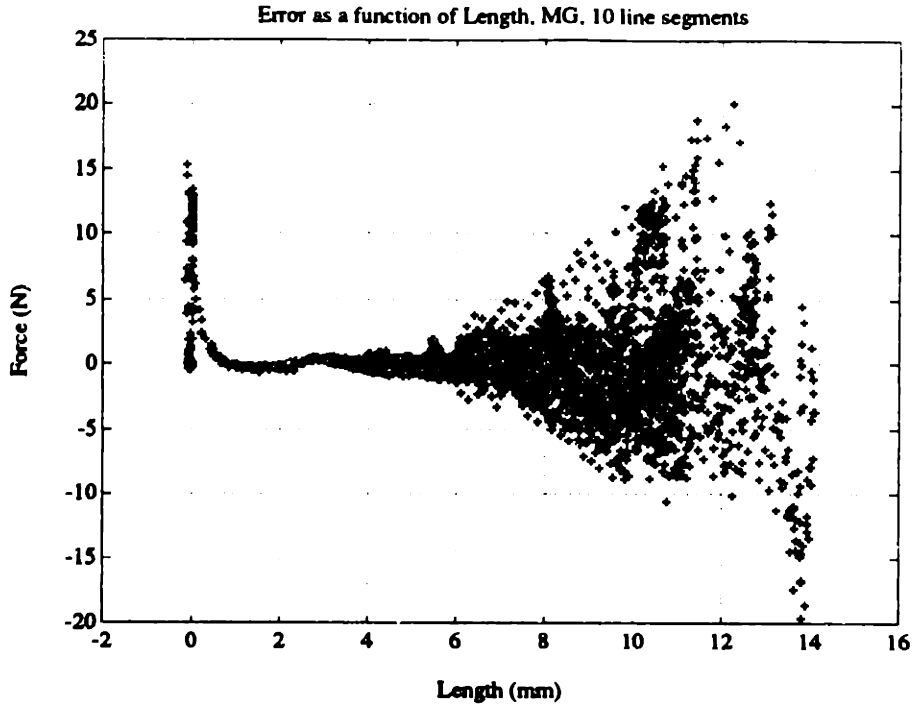

Figure 6.11: Prediction error as a function of length. MG, 10 line segments.

the single line segment parameters calculated from the entire data set. Although the average squared errors were only about twice as high for this one segment prediction, the nature of the error would seriously limit the usefulness of an FES controller. The basic problem is that the errors in Figure 5.74 are well correlated with the length. Figures 6.11 and 6.12 show the errors for the ten segment and the single segment prediction, using the entire data set, plotted as a function of length. Note that the errors associated with the ten segment prediction are approximately evenly distributed with positive and negative error associated with all the lengths, while the single segment prediction underestimates the measured force at lengths shorter than 7.5 mm and consistently overestimates the force at lengths longer than 11 mm. When the error is strongly correlated with a given variable (such as length), the FES controller with limited feedback channels will not perform well. The error associated with the prediction using single segment parameters from the shortened data set are not correlated to length over the entire range, as shown in Figure 6.13. When one segment is used to describe a non-linear relationship, the data set used to estimate the parameters should not contain constant velocity or constant length sections.

The predicted force for the *randclen* protocol using random pulse width 4 are shown in Figures 5.77 and 5.78. These predictions were made assuming no compliance in the series element. Since the servo maintained a constant position throughout the random stimulations, the change in the predicted force over time is a function of the stimulation level only. (The passive force was constant since the total length was

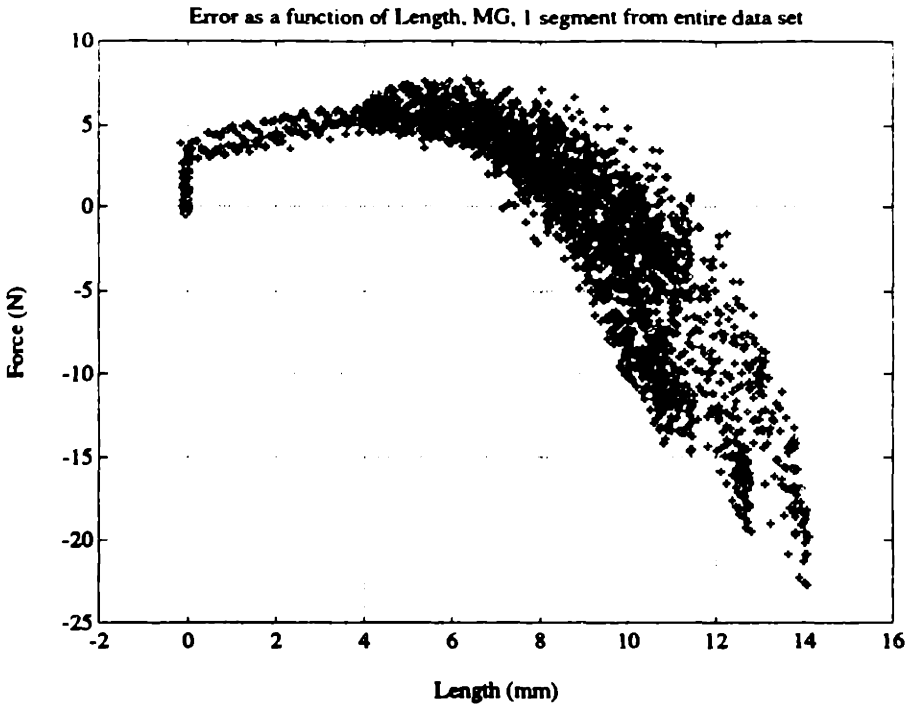

Figure 6.12: Prediction error as a function of length. MG, 1 line segment estimated from entire data set.

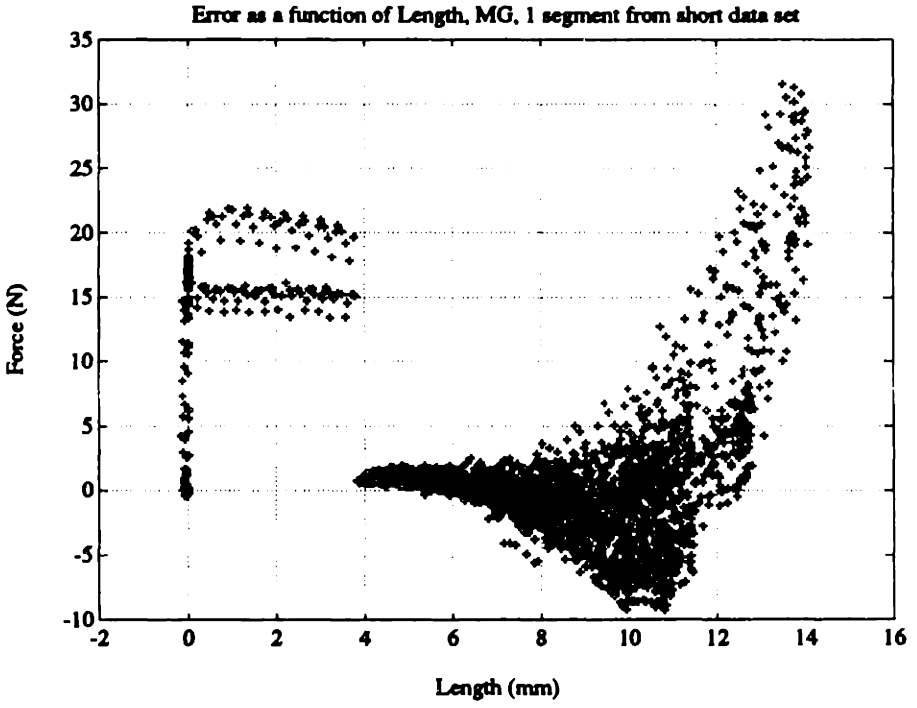

Figure 6.13: Prediction error as a function of length. MG, 1 line segment estimated from short data set.

constant. The forces due to the active length-tension and force-velocity curves are constant since the total length is constant and there is no compliance in the series element.) The predicted force was therefore highly dependent on the accuracy of the isometric recruitment curves which were calculated 238 minutes before the actual force was measured. Note that for the TA, the (constant) passive force was expected to be 6.85 N based on the passive length tension curve shown in Figure 5.61. Since the total force fell below this level, the magnitude of the predicted force does not match the measured at low stimulation levels, although the predicted force oscillates in approximately the same manner as the measured force.

The predicted force for random pulse width 4 and random trajectory 4 are shown in Figures 5.79 and 5.80. For the TA, the total measured force was lower than the predicted passive force at short lengths, so once again, the total predicted force was consistently larger than the measured force at short lengths.

Chapter 7
Conclusions and Recommendations

7.1 Conclusions

The parameter estimation techniques described in Chapter 3 can be used to fit the muscle model to specific muscles. The model can then be used to predict the force of the muscle, using a wide variety of stimulation, length and velocity inputs. The simplifying assumptions used to develop the muscle model (described in Chapter 2) are valid. Observations and conclusions regarding the specific model relationships follow.

The passive length-tension curves developed from the *stepmapl* protocol were similar in shape to the estimated parameters. The curves were also consistent with the findings of Durfee [5] for the same muscles. The passive length-tension relationship is non-linear. Assuming it was linear led to poor force prediction performance by the model.

The passive force-velocity curves which were developed by ramping the length at constant velocity exhibited a discontinuity at zero velocity which are a result of the testing technique. The parameter estimates were of approximately the same magnitude as the classical curves but the discontinuity was not evident in the estimated curves as they were nearly linear. Assuming a linear relationship between the passive force and velocity produced the most accurate force predictions. Linearity, combined with the small magnitude of the passive force-velocity curve in comparison to the passive length-tension curve, indicate that the passive force-velocity relationship is not important when modeling single, isolated muscles. The passive characteristics of non-isolated, whole joint muscles are expected to be more dependent on velocity.

The isometric recruitment curve remained relatively constant in shape over both time and length. Other experiments using the same [6, 13] and different [3, 9] muscles have shown that the shape of the IRC varies with both length and time. The change in peak force during the ramp stimulation as a function of length was similar to the active length-tension curve. The peak force decayed considerably over time.

The active length-tension curves measured by ramping the length at a slow velocity were similar to those measured isometrically. The shape and magnitude of both sets of curves changed as a function of stimulation level. The estimated length tension curves were of approximately the same shape. The length-tension relationship was much steeper for the MG compared to the TA. This was consistent with Durfee's [5] findings. Assuming the active length-tension curves were linear on the logarithmic axes (using parameters calculated from the shortened data set – no constant length and velocity data points) produced force predictions which roughly followed the measured force. However, caution must be used when determining the one line segment parameter

estimate. Using one line segment parameters estimated from the entire data set produced unacceptable errors.

The active force-velocity curves for the MG which were calculated from constant velocity ramp measurements were not the expected shape. At long lengths, the force for fast lengthening was significantly less than for slow lengthening and only slightly larger than the force for fast shortening. This was a result of the timing of the lengthening ramps in relation to when the stimulation started. The estimated active force-velocity curves for the MG did not exhibit this shape phenomena. The active force-velocity curves for the TA were consistent with the parameter estimates and both were the expected shape. Assuming the force-velocity curve was linear on the logarithmic axes produced reasonable force predictions.

The series elastic element was assumed to be linear in the relationship between the force of the contractile element and the difference in length between the musculotendon unit and the contractile element. Using linear series compliance to estimate the active parameters did not improve the fit. Alternative assumptions about the shape of the series elastic relationship should be explored.

7.2 Recommendations

For future animal experiments, the following changes should be implemented:

1. Modify the passive *rlencstm* protocol, which ramps the length at a constant velocity, so that it passively stretches the muscle between the conditioning stimulation and passive ramps. By using a high frequency sinusoidal trajectory or a random length trajectory, any residual cross bridges from the conditioning pulse will be passively broken before the force-velocity data is measured. This addresses the issue of the discontinuity in the passive force-velocity curve. An alternative approach would be to omit the conditioning pulse before passive ramps.

2. Modify the active *rlencstm* protocol to reduce the effects of the time varying characteristics of the muscle which resulted in an unexpected shape of the active force-velocity curve for the MG. Suggested modifications are shown in Figures 6.8 and 6.9.

3. Do all of the stimulations for a single classically determined curve in one file. The active length-tension and force-velocity curves for the TA are not smooth because the data measured during distinct runs of the *rlencstm* and *stepmapl* protocols were not consistent. In general, the MG curves may also be affected by this problem, but it was not evident in the data from this experiment.

4. Use a spline function or other non-constant velocity trajectory to move between the instrumentation zero and the initial and final lengths of the random trajectories in the *cstmrand* protocol. Also consider covering the entire range of test

lengths with the random trajectory. For this experiment, the random trajectories were limited to 4 - 14 mm for the MG and 5 - 17.5 mm for the TA. When the constant velocity ramps were discarded from the data set, there were no force measurements for lengths shorter than 4 and 5 mm, respectively.

Some suggestions for improvements to the model are:

1. Explore alternative structures for the series elastic element as outlined in Section 6.2.2 to improve model force predictions. The assumption of linearity was the simplest to implement, although it is probably not the most suitable.

2. Eliminate the impulse response from the active force calculations. Experimental data often exhibits a slight amount of ripple at the stimulation frequency. Convolving the impulse response with the activation achieves ripple in the model output. However, the calculated ripple is often much larger than the measured, resulting in significant errors. The measured force may be better predicted by a smooth model output.

3. Eliminate the passive force-velocity curve when single muscles are modeled. The magnitude of the force as a function of velocity is small compared to the passive length-tension curve. It may be possible to simplify the model by eliminating the passive force-velocity curve completely. Further testing should be done, particularly with non-isolated muscle preparations which have the passive characteristics of all of the muscles and tissues surrounding the joint contributing to the passive force-velocity characteristics.

Appendix A
Experimental Protocol

This appendix is a record of the animal experiment which was performed on July 11 and 12, 1990. The animal was anesthetized at 8:30 am. The muscles were isolated and the electrodes were implanted during the surgical procedure which lasted from 9:30 am until 1:45 pm. The test system was calibrated between 2:00 and 3:00 pm. Each protocol was run once with the animal on the test bed before the experimental data was collected. Data was collected between 3:50 pm and 1:50 am.

The experiment was divided into six blocks, corresponding to the six protocols outlined in Section 4.2.4. *Fastramp* was run at the beginning of each block to determine the appropriate "zoom limits," or range of stimulation pulse widths. A summary of the blocks is given below, listed in the order in which they were performed.

Block 1: RSTMCLEN

The muscle was held isometrically while the stimulation level was ramped within the zoom limits. Each muscle was tested at eight lengths. The data from this block was used to determine the change in the isometric recruitment curve as a function of length.

Block 2: STEPMAPL

The muscle was held isometrically while a constant stimulation was delivered to the muscle. Each muscle was tested at four stimulation levels, including passive, and at eight lengths. This data was used to produce the passive and active length-tension curves.

Block 3: RANDCLEN

The muscle was stimulated with a predetermined random sequence of pulse widths while the length was held constant. Each muscle was tested at two lengths with four random stimulation sequences. This data was used to verify the force prediction capability of the fitted model.

Block 4: RLENCSTM

The muscle was stimulated at a constant level while the servo lengthened then shortened the muscle at constant velocities. Four stimulation levels, including passive, were used with eight velocities. The passive and active length tension curves were created from this data.

Block 5: CSTMRAND

The muscle was lengthened and shortened following a predetermined random trajectory while it was stimulated at a constant level. Four stimulation levels, including passive, where used with three random length trajectories. This data was used to estimate the passive and active length-tension and force-velocity curves.

Block 6: RANDRAND

The muscle was randomly stimulated while the servo followed a random length trajectory. Four random stimulation sequences were used with three random length patterns. The data was used to verify the force prediction capability of the fitted model.

The details of each block are presented on the following pages. The schedule for the TA and MG are listed in columns one and two, respectively. The pulse widths listed for the stimulation levels should be divided by ten to get the pulse width in μs (i.e., 550 corresponds to 55.0 μs).

Block 1: RSTMCLEN

(Double ramp of stimulation, constant length.)

FASTRAMP			
Time:	3:59	Time:	4:03
Chan:	1	Chan:	2
Length (mm):	10	Length (mm):	8
File # :	3	File # :	4
New Zoom	200 - 700	New Zoom	100 - 600
TORQUE GAIN	750	TORQUE GAIN	250
RSTMCLEN			
Time:	4:12	Time:	4:21
Chan:	1	Chan:	2
File #:	5	File #:	6
Shortest mm:	0	Shortest mm:	0
Longest mm:	7.5	Longest mm:	6
# of lengths:	4	# of lengths:	4
RSTMCLEN			
Time:	4:31	Time:	4:39
Chan:	1	Chan:	2
File #:	7	File #:	8
Shortest mm:	10	Shortest mm:	8.0
Longest mm:	17.5	Longest mm:	14.0
# of lengths:	4	# of lengths:	4

Block 2: STEPMAPL

(Constant length and constant stimulation)

FASTRAMP			
Time:	4:49	Time:	4:51
Chan:	1	Chan:	2
Length (mm):	10	Length (mm):	8
File # :	5	File # :	6
New Zoom	200 - 700	New Zoom	100 - 600
TORQUE GAIN	750	TORQUE GAIN	250
STEPMAPL			
Time:	4:53	Time:	5:55
Chan:	1	Chan:	2
# of stims:	1	# of stims:	1
Stim value:	0	Stim value:	0
Shortest len:	0	Shortest len:	0
Longest len:	17.5	Longest len:	14
# of lengths:	8	# of lengths:	4
File:	2	File:	3

Comments: TA tendon clamp came off during stim # 6 of file 2. Motor zero changed.

STEPMAPL			
Time:	6:02	Time:	6:12
Chan:	1	Chan:	2
# of stims:	3	# of stims:	3
Stim value:	300, 500, 700	Stim value:	200, 400, 600
Shortest len:	0	Shortest len:	0
Longest len:	15	Longest len:	12
# of lengths:	4	# of lengths:	4
File:	4	File:	5

STEPMAPL

Time:	6:28	Time:	6:40
Chan:	1	Chan:	2
# of stims:	3	# of stims:	3
Stim value:	300, 500, 700	Stim value:	200, 400, 600
Shortest len:	2.5	Shortest len:	2
Longest len:	17.5	Longest len:	14
# of lengths:	4	# of lengths:	7
File:	6	File:	7

Block 3: RANDCLEN

(Random stimulation, constant length)

FASTRAMP			
Time:	7:00	Time:	7:02
Chan:	1	Chan:	2
Length (mm):	10	Length (mm):	8
File # :	7	File # :	8
New Zoom	150 - 500	New Zoom	100 - 600
TORQUE GAIN	750	TORQUE GAIN	250
RANDCLEN			
Time:	7:06	Time:	7:08
Chan:	1	Chan:	2
# of stims	1	# of stims	1
rand pw seq	1	rand pw seq	1
mm of travel	17.5	mm of travel	14
time of travel	10	time of travel	10
File #:	3	File #:	4
RANDCLEN			
Time:	7:10	Time:	7:12
Chan:	1	Chan:	2
# of stims	1	# of stims	1
rand pw seq	1	rand pw seq	1
mm of travel	10	mm of travel	8
time of travel	10	time of travel	10
File #:	5	File #:	6
RANDCLEN			
Time:	7:14	Time:	7:16
Chan:	1	Chan:	2
# of stims	1	# of stims	1
rand pw seq	2	rand pw seq	2
mm of travel	17.5	mm of travel	14
time of travel	10	time of travel	10
File #:	7	File #:	8

RANDCLEN			
Time:	7:18	Time:	7:20
Chan:	1	Chan:	2
# of stims	1	# of stims	1
rand pw seq	2	rand pw seq	2
mm of travel	10	mm of travel	8
time of travel	10	time of travel	10
File #:	9	File #:	10

RANDCLEN			
Time:	7:32	Time:	7:34
Chan:	1	Chan:	2
# of stims	1	# of stims	1
rand pw seq	3	rand pw seq	3
mm of travel	17.5	mm of travel	14
time of travel	10	time of travel	10
File #:	11	File #:	12

TORQUE GAIN	750	TORQUE GAIN	500

RANDCLEN			
Time:	7:38	Time:	7:40
Chan:	1	Chan:	2
# of stims	1	# of stims	1
rand pw seq	3	rand pw seq	3
mm of travel	10	mm of travel	8
time of travel	10	time of travel	10
File #:	13	File #:	14

RANDCLEN			
Time:	7:52	Time:	7:54
Chan:	1	Chan:	2
# of stims	1	# of stims	1
rand pw seq	4	rand pw seq	4
mm of travel	17.5	mm of travel	14
time of travel	15	time of travel	15
File #:	15	File #:	16

RANDCLEN

Time:	7:56
Chan:	1
# of stims	1
rand pw seq	4
mm of travel	10
time of travel	15
File #:	17

Time:	7:58
Chan:	2
# of stims	1
rand pw seq	4
mm of travel	10
time of travel	15
File #:	18

Block 4: RLENCSTM

(Constant stimulation, double ramp length at constant velocity)

FASTRAMP			
Time:	8:13	Time:	8:16
Chan:	1	Chan:	2
Length (mm):	10	Length (mm):	8
File # :	9	File # :	10
New Zoom	100 - 400	New Zoom	200 - 500
TORQUE GAIN	750	TORQUE GAIN	500
RLENCSTM			
Time:	8:28	Time:	8:37
Chan:	1	Chan:	2
PW of stim:	0	PW of stim:	0
mm of travel:	17.5	mm of travel:	14.0
# of vel:	4	# of vel:	4
time of travel:	.35,.75,1.5,3.0	time of travel:	.35,.75,1.5,3.0
Flat time:	0.5	Flat time:	0.5
File #:	3	File #:	4
RLENCSTM			
Time:	8:44	Time:	8:55
Chan:	1	Chan:	2
PW of stim:	0	PW of stim:	0
mm of travel:	17.5	mm of travel:	14.0
# of vel:	4	# of vel:	4
time of travel:	.5,1.0,2.0,4.0	time of travel:	.5,1.0,2.0,4.0
Flat time:	0.5	Flat time:	0.5
File #:	5	File #:	6
RLENCSTM			
Time:	9:02	Time:	9:13
Chan:	1	Chan:	2
PW of stim:	225	PW of stim:	350
mm of travel:	17.5	mm of travel:	14.0
# of vel:	4	# of vel:	4
time of travel:	.35,.75,1.5,3.0	time of travel:	.35,.75,1.5,3.0
Flat time:	0.5	Flat time:	0.5
File #:	7	File #:	8

RLENCSTM

Time:	9:23	Time:	9:34
Chan:	1	Chan:	2
PW of stim:	225	PW of stim:	350
mm of travel:	17.5	mm of travel:	14.0
# of vel:	4	# of vel:	4
time of travel:	.5,1.0,2.0,4.0	time of travel:	.5,1.0,2.0,4.0
Flat time:	0.5	Flat time:	0.5
File #:	9	File #:	10

FASTRAMP

Time:	9:43	Time:	9:45
Chan:	1	Chan:	2
Length (mm):	10	Length (mm):	8
File # :	11	File # :	12
New Zoom	100 - 400	New Zoom	200 - 500

RLENCSTM

Time:	9:48	Time:	9:57
Chan:	1	Chan:	2
PW of stim:	275	PW of stim:	425
mm of travel:	17.5	mm of travel:	14.0
# of vel:	4	# of vel:	4
time of travel:	.35,.75,1.5,3.0	time of travel:	.35,.75,1.5,3.0
Flat time:	0.5	Flat time:	0.5
File #:	11	File #:	12

Comments: Analog force input saturated on fastest run of file 12.
Adjust torque gain and rerun as file 14.

TORQUE GAIN	750	TORQUE GAIN	300
		RLENCSTM	
		Time:	10:12
		Chan:	2
		PW of stim:	425
		mm of travel:	14.0
		# of vel:	4
		time of travel:	.35,.75,1.5,3.0
		Flat time:	0.5
		File #:	14

Comments: File 14 is a repeat of file 12. Instrumentation zero position changed on last run of file 14.

RLENCSTM			
Time:	10:24	Time:	10:33
Chan:	1	Chan:	2
PW of stim:	275	PW of stim:	425
mm of travel:	17.5	mm of travel:	14.0
# of vel:	4	# of vel:	4
time of travel:	.5,1.0,2.0,4.0	time of travel:	.5,1.0,2.0,4.0
Flat time:	0.5	Flat time:	0.5
File #:	15	File #:	16

RLENCSTM	
Time:	10:41
Chan:	1
PW of stim:	275
mm of travel:	17.5
# of vel:	4
time of travel:	.35,.75,1.5,3.0
Flat time:	0.5
File #:	17

Comments: File 17 is a repeat of file 11.

RLENCSTM

Time:	10:51
Chan:	1
PW of stim:	350
mm of travel:	17.5
# of vel:	4
time of travel:	.35,.75,1.5,3.0
Flat time:	0.5
File #:	19

TORQUE GAIN 500

RLENCSTM

Time:	11:22
Chan:	1
PW of stim:	350
mm of travel:	17.5
# of vel:	4
time of travel:	.5,1.0,2.0,4.0
Flat time:	0.5
File #:	21

Time:	11:12
Chan:	2
PW of stim:	500
mm of travel:	14.0
# of vel:	4
time of travel:	.35,.75,1.5,3.0
Flat time:	0.5
File #:	20

TORQUE GAIN 300

Time:	11:32
Chan:	2
PW of stim:	500
mm of travel:	14.0
# of vel:	4
time of travel:	.5,1.0,2.0,4.0
Flat time:	0.5
File #:	22

RLENCSTM

Time:	11:42
Chan:	2
PW of stim:	500
mm of travel:	14.0
# of vel:	4
time of travel:	2.0,.5,1.0,4.0
Flat time:	0.5
File #:	18

Comments: File 18 is a repeat of file 22, with constant velocity ramps in different order.

Block 5: CSTMRAND

(Constant stimulation, random length)

FASTRAMP			
Time:	11:52	Time:	11:54
Chan:	1	Chan:	2
Length (mm):	10	Length (mm):	8
File # :	13	File # :	14
New Zoom	100 - 400	New Zoom	200 - 700
TORQUE GAIN	500	TORQUE GAIN	300
CSTMRAND			
Time:	11:57	Time:	12:07
Chan:	1	Chan:	2
# of stims	4	# of stims	4
PW of stims	0, 225, 275, 350	PW of stims	0,350,425,600
mm of travel	5 - 17.5	mm of travel	4 - 14
random curve	1	random curve	1
time of travel	10	time of travel	10
File #:	3	File #:	4
CSTMRAND			
Time:	12:17	Time:	12:27
Chan:	1	Chan:	2
# of stims	4	# of stims	4
PW of stims	0, 225, 275, 350	PW of stims	0,350,425,600
mm of travel	5 - 17.5	mm of travel	4 - 14
random curve	2	random curve	2
time of travel	10	time of travel	10
File #:	5	File #:	6
CSTMRAND			
Time:	12:35	Time:	12:49
Chan:	1	Chan:	2
# of stims	4	# of stims	4
PW of stims	0, 225, 275, 350	PW of stims	0,350,425,600
mm of travel	5 - 17.5	mm of travel	4 - 14
random curve	3	random curve	3
time of travel	10	time of travel	10
File #:	7	File #:	8

Block 6: RANDRAND

(Random stimulation, random length)

TORQUE GAIN	500	TORQUE GAIN	300
FASTRAMP			
Time:	12:57	Time:	12:58
Chan:	1	Chan:	2
Length (mm):	10	Length (mm):	8
File # :	15	File # :	16
New Zoom	100 - 400		
Comments:	Deconvolution error for MG. Reset torque gain. Re-ran as file 18.		
TORQUE GAIN	500	TORQUE GAIN	500
		FASTRAMP	
		Time:	1:00
		Chan:	2
		Length (mm):	8
		File # :	18
		New Zoom	200 - 700
TORQUE GAIN	500	TORQUE GAIN	300
RANDRAND			
Time:	1:02	Time:	1:06
Chan:	1	Chan:	2
# of stims	1	# of stims	1
rand pw seq	1	rand pw seq	1
mm of travel	5 - 17.5	mm of travel	4 - 14
random curve	1	random curve	1
time of travel	10	time of travel	10
File #:	19	File #:	20

RANDRAND			
Time:	1:10	Time:	1:12
Chan:	1	Chan:	2
# of stims	1	# of stims	1
rand pw seq	2	rand pw seq	2
mm of travel	5 - 17.5	mm of travel	4 - 14
random curve	1	random curve	1
time of travel	10	time of travel	10
File #:	21	File #:	22
RANDRAND			
Time:	1:13	Time:	1:15
Chan:	1	Chan:	2
# of stims	1	# of stims	1
rand pw seq	3	rand pw seq	3
mm of travel	5 - 17.5	mm of travel	4 - 14
random curve	1	random curve	1
time of travel	10	time of travel	10
File #:	23	File #:	24
TORQUE GAIN	500	TORQUE GAIN	500
RANDRAND			
Time:	1:18	Time:	1:21
Chan:	1	Chan:	2
# of stims	1	# of stims	1
rand pw seq	1	rand pw seq	1
mm of travel	5 - 17.5	mm of travel	4 - 14
random curve	3	random curve	3
time of travel	10	time of travel	10
File #:	25	File #:	26
TORQUE GAIN	750	TORQUE GAIN	500
RANDRAND			
Time:	1:23	Time:	1:25
Chan:	1	Chan:	2
# of stims	1	# of stims	1
rand pw seq	3	rand pw seq	3
mm of travel	5 - 17.5	mm of travel	4 - 14
random curve	3	random curve	3
time of travel	10	time of travel	10
File #:	27	File #:	28

RANDRAND

Time:	1:27	Time:	1:29
Chan:	1	Chan:	2
# of stims	1	# of stims	1
rand pw seq	4	rand pw seq	4
mm of travel	5 - 17.5	mm of travel	4 - 14
random curve	3	random curve	3
time of travel	10	time of travel	10
File #:	29	File #:	30

RANDRAND

Time:	1:31	Time:	1:33
Chan:	1	Chan:	2
# of stims	1	# of stims	1
rand pw seq	1	rand pw seq	1
mm of travel	5 - 17.5	mm of travel	4 - 14
random curve	4	random curve	4
time of travel	10	time of travel	10
File #:	31	File #:	32

RANDRAND

Time:	1:35	Time:	1:37
Chan:	1	Chan:	2
# of stims	1	# of stims	1
rand pw seq	3	rand pw seq	3
mm of travel	5 - 17.5	mm of travel	4 - 14
random curve	4	random curve	4
time of travel	15	time of travel	15
File #:	33	File #:	34

RANDRAND

Time:	1:40	Time:	1:42
Chan:	1	Chan:	2
# of stims	1	# of stims	1
rand pw seq	4	rand pw seq	4
mm of travel	5 - 17.5	mm of travel	4 - 14
random curve	4	random curve	4
time of travel	15	time of travel	15
File #:	35	File #:	36

FASTRAMP

Time:	1:45	Time:	1:46
Chan:	1	Chan:	2
Length (mm):	10	Length (mm):	8
File # :	17	File # :	20
New Zoom	100 - 400		

Comments: Deconvolution error for MG. Reset torque gain. Re-ran as file 22.

TORQUE GAIN	750	TORQUE GAIN	700

FASTRAMP

Time:	1:48
Chan:	2
Length (mm):	8
File # :	22
New Zoom	200 - 700

Bibliography

[1] S. Brummer and M. Turner. Electrochemical considerations for safe electrical stimulation of the nervous system with platinum electrodes. *IEEE Trans. Biomed. Eng.*, 24:59 - 63, 1977.

[2] R. Burke. Physiological types and histochemical profiles in motor units of the cat gastrocnemius. *J. Physiol.*, 234:723 - 748, 1973.

[3] P. Crago, P. Peckham, and G. Thrope. Modulation of muscle force by recruitment during intramuscular stimulation. *IEEE Trans. Biomed. Eng.*, 27:679–684, 1980.

[4] L. Dum and T. Kennedy. Physiological and histochemical characteristics of motor units in cat tibialis anterior and extensor digitorum longus muscles. *J. of Neurophys.*, 43(6):1615 - 1630, 1980.

[5] W. K. Durfee. *Task Control with an Electrically Stimulated Antagonist Muscle Pair.* PhD thesis, Massachusetts Institute of Technology, June 1985.

[6] W. K. Durfee and K. E. MacLean. Methods for estimating isometric recruitment curves of electrically stimulated muscle. *IEEE Trans. Biomed. Eng.*, 36(7):654–667, July 1989.

[7] G. J. C. Ettema and P. A. Huijing. Architecture and elastic properties of the series elastic element of muscle-tendon complex. In J. M. Winters and S. L-Y. Woo, editors, *Multiple Muscle Systems: Biomechanics and Movement Organization*, chapter 4, pages 46 - 56. Springer-Verlag, 1990.

[8] P. Gorman and J. Mortimer. The effect of stimulus parameters on the recruitment characteristics of direct nerve stimulation. *IEEE Trans. Biomed. Eng.*, 30:407–414, 1983.

[9] J Hausdorff. Gait orthosis combining controllable damping and muscle stimulation. Master's thesis, Massachusetts Institute of Technology, August 1988.

[10] G. C. Joyce, P. M. H. Rack, and D. R. Westbury. The mechanical properties of cat soleus muscle during controlled lengthening and shortening movements. *J. Physiol.*, 204:461–474, 1969.

[11] W. H. Lawton, E. A. Sylvestre, and M. S. Maggio. Self modeling nonlinear regression. *Technometrics*, 14(3):513 - 533, 1972.

[12] J. N. Little and L. Shure. *Signal Processing Toolbox for use with Matlab.* The Math Works, Inc., Sherborn, MA, August 1988.

[13] K. E. MacLean. Estimation of isometric recruitment curves of electrically stimulated muscle. Master's thesis, Massachusetts Institute of Technology, December 1988.

[14] *et. al.* McDonagh, J. A commentary on muscle unit properties in cat hindlimb muscles. *J. Morph.*, 166:217 - 230, 1980.

[15] D. McNeal. Analysis of a model for excitation of myelinated nerve. *IEEE Trans. Biomed. Eng.*, 25:329–337, 1976.

[16] C. Moler, J. Little, and S. Bangert. *PC-Matlab User's Guide.* The Math Works, Inc., Sherborn, MA, Version 3.2-PC edition, June 1987.

[17] D. L. Morgan. Separation of active and passive components of short-range stiffness of muscle. *Am. J. Physiol.*, 232:C45–C49, 1977.

[18] W. H. Press, B. P. Flannery, S. A. Teukolsky, and W. T. Vetterling. *Numerical Recipes in C: The Art of Scientific Computing.* Cambridge University Press, New York, NY, 1988.

[19] P. M. H. Rack and D. R. Westbury. Elastic properties of the cat soleus tendon and their functional importance. *J. Physiol.*, 347:479–495, 1984.

[20] A. H. Robbins. Joint space muscle model for functional electrical stimulation application. Master's thesis, Massachusetts Institute of Technology, February 1990.

[21] R. B. Stein and T. Gordon. Nonlinear stiffness-force relationships in whole mammalian skeletal muscles. *Can. J. Physiol. Pharmacol.*, 64:1236–1244, 1986.

[22] T. E. Stripling. The cost of SCI. *Paraplegia News*, pages 50 - 54, August 1990.

[23] B. Walmsley and U. Proske. Comparison of stiffness of soleus and medial gastrocnemius muscles in cats. *J. Neurophysiol.*, 46:250–259, 1981.

[24] J. M. Winters. Hill-based muscle models: A systems engineering perspective. In J. M. Winters and S. L-Y. Woo, editors, *Multiple Muscle Systems: Biomechanics and Movement Organization*, chapter 5, pages 69 - 93. Springer-Verlag, 1990.

[25] H. J. Woltring. A Fortran package for generalized, cross-validatory spline smoothing and dirrerentiation. *Adv. Eng. Software*, 8(2), 1986.

[26] F. Zajac. Muscle and tendon: properties, models, scaling and application to biomechanics and motor control. *CRC Crit. Rev. Biomed. Engng.*, 17:359–415, 1989.